

Oligomer studies on polymer photovoltaics

Citation for published version (APA):

Karsten, B. P. (2010). *Oligomer studies on polymer photovoltaics*. [Phd Thesis 1 (Research TU/e / Graduation TU/e), Chemical Engineering and Chemistry]. Technische Universiteit Eindhoven.
<https://doi.org/10.6100/IR676738>

DOI:

[10.6100/IR676738](https://doi.org/10.6100/IR676738)

Document status and date:

Published: 01/01/2010

Document Version:

Publisher's PDF, also known as Version of Record (includes final page, issue and volume numbers)

Please check the document version of this publication:

- A submitted manuscript is the version of the article upon submission and before peer-review. There can be important differences between the submitted version and the official published version of record. People interested in the research are advised to contact the author for the final version of the publication, or visit the DOI to the publisher's website.
- The final author version and the galley proof are versions of the publication after peer review.
- The final published version features the final layout of the paper including the volume, issue and page numbers.

[Link to publication](#)

General rights

Copyright and moral rights for the publications made accessible in the public portal are retained by the authors and/or other copyright owners and it is a condition of accessing publications that users recognise and abide by the legal requirements associated with these rights.

- Users may download and print one copy of any publication from the public portal for the purpose of private study or research.
- You may not further distribute the material or use it for any profit-making activity or commercial gain
- You may freely distribute the URL identifying the publication in the public portal.

If the publication is distributed under the terms of Article 25fa of the Dutch Copyright Act, indicated by the "Taverne" license above, please follow below link for the End User Agreement:

www.tue.nl/taverne

Take down policy

If you believe that this document breaches copyright please contact us at:

openaccess@tue.nl

providing details and we will investigate your claim.

Oligomer Studies on Polymer Photovoltaics

PROEFSCHRIFT

ter verkrijging van de graad van doctor aan de
Technische Universiteit Eindhoven, op gezag van
de rector magnificus, prof.dr.ir. C.J. van Duijn,
voor een commissie aangewezen door het College
voor Promoties in het openbaar te verdedigen op
maandag 27 september 2010 om 16.00 uur

door

Bram Pieter Karsten

geboren te Rotterdam

Dit proefschrift is goedgekeurd door de promotor:

prof.dr.ir. R.A.J. Janssen

Omslagfoto: SOHO (ESA & NASA)

Druk: Wöhrmann Print Service, Zutphen

A catalogue record is available from the Eindhoven University of Technology Library

ISBN: 978-90-386-2292-7

The research was supported by a TOP grant of the Chemical Sciences (CW) division of The Netherlands Organization for Scientific Research (NWO) and is part of the Joint Solar Programme (JSP). The JSP is cofinanced by the Foundation for Fundamental Research on Matter (FOM), Chemical Sciences of NWO, and the Foundation Shell Research.

Contents

1	Introduction	1
1.1	Organic solar cells	1
1.2	Small band gap polymers	3
1.3	Energy levels in π -conjugated materials and their determination	5
1.3.1	Measuring the band gap and the HOMO/LUMO levels	5
1.3.2	Triplet states	6
1.3.3	Oxidized oligomers	6
1.4	Photoinduced absorption	7
1.4.1	Triplet energy transfer	8
1.4.2	Photoinduced electron transfer	8
1.5	Aim and scope of this thesis	9
	References and notes	10
2	Electronic structure of oligomers based on CPDT and acceptor units	13
2.1	Introduction	14
2.2	Results and discussion	14
2.2.1	Synthesis	14
2.2.2	Electrochemical and optical properties	14
2.2.3	Triplet excited states and their energies	17
2.2.4	Radical cations	19
2.2.5	Quantum-chemical calculations	20
2.3	Conclusions	22
2.4	Experimental	23
	References and notes	28
3	Small band gap oligothieno[3,4-<i>b</i>]pyrazines	31
3.1	Introduction	32
3.2	Results and discussion	32
3.2.1	Synthesis	32
3.2.2	Optical and electrochemical properties	32
3.2.3	Radical cations	34
3.2.4	Chain length dependence	36
3.3	Conclusions	37
3.4	Experimental	37
	References and notes	41

4	Oligomers with single acceptor units	43
4.1	Introduction	44
4.2	Results and discussion	44
4.2.1	Synthesis	44
4.2.2	Optical and electrochemical properties of the neutral oligomers	45
4.2.3	Theoretical results	48
4.2.4	Triplet excited states	50
4.2.5	Cations and dications of the oligomers	51
4.2.6	Photoinduced electron transfer in solution from oligomers to MP-C ₆₀	52
4.3	Conclusions	56
4.4	Experimental	56
	References and notes	59
5	Double acceptor units and origins of band gap reduction	61
5.1	Introduction	62
5.2	Results and discussion	62
5.2.1	Synthesis	62
5.2.2	Optical and electrochemical properties of the neutral oligomers	63
5.2.3	Triplet states of the neutral oligomers	65
5.2.4	Radical cations of the oligomers	66
5.2.5	Chain length dependence in related systems	67
5.3	Conclusions	72
5.4	Experimental	73
	References and notes	75
6	Charge separation and recombination in triads containing TP units	77
6.1	Introduction	78
6.2	Results and discussion	78
6.2.1	Synthesis	78
6.2.2	Optical properties	80
6.2.3	Photoinduced absorption	81
6.3	Conclusions	88
6.4	Experimental	88
	References and notes	95
7	Charge separation and (triplet) recombination in DPP – fullerene triads	99
7.1	Introduction	100
7.2	Results and discussion	100
7.2.1	Synthesis	100
7.2.2	Optical and electrochemical properties	101
7.2.3	Triplet excited states and cations of the oligomers	102
7.2.4	Photoluminescence of oligomers and triads	103
7.2.5	Charge separation and recombination processes	105
7.3	Conclusions	112
7.4	Experimental	112
	References and notes	116

8 Diketopyrrolopyrroles as acceptor materials in organic photovoltaics	119
8.1 Introduction	120
8.2 Results and discussion	120
8.2.1 Optical and electrochemical properties	120
8.2.2 Acceptor behavior of the compounds	121
8.2.3 Photovoltaic devices	124
8.3 Conclusions	125
8.4 Experimental	126
References and notes	127
 Epilogue	 129
 Summary	 131
 Samenvatting	 133
 Curriculum vitae	 135
 List of publications	 137
 Dankwoord	 139

Chapter 1

Introduction

Over the past four decades, the interest in renewable energy resources has risen. Initially, concerns about the limited availability of fossil fuels were an important motivation for the search for alternatives. In 1972, the Club of Rome published the report 'The Limits to Growth',¹ focussing attention to the finiteness of fossil energy sources. Later in the 1970's, the world was hit by two oil crises, leading to a sudden increase of the oil price and a growing consciousness of the limited availability of natural resources.

In the 1980's, the Brundtland commission was created to address the concerns about environmental pollution and the finiteness of natural resources, and the consequences that these would have for society. In their report 'Our Common Future' from 1987,² the commission defines sustainable development as "development that meets the needs of the present without compromising the ability of future generations to meet their own needs." In an energy perspective this means that, in order to be sustainable, we should use renewable energy and/or provide future generations with technology that renders them independent of fossil resources.

In the years after publication of the Brundtland report, another motivation for abandoning fossil fuels appeared: global warming. Due to the emission of greenhouse gasses, most notably CO₂, upon burning carbon-based fuels (coal, oil and natural gas), the world's climate is changing.³ To circumvent problems, related to climate change, it is thought to be necessary to substantially reduce CO₂ emissions in the near future.⁴ Because the use of energy is only expected to rise in the near future,³ the only way to substantially reduce greenhouse gas emissions will be the use of nuclear power (which is not sustainable, due to the limited availability of nuclear fuel) or renewable energy resources.

1.1 Organic solar cells

Since the development of the first crystalline silicon solar cell by Chapin, Fuller and Pearson in 1954,⁵ with an efficiency of 6%, great improvements have been made in photovoltaic technology. The best published crystalline silicon devices nowadays reach efficiencies of 25%,⁶ and with multi-junction devices efficiencies up to 41% have been reached.⁷ Although the efficiencies obtained with these solar cells based

on inorganic materials are high, the demands on both materials and processing are severe, resulting in very expensive cells.

A possible alternative to inorganic solar cells is formed by organic photovoltaics. Organic materials offer large advantages over inorganic materials, in terms of synthetic accessibility, ease of processing and cost. A large mechanistic difference between organic and inorganic photovoltaics is the nature of the excitation, that is created upon illumination of the materials. In inorganic solar cells, free electrons and holes are created immediately when a photon is absorbed. In organic materials however, the created electron and hole are still coulombically bound, due to the low dielectric constant of organic materials. To create photocurrent, the electron and hole have to be separated. The way to do this has been introduced by Tang in 1986, when he combined an electron-rich donor material (a phthalocyanine, CuPC) and an electron-poor acceptor material (a perylene derivative, PV) in a bilayer architecture and achieved a power conversion efficiency of about 1%.⁸ A schematic representation of the Tang cell and a scheme of the charge separation process are given in figure 1.1. In this architecture, a bound electron-hole pair (an exciton) is formed upon photoexcitation of the donor (process 1 in figure 1.1b).⁹ After separation of the electron and hole, both charges can move to their respective electrodes. The exciton then diffuses to the donor-acceptor interface (2), where the electron and hole are separated by electron transfer to the acceptor (3).

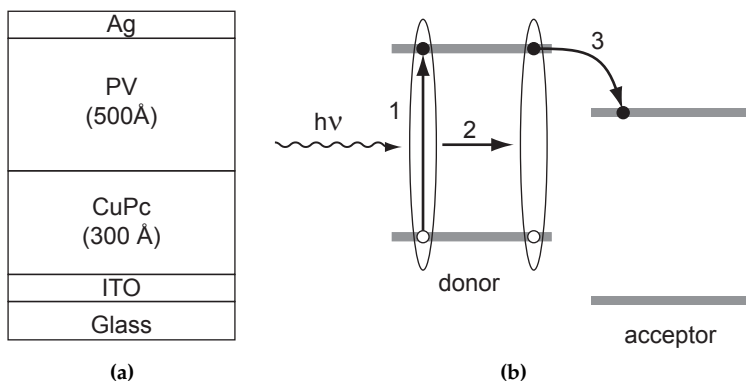


Figure 1.1: Schematic representation of the Tang cell (a) and schematic representation of the processes needed for charge separation (b): excitation (1), excitation diffusion (2) and electron transfer (3).

Since publication of the Tang cell, all efficient organic solar cells are based on the donor-acceptor approach. There are, however different types of organic solar cells. In dye-sensitized solar cells (also called Grätzel cells),¹⁰ the donor material (the dye) consists of small molecules, attached to a mesoporous TiO₂ network. In this case, the TiO₂ acts as the acceptor material, and after exciton separation, the dye is regenerated by a liquid electrolyte (usually I⁻/I₃⁻) that transports the hole to the anode. Efficiencies up to 11.2% have been obtained using this type of solar cell.¹¹ The main advantage in dye-sensitized solar cells is that, due to the attachment of the dye to the acceptor, no exciton diffusion is needed and charge separation takes place

immediately after excitation.

Other approaches are either based on small molecules or polymers as donor materials, combined with a variety of acceptor materials like inorganics, polymers or small molecular compounds (most notably fullerenes). In contrast to dye-sensitized solar cells, exciton diffusion is important in these materials. Because the lifetime of excitons is short, usually in the order of nanoseconds, the path that an exciton can travel is limited to about 5–15 nm for π -conjugated polymers.^{12–15} Excitons created further away from the donor–acceptor interface than this so-called exciton diffusion length, recombine before they can be separated into free charge carriers and, consequently do not contribute to the photocurrent. As a result, the maximum thickness of bilayer devices, like the Tang cell, is limited to about 10–20 nm, which is not enough to absorb all incoming sunlight. To be able to increase the layer thickness, the bulk heterojunction (BHJ) concept was developed.¹⁶ In a BHJ-device, the donor and acceptor materials are intimately mixed in one layer, relying on phase separation between the two materials. As a result, the donor–acceptor interface is dispersed throughout the entire active layer, and every exciton that is generated will be close to this interface. The separated hole and electron are transported to the electrodes through their respective phases. The work described in this thesis focusses on the materials used in BHJ solar cells using polymers as the donor material and small molecules as the acceptor material.

1.2 Small band gap polymers

Since the introduction of the BHJ concept, tremendous advances have been made with regard to device efficiencies of polymer solar cells. The ‘standard’ material combination used in many devices consists of regioregular poly(3-hexylthiophene) (P3HT) as the donor material and [6,6]-phenyl-C₆₁-butyric acid methyl ester (PCBM) as the acceptor, typically yielding efficiencies of 3–4%. The main disadvantage of P3HT as a light absorbing material however, is its relatively high band gap. In figure 1.2, the emission spectrum of the sun, as observed on the earth’s surface is depicted. With a band gap of 1.9 eV, P3HT is only capable of absorbing light with wavelengths lower than ~ 650 nm, indicated with the gray area.

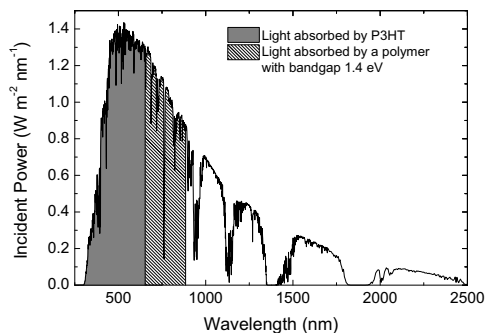


Figure 1.2: Emission spectrum of the sun, as observed on the earth’s surface. Regions where light can be absorbed by P3HT and a polymer with a band gap of 1.4 eV are indicated.

It is clear from figure 1.2, that to increase the amount of light that is absorbed, and hence the efficiency of the photovoltaic device, it is necessary to lower the optical band gap of the light absorbing material. It is estimated, that the optimal band gap for organic photovoltaics is about 1.4–1.5 eV.¹⁷ The extra light absorbed by a polymer with a band gap of 1.4 eV is also indicated in figure 1.2. Of course, the areas marked in this figure represent maxima, obtained when the polymer absorbs *all* photons with an energy below its band gap. In reality however, polymers have an absorption *spectrum*, instead of full absorption below their band gap, and not all of the indicated photons will be absorbed.

Two different strategies exist towards designing and synthesizing polymers with reduced band gaps.^{18–21} The first approach relies on creating polymers based on a single monomer unit that, after polymerization, endows the chain with an electronic structure where aromatic (A) and quinoid (Q) resonance structures are close in energy and bond length alternation is decreased or inverted. The classical example of this class, first described by Wudl et al., is poly(isothionaphthene) (PITN, figure 1.3a), which features a band gap of about 1 eV due to an essentially quinoid ground state.^{22,23} Another example is poly(thienopyrazine) (PTP, figure 1.3b), which has a similarly small optical band gap.^{24–26}

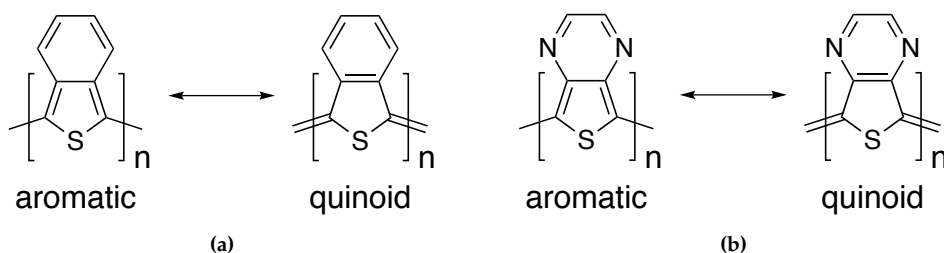


Figure 1.3: Resonance structures of PITN (a) and PTP (b)

The second approach, first described by Havinga et al.^{27,28} and further developed by Tanaka et al.,²⁹ is based on alternating electron-rich (donor) and electron-deficient (acceptor) monomer units along the chain. In this way, the high-lying HOMO of the donor-unit is combined with the low-lying LUMO of the acceptor unit, and a small band gap is obtained (figure 1.4a). Presently, the large majority of small band gap polymers developed for solar cell applications is based on this donor–acceptor approach and polymers with efficiencies in photovoltaic cells up to 7.4% have been published.^{30–32} Frequently, small oligothiophene derivatives with two to four units are used as the electron-rich donor unit with the complementary electron-deficient acceptor units being an aromatic nitrogen heterocyclic system, such as quinoxaline (Q), 1,3,2-benzothiadiazole (BT), or thieno[3,4-b]pyrazine (TP). These acceptors are depicted in figure 1.4b.

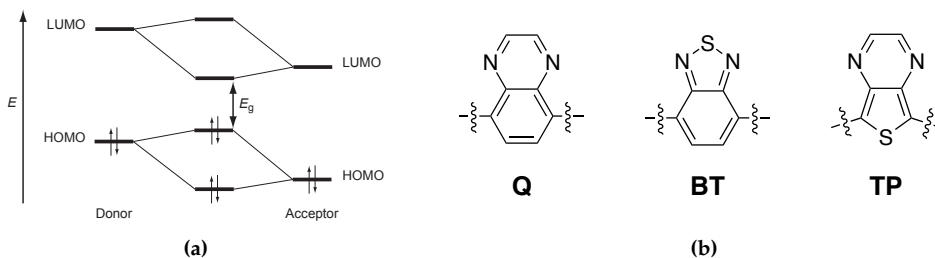


Figure 1.4: Orbital diagram, showing the hybridization of the HOMOs and LUMOs of the donor and acceptor units, creating a small band gap (E_g) in the D-A compound (a), and some commonly used acceptor units (b).

1.3 Energy levels in π -conjugated materials and their determination

The important energy levels in organic photovoltaics are the HOMO and LUMO levels of both the donor and the acceptor material. The difference between the HOMO and LUMO is referred to as the band gap E_g of the material, which can be measured either by optical or electrochemical techniques.

1.3.1 Measuring the band gap and the HOMO/LUMO levels

The most straightforward technique for measuring the band gap is by UV/vis absorption. The long-wavelength onset of the absorption spectrum represents the lowest energy excitation possible (the HOMO \rightarrow LUMO transition, which is equal to the optical band gap, E_g^{opt}). A similar result can be obtained by fluorescence measurements, basically the inverse of absorption.

The other method for determining the band gap of a material is by an electrochemical technique called cyclic voltammetry. In this technique, the material is dissolved in a solvent containing a salt as a supporting electrolyte. By scanning the potential of the working electrode relative to a reference, and recording the current, it is possible to measure at which potentials the compound under study is oxidized or reduced. The onset of the oxidation wave in this experiment is closely related to the HOMO level of the compound under study. The same holds for the onset of the reduction wave and the LUMO level, so the electrochemical band gap E_g^{CV} can be calculated by taking the difference between the two onset potentials. Usually, the electrochemical band gap approximately equals the optical band gap, although slight differences are commonly observed. A possible explanation for these differences can be found in the fact, that in the optical experiment the created electron and hole are bound, forming an exciton, whereas in the electrochemical experiment ions are created. Apart from the exciton binding energy (which lowers the energy of the exciton, relative to that of the free charges), also the solvation of the ions created in the electrochemical experiment has an influence on the observed electrochemical band gap.

Apart from the electrochemical band gap, also the positions of the HOMO and

LUMO levels, relative to some reference, are obtained from CV measurements. In all electrochemical experiments described in this thesis, the ferrocene/ferrocenium (Fc/Fc^+) couple is used as an internal reference, for this purpose. In principle, when knowing the position of this reference level *vs.* vacuum, the position of the HOMO and LUMO levels relative to the vacuum level can be calculated. Unfortunately, exact determination of the Fc/Fc^+ potential *vs.* vacuum is difficult, and values between -4.8 eV and -5.2 eV are frequently found.^{33,34} Therefore in this thesis, HOMO and LUMO levels are always given as oxidation or reduction onset potentials, relative to the Fc/Fc^+ couple rather than to the vacuum level.

1.3.2 Triplet states

In the ground state of a neutral molecule, the HOMO is filled by two electrons with anti-parallel spins (a so-called singlet state). Upon excitation, one of these electrons is promoted to the LUMO, resulting in two singly occupied orbitals. In this excited state, the spins of the electrons can be anti-parallel, like in the ground state, or parallel. If the two spins are parallel, the molecule has net spin, and this state is threefold degenerate. Such a state is called a triplet excited state. A triplet state always has a lower energy than its singlet counterpart (in which the electron spins are anti-parallel), due to quantum mechanics. The difference between the two states equals two times the so-called exchange energy. Basically this exchange energy depends on the overlap between the orbitals containing the two electrons (the HOMO and LUMO in our case). The more overlap, the larger the exchange energy and the singlet–triplet splitting energy ΔE_{ST} . In π -conjugated polymers, the value for ΔE_{ST} usually varies between 0.6 and 1.0 eV.^{35,36} A scheme of the energy levels and possible transitions in any π -conjugated oligomer or polymer is depicted in figure 1.5a

As transitions between states of different spin-multiplicity are forbidden, these transitions are usually weak and not observed. Hence, excitation of a π -conjugated molecule usually yields the first singlet excited state (corresponding to a $S_1 \leftarrow S_0$ transition). The first triplet excited state (T_1) may then be formed by intersystem crossing (ISC) from the S_1 state, which can be weakly allowed by a process called spin-orbit coupling. The triplet state formed is long-lived, because the $S_0 \leftarrow T_1$ transition is spin-forbidden.

1.3.3 Oxidized oligomers

After light absorption in a solar cell, the donor material transfers an electron to the acceptor, forming a charge transfer (CT) state. In this CT state, the positive charge on the donor and the negative charge on the oligomer are in close proximity, and the charges are still weakly bound. In the next step, the charges are fully separated and transported to the electrodes. The final result of these processes is oxidation of the donor material, leaving it with a positive charge. This oxidation induces changes in the electronic structure in the molecule and as a result, the absorption spectrum of the material changes. The changes to the electronic energy levels and the associated transitions are depicted in figure 1.5b.

When a conjugated polymer or oligomer is oxidized, the positive charge induces a more quinoid structure in the backbone of the molecule, thereby decreasing the

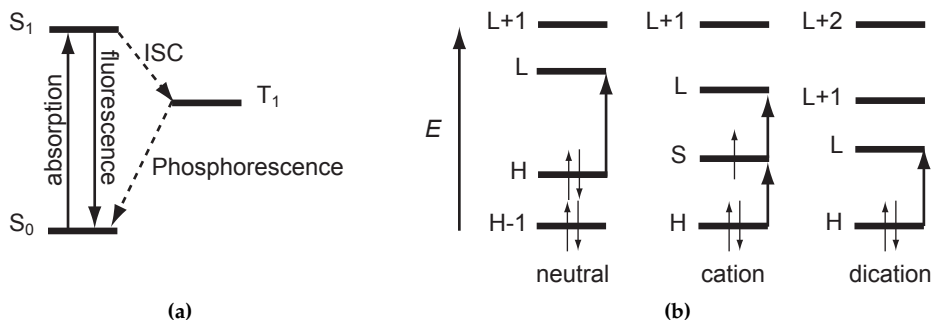


Figure 1.5: (a) Energy diagram of an oligomer, showing singlet and triplet states and the possible transitions between these states. (b) Orbital diagram of an oligomer, showing the possible electronic transitions in the neutral oligomer, the radical cation and the dication (H = HOMO, S = SOMO, L = LUMO).

optical gap.^{37,38} At the same time, two transitions appear at an energy lower than the band gap of the neutral species. One transition takes place from the (new) HOMO to the singly occupied molecular orbital (SOMO, the old HOMO) and one from the SOMO to the LUMO. Further oxidation to the dication leads to a further reduction of the SOMO–LUMO gap, and now only one absorption is visible, in between the absorption bands of the radical cation.

1.4 Photoinduced absorption

As we have seen, several processes can occur after a molecule is excited by a photon. The singlet excited state that is initially formed can decay to the ground state, either radiatively (fluorescence) or non-radiatively, but if intersystem crossing occurs, the long-living triplet state can be formed. The absorption of the different excited states can be investigated by photoinduced absorption (PIA). A schematic of the near steady-state PIA setup used for the work described in this thesis is shown in figure 1.6. In a PIA experiment, a solution of the compound under study is excited by a chopped laser and the transmission of white light is measured. By means of a lock-in amplifier, the difference between light transmission in the excited state (laser "on") and ground state (laser "off") is recorded. In this way an absorption spectrum of the excited state can be reconstructed. The lifetimes of the species that can be detected by this setup are in the μs – ms range and, consequently only long-living species, like triplet excited states, can be detected. For detecting short-lived species and kinetic studies shortly after excitation, also femtosecond PIA has been performed for the work described in chapters 6 and 7. The basic difference between fs-PIA and the steady-state setup described here, is that both excitation and detection are performed by short light pulses (instead of using a continuous wave laser and a halogen lamp). By varying the delay of the probe pulse with respect to the excitation pulse, a series of PIA-spectra can be obtained at various times after excitation.

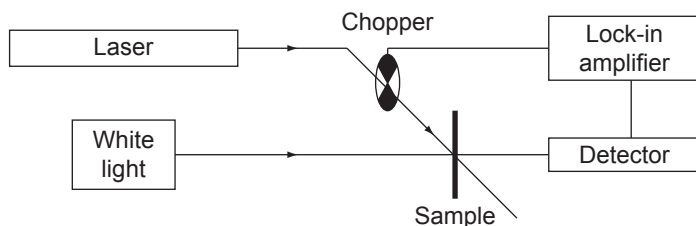


Figure 1.6: Schematic representation of the near steady-state PIA setup

1.4.1 Triplet energy transfer

In most cases described in this thesis, excitation of an oligomer did not give rise to any detectable amount of triplets. Apparently, the singlet excited state has a lifetime that is too short for intersystem crossing to occur. To be able to measure triplet absorption spectra of these compounds, fullerenes (either *N*-methylfulleropyrrolidine, MP-C₆₀, or PCBM) were used as triplet sensitizer. Upon excitation, these fullerenes undergo intersystem crossing with a quantum yield close to unity, yielding the triplet state of the fullerene, with an energy of 1.50 eV.³⁹ If this triplet excited fullerene encounters an oligomer molecule, triplet energy transfer can occur, yielding the triplet excited state of the oligomer, provided that the triplet energy of the oligomer is lower than the triplet energy of the fullerene. This process is schematically depicted in figure 1.7.

The fact that the lowest triplet excited state is observed in near steady-state PIA experiments is not limited to mixtures of only two compounds. Therefore, triplet energy levels of the oligomers can be estimated by adding quenchers with a known triplet energy to the solution. If the triplet energy of the quencher is higher than the triplet energy of the oligomer, the oligomer triplet will not be quenched. If on the other hand the triplet energy of the quencher is lower than the triplet energy of the oligomer, the oligomer triplet is quenched and the triplet absorption of the quencher can be detected.

1.4.2 Photoinduced electron transfer

If a mixture of a fullerene and a conjugated oligomer is photoexcited, there is also the possibility that electron transfer from the oligomer to the fullerene (which is a good electron acceptor) takes place. In this case the radical cation of the oligomer (as described in section 1.3.2) and the radical anion of the fullerene are obtained. It depends on the energy of the charge separated state (CSS), if this process can take place. This energy depends, amongst others, on solvent polarity. The free energy for charged separation (ΔG_{CS}) can be calculated by the Weller equation, which is based on a continuum model.⁴⁰

$$\Delta G_{CS} = e(E_{ox}(D) - E_{red}(A)) - E_{00} - \frac{e^2}{4\pi\epsilon_0\epsilon_s R_{cc}} - \frac{e^2}{8\pi\epsilon_0} \left(\frac{1}{r^+} + \frac{1}{r^-} \right) \left(\frac{1}{\epsilon_{ref}} - \frac{1}{\epsilon_s} \right)$$

In this equation $E_{ox}(D)$ and $E_{red}(A)$ are the oxidation and reduction potentials of the donor (oligomer) and acceptor (fullerene) in the reference solvent. E_{00} is the ex-

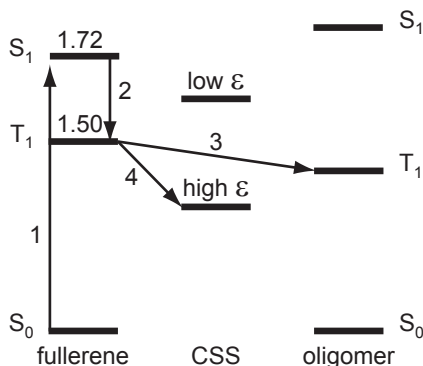


Figure 1.7: Schematic representation of the processes that can take place after exciting a fullerene in a mixture with some π -conjugated oligomer. Excitation (1) is followed by intersystem crossing (2) and either triplet energy transfer (3) or electron transfer (4) from the oligomer to the fullerene, dependent on solvent polarity (represented by the permittivity ϵ). Energies are given in eV.

cited state from which charge transfer takes place (1.50 eV for the triplet level of the fullerene), R_{cc} is the center-to-center distance of the positive and negative charges (infinity for intermolecular charge transfer), r^+ and r^- are the radii of the positive and negative ions, and ϵ_{ref} and ϵ_s are the relative permittivities of the reference solvent (used to measure oxidation and reduction potentials) and the solvent in which the measurements are performed.

From the Weller equation, it can be seen that the charge separated state will be stabilized (more negative ΔE_{CS}) by polar solvents (solvents having a high ϵ). Therefore, in many of the oligomer systems described in this thesis, charge transfer takes place in *o*-dichlorobenzene (ODCB, $\epsilon_r = 10.1$), whereas triplet energy transfer is observed in toluene ($\epsilon_r = 2.4$)

1.5 Aim and scope of this thesis

In the recent past, many new small band gap polymers have appeared in literature. Although there are some general guidelines for the design of these polymers, detailed studies on the influence of the molecular structure on the band gaps and energy levels in these polymers are scarce. In this respect, detailed understanding of the optical and electrochemical properties of short oligomers of small band gap polymers may help developing design rules for new materials. Furthermore, knowledge about the processes limiting the performance of organic solar cells is needed for future device improvement. Therefore, the aim of this thesis is to gain more insight into the electronic properties of small band gap materials and the processes involved in charge separation and recombination in solar cells utilizing these materials. This is achieved by detailed studies, both experimental and theoretical, on oligomeric model compounds.

Chapter 2 deals with a study on the influence of the type of acceptor, used in donor-acceptor oligomers, on the optical and electrochemical properties. The main

focus here, is on band gaps, HOMO and LUMO levels, and the energy of the first excited triplet state. The latter is important, because charge recombination into a triplet state might be important as a loss mechanism in polymer solar cells.

Chapters 3, 4 and 5 deal with different series of small band gap oligomers, based on the thieno[3,4-*b*]pyrazine acceptor unit. Experimental and theoretical studies on the chain length dependence of the band gap and the HOMO and LUMO levels in the different series are performed. This approach yields insight into the cause of the band gap reduction in oligomers and polymers using this specific type of acceptor.

Chapters 6 and 7 are concerned with charge separation and recombination processes. Triads were synthesized, consisting of a small band gap oligomer unit end capped with C₆₀ (acceptor) units. Charge and energy transfer processes in these triads were studied by different spectroscopic techniques. The processes studied serve as models for the charge separation and recombination processes found in BHJ solar cells, consisting of blends of a small band gap polymer with a fullerenes.

Finally, chapter 8 describes the performance of some oligomers, having low lying LUMO levels, as acceptor materials in solar cells. As virtually all efficient solar cells to date use fullerenes as the electron accepting phase, it might be useful to find alternatives. Some of the oligomers described in this thesis might serve this purpose and their behavior in solar cells, when combined with P3HT, is explored.

References and notes

1. Meadows, D. H.; Meadows, D. L.; Randers, J.; Behrens, W. W. *The Limits to Growth*; Universe Books: New York, 1972.
2. World Commission on Environment and Development *Our Common Future*; Oxford University Press: Oxford, 1987.
3. Solomon, S.; Qin, D.; Manning, M.; Chen, Z.; Marquis, M.; Averyt, K. B.; Tignor, M.; Miller, H. L. *Climate Change 2007: The Physical Science Basis*; Cambridge University Press: Cambridge, 2007.
4. Metz, B.; Davidson, O. R.; Bosch, P. R.; Dave, R.; Meyer, L. A. *Climate Change 2007: Mitigation of Climate Change*; Cambridge University Press: Cambridge, 2007.
5. Chapin, D. M.; Fuller, C. S.; Pearson, G. L. *J. Appl. Phys.* **1954**, *25*, 676–677.
6. Green, M. A.; Emery, K.; Hishikawa, Y.; Warta, W. *Prog. Photovolt. Res. Appl.* **2009**, *17*, 320–326.
7. Guter, W.; Schöne, J.; Philipps, S. P.; Steiner, M.; Siefer, G.; Wekkeli, A.; Welsch, E.; Oliva, E.; Bett, A. W.; Dimroth, F. *Appl. Phys. Lett.* **2009**, *94*, 223504.
8. Tang, C. W. *Appl. Phys. Lett.* **1986**, *48*, 183–185.
9. It is also possible to form an exciton in the acceptor material. After diffusion of the exciton to the donor–acceptor interface, the electron and hole are then separated by hole transfer to the donor material.
10. O'Regan, B.; Grätzel, M. *Nature* **1991**, *353*, 737–740.

11. Nazeeruddin, M. K.; De Angelis, F.; Fantacci, S.; Selloni, A.; Viscardi, G.; Liska, P.; Ito, S.; Takeru, B.; Grätzel, M. *J. Am. Chem. Soc.* **2005**, *127*, 16835–16847.
12. Halls, J. J. M.; Pichler, K.; Friend, R. H.; Moratti, S. C.; Holmes, A. B. *Appl. Phys. Lett.* **1996**, *68*, 3120–3122.
13. Haugeneder, A.; Neges, M.; Kallinger, C.; Spirkl, W.; Lemmer, U.; Feldmann, J.; Scherf, U.; Harth, E.; Gugel, A.; Müllen, K. *Phys. Rev. B* **1999**, *59*, 15346–15351.
14. Markov, D. E.; Hummelen, J. C.; Blom, P. W. M.; Sieval, A. B. *Phys. Rev. B* **2005**, *72*, 045216.
15. Markov, D. E.; Amsterdam, E.; Blom, P. W. M.; Sieval, A. B.; Hummelen, J. C. *J. Phys. Chem. A* **2005**, *109*, 5266–5274.
16. Yu, G.; Gao, J.; Hummelen, J. C.; Wudl, F.; Heeger, A. J. *Science* **1995**, *270*, 1789–1791.
17. Scharber, M. C.; Mühlbacher, D.; Koppe, M.; Denk, P.; Waldauf, C.; Heeger, A. J.; Brabec, C. L. *Adv. Mater.* **2006**, *18*, 789–794.
18. Roncali, J. *Chem. Rev.* **1997**, *97*, 173–205.
19. Van Mullekom, H. A. M.; Vekemans, J. A. J. M.; Havinga, E. E.; Meijer, E. W. *Mat. Sci. Eng. R.* **2001**, *32*, 1–40.
20. Kertesz, M.; Choi, C. H.; Yang, S. J. *Chem. Rev.* **2005**, *105*, 3448–3481.
21. Rasmussen, S. C.; Pomerantz, M. *Handbook of Conducting Polymers*, 3rd ed.; CRC Press: Boca Raton, FL, 2007.
22. Wudl, F.; Kobayashi, M.; Heeger, A. J. *J. Org. Chem.* **1984**, *49*, 3382–3384.
23. Kobayashi, M.; Colaneri, N.; Boysel, M.; Wudl, F.; Heeger, A. J. *J. Chem. Phys.* **1985**, *82*, 5717–5723.
24. Pomerantz, M.; Chaloner-Gill, B.; Harding, L. O.; Tseng, J. J.; Pomerantz, W. J. *J. Chem. Soc. Chem. Commun.* **1992**, 1672–1673.
25. Nietfeld, J. P.; Heth, C. L.; Rasmussen, S. C. *Chem. Commun.* **2008**, 981–983.
26. Wen, L.; Duck, B. C.; Dastoor, P. C.; Rasmussen, S. C. *Macromolecules* **2008**, *41*, 4576–4578.
27. Havinga, E. E.; Ten Hoeve, W.; Wynberg, H. *Polym. Bull.* **1992**, *29*, 119–126.
28. Havinga, E. E.; Ten Hoeve, W.; Wynberg, H. *Synth. Met.* **1993**, *55*, 299–306.
29. Kitamura, C.; Tanaka, S.; Yamashita, Y. *Chem. Mater.* **1996**, *8*, 570–578.
30. Park, S. H.; Roy, A.; Beaupré, S.; Cho, S.; Coates, N.; Moon, J. S.; Moses, D.; Leclerc, M.; Lee, K.; Heeger, A. J. *Nat. Photonics* **2009**, *3*, 297–303.
31. Liang, Y.; Feng, D.; Wu, Y.; Tsai, S. T.; Li, G.; Ray, C.; Yu, L. *J. Am. Chem. Soc.* **2009**, *131*, 7792–7799.

32. Liang, Y.; Xu, Z.; Xia, J.; Tsai, S. T.; Wu, Y.; Li, G.; Ray, C.; Yu, L. *Adv. Mater.* **2010**, E135–E138.
33. Bockris, J. O.; Khan, S. U. M. *Surface Electrochemistry: A Molecular Level Approach*; Kluwer Academic/Plenum Publishers: New York, 1993.
34. Pavlishchuk, V. V.; Addison, A. W. *Inorg. Chim. Acta* **2000**, 298, 97–102.
35. Monkman, A. P.; Burrows, H. D.; Hartwell, L. J.; Horsburgh, L. E.; Hamblett, I.; Navaratnam, S. *Phys. Rev. Lett.* **2001**, 86, 1358–1361.
36. Köhler, A.; Beljonne, D. *Adv. Funct. Mater.* **2004**, 14, 11–18.
37. Cornil, J.; Beljonne, D.; Brédas, J. L. *J. Chem. Phys.* **1995**, 103, 834–841.
38. Cornil, J.; Beljonne, D.; Brédas, J. L. *J. Chem. Phys.* **1995**, 103, 842–849.
39. Williams, R. M.; Zwier, J. M.; Verhoeven, J. W. *J. Am. Chem. Soc.* **1995**, 117, 4093–4099.
40. Weller, A. Z. *Phys. Chem. Neue Folge* **1982**, 133, 93–98.

Chapter 2

Electronic structure of small band gap oligomers based on cyclopentadithiophenes and acceptor units

Abstract In this chapter, a combined experimental and theoretical study is presented on a series of well-defined small band gap oligomers. These oligomers comprise two terminal electron-rich cyclopentadithiophene units connected to six different electron deficient aromatic rings that allow tuning the optical band gap from 1.4 to 2.0 eV. Optical absorptions of the ground state, triplet excited state, and radical cation have been investigated. The optical band gaps correlate with the electrochemical oxidation and reduction potentials and are further supported by quantum-chemical calculations at the density functional theory (DFT) level. The optical absorptions of the radical cations show only little variations among the different oligomers, suggesting that the charge is mainly localized on the donor moieties. Triplet energy levels are generally low (<1.2 eV) and the singlet–triplet splitting remains significant when going to smaller band gaps.

This work has been published: Karsten, B. P.; Bijleveld, J. C.; Viani, L.; Cornil, J.; Gierschner, J.; Janssen, R. A. J. *J. Mater. Chem.* **2009**, *19*, 5343–5350.

2.1 Introduction

Detailed understanding of the electrochemical and optical properties of short oligomers of small band gap polymers will help gain valuable insight into the design rules for new materials and into the processes limiting the efficiency of polymer solar cells. In chapters 3, 4 and 5, we demonstrate that in thiophene–thieno[3,4-*b*]pyrazine based small band gap oligomers, the number of acceptor units in the oligomer is a crucial factor that outweighs the importance of extended alternating donor–acceptor conjugation in determining the optical gap. The successful design of new polymers with optimized properties for solar energy conversion will not merely depend on the band gap and HOMO and LUMO levels, but also the triplet energy level. It has been shown that recombination of photogenerated charges into a low-lying triplet state may occur when the energy of the triplet state is below that of the charge transfer state.^{1,2} In fact, triplet recombination might be an important loss mechanism.³ So far, however, very little is known about the exchange energy and the triplet energy level in small band gap polymers, and whether it scales differently with singlet excited state energy than in traditional conjugated polymers.^{4,5} In this chapter the influence of the nature of the acceptor unit on the optical and electrochemical properties of oligomeric small band gap systems is investigated. Oligomers consisting of two cyclopentadithiophene units and six different acceptor units have been synthesized. Their optical absorption spectra, oxidation and reduction potentials, triplet absorptions and triplet energy levels, and corresponding radical cations were investigated in detail. The results are rationalized by density functional theory (DFT) calculations. Clear correlations between the nature of the acceptor and the band gap and the HOMO and LUMO levels have been found. The energy of the triplet excited state of the systems under study has been found to be lower than 1.2 eV.

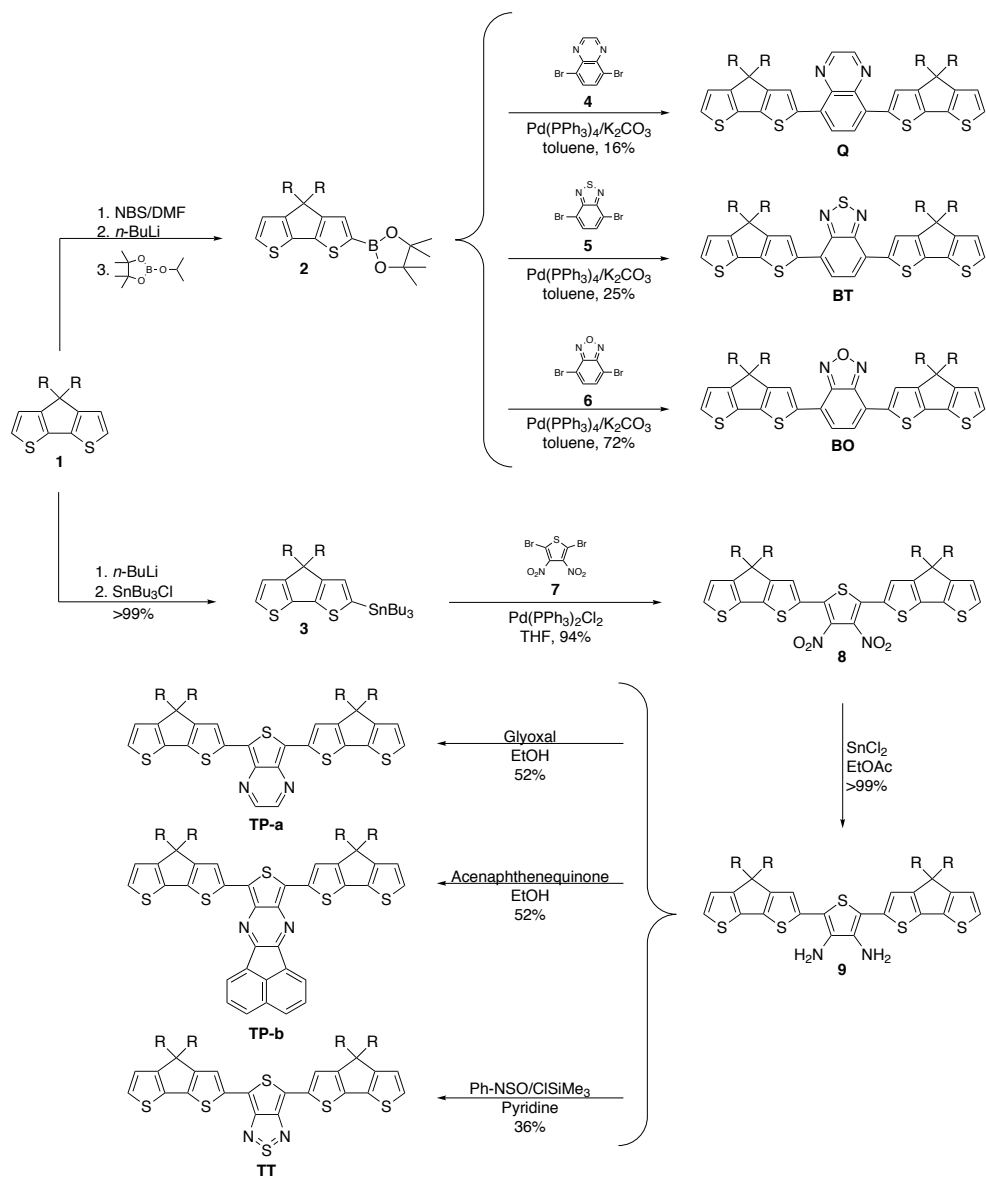
2.2 Results and discussion

2.2.1 Synthesis

The oligomers were synthesized according to scheme 2.1. 4,4-Bis(2-ethylhexyl)-cyclopentadithiophene (CPDT, **1**) was transformed into its boronic ester **2** and tributylstannyl derivative **3**. Oligomers with a benzene-based acceptor (quinoxaline (**Q**), benzothiadiazole (**BT**) and benzoxadiazole (**BO**)) were then prepared by Suzuki coupling of boronic ester **2** with the dibromo-derivative of the acceptor. Tributylstannyl derivative **3** was reacted with 2,5-dibromo-3,4-dinitrothiophene (**7**) and the nitro groups were reduced with tin(II) chloride, to give diamine **9**. The oligomers with a thiophene-based acceptor (thienopyrazine (**TP-a**), acenaphthothienopyrazine (**TP-b**) and thienothiadiazole (**TT**)) were formed by reaction of **9** with a diketone to give **TP-a** and **TP-b**, or with *N*-thionylaniline to give **TT**. All oligomers were characterized by NMR, IR, and MALDI-TOF mass spectrometry.

2.2.2 Electrochemical and optical properties

The redox properties of the oligomers were investigated by cyclic voltammetry (figure 2.1a). The onsets of oxidation (E_{ox}) and reduction (E_{red}) waves determined from



Scheme 2.1: Synthesis of the oligomers, R = 2-ethylhexyl.

the voltammograms and the electrochemical band gap (E_g^{CV}), defined as their difference, are summarized in table 2.1. From these data it can be seen that the nature of the central unit has a major effect on the oxidation and reduction potentials. Changing the acceptor system from a benzene-based (**Q**, **BT** and **BO**) to a thiophene-based (**TP-a**, **TP-b** and **TT**) central unit significantly lowers the oxidation potential. This implies that the HOMO levels of the latter systems are higher in energy, which gives rise to lower open circuit voltages in solar cells, made of polymers using thienopyrazine and thienothiadiazole. The potential difference between the first and second oxidation waves for **Q**, **BT**, and **BO** is ~ 200 mV and significantly less than the ~ 300 mV splitting for **TP-a**, **TP-b** and **TT**. This indicates that the Coulomb interaction between the two positive charges is stronger for the thiophene based systems and signifies the stronger conjugation of the two CPDT units *via* the central unit in this case. At the same time the oligomers with a thiophene-based central unit (**TP-a**, **TP-b**, and **TT**) also have a lower (*i.e.* less negative) reduction potential. This is most clear by comparing the reduction potentials of **Q** and **TP-a** that both have a pyrazine ring or comparing **BT** and **TT** that both have a thiadiazole ring.

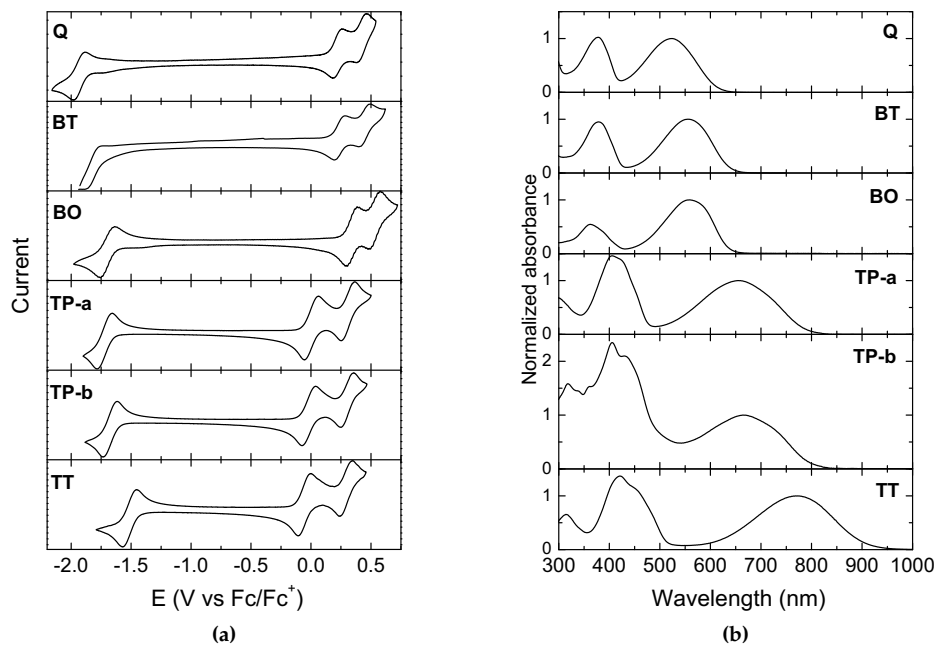


Figure 2.1: Cyclic voltammograms of the oligomers in dichloromethane (a) and normalized UV/vis absorption spectra of the oligomers in toluene (b).

In this series of oligomers, **BO** deviates from the other systems with a benzene-based acceptor by its relatively high oxidation potential. Although the band gap is almost equal to **BT**, the redox potentials are raised by almost 0.1 V, making benzoxadiazole an attractive alternative to the commonly used benzothiadiazole for use in small band gap polymer solar cells, because of the expected higher open-circuit voltages.

Table 2.1: Experimental optical and electrochemical (*vs.* Fc/Fc⁺) data for the oligomers.

Oligomer	E_g^{opt} (eV)	E_{max}^{opt} (eV)	E_{ox} (V)	E_{red} (V)	E_g^{CV} (eV)	$T_n \leftarrow T_1$ (eV)	$D_1 \leftarrow D_0$ (eV)	$D_2 \leftarrow D_0$ (eV)	E_T (eV)	ΔE_{ST} (eV)	
Q	2.02	2.37	0.15	-1.86	2.01	1.72	1.88	0.80	1.45	0.93–1.14	1.0
BT	1.95	2.24	0.18	-1.73	1.91	1.74	1.90	0.82	1.40	1.14	0.8
BO	1.95	2.21	0.26	-1.63	1.89	1.82	1.98	0.81	1.33	1.14	0.8
TP-a	1.57	1.89	-0.07	-1.64	1.57	1.92	2.29	1.02	1.35	0.93	0.6
TP-b	1.55	1.86	-0.10	-1.60	1.50	2.22	1.04	1.36	0.93	0.6	
TT	1.37	1.61	-0.13	-1.44	1.31		0.77	1.32	<0.9	>0.5	

The UV/vis absorption spectra of the oligomers in toluene are depicted in figure 2.1b. The optical band gap E_g^{opt} (calculated from the absorption onset) and electrochemical band gap (E_g^{CV}) are virtually identical (table 2.1), the maximum difference being 0.06 eV, within experimental error. The onset of absorption shifts from 2.02 eV for **Q** to 1.95 eV for **BT** and **BO**. Replacing the benzene ring for a thiophene ring in the central unit, like in the thienopyrazine (**TP-a**) and thienothiadiazole (**TT**) oligomers, causes a significant red shift. Extension of the parent thienopyrazine ring by fusion with naphthalene (**TP-b**) does not have a pronounced effect on the optical band gap, which is reduced by only 0.02 eV going from **TP-a** to **TP-b**. The naphthalene unit does create an enhanced absorption in the 400–500 nm region. Overall the band gap of the CPDT based oligomers presented here can be controlled over a 0.65 eV range by changing the central unit.

2.2.3 Triplet excited states and their energies

Triplet–triplet absorptions were investigated by near steady-state photoinduced absorption (PIA). Because formation of the triplet states of these oligomers by direct $S_1 \leftarrow S_0$ excitation, followed by intersystem crossing to T_1 was not successful, triplet states were populated by using [6,6]-phenyl-C₆₁-butyric acid methyl ester (PCBM) as a triplet sensitizer. In this experiment PCBM is excited by the laser and forms the triplet excited state with a quantum yield of about unity. The triplet energy can then be transferred to the oligomer, yielding the T_1 state of the oligomer and the S_0 ground state of PCBM, provided that the triplet energy of the oligomer is lower than that of PCBM. PIA spectra recorded for the oligomers in toluene in the presence of PCBM are depicted in figure 2.2.

For the oligomers with benzene-based acceptors, strong PIA signals are obtained, showing a $T_n \leftarrow T_1$ absorption band at 1.72–1.92 eV and one or two vibronic peaks at higher energy. In addition, a number of weaker absorptions, extending to below 1 eV are present, showing that the dominant $T_n \leftarrow T_1$ absorption does not correspond to the lowest excited triplet state. The thiophene-based systems, which have smaller band gaps, show only very weak triplet absorptions. This is probably related to the reduced lifetime of the triplet excited states in these oligomers, because the triplet states are actually formed, evidenced by the almost complete quenching of the PCBM triplet (inset in figure 2.2b). The spectra of **TP-a** and **TP-b** show two absorption peaks (one of which probably overlaps with the PCBM signal in case

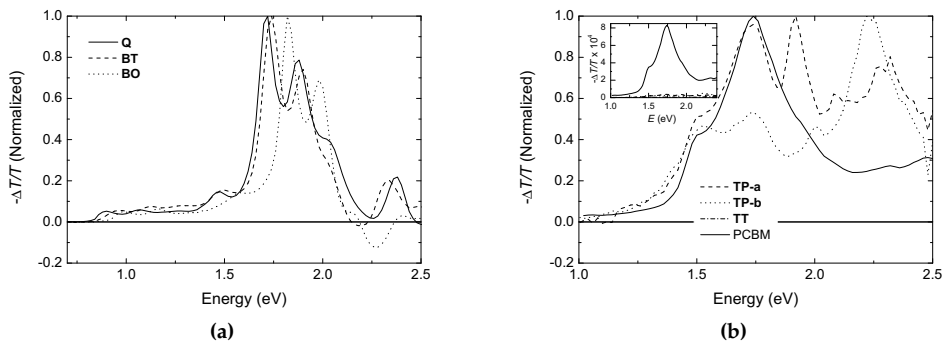


Figure 2.2: Normalized PIA spectra of the oligomers (0.1 mM) in toluene in the presence of PCBM (0.4 mM): benzene-based acceptors (a) and thiophene-based acceptors (b). As a reference, the normalized PIA spectrum of PCBM is also shown in panel b. The inset in panel b shows the unnormalized spectra, illustrating the quenching of the PCBM triplet.

of **TP-b**), located at higher energy than for the benzene-based acceptor systems. For **TT**, no triplet absorptions are observed at all, although the PCBM triplet is quenched completely, indicating triplet energy transfer to the oligomer.

To estimate the energy levels of the triplet excited states (E_T), quenching experiments have been performed. In these experiments, reference compounds with known triplet energy levels are added to the mixture. Depending on the relative triplet energies of the oligomer and reference compound, the triplet state of the oligomer is preserved or quenched. In the latter case the triplet of the reference will be detected. Figure 2.3a shows the partial quenching of the **BO** triplet by rubrene ($E_T = 1.14$ eV)⁶ and the simultaneous formation of the rubrene signal at 2.48 eV. The fact that triplet absorptions of both compounds are visible at the same time indicates that both triplet states have very similar energies. The same experiment for **BT** gives a similar graph, for **Q** no quenching of the triplet signatures or appearance of the rubrene triplet absorption were observed. This leads to the conclusion that both **BT** and **BO** have $E_T \sim 1.14$ eV, while the triplet energy of **Q** is less than 1.14 eV. Quenching experiments of bis(trihexylsiloxy)silicon-2,3-naphthalocyanine ($E_T \sim 0.93$ eV)⁷ with all oligomers result in the spectra shown in figure 2.3b. As expected **BT** and **BO** do not quench the naphthalocyanine triplet absorption, as their triplet energies of around 1.14 eV are well above the triplet energy of the naphthalocyanine. With **Q**, also no quenching of the naphthalocyanine triplet is observed, leading to the conclusion that the triplet energy of **Q** is higher than 0.93 eV. The thienopyrazines (**TP-a** and **TP-b**) partially quench the naphthalocyanine triplet, indicating that their triplet levels are located at about the same energy as the triplet level of naphthalocyanine (0.93 eV). **TT** quenches the naphthalocyanine somewhat more than the thienopyrazines, therefore its triplet level is estimated to be less than 0.9 eV.

The estimated triplet energy levels (E_T) are summarized in table 2.1 together with the singlet–triplet splitting energy (ΔE_{ST}) calculated using the optical band gaps ($\Delta E_{ST} = E_g^{opt} - E_T$). Bearing the experimental uncertainties in mind, there is a trend towards a reduced exchange energy with decreasing band gap.

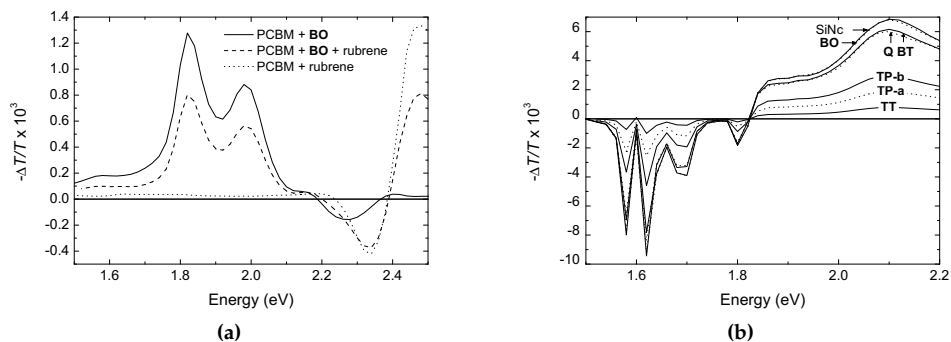


Figure 2.3: Partial quenching of the BO triplet and formation of the rubrene triplet (a) and partial quenching of the bis(trihexylsiloxy)silicon 2,3-naphthalocyanine (SiNc) triplet by the oligomers containing thiophene based acceptors, the benzene based acceptors show no quenching (b).

2.2.4 Radical cations

Chemical oxidation of the oligomers was performed by adding a solution of thianthrenium hexafluorophosphate⁸ to a solution of the oligomers in dichloromethane in small aliquots. UV/vis/NIR absorption spectra were obtained. The spectra for BO are shown in figure 2.4a, the other oligomers gave similar spectra.

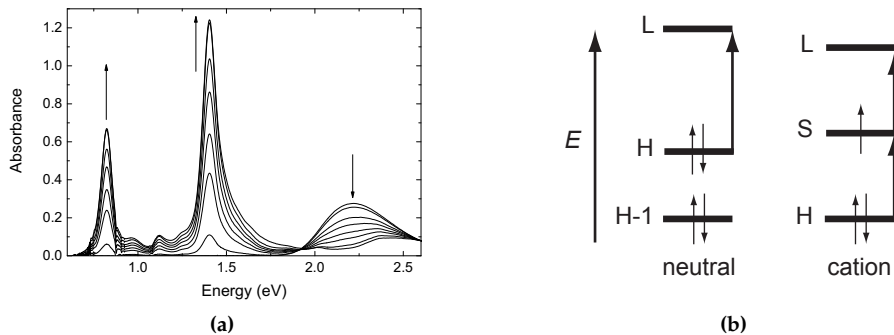


Figure 2.4: (a) Chemical oxidation of BO with thianthrenium hexafluorophosphate in dichloromethane. The appearance and disappearance of bands is shown with arrows. (b) Schematic orbital diagram for the main dipole-allowed transitions of the neutral oligomer and the radical cation, H = HOMO, S = SOMO and L = LUMO.

Upon addition of thianthrenium hexafluorophosphate, the absorption band of the neutral oligomer disappears and two new bands at lower energy appear. These bands are attributed to the dipole-allowed $D_1 \leftarrow D_0$ and $D_2 \leftarrow D_0$ transitions of the doublet-state radical cation that, in first approximation, correspond to electron excitations from $HOMO \rightarrow SOMO$ (singly occupied molecular orbital) and $SOMO \rightarrow LUMO$ (see figure 2.4b). The energy maxima of these absorptions are summarized in table 2.1. The position of these maxima does not show great variation upon changing the acceptor strength, with a $D_1 \leftarrow D_0$ transition around 0.8 eV (the only exception

being the thienopyrazines, which have this transition at about 1 eV) and a $D_2 \leftarrow D_0$ transition around 1.3–1.4 eV. This limited variation points to a localization of the excitations on the donor units of the oligomers, instead of a strong charge-transfer character of the absorption, as is observed when exciting the neutral oligomers.

2.2.5 Quantum-chemical calculations*

The evolution of the electronic and optical properties of the oligomers upon variation of the acceptor unit has also been characterized at the theoretical level in order to provide a deeper insight into the experimental data. We have optimized the ground-state geometry of the six oligomers at the DFT level using the standard B3LYP functional and a 6–31G (d,p) basis set using the Gaussian 2003 package.⁹ The alkyl substituents have been replaced by hydrogen atoms and planarity has been imposed on the conjugated backbone. The geometry in the lowest triplet excited state has been optimized at the same level of theory, as motivated by the reliable triplet energies provided by this approach.¹⁰ The energy of the vertical $S_1 \leftarrow S_0$ transition, to be compared to the experimental E_{max}^{opt} values, has been obtained by coupling the DFT approach to a time-dependent (TD) formalism; the energy of the fully relaxed S_1 state has been inferred by subtracting from the vertical transition energy the reorganization energy in the excited state; the latter is directly accessible from the experimental data as the energy difference between E_{max}^{opt} and E_g^{opt} ($E_{reorg} = E_{max}^{opt} - E_g^{opt}$). A summary of the theoretical data is given in table 2.2.

Table 2.2: Calculated HOMO/LUMO energies, distribution of these orbitals over the donor (D) and acceptor (A) parts calculated from the LCAO (linear combination of atomic orbitals) coefficients, $S_1 \leftarrow S_0$ and $T_n \leftarrow T_1$ transition energies, energies of the lowest triplet state in the fully relaxed geometry (E_T), and energy difference between the lowest fully relaxed singlet versus triplet excited states (ΔE_{ST}).

Oligomer	HOMO (eV)	LUMO (eV)	Distribution HOMO		Distribution LUMO		E_{max}		E_T (eV)	ΔE_{ST} (eV)
			D (%)	A (%)	D (%)	A (%)	$S_1 \leftarrow S_0$ (eV)	$T_n \leftarrow T_1$ (eV)		
Q	-4.69	-2.34	80	20	33	67	2.06	1.96	1.23	0.48
BT	-4.74	-2.68	78	22	34	66	1.90	2.05	0.93	0.68
BO	-4.84	-2.64	79	21	35	65	1.99	2.08	1.02	0.72
TP-a	-4.48	-2.61	71	29	32	68	1.66	2.00	0.66	0.68
TP-b	-4.40	-2.50	68	32	30	70	1.66	2.15	0.75	0.60
TT	-4.40	-2.93	69	31	27	73	1.34	2.35	0.31	0.79

The $S_1 \leftarrow S_0$ transition is mostly described for all oligomers by a HOMO to LUMO one-electron excitation. The calculated and experimental values of the vertical transition energies (E_{max}) are plotted in figure 2.5a. The experimental evolution is reproduced very well, though the TD-DFT values underestimate E_{max} by about 0.3 eV.¹¹ There is a drop in the lowest optical transition energy by 0.72 eV going from **Q** to **TT**, in full consistency with the experimental value of 0.65 eV. The calculated HOMO

*The calculations were performed by L. Viani at the university of Mons–Hainaut.

and LUMO levels are depicted in figure 2.5b together with the corresponding experimental oxidation and reduction potentials. This graph shows that the general experimental trends are once again reproduced very well. In particular, the calculations confirm that there is a marked increase in the HOMO energy when changing the acceptor from a benzene-based to a thiophene-based unit and that **BO** has the highest ionization potential. The results also rationalize the reduction of the band gap with the increase of the acceptor strength (**BT** and **BO** vs. **Q**, **TP-a** vs. **TP-b**), mainly due to stabilization of the LUMO. No conclusions can be made about the exact offsets between the calculated and experimental HOMO and LUMO levels, as the potential of Fc/Fc^+ vs. vacuum is set arbitrarily in figure 2.5b.

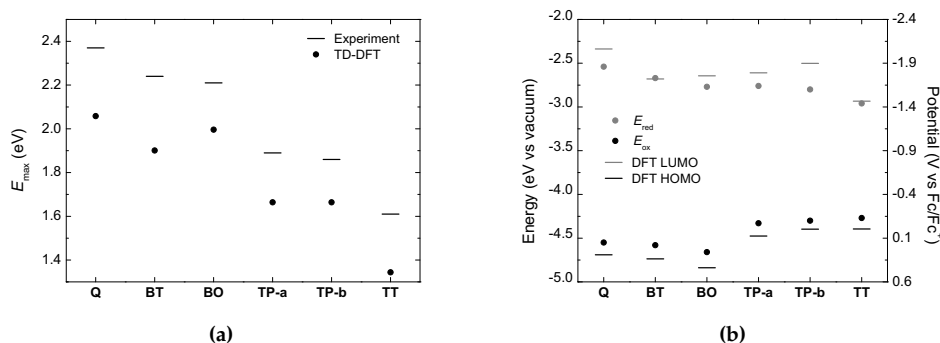


Figure 2.5: Theoretical and experimental vertical transition energies (a) and calculated frontier orbital energies and measured redox potentials (b). Values calculated at the DFT level are depicted as horizontal bars and experimental values by dots.

Table 2.2 shows that in the oligomers with a thiophene-based acceptor (**TP-a**, **TP-b**, **TT**), the HOMO is more or less delocalized evenly over the entire molecule since the distribution over the donor and acceptor units is close to the statistical expectation of $\sim 70\%$ and $\sim 30\%$, respectively, which follows from simply counting the sp^2 hybridized atoms on the donor and acceptor parts (neglecting the naphthalene unit in **TP-b** which does not affect the band gap according to table 2.1). For the oligomers containing a benzene-based acceptor, the HOMO gets localized in a more pronounced way on the donor units. The larger delocalization in the thiophene-based acceptors is consistent with the higher HOMO levels calculated and measured for these systems. Table 2.2 further indicates that the LUMO is located mostly on the acceptor unit for all oligomers (by 68% on average). Among the various molecules, the differences between the distribution of the LUMO level are less pronounced than for the HOMO level, although the LUMO becomes somewhat more confined on the acceptor unit for the strongest acceptor (**TT**).

The calculated triplet $T_n \leftarrow T_1$ absorption energies are fairly close to the experimental values while a larger discrepancy is observed for the lowest triplet energies (E_T) (figure 2.6a). The latter can be attributed in part to the experimental uncertainties in determining the triplet energy levels by quenching experiments though this cannot reconcile all differences between experiment and theory, in particular the relative order of **Q** and **BT**. The experimentally determined triplet energies are in a quite narrow range (0.9–1.14 eV) while the calculated values show a much stronger

variation with the choice of the acceptor. The calculated value for the triplet energy of the thienothiadiazole oligomer of 0.3 eV is very low for an electronically excited state; we stress, however, that the experimental value of 0.9 eV can only be considered as an upper limit in this case.

The calculated singlet–triplet energy splittings $\Delta E_{ST} = E_{max} - E_{reorg} - E_T$ are compared to the experimental values in figure 2.6b. While the experimentally determined ΔE_{ST} shows a clear decrease with increasing acceptor strength, the calculated values do not show a clear trend and changes are sometimes opposite to the experimental observations. Similarly, large ΔE_{ST} values (between 0.6 and 0.8 eV) are obtained at both the theoretical and experimental levels for **BT**, **BO**, **TP-a**, and **TP-b**. A larger discrepancy is observed for **Q** while the comparison for **TT** is hampered by the uncertainty in the experimental E_T value.

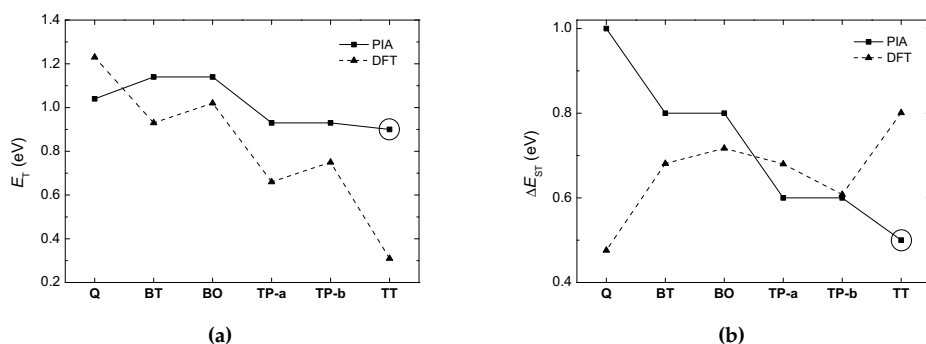


Figure 2.6: Experimental and calculated triplet energies E_T (a) and singlet–triplet energy splitting ΔE_{ST} (b). The experimental value of E_T for **TT** (circled entries) is an upper limit, so that the corresponding ΔE_{ST} is a lower limit.

ΔE_{ST} reflects the exchange energy, which at first approximation is determined by the extent to which the HOMO and LUMO levels share the same regions of space. Naively, one might expect that by introducing stronger acceptor units, the exchange energy is reduced because the LUMO would get more strongly confined on the acceptor and the HOMO on the donor. In fact, this expectation seems to coincide with the experimental trend for ΔE_{ST} shown in figure 2.6b. However, by inspecting the contributions of the donor and acceptor units over the frontier orbitals (table 2.2), there is fairly little variation among the oligomers. The calculated values do not show any appreciable trend, strongly suggesting that changes in ΔE_{ST} are determined by more subtle effects that go beyond the simple rationale mentioned above. In fact, the molecule with the strongest acceptor (**TT**) is predicted to have the largest ΔE_{ST} value.

2.3 Conclusions

Oligomers consisting of two cyclopentadithiophene units and six different electron-deficient aromatic ring systems have been prepared. The influence of the acceptor on the optical and electrochemical properties has been investigated both experimen-

tally and theoretically on the basis of density functional theory calculations. The experimental values for optical and electrochemical band gaps are almost similar and fully supported by (TD-)DFT calculations that show a similar evolution of the lowest singlet transition energy compared to experiments and a good correlation between the calculated energies of the frontier electronic levels and the experimental redox potentials.

The optical band gap of the oligomers changes from 1.4 to 2 eV depending on the acceptor as a consequence of substantial changes in both the oxidation and reduction potentials, because the HOMO is delocalized over the entire molecule while the LUMO is mainly localized on the acceptor. The optical absorption spectra of the radical cations of the oligomers show little variation when changing the acceptors, suggesting that the electronic structures are dominated by the cyclopentadithiophene units. Triplet energies have been determined from near steady-state PIA experiments using triplet quenchers. Experimentally estimated values lead to triplet energies that are relatively constant, between <0.9 and 1.14 eV. DFT predicts much larger variations from 1.23 eV for **Q**, going down to a value as low as 0.66 eV for **TP-a**, and 0.31 eV for **TT**. The low triplet energies might cause charge recombination into a triplet state to become an important loss mechanism in the application of small band gap materials in organic solar cells. Predicting or rationally controlling the exchange energy in these small band gap systems by simple arguments is presently not possible.

2.4 Experimental

General methods $^1\text{H-NMR}$ and $^{13}\text{C-NMR}$ spectra were recorded in CDCl_3 on a 400 MHz NMR (Varian Mercury, 400 MHz for $^1\text{H-NMR}$ and 100 MHz for $^{13}\text{C-NMR}$), chemical shifts are reported in ppm downfield from tetramethylsilane (TMS). IR spectra were recorded on a Perkin Elmer 1600 FT-IR. Matrix-assisted laser desorption ionization time-of-flight (MALDI-TOF) mass spectrometry was performed on a PerSeptive Biosystems Voyager-DE PRO spectrometer. Recycling GPC was performed on a LC system equipped with JAIGEL 2H and JAIGEL 2.5H columns and a UV-detector, using a preparative flow cell (path length 0.5 mm). The eluent was chloroform at 3.5 mL/min, the injection volume was 2 mL. UV/vis spectra were recorded on a Perkin Elmer Lambda 900 UV/vis/NIR spectrometer. Cyclic voltammograms were recorded in an inert atmosphere with 0.1 M tetrabutyl ammonium hexafluorophosphate (TBAPF_6) in dichloromethane as supporting electrolyte. The working electrode was a platinum disc (0.2 cm^2) and the counter electrode was a silver electrode. The samples were measured using an Ag/AgCl reference electrode with Fc/Fc^+ as an internal standard using a $\mu\text{Autolab II}$ with a PGSTAT30 potentiostat. PIA spectra were recorded by exciting with a mechanically modulated cw Ar-ion laser ($\lambda = 351$ and 364 nm, 275 Hz) pump beam and monitoring the resulting change in transmission of a tungsten-halogen probe light through the sample (ΔT) with a phase-sensitive lock-in amplifier after dispersion by a grating monochromator and detection, using Si, InGaAs, and cooled InSb detectors. The pump power incident on the sample was typically 25 mW with a beam diameter of 2 mm. The PIA ($\Delta T/T$) was corrected for the photoluminescence, which was recorded in a separate

experiment. Photoinduced absorption spectra and photoluminescence spectra were recorded with the pump beam in a direction almost parallel to the direction of the probe beam. The solutions were studied in a 1 mm near-IR grade quartz cell at room temperature.

Materials Solvents were purchased from Biosolve and used without further purification, unless stated otherwise. THF was distilled over 4 Å molsieves, pyridine was dried over 4 Å molsieves before use. Chemicals were purchased from Acros or Aldrich and used without purification. PCBM was obtained from Solenne. CPDT (**1**) and 2,5-dibromo-3,4-dinitrothiophene (**7**) were prepared following literature procedures.^{12,13} Oxygen and moisture-sensitive reactions were performed under an argon atmosphere.

(4,4,5,5-Tetramethyl-1,3,2-dioxaborolane-2-yl)-4,4-bis(2-ethylhexyl)-4H-cyclopenta[2,1-*b*:3,4-*b'*]dithiophene (2**)** This product was obtained as a by-product in the synthesis of 2,6-di-(4,4,5,5-tetramethyl-1,3,2-dioxaborolane-2-yl)-4,4-bis(2-ethylhexyl)-4H-cyclopenta[2,1-*b*:3,4-*b'*]dithiophene, following a literature procedure.¹³ The title compound was separated from the main product by recycling GPC. ¹H-NMR: δ 7.43 (m, 2H, Ar-*H*), 7.17 (m, 2H, Ar-*H*), 6.92 (m, 2H, Ar-*H*), 1.85 (m, 4H, -CH₂CH(C₂H₅)(C₄H₉)), 1.35 (s, 12H, -BO₂C₂(CH₃)₄), 0.85 (m, 18H, alkyl-*H*), 0.74 (m, 6H, -CH₃), 0.58 (m, 6H, -CH₃). ¹³C-NMR: δ 160.97, 144.07, 131.87, 83.97, 52.66, 43.20, 35.13, 33.80, 28.31, 27.43, 24.77, 22.77, 14.08, 10.57. MALDI-TOF-MS: *m/z* 527.21 (20%), 528.20 (100), 529.21 (35), 530.20 (15), 531.20 (5).

2-(Tributylstannyl)-4,4-bis(2-ethylhexyl)-4H-cyclopenta[2,1-*b*:3,4-*b'*]dithiophene (3**)** Compound **1** (215 mg, 0.53 mmol) was dissolved in THF (2 mL). At -78°C, *n*-Butyllithium (0.215 mL, 2.5 M, 0.54 mmol) was added and the mixture was stirred at -78°C for 2 h. Tributyltin chloride (0.145 mL, 0.53 mmol) was added and the mixture was stirred for 16 h, while warming to room temperature. Diethyl ether (15 mL) was added and the mixture was washed with water (3.5 mL), dried with MgSO₄ and the solvent was evaporated. Yield: 369 mg (>99%). ¹H-NMR: δ 7.05 (d, *J* = 4.8 Hz, 1H, Ar-*H*), 6.93–6.88 (m, 2H, Ar-*H*), 1.90–1.82 (m, 4H, -CH₂CH(C₂H₅)(C₄H₉)), 1.63–1.52 (m, 6H, -CH₂C₃H₇), 1.40–1.30 (m, 6H, -CH₂CH₂C₂H₅), 1.13–1.06 (m, 6H, -C₂H₄CH₂CH₃), 1.06–0.82 (m, 27H, alkyl-*H*), 0.75 (t, *J* = 6.7 Hz, 6H, -CH₃), 0.58 (t, *J* = 7.6 Hz, 6H, -CH₃)

5,8-Dibromoquinoxaline (4**)** 2,3-Diamino-1,4-dibromobenzene (2.45 g, 0.39 mmol) was dissolved in ethanol (30 mL). Glyoxal (1.5 mL, 40 wt. % solution in water) and two drops of dry triethylamine were added. The mixture was stirred at room temperature overnight. The white crystals that had formed were filtered off and recrystallized from ethanol to give white needles. Yield: 0.76 g (76%). ¹H-NMR: δ 9.01 (s, 2H, Ar-*H*), 8.00 (s, 2H, Ar-*H*). ¹³C-NMR: δ 146.03, 141.56, 133.72, 123.97.

4,7-Dibromo-2,1,3-benzothiadiazole (5**)** 2,1,3-Benzothiadiazole (10.18 g, 79.3 mmol) was dissolved in aqueous HBr (48 wt. %, 100 mL). At 150°C, bromine (12 mL, 233 mmol) was added slowly. This mixture was stirred at 150°C for 2 h and reaction

mixture was cooled to room temperature. The mixture was filtered over a Büchner funnel; solids were washed extensively with water. Solids were dissolved in diethyl ether (1 L) and the mixture was washed with water and saturated NaCl. The solvent was evaporated and the product was recrystallized from methanol to give off-white needles. Yield: 17.18 g (78 %). $^1\text{H-NMR}$: δ 7.72 (s, 2H, Ar-H) $^{13}\text{C-NMR}$: δ 152.96, 132.31, 113.87.

4,7-Dibromo-2,1,3-benzoxadiazole (6) To a melt of 2,1,3-benzoxadiazole (8.46 g, 40.4 mmol) with iron dust (93 mg, 1.6 mmol), bromine (15.2 g, 95 mmol) was added dropwise. The mixture was stirred at 90°C for 2 h and the mixture was poured into water. A solution of sodium bisulfite was added until no gas evolution was observed. Solids were filtered, impregnated on silica and purified by column chromatography on silica, using heptane as the eluent. The product was recrystallized from ethanol to give yellow crystals. Yield: 8.40 g (75 %). $^1\text{H-NMR}$: δ 7.51 (s, 2H, Ar-H). $^{13}\text{C-NMR}$: δ 149.38, 134.17, 108.70.

5,8-Di(4,4-bis(2-ethylhexyl)-4H-cyclopenta[2,1-b:3,4-b']dithiophene-2-yl)-quinoxaline (Q) To a mixture of compound 2 (36 mg, 68 μmol), 5,8-dibromoquinoxaline (4) (8 mg, 28 μmol), Aliquat 336 (one drop) and degassed aqueous 2 M K_2CO_3 (0.3 mL) in degassed toluene (3 mL), a few grains of tetrakis(triphenylphosphine)palladium were added. The mixture was stirred overnight at 120°C. Heptane (10 mL) was added and the mixture was washed with water. The product was purified by column chromatography on silica, using ethyl acetate/heptane as the eluent. Yield: 10 mg (16 %). $^1\text{H-NMR}$: δ 8.98 (s, 2H, Ar-H), 8.11 (s, 2H, Ar-H), 7.72 (s, 2H, Ar-H), 7.18 (m, 2H, Ar-H), 6.97 (m, 2H, Ar-H), 1.90 (m, 8H, $-\text{CH}_2\text{CH}(\text{C}_2\text{H}_5)(\text{C}_4\text{H}_9)$), 0.95 (m, 36H, alkyl-H), 0.76, (m, 12H, $-\text{CH}_3$), 0.64 (m, 12H, $-\text{CH}_3$). $^{13}\text{C-NMR}$: δ 157.85, 157.10, 142.81, 139.60, 137.36, 131.90, 126.28, 124.83, 122.33, 122.29, 121.50, 121.42, 53.48, 53.41, 43.25, 35.10, 35.07, 34.22, 29.68, 28.62, 28.56, 28.05, 27.41, 27.33, 22.79, 22.76, 22.68, 14.07, 10.72, 10.60. IR: $\tilde{\nu}_{\text{max}}$ (cm^{-1}) 2955, 2921, 2870, 2855, 1731, 1661, 1567, 1504, 1458, 1428, 1406, 1377, 1321, 1275, 1078, 939, 891, 861, 828, 798, 725, 708, 658. MALDI-TOF-MS: m/z 930.65 (100 %), 931.65 (70), 932.65 (40), 933.65 (15), 934.65 (5).

4,7-Di(4,4-bis(2-ethylhexyl)-4H-cyclopenta[2,1-b:3,4-b']dithiophene-2-yl)-2,1,3-benzothiadiazole (BT) This compound was prepared following the same procedure as for **Q**, using compound 2 (325 mg, 0.61 mmol) and 4,7-dibromo-2,1,3-benzothiadiazole (5) (90 mg, 0.30 mmol). Yield: 71 mg (25 %). $^1\text{H-NMR}$: δ 8.05 (m, 2H, Ar-H), 7.82 (m, 2H, Ar-H), 7.19 (m, 2H, Ar-H), 6.97 (m, 2H, Ar-H), 1.97 (m, 8H, $-\text{CH}_2\text{CH}(\text{C}_2\text{H}_5)(\text{C}_4\text{H}_9)$), 0.95 (m, 36H, alkyl-H), 0.75 (m, 12H, $-\text{CH}_3$), 0.63 (m, 12H, $-\text{CH}_3$). $^{13}\text{C-NMR}$: δ 158.55, 158.29, 152.53, 139.04, 138.73, 136.97, 126.04, 125.23, 124.15, 53.72, 43.27, 43.16, 35.16, 35.13, 34.18, 29.70, 28.63, 28.53, 27.45, 27.33, 22.77, 14.12, 14.08, 14.04, 10.76, 10.63. IR: $\tilde{\nu}_{\text{max}}$ (cm^{-1}) 2955, 2921, 2854, 1668, 1574, 1563, 1533, 1505, 1478, 1458, 1428, 1397, 1377, 1339, 1269, 1181, 1082, 885, 859, 826, 798, 708, 659. MALDI-TOF-MS: m/z 936.23 (100 %), 937.24 (70), 938.23 (45), 939.23 (20), 940.23 (5).

4,7-Di(4,4-bis(2-ethylhexyl)-4H-cyclopenta[2,1-*b*:3,4-*b'*]dithiophene-2-yl)-2,1,3-benzoxadiazole (BO) This compound was prepared following the same procedure as for **Q**, using compound **2** (32 mg, 61 μ mol) and 4,7-dibromo-2,1,3-benzoxadiazole (**6**) (8 mg, 29 μ mol). Yield: 20 mg (72%). $^1\text{H-NMR}$: δ 8.05 (s, 2H, Ar-*H*), 7.53 (s, 2H, Ar-*H*), 7.22 (m, 2H, Ar-*H*), 6.98 (m, 2H, Ar-*H*), 1.96 (m, 8H, $-\text{CH}_2\text{CH}(\text{C}_2\text{H}_5)(\text{C}_4\text{H}_9)$), 0.90 (m, 36H, alkyl-*H*), 0.75 (m, 12H, $-\text{CH}_3$), 0.63 (m, 12H, $-\text{CH}_3$). $^{13}\text{C-NMR}$: δ 159.19, 158.95, 147.86, 138.61, 137.59, 136.57, 125.89, 124.46, 124.07, 122.48, 121.88, 53.88, 43.18, 43.14, 43.05, 35.17, 34.15, 28.61, 28.50, 27.43, 27.31, 22.75, 14.05, 13.95, 13.91, 10.74, 10.60. IR: $\tilde{\nu}_{\text{max}}$ (cm^{-1}) 2956, 2921, 2855, 1668, 1591, 1531, 1459, 1425, 1407, 1378, 1326, 1261, 1188, 1113, 1079, 1015, 895, 873, 832, 799, 709, 661. MALDI-TOF-MS: m/z 920.46 (100%), 921.46 (70), 922.46 (40), 923.45 (15).

2,5-Di(4,4-bis(2-ethylhexyl)-4H-cyclopenta[2,1-*b*:3,4-*b'*]dithiophene-2-yl)-3,4-dinitrothiophene (8) Compound **3** (396 mg, 0.53 mmol) and 2,5-dibromo-3,4-dinitrothiophene (**7**) were dissolved in THF (2 mL). Bis(triphenylphosphine)palladium(II) dichloride (9 mg, 13 μ mol) was added and the mixture was stirred at 70°C for 2 h. The solvent was evaporated and the crude product was purified by flash chromatography on silica, using ethyl acetate/heptane as the eluent. Yield: 234 mg (94%). $^1\text{H-NMR}$: δ 7.24 (t, $J=1.8$ Hz, 2H, Ar-*H*), 7.31 (d, $J=4.9$ Hz, 2H, Ar-*H*), 6.98 (m, 2H, Ar-*H*), 1.99–1.86 (m, 8H, $-\text{CH}_2\text{CH}(\text{C}_2\text{H}_5)(\text{C}_4\text{H}_9)$), 1.44–1.31 (m, 4H, $-\text{CH}_2\text{CH}(\text{C}_2\text{H}_5)(\text{C}_4\text{H}_9)$), 1.10–0.82 (m, 32H, alkyl-*H*), 0.80–0.73 (m, 12H, $-\text{CH}_3$), 0.66–0.54 (m, 12H, $-\text{CH}_3$). $^{13}\text{C-NMR}$: δ 160.18, 158.41, 143.95, 135.78, 134.65, 127.87, 126.79, 126.08, 125.98, 122.50, 54.06, 43.10, 35.16, 34.27, 34.16, 28.61, 28.57, 28.27, 27.38, 27.28, 26.76, 22.79, 22.71, 17.28, 14.09, 14.04, 13.57, 10.63. IR: $\tilde{\nu}_{\text{max}}$ (cm^{-1}) 2956, 2922, 2871, 2855, 1546, 1459, 1425, 1376, 1308, 1181, 733, 709, 664. MALDI-TOF-MS: m/z 974.23 (100%), 975.23 (65), 976.23 (40), 977.22 (20), 978.22 (10).

2,5-Di(4,4-bis(2-ethylhexyl)-4H-cyclopenta[2,1-*b*:3,4-*b'*]dithiophene-2-yl)-3,4-diaminothiophene (9) Compound **8** (234 mg, 0.24 mmol) and tin(II) chloride (650 mg, 2.9 mmol) were dissolved in ethyl acetate (5 mL). The mixture was stirred at reflux for 2 h, cooled to room temperature and added to Na_2CO_3 (0.25 M, 20 mL). Dichloromethane (20 mL) was added, the mixture was stirred vigorously and filtered over celite. Phases were separated and the organic phase was washed with water (3×30 mL), dried with MgSO_4 and the solvent was evaporated. Yield: 220 mg (>99%). $^1\text{H-NMR}$: δ 7.12 (d, $J=4.8$ Hz, 2H, Ar-*H*), 6.97–6.91 (m, 4H, Ar-*H*), 3.73 (s, 4H, $-\text{NH}_2$), 1.95–1.82 (m, 8H, $-\text{CH}_2\text{CH}(\text{C}_2\text{H}_5)(\text{C}_4\text{H}_9)$), 1.41–1.22 (m, 4H, $-\text{CH}_2\text{CH}(\text{C}_2\text{H}_5)(\text{C}_4\text{H}_9)$), 1.14–0.83 (m, 32H, alkyl-*H*), 0.83–0.71 (m, 12H, $-\text{CH}_3$), 0.71–0.56 (m, 12H, $-\text{CH}_3$). $^{13}\text{C-NMR}$: δ 158.03, 157.17, 136.77, 135.76, 134.93, 133.12, 124.27, 122.29, 119.28, 111.36, 53.64, 43.21, 35.07, 35.04, 34.22, 34.19, 28.68, 28.59, 27.82, 27.33, 22.81, 22.74, 14.09, 14.06, 10.71, 10.64. IR: $\tilde{\nu}_{\text{max}}$ (cm^{-1}) 2956, 2922, 2871, 2855, 1613, 1457, 1377, 906, 732. MALDI-TOF-MS: m/z 914.37 (100%), 915.37 (65), 916.36 (45), 917.36 (20), 918.36 (5).

5,7-Di(4,4-bis(2-ethylhexyl)-4H-cyclopenta[2,1-*b*:3,4-*b'*]dithiophene-2-yl)thieno[3,4-*b*]pyrazine (TP-a) Compound **9** (110 mg, 0.12 mmol) was dissolved in

ethanol (3 mL). Glyoxal (40 %, 0.1 mL) was added and the mixture was stirred at reflux for 2 h. The solvent was evaporated and the product was purified by flash chromatography on silica, using ethyl acetate/heptane and dichloromethane/heptane as the eluents. The product was further purified by recycling GPC. Yield: 59 mg (52 %). $^1\text{H-NMR}$: δ 8.47 (s, 2H, Ar-*H*), 7.43 (m, 2H, Ar-*H*), 7.18 (m, 2H, Ar-*H*), 6.95 (m, 2H, Ar-*H*), 2.00–1.85 (m, 8H, $-\text{CH}_2\text{CH}(\text{C}_2\text{H}_5)(\text{C}_4\text{H}_9)$), 1.10–0.85 (m, 36H, alkyl-*H*), 0.80–0.58 (m, 24H, $-\text{CH}_3$). $^{13}\text{C-NMR}$: δ 158.10, 158.79, 143.70, 139.31, 139.02, 136.95, 133.74, 125.56, 125.21, 122.35, 119.44, 53.55, 43.31, 43.25, 43.16, 35.13, 34.18, 28.62, 28.55, 28.33, 27.42, 27.33, 22.82, 22.79, 22.75, 14.07, 10.73, 10.60, 10.57, 43.36. IR: $\tilde{\nu}_{\text{max}}$ (cm^{-1}) 2955, 2919, 2870, 2854, 1509, 1457, 1406, 1377, 1179, 1113, 1020, 974, 891, 852, 797, 706. MALDI-TOF-MS: m/z 936.36 (100 %), 937.36 (70), 938.36 (45), 939.35 (20), 940.35 (5).

8,10-Di(4,4-bis(2-ethylhexyl)-4H-cyclopenta[2,1-*b*:3,4-*b'*]dithiophene-2-yl)acenaphtho[1,2-*e*]thieno[3,4-*b*]pyrazine (TP-*b*) Compound **9** (110 mg, 0.12 mmol) and acenaphthenequinone (33 mg, 0.18 mmol) were dissolved in ethanol (3 mL) and the mixture was stirred at reflux for 16 h. The solvent was evaporated and the product was purified by flash chromatography on silica, using ethyl acetate/heptane and dichloromethane/heptane as the eluents. Yield: 66 mg (52 %). $^1\text{H-NMR}$: δ 8.41 (d, $J=6.9$ Hz, 2H, Ar-*H*), 8.08 (d, $J=8.2$ Hz, 2H, Ar-*H*), 7.85 (t, $J=7.4$ Hz, 2H, Ar-*H*), 7.49 (s, 2H, Ar-*H*), 7.20 (s, 2H, Ar-*H*), 6.98 (s, 2H, Ar-*H*), 2.04–1.87 (m, 8H, $-\text{CH}_2\text{CH}(\text{C}_2\text{H}_5)(\text{C}_4\text{H}_9)$), 1.10–0.85 (m, 36H, alkyl-*H*), 0.82–0.60 (m, 24H, $-\text{CH}_3$). $^{13}\text{C-NMR}$: δ 158.01, 157.60, 153.14, 139.48, 138.16, 137.64, 137.26, 134.59, 131.51, 130.04, 128.77, 128.44, 125.58, 124.94, 122.38, 121.08, 119.11, 53.49, 43.41, 43.30, 35.17, 34.26, 34.21, 29.70, 28.68, 28.62, 28.59, 27.41, 22.92, 22.88, 22.82, 22.69, 14.15, 14.12, 10.77, 10.70, 10.67. IR: $\tilde{\nu}_{\text{max}}$ (cm^{-1}) 2955, 2919, 2870, 2854, 1458, 1418, 1377, 1282, 1214, 1176, 1115, 1078, 1033, 891, 823, 798, 769, 706. MALDI-TOF-MS: m/z 1060.45 (100 %), 1061.45 (75), 1062.45 (50), 1063.45 (25), 1064.45 (10).

4,6-Di(4,4-bis(2-ethylhexyl)-4H-cyclopenta[2,1-*b*:3,4-*b'*]dithiophene-2-yl)thieno[3,4-*c*][1,2,5]thiadiazole (TT) Compound **9** (89 mg, 0.10 mmol) was dissolved in pyridine (3 mL). *N*-thionylaniline (0.03 mL, 0.26 mmol) and chlorotrimethylsilane (0.03 mL, 0.23 mmol) were added and the mixture was stirred for 16 h at 80°C. The solvent was evaporated and the mixture was purified by flash chromatography on silica, using ethyl acetate/heptane and dichloromethane/heptane as the eluents. The product was further purified by recycling GPC. Yield: 33 mg (36 %). $^1\text{H-NMR}$: δ 7.41 (t, $J=4.8$ Hz, 2H, Ar-*H*), 7.18 (d, $J=4.8$ Hz, 2H, Ar-*H*), 6.95 (m, 2H, Ar-*H*), 1.98–1.85 (m, 8H, $-\text{CH}_2\text{CH}(\text{C}_2\text{H}_5)(\text{C}_4\text{H}_9)$), 1.10–0.85 (m, 36H, alkyl-*H*), 0.79–0.58 (m, 24H, $-\text{CH}_3$). $^{13}\text{C-NMR}$: δ 159.16, 158.18, 156.29, 137.50, 136.84, 135.11, 125.33, 122.41, 118.91, 112.14, 53.67, 43.31, 43.20, 43.16, 35.17, 34.15, 28.62, 28.53, 27.39, 27.33, 22.80, 22.77, 14.07, 10.73, 10.61. IR: $\tilde{\nu}_{\text{max}}$ (cm^{-1}) 2955, 2918, 2870, 2854, 1504, 1480, 1457, 1398, 1377, 1181, 829, 797, 706. MALDI-TOF-MS: m/z 942.19 (100 %), 943.19 (70), 944.19 (50), 945.19 (20), 946.18 (10).

References and notes

1. Ford, T. A.; Avilov, I.; Beljonne, D.; Greenham, N. C. *Phys. Rev. B* **2005**, *71*, 125212.
2. Offermans, T.; Van Hal, P. A.; Meskers, S. C. J.; Koetse, M. M.; Janssen, R. A. J. *Phys. Rev. B* **2005**, *72*, 045213.
3. Ford, T. A.; Ohkita, H.; Cook, S.; Durrant, J. R.; Greenham, N. C. *Chem. Phys. Lett.* **2008**, *454*, 237–241.
4. Monkman, A. P.; Burrows, H. D.; Hartwell, L. J.; Horsburgh, L. E.; Hamblett, I.; Navaratnam, S. *Phys. Rev. Lett.* **2001**, *86*, 1358–1361.
5. Köhler, A.; Beljonne, D. *Adv. Funct. Mater.* **2004**, *14*, 11–18.
6. Herkstroeter, W. G.; Merkel, P. B. *J. Photochem.* **1981**, *16*, 331–341.
7. Firey, P. A.; Ford, W. E.; Sounik, J. R.; Kenney, M. E.; Rodgers, M. A. J. *J. Am. Chem. Soc.* **1988**, *110*, 7626–7630.
8. Shine, H. J.; Zhao, B. J.; Marx, J. N.; Ould-Ely, T.; Whitmire, K. H. *J. Org. Chem.* **2004**, *69*, 9255–9261.
9. Frisch, M. J.; Trucks, G. W.; Schlegel, H. B.; Scuseria, G. E.; Robb, M. A.; Cheeseman, J. R.; Montgomery, Jr., J. A.; Vreven, T.; Kudin, K. N.; Burant, J. C.; Millam, J. M.; Iyengar, S. S.; Tomasi, J.; Barone, V.; Mennucci, B.; Cossi, M.; Scalmani, G.; Rega, N.; Petersson, G. A.; Nakatsuji, H.; Hada, M.; Ehara, M.; Toyota, K.; Fukuda, R.; Hasegawa, J.; Ishida, M.; Nakajima, T.; Honda, Y.; Kitao, O.; Nakai, H.; Klene, M.; Li, X.; Knox, J. E.; Hratchian, H. P.; Cross, J. B.; Bakken, V.; Adamo, C.; Jaramillo, J.; Gomperts, R.; Stratmann, R. E.; Yazyev, O.; Austin, A. J.; Cammi, R.; Pomelli, C.; Ochterski, J. W.; Ayala, P. Y.; Morokuma, K.; Voth, G. A.; Salvador, P.; Dannenberg, J. J.; Zakrzewski, V. G.; Dapprich, S.; Daniels, A. D.; Strain, M. C.; Farkas, O.; Malick, D. K.; Rabuck, A. D.; Raghavachari, K.; Foresman, J. B.; Ortiz, J. V.; Cui, Q.; Baboul, A. G.; Clifford, S.; Cioslowski, J.; Stefanov, B. B.; Liu, G.; Liashenko, A.; Piskorz, P.; Komaromi, I.; Martin, R. L.; Fox, D. J.; Keith, T.; Al-Laham, M. A.; Peng, C. Y.; Nanayakkara, A.; Challacombe, M.; Gill, P. M. W.; Johnson, B.; Chen, W.; Wong, M. W.; Gonzalez, C.; and Pople, J. A.; *Gaussian 03, Revision C.02*; Gaussian, Inc., Wallingford, CT, 2004.
10. Wasserberg, D.; Marsal, P.; Meskers, S. C. J.; Janssen, R. A. J.; Beljonne, D. *J. Phys. Chem. B* **2005**, *109*, 4410–4415.
11. This is due to the inherent overestimation of long range interactions of standard functionals (without or with small HF exchange like B3LYP). This is already quite pronounced for the size of oligomers considered here, *i.e.* 5 rings, see *e.g.* Gierschner, J.; Cornil, J.; Egelhaaf, H.J. *Adv. Mater.* **2007**, *19*, 173–191. However, different oligomers can be well compared if they have a similar conjugation length as is the case here.
12. Kenning, D. D.; Mitchell, K. A.; Calhoun, T. R.; Funfar, M. R.; Sattler, D. J.; Rasmussen, S. C. *J. Org. Chem.* **2002**, *67*, 9073–9076.

13. Gaudiana, R.; Kingsborough, R.; Waller, D.; Zhu, Z.; US Patent 2007014939; 2007.

Chapter 3

Small band gap oligothieno[3,4-*b*]pyrazines

Abstract In this chapter, the synthesis and optical and electrochemical properties of thiophene end-capped oligo(2,3-alkylthieno[3,4-*b*]pyrazine)s are presented. The optical absorption rapidly shifts to lower energies with increasing chain length, caused in almost equal amounts by a rise of the HOMO and a lowering of the LUMO. The optical band gap of the polymer is estimated to be 1.13 ± 0.07 eV. Extrapolated redox potentials indicate that the polymer is a small band gap *p*-type material.

This work has been published: Karsten, B. P.; Janssen, R. A. J. *Org. Lett.* **2008**, *10*, 3513–3516.

3.1 Introduction

As described in section 1.2, various approaches for the design of small band gap polymers exist. One of these approaches is the homopolymerization of heterocyclic units that favor a quinoidal structure. Classical examples here are poly(isothianaphthene)¹⁻³ and poly(thieno[3,4-*b*]pyrazine)^{4,5} that feature very small band gaps (~ 1 eV). Theoretical calculations and IR and Raman studies have shown that the small band gaps are caused by their quinoid ground state.⁶

We are interested in considering poly(2,3-dialkylthieno[3,4-*b*]pyrazine)s for use in solar cells. Until recently, the only way to make poly(2,3-dialkylthieno[3,4-*b*]pyrazine)s in significant amounts was by oxidative polymerization using iron(III)chloride. In these polymers, residual iron is complexed to the polymers and cannot be removed.^{4,7} This ambiguity on residual doping has led to some discussion in the literature on the actual band gap of poly(2,3-alkylthieno[3,4-*b*]pyrazine)s.^{4,7} Moreover, for electrochemically polymerized poly(2,3-alkylthieno[3,4-*b*]pyrazine)s there is a rather unexpected strong dependence of the oxidation and reduction potentials of up to 0.5 V on the length of the alkyl chain.⁷ Such large differences can even change the material from electron-donating to electron-accepting in combination with a second semiconductor in a solar cell.

The synthesis of poly(2,3-dihexylthieno[3,4-*b*]pyrazine) by Grignard methathesis polymerization and of trimethylsilyl end capped oligomers of 2,3-dimethylthieno[3,4-*b*]pyrazine have recently been reported by Wen and Rasmussen.^{8,9} In this chapter, we present a series of well-defined oligothieno[3,4-*b*]pyrazines with thiophene end caps and study the electrochemistry and the optical properties of these oligomers as function of chain length. Using these oligomers we are able to resolve some of the existing questions for the corresponding polymer.

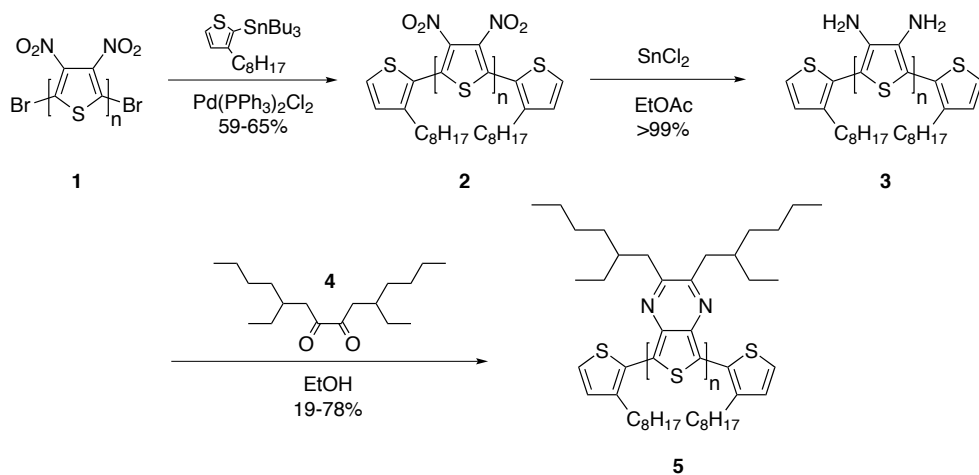
3.2 Results and discussion

3.2.1 Synthesis

The synthesis of the oligomers is outlined in scheme 3.1. The α, ω -dibromo-oligo(dinitrothiophene)s **1** ($n = 1-3$) were prepared from the dibromothiophenes (for $n = 1, 2$) or from 5,5''-dibromo-3',4'-dinitro [2,2';5',2'']terthiophene (for $n = 3$), by nitration with either $\text{HNO}_3/\text{H}_2\text{SO}_4$ (for $n = 1$) or NO_2BF_4 ^{10,11} (for $n = 2, 3$), with yields close to 70 %. The resulting nitro compounds were reacted in a Stille coupling with tributyl-(3-octylthiophen-2-yl)-stannane, followed by reduction of the nitro groups using tin(II)chloride. The final step consisted of the condensation of the amine compounds with diketone **4** to give end capped oligomers **5**. The oligomers were characterized by NMR, IR, and MALDI-TOF mass spectrometry.

3.2.2 Optical and electrochemical properties

UV/vis absorption spectra of the oligomers, both at room temperature and at low temperature (down to 80 K), are depicted in figure 3.1. It is clear from this figure that adding extra thieno[3,4-*b*]pyrazine units causes a large red shift and an increase of the molar absorption coefficient of the low energy absorption band. The optical band



Scheme 3.1: Synthesis of the oligomers ($n = 1-3$)

gaps E_g^{opt} , as estimated from the onsets of absorption, are summarized in table 3.1. When cooling down, the spectra exhibit a gradually enhanced vibronic fine structure on the low-energy absorption. The relative intensity of the 0-0 transition increases with chain length. This points to a lesser degree of structural deformation in the excited state for the longer oligomers, consistent with an extensive delocalization of both HOMO and LUMO over the whole molecule. As can be seen clearly, the onset of absorption does not shift upon cooling. This indicates that the changes with temperature are due to a reduction of inhomogeneous line-broadening, as a result of less intramolecular motions at lower temperature, rather than aggregation.

Table 3.1: UV/vis absorption data and onsets of oxidation and reduction (E_{ox} and E_{red} vs. Fc/Fc^+) in dichloromethane.

n	λ_{max} (nm)	λ_{onset} (nm)	E_g^{opt} (eV)	E_{ox} (V)	E_{red} (V)	E_g^{CV} (eV)	E_{max}^{RC} (eV)
1	479	591	2.10	0.24	-1.97	2.21	
2	620	745	1.66	-0.06	-1.71	1.65	1.59
3	745	871	1.42	-0.24	-1.59	1.35	1.34

The redox behavior of the oligomers was investigated by cyclic voltammetry. Cyclic voltammograms are shown in figure 3.2. For all oligomers one or two quasi-reversible reductions are visible. For $n = 2$ and 3 also two quasi-reversible oxidations are observed, but for $n = 1$, the oxidation is irreversible and an extra peak is observed in the backward scan. This peak can be attributed to the product of dimerization of the radicals formed upon oxidation (see section 4.2.5). From these voltammograms, the onset potentials of oxidation (E_{ox}) and reduction (E_{red}) can be determined and the electrochemical band gap can be calculated as $E_g^{CV} = E_{ox} - E_{red}$. The values are represented in table 3.1. The electrochemical band gaps are close to the optical band gaps.

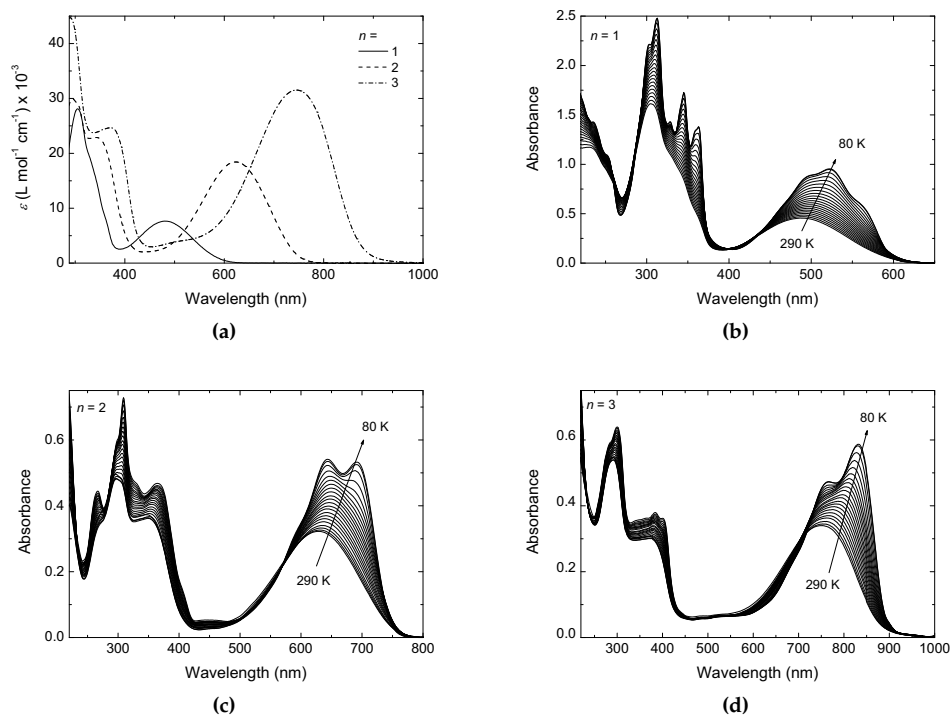


Figure 3.1: UV/vis absorption spectra of compounds **5** ($n=1-3$) in dichloromethane (a) and low temperature UV/vis absorption in 2-methyltetrahydrofuran (b-d).

3.2.3 Radical cations

Chemical oxidation of the oligomers can be accomplished by addition of a strong oxidant. In this case, thianthrenium hexafluorophosphate¹² was added to a solution of the oligomers **5** ($n=2, 3$) in dichloromethane in small aliquots. The UV/vis/NIR absorption spectra of the radical cations that are produced in solution with increasing equivalents of thianthrenium are shown in figure 3.3. For oligomer **5** ($n=1$), the formed radical cation dimerizes and the spectrum (not shown) exhibits the absorption band of the corresponding cation of the dimer (see section 4.2.5).

It can be seen from figure 3.3 that the radical cations have a very intense absorption band located at lower energy, slightly below the onset of the absorption of the neutral molecules, and that additional low intensity bands appear at very low energy. The absorption maxima (E_{max}^{RC}) are summarized in table 3.1. Compared to the onset of absorption of the neutral oligomer, the new strong absorption of the oxidized state exhibits a relatively small red shift of only around 0.15 eV. Therefore, oxidation of electrochemically polymerized poly(thieno[3,4-*b*]pyrazine) might explain the reported reduction in band gap compared to the same polymer that was made via oxidative polymerization using FeCl_3 .^{4,5}

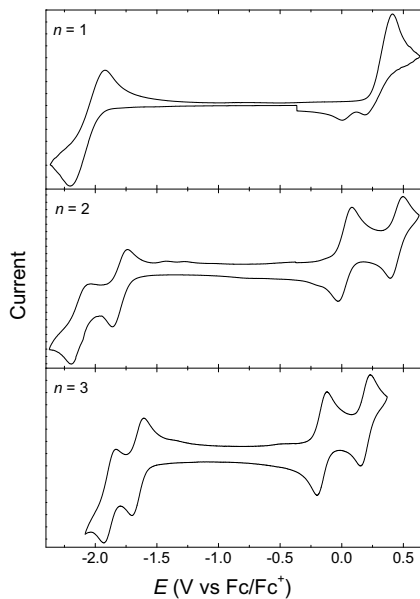


Figure 3.2: Cyclic voltammograms of oligomers **5** recorded in dichloromethane

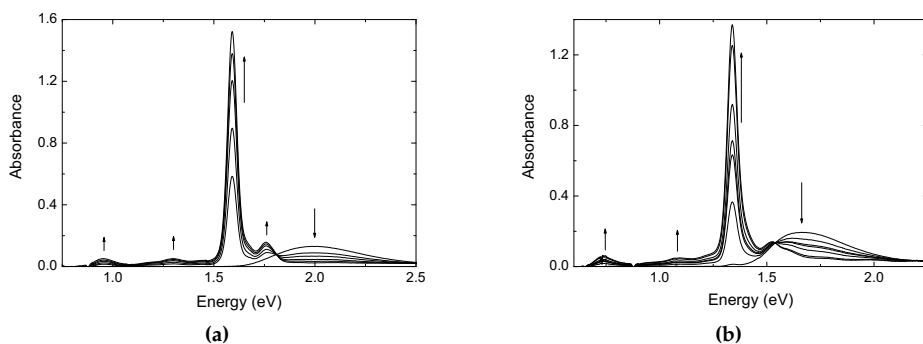


Figure 3.3: Chemical oxidation of oligomers **5** ($n=2$) (a) and ($n=3$) (b) in dichloromethane, by adding a solution of thianthrenium hexafluorophosphate. The appearance and disappearance of absorption bands is indicated with arrows.

3.2.4 Chain length dependence

The evolution of the optical band gap and the oxidation and reduction potentials with the increasing number of thieno[3,4-*b*]pyrazine units is depicted in figure 3.4, plotted versus the reciprocal number of rings in the conjugated backbone, $1/(n+2)$.

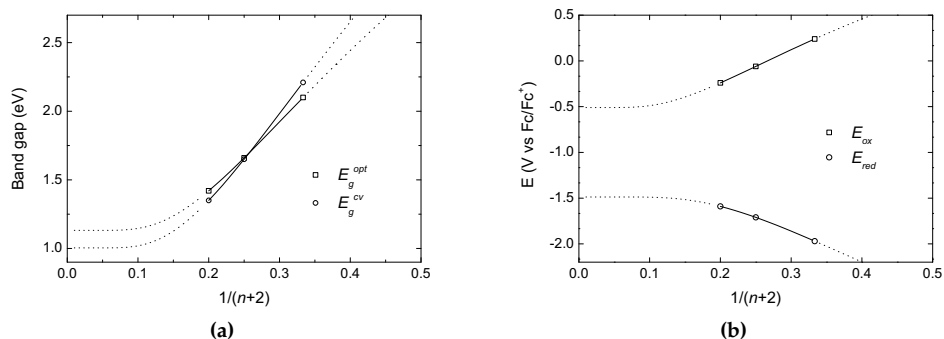


Figure 3.4: Evolution of the optical and electrochemical band gap (a) and oxidation and reduction potentials (b) with the amount of thieno[3,4-*b*]pyrazine. Fits are according to equation 3.1.

The interesting issue is that the dependence of the band gap on chain length is much stronger for these oligothieno[3,4-*b*]pyrazines than for small band gap oligomers based on alternating electron-rich and electron-deficient units.¹³ The likely explanation for the much stronger chain length dependence is the stronger dispersion of both HOMO and LUMO in the homo-oligomers, compared to alternating systems where the different units tend to localize the frontier orbitals. As observed in chapter 2, the LUMO is mainly localized on the acceptor units in mixed donor–acceptor systems, whereas the HOMO is more delocalized.

It is well-known that for conjugated oligomers the evolution of the optical properties with chain length are described by the following equation:¹⁴

$$E_m = E_\infty + (E_1 - E_\infty) \exp[-a(m-1)] \quad (3.1)$$

In this equation, E_m is the value of the transition energy (*e.g.*, band gap) for the oligomer with length m , E_1 is the transition energy for the oligomer with $m = 1$ and a is a parameter which describes how fast the optical property saturates toward its polymer value. Fitting the optical band gap to equation 3.1 using $m = n + 2$ for the end capped oligothieno[3,4-*b*]pyrazines gives a value for E_∞ of 1.13 ± 0.07 eV, which agrees quite well with the literature value of 1.14 eV of poly(2,3-dihexylthieno[3,4-*b*]pyrazine) in chloroform solution.⁴ The obtained value for a of 0.61 implies that 99% of the band gap reduction will be accomplished when $m = 9$, which corresponds to an oligomer containing 7 thieno[3,4-*b*]pyrazine units. The observed chain-length dependence of the band gap is consistent with the results obtained recently by Rasmussen *et al.*^{8,9} Although the number of data points fitted is equal to the number of parameters in equation 3.1, we think the extrapolation for the band gap to the polymer is valid, because the optical and electrochemical data provide consistent results.

The electrochemical data clearly demonstrate that the band gap reduction is caused by a rise of the HOMO (lowering of oxidation potential) and a lowering of the LUMO (rise of reduction potential) in almost equal amounts (figure 3.4b). Oxidation and reduction potentials can also be fitted to equation 3.1. This yields values of -0.51 ± 0.08 V for the oxidation potential and -1.49 ± 0.06 V for the reduction potential of the polymer. These values indicate that the polymer would be easily oxidized, but that the electron-accepting properties are not very good. Hence, poly(thieno[3,4-*b*]pyrazine)s are probably not the most viable candidates to function as *n*-type materials in devices like solar cells but are rather *p*-type polymers, although the low oxidation potentials would lead to a low open-circuit voltage in combination with commonly used fullerene derivatives as acceptor.

3.3 Conclusions

Oligothiено[3,4-*b*]pyrazines with up to three consecutive units and two thiophene end caps were prepared and their optical and electrochemical properties were investigated. As the number of thieno[3,4-*b*]pyrazine units increases, the optical absorption of the compound rapidly shifts to lower wavelengths, having an absorption onset of close to 900 nm for the system with three thieno[3,4-*b*]pyrazines. Extrapolation yields a value of 1.13 ± 0.07 eV for the optical band gap of the corresponding polymer. Electrochemistry reveals that this reduction in band gap is caused by a decrease in LUMO level and a concomitant rise in HOMO level. This points to frontier orbitals that are delocalized over the entire system. This observation is supported by UV/vis absorption experiments at low temperature. Chemical oxidation of the oligomers reduces the optical band gap by ~ 0.15 eV compared to the neutral compounds. Extrapolation of the oxidation and reduction potentials to the polymer values gives $E_{ox} = -0.51 \pm 0.08$ V and $E_{red} = -1.49 \pm 0.06$ V. These extrapolated redox potentials lead to the conclusion that poly(thieno[3,4-*b*]pyrazine)s are small band gap *p*-type polymers rather than *n*-type.

3.4 Experimental

General methods $^1\text{H-NMR}$ and $^{13}\text{C-NMR}$ spectra were recorded in CDCl_3 or DMSO on a 400 MHz NMR (Varian Mercury, 400 MHz for $^1\text{H-NMR}$ and 100 MHz for $^{13}\text{C-NMR}$) or on a 200 MHz NMR (Varian Mercury, 200 MHz for $^1\text{H-NMR}$ and 50 MHz for $^{13}\text{C-NMR}$), chemical shifts are reported in ppm downfield from tetramethylsilane (TMS). IR spectra were recorded on a Perkin Elmer 1600 FT-IR. Matrix-assisted laser desorption ionization time-of-flight (MALDI-TOF) mass spectrometry was performed on a PerSeptive Biosystems Voyager-DE PRO spectrometer. UV/vis spectra were recorded on a Perkin Elmer Lambda 900 UV/vis/NIR spectrometer. Temperature was controlled by using an Oxford Optistat continuous flow cryostat. Cyclic voltammograms were recorded in an inert atmosphere with 0.1 M tetrabutyl ammonium hexafluorophosphate (TBAPF_6) in dichloromethane as supporting electrolyte. The working electrode was a platinum disc (0.2 cm^2) and the counter electrode was a silver electrode. The scan speed was 200 mV/s. The samples were measured using an Ag/AgCl reference electrode with Fc/Fc^+ as an internal standard

using a μ Autolab II with a PGSTAT30 potentiostat.

Materials Solvents were purchased from Biosolve and used without further purification, unless stated otherwise, THF was distilled over 4Å molsieves before use. Chemicals were purchased from Acros or Aldrich and used without purification. 2,5-Dibromo-3,4-dinitrothiophene (**1**, $n = 1$), 3,3-dioctyl-3,4-dinitro[2,2;5,2]terthiophene (**2**, $n = 1$), 3,3-dioctyl[2,2;5,2]terthiophene-3,4-diamine (**3**, $n = 1$), 3,4-dinitro[2,2;5,2]terthiophene and tributyl(3-octyl-thiophen-2-yl)stannane were prepared according to literature procedures.^{15,16} Oxygen and moisture-sensitive reactions were performed under an argon atmosphere.

5,5'-dibromo-3,3',4,4'-tetranitro-2,2'-bithiophene (1, $n = 2$) 5,5-dibromo-2,2-bithiophene (0.97 g, 3.0 mmol) was dissolved in tetramethylene sulfone (10 mL). At 100°C, NO₂BF₄ (30 mL, 15.0 mmol, 0.5 M solution in tetramethylene sulfone) was added and the mixture was stirred at 100°C for 22 h. The product was precipitated in water (200 mL), filtered off and washed repeatedly with water and methanol. Yield: 1.02 g (68 %). ¹³C-NMR (50 MHz, DMSO): δ 140.28, 138.78, 130.16, 118.98. IR: $\tilde{\nu}_{max}$ (cm⁻¹) 1545, 1499, 1442, 1398, 1322, 881, 743. MALDI-TOF-MS: m/z 501.84 (50 %), 503.84 (100), 505.84 (70).

5,5-dibromo-3,4-dinitro[2,2;5,2]terthiophene 3,4-dinitro[2,2;5,2]terthiophene (1.25 g, 3.7 mmol) was dissolved in DMF (25 mL). A solution of NBS (1.4 g, 7.8 mmol) in DMF (25 mL) was added and the mixture was stirred overnight at 50°C. The reaction mixture was poured into methanol (100 mL) the bright orange product was filtered off and washed repeatedly with methanol. Yield: 1.35 g (73 %). ¹H-NMR (400 MHz, CDCl₃): δ 7.30 (d, $J = 4.1$ Hz, 2H, Ar-*H*), 7.15 (d, $J = 4.0$ Hz, 2H, Ar-*H*). IR: $\tilde{\nu}_{max}$ (cm⁻¹) 3098, 3074, 1526, 1383, 795.

5,5''-dibromo-3,3',3'',4,4',4''-hexanitro[2,2';5',2'']terthiophene (1, $n = 3$) NO₂BF₄ (7.1 mL, 3.5 mmol, 0.5 M solution in tetramethylene sulfone) was added to 5,5-dibromo-3,4-dinitro[2,2;5,2]terthiophene (350 mg, 0.71 mmol). The mixture was stirred at room temperature for 2 h and subsequently precipitated in water (30 mL). The product was collected by filtration and washed repeatedly with water and methanol. Yield: 308 mg (65 %). IR: $\tilde{\nu}_{max}$ (cm⁻¹) 1546, 1530, 1502, 1455, 1404, 1343, 1323, 788, 746. MALDI-TOF-MS: m/z 673.99 (20 %), 675.99 (35), 677.99 (20) and signals of the product that lost a nitro group ($M - 46$): m/z 628.00 (50 %), 629.00 (15), 629.99 (100), 631.00 (30), 631.99 (65), 632.99 (20), 633.99 (10).

5,5'-bis(3-octyl-thiophen-2-yl)-3,3',4,4'-tetranitro-2,2'-bithiophene (2, $n = 2$) Compound **1** ($n = 2$) (1.50 g, 3.0 mmol) and tributyl(3-octyl-thiophen-2-yl)stannane (3.07 g, 6.3 mmol) were dissolved in THF (20 mL). Bis(triphenylphosphine)palladium(II)dichloride (100 mg, 0.14 mmol) was added and the mixture was stirred at reflux for 16 h. The solvent was evaporated and the crude mixture was purified by column chromatography on silica (1:1 dichloromethane/heptane). Yield: 1.43 g (65 %). ¹H-NMR (400 MHz, CDCl₃): δ 7.54 (d, $J = 5.2$ Hz, 2H, Ar-*H*), 7.06 (d, $J = 5.2$ Hz, 2H, Ar-*H*), 2.61 (t, $J = 7.6$ Hz,

4H, $-\text{CH}_2\text{C}_7\text{H}_{15}$), 1.60 (m, 4H, $-\text{CH}_2\text{CH}_2\text{C}_6\text{H}_{13}$), 1.5–1.2 (m, 20H, $-\text{CH}_2-$), 0.86 (t, $J = 6.8$ Hz, 6H, $-\text{CH}_3$). ^{13}C -NMR (100 MHz, CDCl_3): δ 147.28, 139.23, 139.15, 136.81, 130.10, 129.61, 126.94, 118.89, 31.81, 30.50, 29.34, 29.31, 29.24, 29.14, 22.63, 14.08. IR: $\tilde{\nu}_{\text{max}}$ (cm^{-1}) 2924, 2854, 1541, 1460, 1399, 1325, 792, 750, 724. MALDI-TOF-MS: m/z 743.10 (15 %) and signals of the product that lost a nitro group ($M - 46$): m/z 688.15 (10 %), 689.15 (45), 690.15 (30), 691.13 (15).

5,5'-bis(3-octyl-thiophen-2-yl)-3,3',3'',4,4',4''-hexanitro[2,2';5',2'']terthiophene (2, $n = 3$) Compound **1** ($n = 3$) (38 mg, 0.06 mmol) and tributyl(3-octyl-thiophen-2-yl)stannane (61 mg, 0.13 mmol) were dissolved in THF (1.5 mL). Bis(triphenylphosphine)palladium(II)dichloride (2 mg, 3 μmol) was added and the mixture was stirred at reflux for 2.5 h. The solvent was evaporated and the crude mixture was purified by column chromatography on silica (3:1 dichloromethane/heptane). Yield: 30 mg (59 %). ^1H -NMR (400 MHz, CDCl_3): δ 7.57 (d, $J = 4.9$ Hz, 2H, Ar- H), 7.07 (d, $J = 5.1$ Hz, 2H, Ar- H), 2.62 (t, $J = 7.6$ Hz, 4H, $-\text{CH}_2\text{C}_7\text{H}_{15}$), 1.67–1.55 (m, 4H, $-\text{CH}_2\text{CH}_2\text{C}_6\text{H}_{13}$), 1.37–1.18 (m, 20H, $-\text{CH}_2-$), 0.87 (t, $J = 5.9$ Hz, 6H, $-\text{CH}_3$). ^{13}C -NMR (100 MHz, CDCl_3): δ 147.51, 139.10, 137.95, 130.41, 129.71, 129.30, 124.74, 118.60, 31.86, 13.79, 30.52, 29.35, 29.30, 29.12, 22.61, 14.07. IR: $\tilde{\nu}_{\text{max}}$ (cm^{-1}) 2923, 2853, 1540, 1507, 1468, 1402, 1347, 1324. MALDI-TOF-MS: m/z 905.95 (15 %) and signals of the product that lost a nitro group ($M - 46$): m/z 860.02 (100 %), 861.02 (55), 862.01 (40), 863.02 (15).

5,5'-bis(3-octyl-thiophen-2-yl)-3,3',4,4'-tetraamino-2,2'-bithiophene (3, $n = 2$) Compound **2** ($n = 2$) (0.91 g, 1.2 mmol) and tin(II)chloride dihydrate (6.7 g, 30 mmol) were dissolved in ethyl acetate (50 mL) and stirred at reflux for 2 h. The mixture was added to a solution of Na_2CO_3 (200 mL, 0.25 M), stirred vigorously with dichloromethane (200 mL) and the mixture was filtered over celite. The phases were separated and the organic phase was washed with water (3×100 mL), dried with MgSO_4 and the solvent was evaporated. Yield: 0.76 g (>99 %). ^1H -NMR (400 MHz, CDCl_3): δ 7.27 (d, $J = 5.2$ Hz, 2H, Ar- H), 6.97 (d, $J = 5.2$ Hz, 2H, Ar- H), 3.69 (s, 4H, $-\text{NH}_2$), 3.55 (s, 4H, $-\text{NH}_2$), 2.60 (t, $J = 7.8$ Hz, 4H, $-\text{CH}_2\text{C}_7\text{H}_{15}$), 1.58 (m, 4H, $-\text{CH}_2\text{CH}_2\text{C}_6\text{H}_{13}$), 1.4–1.2 (m, 20H, $-\text{CH}_2-$), 0.86 (t, $J = 7.2$ Hz, 6H, $-\text{CH}_3$). ^{13}C -NMR (100 MHz, CDCl_3): δ 142.20, 134.86, 133.54, 129.22, 127.95, 125.43, 108.99, 108.66, 31.89, 30.84, 29.47, 29.44, 29.26, 28.96, 22.68, 14.13. IR: $\tilde{\nu}_{\text{max}}$ (cm^{-1}) 3399, 3326, 2922, 2853, 1728, 1614, 1447, 1373, 1242, 1044, 824, 721. MALDI-TOF-MS: m/z 614.36 (100 %), 615.36 (45), 616.36 (25).

5,10-Diethyl-tetradecane-7,8-dione (4) 2-Ethylhexyl bromide (10.7 mL, 60 mmol) was added dropwise to iodine-activated magnesium (1.61 g, 66 mmol) in diethyl ether (50 mL). The mixture was stirred for 30 min at reflux. A mixture of LiBr (11.2 g, 130 mmol) and CuBr (8.7 g, 61 mmol) was dissolved in THF (200 mL). The Grignard solution was added dropwise at -100°C . Oxalyl chloride (1.8 mL, 20 mmol) was added dropwise and the mixture was kept stirring at -100°C for 40 min. The mixture was quenched with a small amount of water and allowed to warm to room temperature. Saturated NH_4Cl (300 mL) was added and the product was extracted with ethyl acetate (2×100 mL), the organic phase was dried with MgSO_4

and the solvent was evaporated. The crude product was purified by column chromatography on silica (95/5 heptane/ethyl acetate), the product eluted as the first band and was obtained as a yellow liquid. Yield: 4.5 g (66%). ¹H-NMR (400 MHz, CDCl₃): δ 2.65 (d, J = 6.6 Hz, 4H, -(CO)CH₂CH(C₄H₉)(C₂H₅)), 1.86 (m, 2H, -(CO)CH₂CH(C₄H₉)(C₂H₅)), 1.45–1.10 (m, 16H, -CH₂-), 0.95–0.75 (m, 12H, -CH₃). ¹³C-NMR (100 MHz, CDCl₃): δ 200.62, 40.26, 34.96, 33.24, 28.83, 26.48, 22.87, 14.03, 10.81. IR: $\tilde{\nu}_{max}$ (cm⁻¹) 2959, 2926, 2860, 1710, 1460, 1380.

2,3-Bis(2'-ethylhexyl)-5,7-bis(3-octylthiophen-2-yl)thieno[3,4-*b*]pyrazine

(5, *n* = 1) Compound **3** (*n* = 1) (1.1 g, 2.1 mmol) and compound **4** (0.7 g, 2.3 mmol) were dissolved in ethanol (25 mL) and stirred at reflux for 22 h. The solvent was evaporated and the crude product was purified by column chromatography on silica (1:3 dichloromethane/heptane). The product was isolated as a dark red oil. Yield: 1.31 g (78%). ¹H-NMR (400 MHz, CDCl₃): δ 7.35 (d, J = 5.2 Hz, 2H, Ar-*H*), 7.00 (d, J = 5.3 Hz, 2H, Ar-*H*), 2.95 (t, J = 7.9 Hz, 4H, -CH₂C₇H₁₅), 2.84 (d, J = 6.9 Hz, 4H, -CH₂CH(C₄H₉)(C₂H₅)), 2.20 (m, 2H, -CH₂CH(C₄H₉)(C₂H₅)), 1.72 (qu, J = 7.7 Hz, 4H, -CH₂CH₂C₆H₁₃), 1.50–1.20 (m, 36H, -CH₂-), 0.96–0.83 (m, 18H, -CH₃). ¹³C-NMR (100 MHz, CDCl₃): δ 155.65, 140.24, 137.77, 129.27, 128.32, 126.19, 123.70, 39.48, 37.68, 32.85, 31.89, 30.38, 30.36, 29.78, 29.54, 29.32, 28.94, 25.93, 23.14, 22.67, 14.16, 14.08, 10.89. IR: $\tilde{\nu}_{max}$ (cm⁻¹) 2956, 2924, 2855, 1463, 1378. MALDI-TOF-MS: *m/z* 748.38 (100%), 749.38 (70), 750.37 (50), 751.37, 752.38.

2,2',3,3'-tetrakis(2-ethylhexyl)-7,7'-bis(3-octylthiophen-2-yl)-5,5'-bithieno[3,4-*b*]pyrazine (5, *n* = 2)

Compound **3** (*n* = 2) (0.76 g, 1.2 mmol) compound **4** (0.72 g, 2.54 mmol) were dissolved in ethanol (15 mL) and stirred at reflux for 2.5 h. The solvent was evaporated and the crude mixture was purified by column chromatography on silica (1:3 dichloromethane/heptane). Yield: 0.69 g (50%). ¹H-NMR (400 MHz, CDCl₃): δ 7.37 (d, J = 5.2 Hz, 2H, Ar-*H*), 7.03 (d, J = 5.2 Hz, 2H, Ar-*H*), 3.07 (t, J = 7.6 Hz, 4H, -CH₂C₇H₁₅), 2.93 (d, J = 7.0 Hz, 4H, -CH₂CH(C₄H₉)(C₂H₅)), 2.88 (d, J = 6.9 Hz, 4H, -CH₂CH(C₄H₉)(C₂H₅)), 2.34–2.19 (m, 4H, -CH₂CH(C₄H₉)(C₂H₅)), 1.76 (qu, J = 7.5 Hz, 4H, -CH₂CH₂C₆H₁₃), 1.54–1.17 (m, 52H, -CH₂-), 0.98–0.80 (m, 30H, -CH₃). ¹³C-NMR (100 MHz, CDCl₃): δ 155.87, 155.14, 140.26, 138.01, 137.91, 129.33, 129.16, 126.17, 125.99, 123.12, 39.55, 37.91, 37.82, 33.02, 33.03, 32.89, 31.89, 30.38, 30.29, 29.71, 29.65, 29.32, 28.96, 28.94, 25.97, 25.92, 23.19, 23.15, 22.65, 14.16, 14.10, 14.06, 10.91, 10.88. IR: $\tilde{\nu}_{max}$ (cm⁻¹) 2955, 2923, 2871, 2852, 1457, 1441, 1378, 1237, 1139, 833, 709. MALDI-TOF-MS: *m/z* 1106.58 (100%), 1107.59 (80), 1108.58 (50), 1109.58 (25), 1110.59 (10).

2,2',2'',3,3',3'''-hexakis(2-ethylhexyl)-7,7''-bis(3-octylthiophen-2-yl)[5,5';7',5'']-terthieno[3,4-*b*]pyrazine (5, *n* = 3)

Compound **2** (*n* = 3) (29 mg, 0.03 mmol) and tin(II)chloride dihydrate (260 mg, 1.2 mmol) were dissolved in ethyl acetate (1 mL) and stirred at reflux for 1.5 h. The mixture was added to a solution of Na₂CO₃ (10 mL, 0.25 M), stirred vigorously with dichloromethane (10 mL) and the mixture was filtered over celite. The phases were separated and the organic phase was washed with water (3 × 20 mL), dried with MgSO₄ and the solvent was evaporated. The hexamine product and compound **4** (30 mg, 0.11 mmol) were dissolved

in ethanol (1 mL) and stirred at reflux for 2.5 h. The solvent was evaporated and the crude mixture was purified by column chromatography on silica (1:3 dichloromethane/heptane). Yield: 9 mg (19 %). $^1\text{H-NMR}$ (400 MHz, CDCl_3): δ 7.37 (d, $J=4.8$ Hz, 2H, Ar-H), 7.04 (d, $J=5.2$ Hz, 2H, Ar-H), 3.15–2.85 (m, 16H, $-\text{CH}_2\text{C}_7\text{H}_{15}$, $-\text{CH}_2\text{CH}(\text{C}_4\text{H}_9)(\text{C}_2\text{H}_5)$), 2.40–2.25 (m, 4H, $-\text{CH}_2\text{CH}(\text{C}_4\text{H}_9)(\text{C}_2\text{H}_5)$), 2.1–2.0 (m, 2H, $-\text{CH}_2\text{CH}(\text{C}_4\text{H}_9)(\text{C}_2\text{H}_5)$), 1.78 (qu, $J=7.2$ Hz, 4H, $-\text{CH}_2\text{CH}_2\text{C}_6\text{H}_{13}$), 1.6–1.2 (m, 68H, $-\text{CH}_2-$), 1.0–0.75 (m, 42H, $-\text{CH}_3$). IR: $\tilde{\nu}_{\text{max}}$ (cm^{-1}) 2957, 2921, 2872, 2855, 1514, 1483, 1448, 1377, 1351, 1280, 1254, 1182, 1136, 1096, 828, 692. MALDI-TOF-MS: m/z 1465.03 (90 %), 1466.03 (100), 1467.04 (75), 1468.03 (45), 1469.04 (20) 1470.03 (10).

References and notes

1. Wudl, F.; Kobayashi, M.; Heeger, A. J. *J. Org. Chem.* **1984**, *49*, 3382–3384.
2. Kobayashi, M.; Colaneri, N.; Boysel, M.; Wudl, F.; Heeger, A. J. *J. Chem. Phys.* **1985**, *82*, 5717–5723.
3. Hoogmartens, I.; Adriaensens, P.; Vanderzande, D.; Gelan, J.; Quattrocchi, C.; Lazzaroni, R.; Brédas, J. L. *Macromolecules* **1992**, *25*, 7347–7356.
4. Pomerantz, M.; Chaloner-Gill, B.; Harding, L. O.; Tseng, J. J.; Pomerantz, W. J. *J. Chem. Soc. Chem. Commun.* **1992**, 1672–1673.
5. Nietfeld, J. P.; Heth, C. L.; Rasmussen, S. C. *Chem. Commun.* **2008**, 981–983.
6. Brédas, J. L.; Heeger, A. J.; Wudl, F. *J. Chem. Phys.* **1986**, *85*, 4673–4678.
7. Kenning, D. D.; Rasmussen, S. C. *Macromolecules* **2003**, *36*, 6298–6299.
8. Wen, L.; Rasmussen, S. C. *Polym. Prepr.* **2007**, *48*, 132–133.
9. Wen, L.; Duck, B. C.; Dastoor, P. C.; Rasmussen, S. C. *Macromolecules* **2008**, *41*, 4576–4578.
10. Kuhn, S. J.; Olah, G. A. *J. Am. Chem. Soc.* **1961**, *83*, 4564–4571.
11. Tanaka, S.; Yamashita, Y. *Synth. Met.* **1999**, *101*, 532–533.
12. Shine, H. J.; Zhao, B. J.; Marx, J. N.; Ould-Ely, T.; Whitmire, K. H. *J. Org. Chem.* **2004**, *69*, 9255–9261.
13. Van Mullekom, H. A. M.; Vekemans, J. A. J. M.; Meijer, E. W. *Chem. Eur. J.* **1998**, *4*, 1235–1243.
14. Meier, H.; Stalmach, U.; Kolshorn, H. *Acta Polym.* **1997**, *48*, 379–384.
15. Kitamura, C.; Tanaka, S.; Yamashita, Y. *Chem. Mater.* **1996**, *8*, 570–578.
16. Campos, L. M.; Tontcheva, A.; Gunes, S.; Sonmez, G.; Neugebauer, H.; Sariciftci, N. S.; Wudl, F. *Chem. Mater.* **2005**, *17*, 4031–4033.

Chapter 4

Oligomers with single acceptor units

Abstract In this chapter, a combined experimental and theoretical study on the optical and electrochemical properties of a series of well-defined, extended, small band gap oligo(5,7-bis(thiophen-2-yl)thieno[3,4-*b*]pyrazine)s having alternating donor and acceptor units is presented. The optical absorptions of the ground state, triplet excited state, radical cation, and dication are identified and found to shift to lower energy with increasing chain length. The reduction of the band gap in these alternating small band gap oligomers mainly results from an increase of the HOMO level. The S_1 - T_1 singlet-triplet splitting is reduced from ~ 0.9 eV for the trimeric monomer to ~ 0.5 eV for the pentamer. This significant exchange energy is consistent with the fact that both the HOMO and the LUMO remain distributed over virtually all units, rather than being localized on the donor and acceptor units.

This work has been published: Karsten, B. P.; Viani, L.; Gierschner, J.; Cornil, J.; Janssen, R. A. J. *Phys. Chem. A* **2008**, *112*, 10764–10773.

4.1 Introduction

As the field of small band gap polymers is rapidly expanding, it is important to investigate the detailed electro-optical properties of these systems and understand how these characteristics can evolve with chain length. To date, experimental studies on small band gap oligomers have been restricted to short-chain oligomers;^{1,2} extended systems have been studied by quantum chemical methods.^{3,4} Knowledge about the electrochemical and optical properties of oligomers of small band gap systems will help in gaining valuable insight into the design rules for new materials and into the processes limiting the efficiency of polymer solar cells. Knowledge of the chain-length dependence of, *e.g.*, band gap, highest occupied molecular orbital (HOMO) and lowest unoccupied molecular orbital (LUMO) levels, and triplet energies can help with the design of new polymers with optimized properties for solar energy conversion.

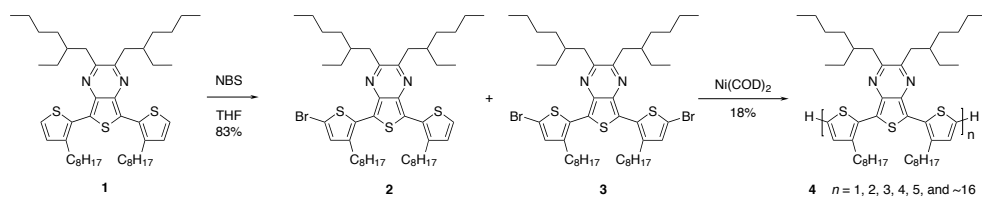
In this chapter, we present a combined experimental and theoretical study on the properties of small band gap oligomers that comprise electron-rich thiophene units alternating with an electron-deficient thienopyrazine, similar to materials recently described for solar cells.⁵ Oligomers were synthesized by polymerizing the monomer in the presence of a chain stopper, yielding a mixture of short oligomers. The oligomers produced in this way could be efficiently separated by recycling gel permeation chromatography (GPC). Subsequently, the chain length dependence of the absorption spectra, oxidation and reduction potentials, triplet levels, triplet absorptions, and the properties of the oxidized species were investigated. The electronic and optical properties of the neutral oligomers were estimated at a quantum-chemical level.

4.2 Results and discussion

4.2.1 Synthesis

The synthesis of the oligomers is outlined in scheme 4.1. The synthesis of monomer **1** was described in chapter 3. This compound was (partially) brominated with NBS, yielding a mixture of mono- and dibrominated monomers (**2** and **3**). This mixture was then subjected to a nickel(0)-mediated Yamamoto coupling,⁶ yielding a mixture of shorter oligomers **4** of various lengths. A rough separation of this mixture was accomplished by Soxhlet extraction. The different oligomers were further separated by recycling GPC. Recycling GPC is a preparative-scale GPC technique, in which the eluted products are fed back into the column, thereby virtually creating a GPC column of very high length, without having the problem of a very high pressure drop. During the run, the several oligomers can be collected, by temporarily switching the recycle valve to the collect position. This strategy yielded the monomer up to the pentamer ($n = 1-5$) in pure form as evidenced from GPC, MALDI-TOF mass spectrometry, and NMR. In the pentamer, the longest well-defined oligomer that was isolated in pure form, 15 aromatic units form the chain.

The corresponding polymer was also prepared by Yamamoto coupling from the dibrominated monomer. The polymer thus prepared had $M_n = 12\,300$ g/mol, $M_w = 32\,500$ g/mol, resulting in a polydispersity of 2.7, as determined by GPC against pol-



Scheme 4.1: Synthesis of the Oligomers and Polymer of 2,3-Bis(2'-ethylhexyl)-5,7-bis(3-octylthiophen-2-yl)thieno[3,4-*b*]pyrazine

ystyrene standards. The number average degree of polymerization of the polymer is $n \sim 16$, corresponding to ~ 48 aromatic units.

4.2.2 Optical and electrochemical properties of the neutral oligomers

UV/vis absorption spectra of the oligomers, $n = 1-5$, are shown in figure 4.1a. As expected, the absorption maxima (λ_{max}) and onsets (λ_{onset}) show a shift to longer wavelengths going from the monomer to the polymer. The extinction coefficients increase superlinearly with chain length. The optical band gaps (E_g^{opt}) estimated from the onsets of absorption are summarized in table 4.1. The absorption spectrum of the polymer in ODCB (figure 4.1b) exhibits an extra shoulder at the low-energy side of the absorption spectrum. This is a clear signature of (partial) aggregation at room temperature in solution. At higher temperatures (above 40°C) the polymer is molecularly dissolved. The onset of absorption for the polymer at 1.50 eV (when dissolved) and at 1.31 eV, (when aggregated), clearly identifies it as a small band gap conjugated polymer. In solution, the oligomers with $n > 1$ do not fluoresce, which indicates a high efficiency of internal conversion for these systems.

Table 4.1: UV/Vis absorption and PIA data in toluene and onset of redox potentials (E_{ox} and E_{red} , vs. Fc/Fc^+) in ODCB for the oligomers and polymer.^a

Oligomer	λ_{max} (nm)	E_{max} (eV)	E_{cal}^{ver} (eV)	λ_{onset} (nm)	E_g^{opt} (eV)	E_{ox} (V)	E_{red} (V)	E_g^{CV} (eV)	$E_g^{opt} - E_g^{CV}$ (eV)	$T_n \leftarrow T_1$ (eV)	E_T^{cal} (eV)
Monomer	493	2.52	2.67	605	2.05	0.20	-2.00	2.20	0.15	1.60 ^b	0.97
Dimer	587	2.11	2.30	706	1.76	-0.10	-1.92	1.82	0.06	1.40	0.90
Trimer	632	1.96	2.11	768	1.61	-0.18	-1.92	1.74	0.13	1.32	0.88
Tetramer	648	1.91	2.04	795	1.56	-0.21	-1.89	1.68	0.12	1.22	0.87
Pentamer	669	1.85	2.01	809	1.53	-0.24	-1.87	1.63	0.10	1.20	0.87
Polymer	671 ^c	1.85 ^c		828 ^c	1.50 ^c	-0.26	-1.89	1.63	0.13	1.20 ^d	

^a $T_n \leftarrow T_1$ absorption in toluene.

^b Expected value based on equation 4.1.

^c In ODCB at 80°C.

^d In chlorobenzene at 80°C.

The redox behavior of the oligomers was investigated by cyclic voltammetry. The resulting voltammograms are shown in figure 4.2. For the dimer to tetramer, two quasi-reversible oxidations are observed, which start to overlap in the pentamer. The reduction waves are irreversible, except for the monomer. The onset potentials

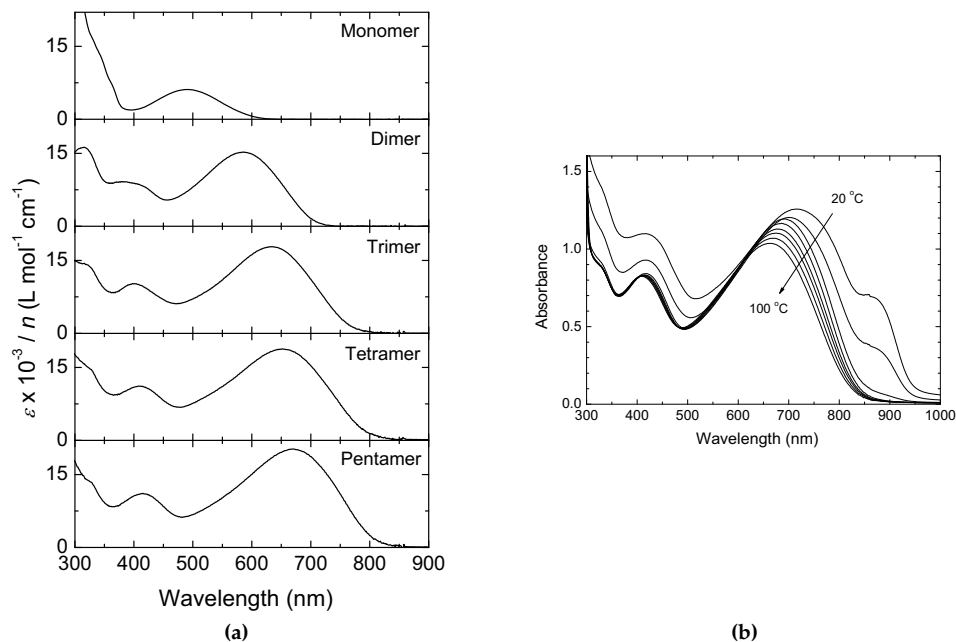


Figure 4.1: UV/vis absorption of (a) the monomer to the pentamer in toluene (the ordinate is the molar absorption coefficient (ϵ) divided by n , the number of monomeric units in the oligomer) at room temperature, and (b) the polymer at various temperatures in ODCB.

of both oxidation (E_{ox}) and reduction (E_{red}) and the electrochemical band gap ($E_g^{CV} = E_{ox} - E_{red}$) are presented in table 4.1.

The band gap of the oligomers decreases with increasing chain length (table 4.1). The electrochemical band gap is slightly higher by 0.10 ± 0.05 eV than the optical band gap. Apart from experimental uncertainties, this difference reflects the fact that free ions are created in the electrochemical experiment rather than a neutral exciton. Apparently, this, combined with different solvation energies for the ions and the neutral molecule, causes E_g^{opt} and E_g^{cv} to be different. Both the dependence of the electrochemical and optical band gap on the inverse chain length and the dependence of the oxidation and reduction potentials on the inverse chain length ($1/n$) are shown in figure 4.3.

In first approximation, both the oxidation and the reduction potentials follow a linear dependence with $1/n$. With increasing chain length the rise of the HOMO level (as reflected in the lowering of the oxidation potential) is responsible for most of the reduction of the band gap. The LUMO (reflected in the reduction potential) varies less. While a linear relation of the band gap with $1/n$ also seems valid for the band gap of the oligomers, the value for polymer deviates significantly from this straight line. It is well-known from literature that the optical band gaps of conjugated polymers can be fitted to the following equation:⁷

$$E(n) = E_{\infty} + (E_1 - E_{\infty}) \exp[-a(n-1)] \quad (4.1)$$

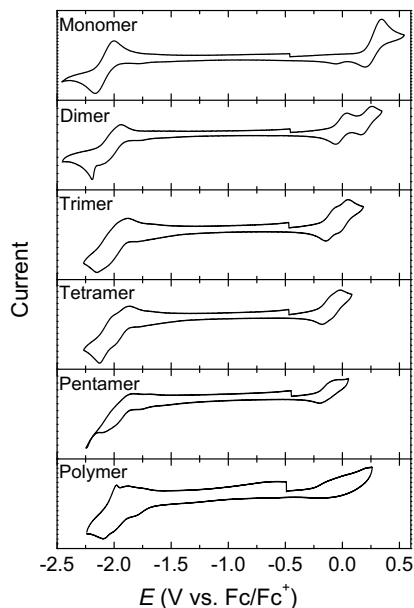


Figure 4.2: Cyclic voltammograms of the oligomers and the polymer recorded in ODCB.

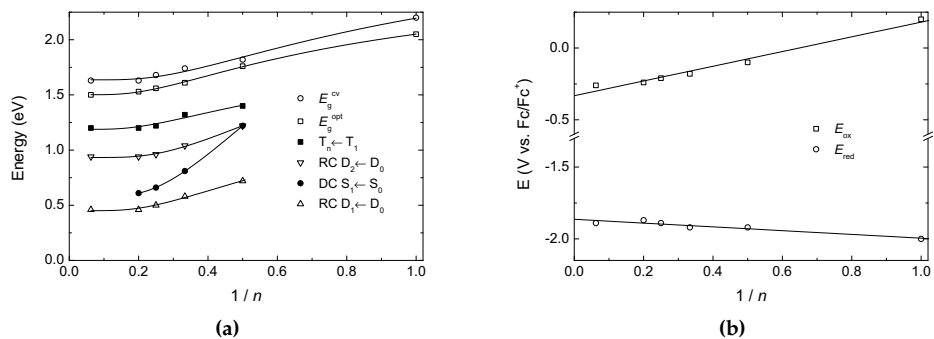


Figure 4.3: (a) Chain length dependence of energies for the optical E_g^{opt} and electrochemical band gap E_g^{CV} , the triplet $T_n \leftarrow T_1$ absorption, the radical cation (RC) absorptions ($D_1 \leftarrow D_0$ and $D_2 \leftarrow D_0$), and the dication (DC) absorption ($S_1 \leftarrow S_0$) versus reciprocal chain length ($1/n$). (b) Onsets of oxidation and reduction potentials *vs.* $1/n$. Fits of the data (solid lines) in panel a are to equation 4.1, and those in panel b are to a linear relation with $1/n$.

Here, E_1 and E_∞ are the excitation energies for the monomer and the (infinitely long) polymer, n is the number of repeat units, and a is a parameter that describes how fast $E(n)$ saturates to E_∞ . This empirical relation can be rationalized in terms of intrinsic length scales (electron-hole distances) and extrinsic length scales set by disorder.⁸ If the optical band gaps for the oligomers are fitted to equation 4.1, a value of $E_\infty = 1.505$ eV is obtained, very close to the experimental value of 1.50 for the polymer. This fit is also shown in figure 4.3. The value for a of 0.78 implies that the band gap stops decreasing between 7 and 10 repeat units (99 % or 99.9 % of the difference $E_1 - E_\infty$ has been reached, respectively). The data for the oligomers were also fitted according to the method by Kuhn⁹ (figure 4.4a), where all N double bonds are regarded as identical, coupled oscillators. For the Kuhn model, only the double bonds in the conjugated chain are used, which, for the present oligomers, is given by $N = 6n$. This approach yields the same value of 1.5 eV for the optical band gap of the polymer (figure 4.4a).

4.2.3 Theoretical results*

The electronic and optical properties of the oligomers have also been characterized at a quantum chemical level. The long alkyl side chains of the oligomers influence the solubility and the organization of the molecules in the solid state, but to a much lesser extent the electronic properties; we have thus substituted all of them by methyl groups to minimize the computational efforts. Since the correct determination of the actual torsion angles in solution is a rather challenging task, all molecular geometries were optimized by imposing the planarity of the systems. In view of the large size of the longest oligomers, we have optimized the ground-state geometry of the systems with the help of semi-empirical Hartree–Fock techniques that generally provide the best compromise between computer times and accuracy of the geometric parameters. We have chosen here the semi-empirical Hartree–Fock MNDO (modified neglect of differential overlap) method, as implemented in the AMPAC package,¹⁰ which is known to provide geometric parameters in good agreement with experimental values for thiophene-based compounds;¹¹ in particular, MNDO yields a much better description of the C–C bond alternation compared to the widely used AM1 (Austin model 1) method.^{11,12} The electronic structure was then calculated with the semi-empirical Hartree–Fock INDO (intermediate neglect of differential overlap) method, as parametrized by Zerner and co-workers, and using the Ohno-Klopman potential.¹³ INDO has been coupled to a single configuration interaction scheme including all $\pi \rightarrow \pi^*$ transitions to access the vertical transition energies between the ground and lowest excited states ($S_1 \leftarrow S_0$). This approach has been found to be the best compromise to depict the chain-length dependence of the optical properties of conjugated oligomers.¹⁴ Note also that the combination of these two semi-empirical techniques proves reliable to rationalize the optical properties of oligothiophenes.¹⁵

The vertical $S_1 \leftarrow S_0$ transition energies E_{ver}^{cal} calculated for all oligomers are shown in figure 4.4a and are collected in table 4.1. The experimental chain-size evolution is very well reproduced by the calculations. Moreover, we observe a fairly

*The calculations were performed by L. Viani at the university of Mons–Hainaut.

good quantitative agreement between the calculated transition energies and the experimental values of E_{max} that correspond to λ_{max} and that can be associated in first approximation to the vertical transition energies. Extrapolations to obtain the transition energies for the polymer were done using the Kuhn method⁹ (solid line in figure 4.4a), which predicts the vertical transition for the polymer at $E_{ver}^{cal} = 1.93$ eV, while a slightly larger value of $E_{ver}^{cal} = 1.97$ eV is obtained with equation 4.1 (dashed line in figure 4.4a). These two values are in good agreement with the experimental value of $E_{max} = 1.85$ eV.

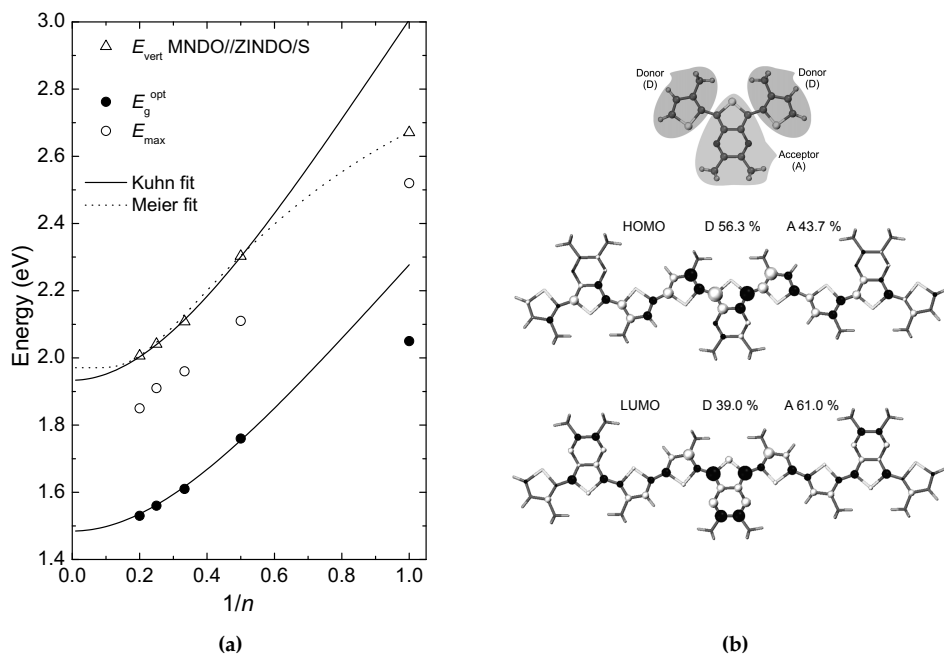


Figure 4.4: (a) Calculated vertical transitions at the MNDO//ZINDO/S level of theory and experimental values for optical band gap and absorption maxima. Lines are extrapolation fits, following Kuhn⁹ (solid line) and Meier⁷ (equation 4.1, dotted line). n is the number of units in the oligomer and proportional to the number of double bonds along the conjugated chain $N = 6n$. (b) Shape of the frontier molecular orbitals and relative contributions of the donor (D) and acceptor (A) units; the color and size of the balls reflect the sign and amplitude of the linear combination of atomic orbitals (LCAO) coefficients.

The $S_1 \leftarrow S_0$ transition of the monomer is mainly described by a HOMO \rightarrow LUMO excitation. The corresponding shapes of the frontier molecular orbitals are shown in figure 4.4b. Despite the donor *vs.* acceptor character of the two building blocks in the oligomers, the electronic density in the HOMO level is found to have a homogeneous distribution over the units while the LUMO has a more pronounced weight over the acceptor parts.¹⁶ This delocalization rationalizes the significant transition dipole moment (and hence oscillator strength) associated with the lowest optical transition. Another consequence is that a significant intramolecular charge transfer ($\sim 0.17e$ for the monomer) occurs upon promotion of an electron from the HOMO

to the LUMO level.

4.2.4 Triplet excited states

Triplet–triplet absorptions were investigated using near steady-state PIA. Because formation of the triplet states of the oligomers by direct excitation to S_1 , followed by intersystem crossing to T_1 was not successful, triplet states were populated by sensitization with a fullerene derivative (*N*-methylfulleropyrrolidine, MP-C₆₀).¹⁷ In this experiment, the fullerene is excited by the laser, and the triplet state of the fullerene is formed with a quantum yield of about unity. The triplet energy is then transferred from MP-C₆₀ to the oligomer, yielding the triplet state of the oligomer. Mixtures of the oligomer (0.1 mM) and MP-C₆₀ (0.4 mM) in toluene were excited by laser irradiation at 351 and 364 nm. The PIA spectra in toluene are shown in figure 4.5. The PIA spectra of the oligomers exhibit a single strong absorption peak that shifts to lower energy with increasing n . In the case of the monomer, the triplet state of the monomer is not observed, but the typical PIA spectrum of MP-C₆₀ with a peak at 1.78 and a shoulder at 1.52 eV is obtained.¹⁷ Compared to a solution of pure MP-C₆₀, the triplet spectrum in the mixture is quenched by a factor of 15, indicating that the triplet state of the monomer is actually formed, yet not visible. Because of its poor solubility in toluene, the PIA spectrum of the polymer (375 $\mu\text{g}/\text{mL}$) was recorded in chlorobenzene, at 80°C.

As can be seen, the $T_n \leftarrow T_1$ absorptions shift to lower energy as the length of the molecule increases. An overview of the $T_n \leftarrow T_1$ absorption maxima in toluene is given in table 4.1. In the case of the polymer, also polaronic absorptions are visible in the PIA spectrum; this is due to the higher polarity of chlorobenzene compared to toluene. The more polar solvent stabilizes the charge separated state, where an electron is transferred from the polymer to MP-C₆₀.

The dependence of the $T_n \leftarrow T_1$ absorption maxima on the inverse chain length is depicted in figure 4.3a. Again, the absorption maxima for the dimer to the pentamer can be fitted to equation 4.1 to give $E_1 = 1.64$ eV, $E_\infty = 1.19$ eV, and $a = 0.73$. Careful inspection of the PIA spectrum of MP-C₆₀ with the monomer leads to the observation of an extra shoulder in the MP-C₆₀ triplet absorption around 1.6 eV. This is exactly the region where the monomer triplet absorption would be expected, based on the fit discussed before. The extra shoulder is indicated in figure 4.5 with an asterisk.

To estimate the energies of the T_1 state of the oligomers (E_T), quenching experiments were conducted. In these experiments, a triplet quencher with known triplet energy was added to the monomer/fullerene mixture. Quenching of the oligomer triplet indicates that the triplet energy of the oligomer is above the triplet energy of the quencher and vice versa. In this way, the T_1 triplet energies for the dimer to the pentamer were estimated to be between 0.93 eV (the triplet energy of bis(trihexylsiloxy)-silicon-2,3-naphthalocyanine)¹⁸ and 1.14 eV (the triplet energy of rubrene).¹⁹ The triplet level of the monomer was estimated to be around 1.14 eV (the triplet state of rubrene is only partially quenched by the monomer). In this way, the S_1 – T_1 singlet–triplet splitting is estimated to be around 0.9 eV for the monomer, going to around 0.5 eV for the pentamer; the splitting for the dimer up to the tetramer is located somewhere in between. These values are roughly in correspondence with literature values of $\Delta E_{ST} \approx 0.7$ eV for most conjugated polymers.²⁰

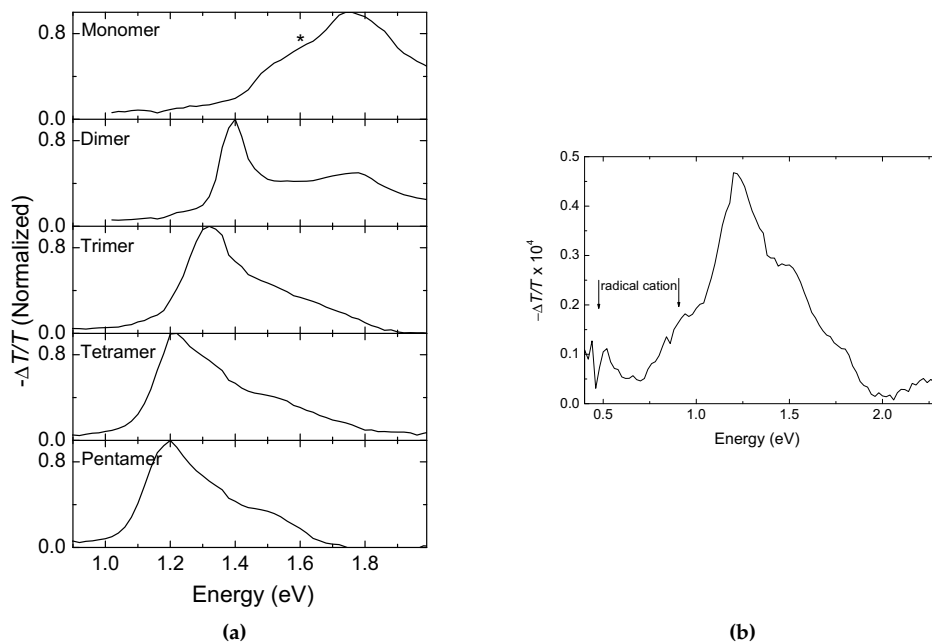


Figure 4.5: PIA spectra of (a) the oligomers recorded in toluene at room temperature and (b) the polymer in chlorobenzene at 80°C. The expected location of the monomer triplet absorption is indicated with an asterisk in panel a. In panel b, the radical cation absorptions of the polymer are indicated with arrows.

Theoretical support for these estimates for E_T was obtained by calculating the energies of the vertical $T_1 \leftarrow S_0$ transitions (E_T^{cal}) for the planar oligomers at the INDO/SCI level (table 4.1). These vary from $E_T^{cal} = 0.97$ eV for the monomer to 0.87 eV for the pentamer and are, hence, slightly less than the experimental estimates ($0.93 < E_T \leq 1.14$ eV). In these calculations, the relaxation of the geometry in the triplet state, which will further reduce E_T^{cal} , was not taken into account. The overall small change in E_T compared to E_{ver}^{cal} with increasing chain length (n) suggests that the natural size of the triplet exciton is smaller than that of the singlet exciton.

4.2.5 Cations and dications of the oligomers

When applied in organic solar cells, photoexcited small band gap polymers donate an electron to an acceptor molecule, often a C_{60} derivative. The electron and hole are then separated, producing the photocurrent. To investigate the optical properties of the resulting oxidized species, chemical oxidation experiments and PIA experiments were performed.

Chemical oxidation of the oligomers can be accomplished by the addition of a strong oxidant. In this case, thianthrenium hexafluorophosphate²¹ was added to a solution of the oligomers in dichloromethane in small aliquots. The UV/vis/NIR absorption spectra of the radical cations and of the dications that are produced in

solution with increasing equivalents of thianthrenium were recorded. Results are shown in figure 4.6. Chemical oxidation of the polymer was not performed, because of the poor solubility of the polymer in dichloromethane.

Upon oxidation of the monomer, bands corresponding to the radical cation or the dication of the monomer are absent (figure 4.6a). Instead, the monomer radical cation is reactive and dimerizes to produce the dication of the dimer. As a result, the spectra of the monomer (figure 4.6a) and the dimer (figure 4.6b) both show a similar band at 1.22 eV. This observation is consistent with the fact that the first oxidation potential of monomer is higher than the second oxidation potential of the dimer (figure 4.2). This dimerization is also visible in cyclic voltammetry. The first two scans for the monomer are depicted in figure 4.7. In the second scan, the peaks of the dimer are clearly visible. In addition to the peak at 1.22 eV, the spectra of the oxidized monomer also show clear transitions at 1.92 and 2.13 eV. These are not related to the dimer dication, but, at present, we have no clear explanation for these features. Extrapolation of the determined $D_2 \leftarrow D_0$ transition energies for the other oligomers according to equation 4.1 (figure 4.3a) yields a value of 1.77 eV for the monomer. This value is much lower than 1.92 eV, and hence traces of monomer radical cation cannot satisfactorily explain the features at 1.92 and 2.13 eV.

For the dimer through the pentamer, the absorption band of the neutral oligomer decreases upon addition of the first equivalent thianthrenium hexafluorophosphate, while, at the same time, two new bands appear at lower energy. The new bands are attributed to the dipole-allowed $D_1 \leftarrow D_0$ and $D_2 \leftarrow D_0$ transitions of the doublet-state radical cation that, in first approximation, correspond to electron excitations from HOMO \rightarrow SOMO (singly occupied molecular orbital) and SOMO \rightarrow LUMO (see figure 4.6f). For the pentamer, the low-energy $D_1 \leftarrow D_0$ band of the radical cation cannot be clearly observed, because it is located in the same region where the IR overtones of the solvent (dichloromethane) appear. Upon addition of a second equivalent of thianthrenium hexafluorophosphate, the radical cation bands decrease again, while an essentially single, new band with a vibronic feature at higher energy appears, located between the two bands of the radical cation. This band is attributed to the $S_1 \leftarrow S_0$ transition of the (singlet state) dication. In the case of the dimer, the high energy band of the radical cation overlaps with the band of the dication, and, with increasing conjugation length, the position of the dication band moves from the position close to the $D_2 \leftarrow D_0$ band for the dimer to that of the $D_1 \leftarrow D_0$ band for the pentamer (figure 4.6). The positions of the radical cation and dication bands are collected in table 4.2 and plotted versus $1/n$ in figure 4.3a. In figure 4.3a it can be seen that dispersion of the dication transition with chain length is much stronger than that for the other transitions.

4.2.6 Photoinduced electron transfer in solution from oligomers to MP-C₆₀

In a PIA experiment with a mixture of the oligomers and MP-C₆₀, the nature of the formed excited state depends on the polarity of the solvent. In apolar solvents, the triplet state energy of MP-C₆₀ is transferred to the oligomer, giving rise to the triplet state of the oligomer (T_1), and the corresponding $T_n \leftarrow T_1$ absorption as shown in figure 4.5. In polar solvents like ODCB, however, the same experiment can result

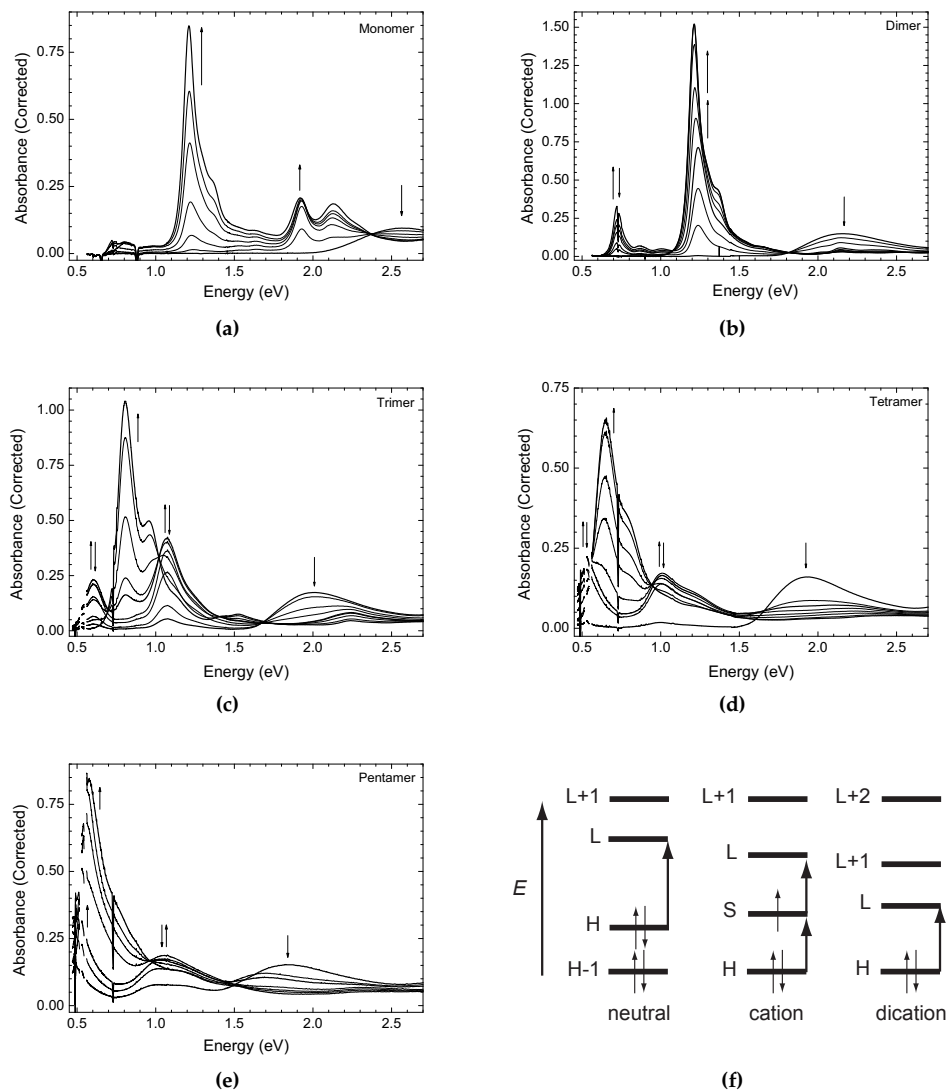


Figure 4.6: (a–e) Chemical oxidation of the oligomers in dichloromethane, by adding a solution of thianthrenium hexafluorophosphate. The appearance and disappearance of absorption bands is indicated with arrows. First, radical cations are produced, that are subsequently transformed into the dications. (f) Schematic orbital diagram for the main dipole-allowed transitions of the neutral oligomer, the cation, and the dication in a one electron picture. (H = HOMO, S = SOMO, L = LUMO).

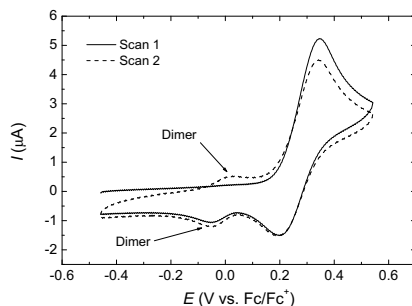


Figure 4.7: The first two scans in the cyclic voltammogram of the monomer; peaks belonging to the dimer are indicated.

Table 4.2: Absorption maxima (eV) of the principal transitions of the radical cation (RC) and dication (DC) of the oligomers ($n = 2-5$) and the polymer determined from chemical oxidation and PIA experiments.

Oligomer	chemical oxidation			PIA	
	RC D ₁ ← D ₀	RC D ₂ ← D ₀	DC S ₁ ← S ₀	RC D ₁ ← D ₀	RC D ₂ ← D ₀
Dimer	0.72	1.22	1.22	0.72	1.22
Trimer	0.60	1.07	0.81	0.58	1.04
Tetramer	0.53	1.01	0.66	0.50	0.96
Pentamer	0.46	1.04	0.61	0.46	0.94
Polymer				0.46	0.94

in an electron being transferred from the oligomer to the triplet state of MP-C₆₀, resulting in the radical cation of the oligomer and the radical anion of MP-C₆₀. The free energy for charge separation (ΔG_{CS}) in different solvents can be calculated by the Weller equation, based on a continuum model:²²

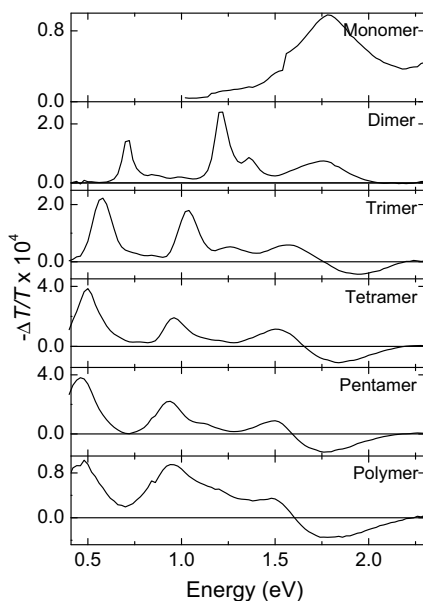
$$\Delta G_{CS} = e(E_{ox}(D) - E_{red}(A)) - E_{00} - \frac{e^2}{4\pi\epsilon_0\epsilon_s R_{cc}} - \frac{e^2}{8\pi\epsilon_0} \left(\frac{1}{r^+} + \frac{1}{r^-} \right) \left(\frac{1}{\epsilon_{ref}} - \frac{1}{\epsilon_s} \right) \quad (4.2)$$

Here $E_{ox}(D)$ and $E_{red}(A)$ are the oxidation and reduction potentials of the donor (oligomer) and acceptor (MP-C₆₀, $E_{red}(A) = -1.20$ V vs. Fc/Fc⁺) in the reference solvent, respectively, E_{00} is the excited state from which charge transfer takes place (1.50 eV for the triplet level of MP-C₆₀),²³ R_{cc} is the center-to-center distance of the positive and negative charges (set to infinity for intermolecular charge transfer), r^+ and r^- are the radii of the positive and negative ions, and ϵ_{ref} and ϵ_s are the relative permittivities of the reference solvent (used to measure oxidation and reduction potentials) and the solvent in which electron transfer is studied. r^- is calculated in literature to be 5.6 Å for C₆₀, based on the density of C₆₀.²³ r^+ can be estimated using a similar approach, using a density of 1.5, the value for unsubstituted terthiophene.²⁴ This calculation for the different oligomers yields the values given in table 4.3. On the basis of these data we indeed expect triplet absorptions in toluene, but photoinduced electron transfer in ODCB.

Table 4.3: Free energies for charge separation, calculated using equation 4.2

Oligomer	E_{ox}^0 (ODCB) (V vs. Fc/Fc ⁺)	r^+ (Å)	ΔG_{CS} (eV)	
			toluene	ODCB
Monomer	0.27	4.3	0.92	-0.03
Dimer	-0.01	5.4	0.53	-0.31
Trimer	-0.10	6.2	0.39	-0.40
Tetramer	-0.13	6.8	0.32	-0.43
Pentamer	-0.16	7.4	0.27	-0.46

The PIA spectra recorded of the oligomers in ODCB in the presence of MP-C₆₀ are depicted in figure 4.8. In order to prevent aggregation, the PIA spectrum of the polymer was recorded at 80°C. As expected, the PIA spectra in ODCB show the two peaks of the radical cation of the oligomers ($n=2-5$) and the polymer at low energies and a bleaching band at the absorption energies of the neutral compounds. Absorption maxima of the oxidized oligomers determined by chemical oxidation and PIA in ODCB are given in table 4.2; the data are also depicted in figure 4.3a. The radical anion of MP-C₆₀, which is expected to give a less intense transition at 1.24 eV,¹⁷ is not clearly apparent from the spectra shown in figure 4.8.

**Figure 4.8:** PIA spectra of the oligomers ($n=1-5$) and the polymer recorded in ODCB in the presence of MP-C₆₀.

The values determined by PIA and chemical oxidation are in good agreement. The values determined in the PIA experiment are probably more reliable, because radical concentrations are much lower and reactions of these radicals are of less im-

portance. Moreover, the low energy absorption bands of the longer oligomers are more visible in the PIA experiment, because of the lock-in detection. Going from pentamer to polymer, there is no decrease in transition energy anymore for both radical cation bands.

4.3 Conclusions

Well-defined, extended oligomers, having up to 15 aromatic units, of a soluble poly-(5,7-bis(thiophen-2-yl)thieno[3,4-*b*]pyrazine) were prepared. As expected, the optical band gap (E_g^{opt}) of the oligomers decreases with increasing chain length, and reaches a constant value of ~ 1.50 eV for seven repeating (trimeric) units. The electrochemical band gaps are slightly higher (0.10 ± 0.05 eV) than the optical band gaps. The redox potentials reveal that the major contribution ($\sim 75\%$) to the reduction of the optical band gap is the increase of the HOMO level with increasing chain length, rather than a reduction of the LUMO level ($\sim 25\%$). PIA experiments of a mixture of the oligomer with MP-C₆₀ as sensitizer were used to generate the triplet state of the oligomers in toluene, via triplet-energy transfer. Going from monomer to polymer, the triplet ($T_n \leftarrow T_1$) absorption decreases in energy, showing the same trend as the $S_1 \leftarrow S_0$ absorption. The triplet state energies were estimated by quenching experiments, revealing that $\Delta E_{ST} \approx 0.9$ eV for the monomer, decreasing to around ~ 0.5 eV for the pentamer. These values are in agreement with previously reported values for conjugated systems.²⁰ In a more polar solvent, ODCB, electron transfer from the oligomer to the T_1 state of MP-C₆₀ takes place rather than energy transfer, consistent with the estimated energy levels from a continuum model. The absorption bands determined for the oligomer radical cations produced in this way also shift to lower energy with increasing chain length. These are confirmed by chemical oxidation measurements that additionally provide insight into the absorption of the corresponding dications. The electronic and optical properties of the neutral oligomers were supported by quantum-chemical calculations. Inspection of the orbital coefficients for the HOMO and LUMO leads to the conclusion that both are roughly located on the same atoms (the LUMO is not solely localized on the acceptor units). This would give rise to a relatively large exchange energy and hence, to relatively large values for the singlet–triplet splitting, in agreement with experiment.

4.4 Experimental

General methods ¹H-NMR and ¹³C-NMR spectra were recorded in CDCl₃ on a 400 MHz NMR (Varian Mercury, 400 MHz for ¹H-NMR and 100 MHz for ¹³C-NMR), chemical shifts are reported in ppm downfield from tetramethylsilane (TMS). IR spectra were recorded on a Perkin Elmer 1600 FT-IR. Matrix-assisted laser desorption ionization time-of-flight (MALDI-TOF) mass spectrometry was performed on a PerSeptive Biosystems Voyager–DE PRO spectrometer. UV/vis spectra were recorded on a Perkin Elmer Lambda 900 UV/vis/NIR spectrometer. GPC analysis of the oligomers was performed on a LC system, equipped with two PLgel 3 μ m 100 Å GPC columns and a photodiode array detector. The eluent was chloroform, using

a flow of 1 mL/min and an injection volume of 20 μ L. GPC analysis of the polymer was performed at 80°C on a LC system equipped with a PLgel 5 μ m Mixed-C column and UV and refractive index detectors. The eluent was ODCB, using a flow of 1 mL/min and an injection volume of 20 μ L. Recycling GPC was performed on a LC system equipped with JAIGEL 2H and JAIGEL 2.5H columns and a UV-detector set at 400 nm and 600 nm, using a preparative flow cell (path length 0.5 mm). The eluent was chloroform at 3.5 mL/min, the injection volume was 2 mL. Cyclic voltammograms were recorded in an inert atmosphere with 0.1 M tetrabutyl ammonium hexafluorophosphate (TBAPF₆) in ODCB as supporting electrolyte. The working electrode was a platinum disc (0.2 cm²) and the counter electrode was a silver electrode. The scan speed was 200 mV/s. The samples were measured using an Ag/AgCl reference electrode with Fc/Fc⁺ as an internal standard using a μ Autolab II with a PGSTAT30 potentiostat. PIA spectra were recorded by exciting with a mechanically modulated cw Ar-ion laser ($\lambda = 351$ and 364 nm, 275 Hz) pump beam and monitoring the resulting change in transmission of a tungsten-halogen probe light through the sample (ΔT) with a phase-sensitive lock-in amplifier after dispersion by a grating monochromator and detection, using Si, InGaAs, and cooled InSb detectors. The pump power incident on the sample was typically 25 mW with a beam diameter of 2 mm. The PIA ($\Delta T/T$) was corrected for the photoluminescence, which was recorded in a separate experiment. Photoinduced absorption spectra and photoluminescence spectra were recorded with the pump beam in a direction almost parallel to the direction of the probe beam. The solutions were studied in a 1 mm near-IR grade quartz cell at room temperature, except for the polymer which was studied at 80°C.

Materials Solvents were purchased from Biosolve and used without further purification, unless stated otherwise, THF was distilled over 4 Å molsieves before use. Chemicals were purchased from Acros or Aldrich and used without purification. MP-C₆₀ was obtained from Solenne. *N*-bromosuccinimide (NBS) was recrystallized from water. The synthesis of 2,3-Bis(2'-ethylhexyl)-5,7-bis(3-octylthiophen-2-yl)thieno[3,4-*b*]pyrazine **1** was described in chapter 3. Oxygen and moisture-sensitive reactions were performed under an argon atmosphere.

Monobromo and Dibromo 2,3-bis(2'-ethylhexyl)-5,7-bis-(3-octylthiophen-2-yl)-thieno[3,4-*b*]pyrazine (2, 3) Monomer **1** (433 mg, 0.58 mmol) was dissolved in THF (25 mL). NBS (166 mg, 0.93 mmol) was added at 0°C, in the absence of light. The mixture was stirred overnight, while warming to room temperature. Diethyl ether (100 mL) was added and the mixture was washed with water (3 × 40 mL) and saturated NaCl (2 × 40 mL). The organic phase was dried with MgSO₄ and the solvent was evaporated. The crude product contained a mixture of mono- and dibrominated compounds. The compounds were separated by column chromatography on silica (1:9 dichloromethane/heptane). Two fractions were collected, the first fraction contained dibrominated product **3** (305 mg, 58 %), the second fraction contained monobrominated product **2** (122 mg, 25 %)

Compound 2: ¹H-NMR: δ 7.36(d, J = 5.2 Hz, 1H, Ar-*H*), 7.00 (d, J = 5.2 Hz, 1H, Ar-*H*), 6.94 (s, 1H, ArBr-*H*), 2.96–2.82 (m, 8H, Ar-CH₂-), 2.20 (m, 2H, -CH₂CH(C₄H₉)(C₂H₅)), 1.76–1.66 (m, 4H, -CH₂CH₂C₆H₁₃), 1.55–1.18 (m, 36H, -CH₂-), 0.98–0.83 (m, 18H, -CH₃). ¹³C-NMR: δ 155.94, 155.78, 140.45, 139.97, 131.73,

130.23, 129.33, 126.45, 113.55, 39.43, 37.90, 37.67, 37.52, 32.85, 32.76, 31.89, 30.55, 30.37, 30.04, 29.78, 29.71, 29.53, 29.50, 29.32, 29.28, 28.93, 25.94, 23.13, 22.65, 14.20, 14.15, 14.08, 10.93, 10.89. IR: $\tilde{\nu}_{max}$ (cm^{-1}) 2956, 2923, 2854, 1638, 1521, 1460, 1407, 1378. MALDI-TOF-MS: m/z 826.45 (80%), 827.45 (45), 828.45 (100), 829.45 (100), 830.45, 831.45.

Compound 3: $^1\text{H-NMR}$: δ 6.93 (s, 2H, Ar-H), 2.91–2.82 (m, 8H, Ar-CH₂-), 2.20 (m, 2H, -CH₂CH(C₄H₉)(C₂H₅)), 1.70 (m, 4H, -CH₂CH₂C₆H₁₃), 1.52–1.20 (m, 36H, -CH₂-), 0.98–0.84 (m, 18H, -CH₃). $^{13}\text{C-NMR}$: δ 156.04, 140.20, 137.42, 131.77, 130.00, 122.85, 113.88, 39.39, 37.53, 32.78, 31.90, 30.60, 30.01, 29.73, 29.52, 29.30, 28.91, 25.92, 23.14, 22.67, 14.20, 14.09, 10.94. IR: $\tilde{\nu}_{max}$ (cm^{-1}) 2956, 2923, 2854, 1460, 1427, 1378, 827. MALDI-TOF-MS: m/z 904 (50%), 905 (30), 906.27 (100), 907.27 (55), 908.27 (60), 909.27 (35), 910.26.

Poly(2,3-bis(2'-ethylhexyl)-5,7-bis(3-octylthiophen-2-yl)thieno[3,4-b]pyrazine)

(4) Bis(1,5-cyclooctadiene)nickel(0) (Ni(COD)₂) (91 mg, 0.33 mmol) and 2,2'-bipyridyl (53 mg, 0.33 mmol) were dissolved in dry and oxygen-free toluene (2 mL) and heated to 80°C. Compound **3** (93 mg, 0.10 mmol) was added and the mixture was stirred for 22 h at 80°C. A 1:1:1 methanol/acetone/0.1 M HCl mixture (35 mL) was added and the mixture was stirred for 6 h. The product was extracted with chloroform (2×35 mL), EDTA (disodium salt, 0.5 g) was added and the mixture was stirred overnight. The mixture was washed with water (3×75 mL), concentrated and precipitated in methanol (200 mL). The crude polymer was filtered into a Soxhlet thimble and fractionated by Soxhlet extraction with methanol, hexane, dichloromethane, chloroform, and ODCB. Yield (ODCB-fraction): 32 mg (42%). $^1\text{H-NMR}$: δ 7.15 (Ar-H), 2.93 (Ar-CH₂-), 2.36 (-CH₂CH(C₄H₉)(C₂H₅)), 1.79 (-CH₂CH₂C₆H₁₃), 1.5–1.1 (-CH₂-), 1.1–0.6 (-CH₃). IR: $\tilde{\nu}_{max}$ (cm^{-1}) 3372 (br), 2956, 2923, 2853, 1627, 1517, 1483, 1456, 1377, 1305, 1232, 1179, 1122, 982, 824. GPC (UV-detector, 424 nm): M_n = 12300 g/mol, M_w = 32500 g/mol, PDI = 2.7.

Oligo(2,3-bis(2'-ethylhexyl)-5,7-bis(3-octylthiophen-2-yl)thieno[3,4-b]pyrazine)

(4, n = 2, 3, 4, 5) Monomer **1** (801 mg, 1.07 mmol) was dissolved in THF (10 mL). NBS (238 mg, 1.34 mmol) was added at 0°C, in the absence of light. The mixture was stirred overnight, while warming to room temperature. Diethyl ether (150 mL) was added and the mixture was washed with water (3×50 mL) and saturated NaCl (2×50 mL). The organic phase was dried with MgSO₄ and the solvent was evaporated. The resulting monomer mixture was brought under an argon atmosphere. Ni(COD)₂ (555 mg, 2.02 mmol) and 2,2'-bipyridyl (315 mg, 2.02 mmol) were dissolved in toluene (20 mL) and stirred 0.5 h at 80°C. The Ni(COD)₂/bipyridyl mixture was added to the monomer mixture and stirred at 80°C for 18 h. A 1:1:1 methanol/acetone/0.1 M HCl mixture (300 mL) was added and the mixture was stirred for 1.5 h. The product was extracted with chloroform (2×150 mL), EDTA (disodium salt, 2 g) was added and the mixture was stirred over night. The mixture was washed with water (3×300 mL), concentrated and precipitated in methanol (500 mL). The crude product mixture was filtered into a Soxhlet thimble and fractionated by Soxhlet extraction with methanol, acetone, hexane, dichloromethane, and chloroform. The hexane and dichloromethane extracts were separated by

recycling GPC, yielding pure oligomers. Yields: dimer: 57 mg, trimer: 48 mg, tetramer: 33 mg, pentamer: 6 mg.

Dimer $^1\text{H-NMR}$: δ 7.36 (d, $J=5.2$ Hz, 2H, Ar-H), 7.14 (s, 2H, Ar-H), 7.01 (d, $J=5.2$ Hz, 2H, Ar-H), 2.97 (t, $J=2.7$ Hz, 8H, $-\text{CH}_2\text{C}_7\text{H}_{15}$), 2.87 (m, 8H, $-\text{CH}_2\text{CH}(\text{C}_4\text{H}_9)(\text{C}_2\text{H}_5)$), 2.40–2.30 (m, 2H, $-\text{CH}_2\text{CH}(\text{C}_4\text{H}_9)(\text{C}_2\text{H}_5)$), 2.25–2.15 (m, 2H, $-\text{CH}_2\text{CH}(\text{C}_4\text{H}_9)(\text{C}_2\text{H}_5)$), 1.85–1.65 (m, 8H, $-\text{CH}_2\text{CH}_2\text{C}_6\text{H}_{13}$), 1.56–1.20 (m, 72H, $-\text{CH}_2-$), 1.04–0.84 (m, 36H, $-\text{CH}_3$). IR: $\tilde{\nu}_{\text{max}}$ (cm^{-1}) 3079, 2956, 2922, 2872, 2853, 1516, 1487, 1457, 1377, 1235, 1182, 1122, 823, 813, 712. MALDI-TOF-MS: m/z 1494.61 (90%), 1495.60 (100), 1496.60 (80), 1497.60 (50), 1498.60 (24), 1499.60 (10). GPC: 1 peak at 12.9 min.

Trimer $^1\text{H-NMR}$: δ 7.36 (d, $J=5.2$ Hz, 2H, Ar-H), 7.14 (s, 4H, Ar-H), 7.01 (d, $J=5.2$ Hz, 2H, Ar-H), 3.02–2.94 (m, 12H, $-\text{CH}_2\text{C}_7\text{H}_{15}$), 2.93–2.84 (m, 12H, $-\text{CH}_2\text{CH}(\text{C}_4\text{H}_9)(\text{C}_2\text{H}_5)$), 2.40–2.30 (m, 4H, $-\text{CH}_2\text{CH}(\text{C}_4\text{H}_9)(\text{C}_2\text{H}_5)$), 2.26–2.16 (m, 2H, $-\text{CH}_2\text{CH}(\text{C}_4\text{H}_9)(\text{C}_2\text{H}_5)$), 1.85–1.70 (m, 12H, $-\text{CH}_2\text{CH}_2\text{C}_6\text{H}_{13}$), 1.60–1.20 (m, 108H, $-\text{CH}_2-$), 1.05–0.80 (m, 54H, $-\text{CH}_3$). IR: $\tilde{\nu}_{\text{max}}$ (cm^{-1}) 3079, 2956, 2922, 2871, 2853, 1517, 1485, 1457, 1377, 1350, 1239, 1181, 1122, 824, 813. MALDI-TOF-MS: m/z 2240.93 (55%), 2241.93 (90), 2242.93 (100), 2243.92 (80), 2244.9 (50), 2245.92 (30), 2246.92 (15). GPC: 1 peak at 12.3 min.

Tetramer $^1\text{H-NMR}$: δ 7.36 (d, $J=5.2$ Hz, 2H, Ar-H), 7.15 (m, 6H, Ar-H), 7.01 (d, $J=5.2$ Hz, 2H, Ar-H), 3.04–2.84 (m, 32H, Ar- CH_2-), 2.42–2.30 (m, 6H, $-\text{CH}_2\text{CH}(\text{C}_4\text{H}_9)(\text{C}_2\text{H}_5)$), 2.26–2.16 (m, 2H, $-\text{CH}_2\text{CH}(\text{C}_4\text{H}_9)(\text{C}_2\text{H}_5)$), 1.87–1.70 (m, 16H, $-\text{CH}_2\text{CH}_2\text{C}_6\text{H}_{13}$), 1.60–1.20 (m, 144H, $-\text{CH}_2-$), 1.06–0.82 (m, 72H, $-\text{CH}_3$). IR: $\tilde{\nu}_{\text{max}}$ (cm^{-1}) 3079, 2956, 2922, 2871, 2853, 1731, 1627, 1516, 1484, 1457, 1377, 1351, 1239, 1181, 1122, 824, 813. MALDI-TOF-MS m/z : 2987.58 (33%), 2988.58 (70), 2989.6 (97), 2990.57 (100), 2991.57 (85), 2992.57 (60), 2993.57 (40), 2994.58 (25), 2995.57 (15). GPC: 1 peak at 11.9 min.

Pentamer $^1\text{H-NMR}$: δ 7.36 (d, $J=4.6$ Hz, 2H, Ar-H), 7.15 (m, 8H, Ar-H), 7.01 (d, $J=5.2$ Hz, 2H, Ar-H), 3.04–2.84 (m, 40H, Ar- CH_2-), 2.42–2.30 (m, 8H, $-\text{CH}_2\text{CH}(\text{C}_4\text{H}_9)(\text{C}_2\text{H}_5)$), 2.26–2.16 (m, 2H, $-\text{CH}_2\text{CH}(\text{C}_4\text{H}_9)(\text{C}_2\text{H}_5)$), 1.87–1.70 (m, 20H, $-\text{CH}_2\text{CH}_2\text{C}_6\text{H}_{13}$), 1.60–1.20 (m, 180H, $-\text{CH}_2-$), 1.06–0.82 (m, 90H, $-\text{CH}_3$). IR: $\tilde{\nu}_{\text{max}}$ (cm^{-1}) 3077, 2955, 2922, 2871, 2853, 1516, 1483, 1457, 1377, 1350, 1239, 1180, 1134, 1122, 824, 813. MALDI-TOF-MS: m/z 3735.62 (80%), 3736.60 (100), 3737.60 (98), 3738.49 (90), 3739.44 (70). GPC: 1 peak at 11.6 min.

References and notes

1. Van Mullekom, H. A. M.; Vekemans, J. A. J. M.; Meijer, E. W. *Chem. Eur. J.* **1998**, *4*, 1235–1243.
2. Van Mullekom, H. A. M.; Vekemans, J. A. J. M.; Havinga, E. E.; Meijer, E. W. *Mat. Sci. Eng. R.* **2001**, *32*, 1–40.
3. Ozen, A. S.; Atilgan, C.; Sonmez, G. *J. Phys. Chem. C* **2007**, *111*, 16362–16371.
4. Salzner, U.; Karalti, O.; Durdagi, S. *J. Mol. Model.* **2006**, *12*, 687–701.
5. Wienk, M. M.; Turbiez, M. G. R.; Struijk, M. P.; Fonrodona, M.; Janssen, R. A. J. *Appl. Phys. Lett.* **2006**, *88*, 153511.

6. Yamamoto, T.; Morita, A.; Miyazaki, Y.; Maruyama, T.; Wakayama, H.; Zhou, Z.; Nakamura, Y.; Kanbara, T.; Sasaki, S.; Kubota, K. *Macromolecules* **1992**, *25*, 1214–1223.
7. Meier, H.; Stalmach, U.; Kolshorn, H. *Acta Polym.* **1997**, *48*, 379–384.
8. Rissler, J. *Chem. Phys. Lett.* **2004**, *395*, 92–96.
9. Kuhn, W. *Helv. Chim. Acta* **1948**, *31*, 1780–1799.
10. AMPAC 6.55, Semichem: Shawnee, KS, 1997.
11. Adant, C.; Beljonne, D.; Brédas, J. L. *J. Chem. Phys.* **1994**, *101*, 8048–8054.
12. Cornil, J.; Beljonne, D.; Brédas, J. L. *J. Chem. Phys.* **1995**, *103*, 842–849.
13. Ridley, J.; Zerner, M. *Theor. Chim. Acta* **1973**, *32*, 111–134.
14. Gierschner, J.; Cornil, J.; Egelhaaf, H. J. *Adv. Mater.* **2007**, *19*, 173–191.
15. Beljonne, D.; Cornil, J.; Friend, R. H.; Janssen, R. A. J.; Brédas, J. L. *J. Am. Chem. Soc.* **1996**, *118*, 6453–6461.
16. A similar pattern is obtained at the density functional theory (DFT) level, using the widely used B3LYP functional and a 6–31G* basis set, thus demonstrating the reliability of the semi-empirical approaches.
17. Van Hal, P. A.; Beckers, E. H. A.; Peeters, E.; Apperloo, J. J.; Janssen, R. A. J. *Chem. Phys. Lett.* **2000**, *328*, 403–408.
18. Firey, P. A.; Ford, W. E.; Sounik, J. R.; Kenney, M. E.; Rodgers, M. A. J. *J. Am. Chem. Soc.* **1988**, *110*, 7626–7630.
19. Herkstroeter, W. G.; Merkel, P. B. *J. Photochem.* **1981**, *16*, 331–341.
20. Köhler, A.; Beljonne, D. *Adv. Funct. Mater.* **2004**, *14*, 11–18.
21. Shine, H. J.; Zhao, B. J.; Marx, J. N.; Ould-Ely, T.; Whitmire, K. H. *J. Org. Chem.* **2004**, *69*, 9255–9261.
22. Weller, A. *Z. Phys. Chem. Neue Folge* **1982**, *133*, 93–98.
23. Williams, R. M.; Zwier, J. M.; Verhoeven, J. W. *J. Am. Chem. Soc.* **1995**, *117*, 4093–4099.
24. Van Bolhuis, F.; Wynberg, H.; Havinga, E. E.; Meijer, E. W.; Staring, E. G. *J. Synth. Met.* **1989**, *30*, 381–389.

Chapter 5

Oligomers with double acceptor units and the origins of band gap reduction in alternating thiophene – thienopyrazine oligomers

Abstract In this chapter, experimental and theoretical studies on the optical and electrochemical properties of small band gap oligo(7,7'-bis(thiophen-2-yl)-5,5'-bisthieno[3,4-*b*]pyrazine)s are presented. The oligomers consist of alternating blocks of bithiophene units and bisthienopyrazine units, up to a total length of 16 units. The optical absorptions of the ground state, the triplet excited state, and the corresponding radical cation have been identified and shift to lower energy with increasing chain length. The optical absorption correlates well with quantum chemical calculations and the electrochemical band gap. We show that reduction of the band gap with chain length results from a significant rise of the HOMO level and a moderate reduction of the LUMO energy. Comparison of the chain length dependence of the transition energy at maximum absorption (E_{max}) and of the redox potentials with previously published data on oligothiophenes and the mixed thiophene–thienopyrazine oligomers described in chapters 3 and 4 shows that the reduction of E_{max} is more easily induced by increasing the number of thienopyrazine units than by extending the chain, mainly because thienopyrazine is both a better donor and a better acceptor than thiophene. Strong interactions between neighboring thienopyrazine units, with some possible admixing of quinoid character, are the main cause of the small band gap in these oligomers.

This work has been published: Karsten, B. P.; Viani, L.; Cornil, J.; Gierschner, J.; Janssen, R. A. J. *J. Phys. Chem. A* **2009**, *113*, 10343–10350.

5.1 Introduction

As described in chapter 1, two different strategies exist toward designing and synthesizing small band gap polymers.¹⁻⁴ The first approach relies on creating polymers based on a single monomer unit that, after polymerization, endows the chain with an electronic structure where aromatic (A) and quinoid (Q) resonance structures are close in energy and bond length alternation is decreased or inverted. Classical examples are poly(isothianaphthene) and poly(thienopyrazine).⁵⁻¹⁰ The second approach is based on alternating electron-rich (donor) and electron-deficient (acceptor) monomer units along the chain that cause partial intramolecular charge transfer (ICT) and lead to small band gap semiconducting polymers. Presently, the large majority of small band gap polymers developed for solar cell applications is based on this donor-acceptor approach. Kertesz *et al.*, however, have pointed out on the basis of theoretical considerations that alternating donor-acceptor (DA) copolymers might also be considered as alternating aromatic-quinoid (AQ) copolymers, reflecting that the A units tend to be aromatic in poly-A and the Q units quinoid in poly-Q.³

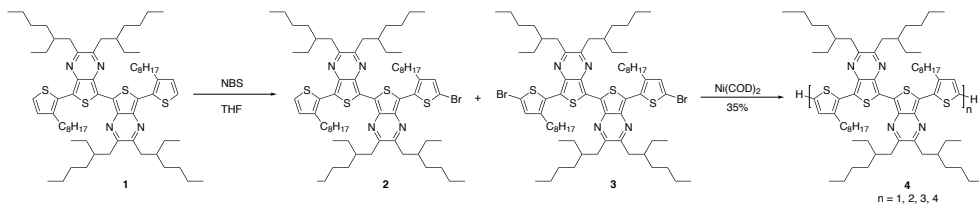
Virtually all small band gap polymers reported to date have a single acceptor unit alternating with more extended donor segments along the chain. In this chapter, we present the synthesis and optical properties of a new series of oligomers comprising two electron-rich thiophene (T) units alternating with two electron-deficient thienopyrazine (TP) units. These (T-TP₂-T)_n oligomers are homologues of the (T-TP-T)_n and T-TP_n-T series presented in chapters 3 and 4. Comparison of the optical and electrochemical signatures of the different series at the experimental and theoretical levels reveals that for these T-TP oligomers donor-acceptor interactions are not the principal reason for the small band gap. The experiments and calculations reveal that the TP unit is both a better donor *and* a better acceptor than T. Hence, for a fixed number of repeat units ($n + m$), the band gap of a T_nTP_m oligomer decreases when n decreases in favor of m .

5.2 Results and discussion

5.2.1 Synthesis

(T-TP₂-T)_n oligomers of different length were synthesized in a one-step procedure outlined in scheme 5.1 and subsequently separated using recycling GPC. The synthesis of the T-TP₂-T monomer (**1**) has been described in chapter 3. Partial bromination using NBS yielded a mixture of monobrominated and dibrominated compounds (**2** and **3**). This mixture was then subjected to a nickel(0)-mediated Yamamoto oligomerization¹¹ in which **2** acts as a chain stopper to provide a mixture of shorter oligomers (**4**) of various lengths. After a first separation of this mixture by Soxhlet extraction, we used recycling GPC to obtain the oligomers in pure form. Recycling GPC is a preparative scale GPC technique, in which the eluted products are fed back into the column, thereby virtually creating a GPC column of very long length, without having the problem of a very high pressure drop. The consecutive oligomers were collected during the repetitive cycles by temporarily switching the recycle valve to the collect position. This technique provides monodisperse, pure oligomers ($n = 1-4$)

as evidenced from MALDI-TOF mass spectrometry, NMR, and FT-IR. The longest oligomer that was isolated in pure form ($n = 4$) has 16 units along the chain.



Scheme 5.1: Synthesis of the oligomers of 2,2',3,3'-tetrakis(2-ethylhexyl)-7,7'-bis(3-octylthiophen-2-yl)-5,5'-bisthieno[3,4-*b*]pyrazine

5.2.2 Optical and electrochemical properties of the neutral oligomers

The $\pi \rightarrow \pi^*$ optical absorption of the (T-TP₂-T)_{*n*} oligomers shifts to longer wavelengths when *n* increases from 1 to 4 (figure 5.1a). Already for $n = 1$ the onset of absorption (λ_{onset}) is outside the visible region of the spectrum. The energies of maximum absorption (E_{max}) and the onsets (E_g^{opt}) in solution are collected in table 5.1.

Table 5.1: UV/vis/NIR absorption data in toluene and onset of redox potentials (E_{ox} and E_{red} , vs. Fc/Fc⁺) in ODCB for the oligomers.^a

<i>n</i>	neutral oligomers									radical cations	
	λ_{max} (nm)	E_{max} (eV)	λ_{onset} (nm)	E_g^{opt} (eV)	E_{ox} (V)	E_{red} (V)	E_g^{CV} (eV)	$E_g^{CV} - E_g^{opt}$ (eV)	$T_n \leftarrow T_1$ (eV)	$D_2 \leftarrow D_0$ (eV)	$D_1 \leftarrow D_0$ (eV)
1	629	1.97	756	1.64	-0.08	-1.78	1.70	0.06		1.58	0.96
2	736	1.68	882	1.41	-0.26	-1.69	1.43	0.02	1.22	0.93	0.52
3	775	1.60	948	1.31	-0.35	-1.68	1.33	0.02	1.18	0.83	0.48
4	792	1.57	975	1.27	-0.39	-1.67	1.28	0.01	0.01	0.83	0.46

^a $T_n \leftarrow T_1$ absorption in toluene. $D_2 \leftarrow D_0$ and $D_1 \leftarrow D_0$ absorptions of the radical cations in benzonitrile.

The optical band gap (E_g^{opt}) of the (T-TP₂-T)_{*n*} oligomers is plotted versus $1/n$ in figure 5.2a. To describe the dispersion of the optical band gap with chain length we have used an empirical relation that accounts for the leveling off of the curve at longer chain lengths:¹²

$$E(n) = E_\infty + (E_1 - E_\infty) \exp[-a(n - 1)] \quad (5.1)$$

In this relation, E_1 and E_∞ are the excitation energies for the monomer and the (infinitely long) polymer, n is the number of repeat units, and a is a parameter that describes how fast $E(n)$ saturates to E_∞ . Fitting the optical band gaps E_g^{opt} of the oligomers to equation 5.1 yields $E_\infty = 1.24$ eV, $E_1 = 1.64$ eV, and $a = 0.85$. From the value of a , it follows that 99% of the band gap reduction will be completed at about six repeat units, similar to the conversion of the (T-TP-T)_{*n*} series of oligomers.

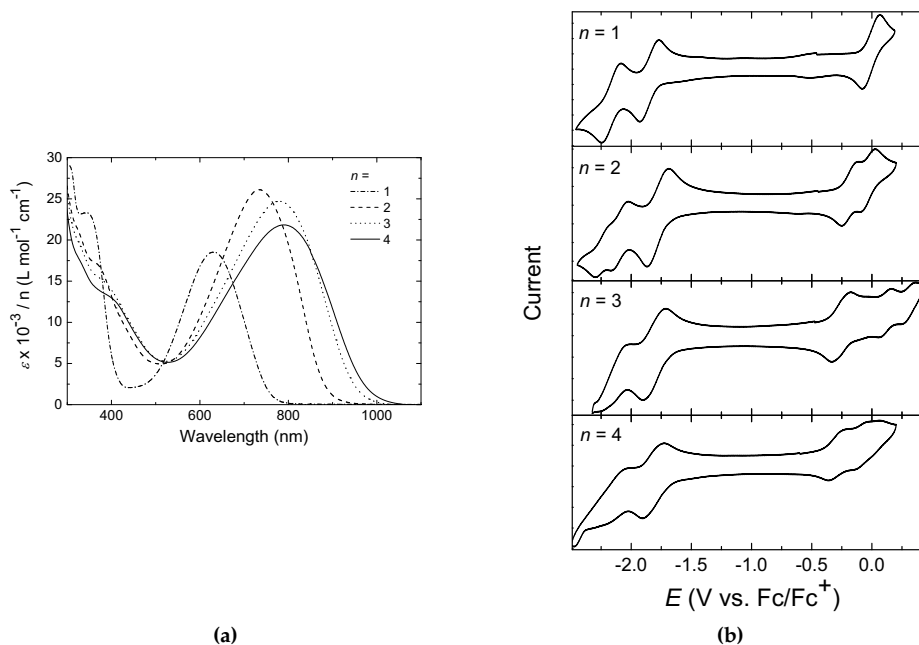


Figure 5.1: (a) UV/vis/NIR absorption spectra of the $(T-TP_2-T)_n$ oligomers in toluene, given in molar extinction coefficients per repeating unit. (b) Cyclic voltammograms of the oligomers in ODCB.

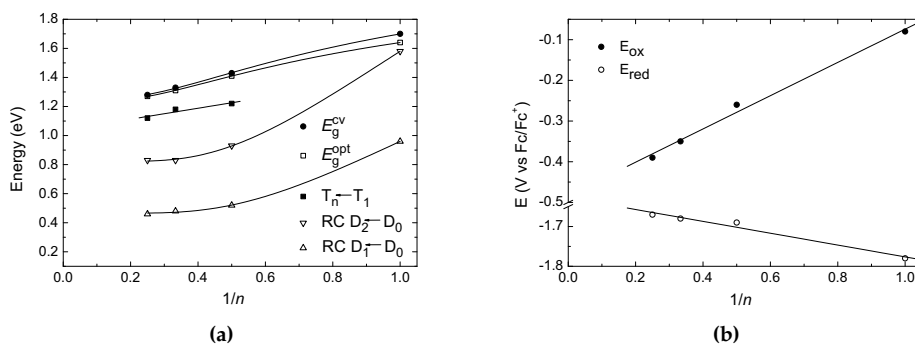


Figure 5.2: (a) Chain length dependence of the energies for the optical and electrochemical band gap, the triplet $T_n \leftarrow T_1$ absorption, and the radical cation absorptions ($D_1 \leftarrow D_0$ and $D_2 \leftarrow D_0$) vs. reciprocal chain length ($1/n$) for the $(T-TP_2-T)_n$ oligomers. (b) Onsets of oxidation and reduction vs. $1/n$. Fits of the data are to equation 5.1 for the band gaps and the radical cation absorption; other data are fitted to a linear relation with $1/n$.

The cyclic voltammograms recorded for each of the four (T-TP₂-T)_n oligomers dissolved in ODCB (figure 5.1b) reveal one or more quasi reversible oxidation and reduction waves. Oxidation of the oligomers occurs at rather low potentials, even below 0 V *vs.* Fc/Fc⁺. From the relative intensities of the oxidation and reduction waves in the voltammogram, it can be seen that, for the longer oligomers ($n > 1$), the first reduction wave corresponds to a multi electronic process. The same holds for the first oxidation wave when $n > 2$.

The potentials at the onsets of the redox waves (E_{ox} and E_{red}) have been used to estimate the electrochemical band gap ($E_g^{CV} = E_{ox} - E_{red}$) (table 5.1). These onsets were determined as the crossing of the tangents to the baseline and the redox wave in its inflection point. The electrochemical band gap, E_g^{CV} , is slightly larger than the optical band gap, E_g^{opt} , but decreases in a similar fashion with chain length. Apart from experimental uncertainties, the difference between E_g^{opt} and E_g^{CV} reflects the fact that free ions are created and solvated in the electrochemical experiment rather than a neutral exciton under optical excitation. E_g^{opt} and E_g^{CV} increase almost linearly with the reciprocal chain length ($1/n$) (figure 5.2a). Figure 5.2b shows that the oxidation and reduction potentials change almost linearly with $1/n$ in the range studied. This figure shows furthermore, that the decrease in the electrochemical band gap is mainly (for ~75 %) due to a lowering of the oxidation potential, because the change of reduction potentials with chain length is much less pronounced. The same has been observed for the (T-TP-T)_n oligomers that contain only one TP unit per two T units (see chapter 4). Compared to (T-TP-T)_n, the (T-TP₂-T)_n series has a lower oxidation and lower reduction potential. This is maybe somewhat unexpected because lowering of the oxidation potential, with increasing number of TP acceptor units, implies that they also have significant donor characteristics; this is actually supported by the delocalized character of the HOMO level suggested by the calculations (see section 5.2.5). On the other hand, the interaction between the acceptor parts of the molecule is less pronounced due to their localized character.

5.2.3 Triplet states of the neutral oligomers

Direct excitation of the (T-TP₂-T)_n oligomers in toluene did not produce any detectable amount of the corresponding triplet states using near steady-state photoinduced absorption (PIA). The triplet states for $n > 1$, however, could readily be populated and studied using a fullerene derivative ([6,6]-phenyl-C₆₁-butyric acid methyl ester, PCBM) as triplet sensitizer.¹³ PCBM has a very high quantum yield for triplet formation after absorbing a photon. In a toluene solution the triplet excited PCBM can transfer its energy to the (T-TP₂-T)_n oligomer, producing the corresponding triplet state. The PIA spectra recorded for mixtures of the oligomer (0.1 mM) and PCBM (0.4 mM) in toluene with excitation at 351 and 364 nm are shown in figure 5.3a. Although the signals are rather weak, the $T_n \leftarrow T_1$ absorption peak clearly shifts to lower energy with increasing n . For the monomer, the triplet state is not observed in this experiment. Instead, for $n = 1$ the PIA spectrum is characteristic for that of the triplet state of PCBM with a peak at 1.78 and a shoulder at 1.52 eV.¹⁴ This signal can also be observed in the PIA spectra of the other oligomers and overlaps with the bleaching band of the ground state absorption. The $T_n \leftarrow T_1$ absorption maximum

for the three longer oligomers ($n = 2-4$) is plotted versus $1/n$ in figure 5.2a. Because the data is limited to only three points, only a linear fit has been made, which suggests that the $T_n \leftarrow T_1$ absorption for the polymer would be located around 1.05 eV.

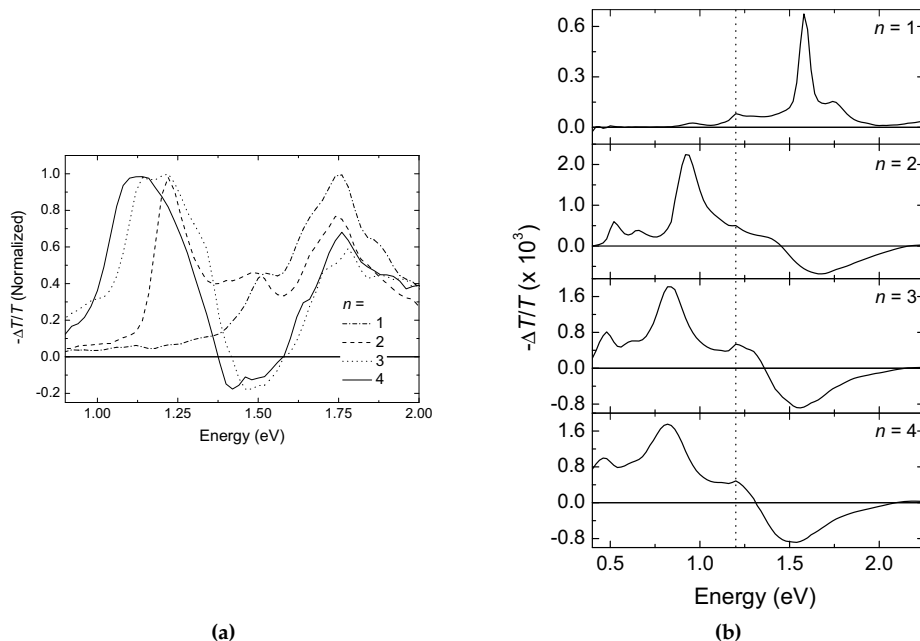


Figure 5.3: PIA spectra of the mixtures of the $(T-TP_2-T)_n$ oligomers (0.1 mM) and PCBM (0.4 mM) dissolved in toluene (a) and benzonitrile (b), recorded at room temperature with excitation at 351 and 364 nm. The vertical dotted line in panel b indicates the position of the PCBM radical anion.

5.2.4 Radical cations of the oligomers

When using PCBM as a triplet sensitizer in PIA experiments, the polarity of the solvent is an important parameter for the outcome of the reaction. As shown in section 5.2.3, in an apolar solvent like toluene ($\epsilon_r = 2.4$) the T_1 state of PCBM can transfer its triplet excitation energy to the oligomer. However, as PCBM is also an electron acceptor in the triplet state, the same experiment can also result in an electron transfer reaction between PCBM and the oligomer, producing the radical cation of the latter and the PCBM radical anion. Electron transfer is favored in more polar solvents (*e.g.* in benzonitrile, $\epsilon_r = 25.9$), because the solvent may stabilize the charge-separated state solvation and screening of the ions. The discrimination between the two processes can be described by the Weller equation in terms of the free energy for

charge separation (ΔG_{CS}):¹⁵

$$\Delta G_{CS} = e(E_{ox}(D) - E_{red}(A)) - E_{00} - \frac{e^2}{4\pi\epsilon_0\epsilon_s R_{cc}} - \frac{e^2}{8\pi\epsilon_0} \left(\frac{1}{r^+} + \frac{1}{r^-} \right) \left(\frac{1}{\epsilon_{ref}} - \frac{1}{\epsilon_s} \right) \quad (5.2)$$

In this equation $E_{ox}(D)$ and $E_{red}(A)$ represent the redox potentials of the donor (oligomer) and acceptor (PCBM, $E_{red}(A) = -1.08$ V *vs.* Fc/Fc⁺),¹⁶ E_{00} is the energy of the photoexcited state (1.50 eV for the triplet level of fullerene derivatives like PCBM),¹⁷ and R_{cc} is the center-to-center distance of the positive and negative charges (set to infinity for intermolecular charge transfer), r^+ and r^- are the radii of the positive and negative ions, and ϵ_{ref} and ϵ_s are the relative permittivities of the reference solvent (used to measure oxidation and reduction potentials) and the solvent in which is measured. r^- is calculated in literature to be 5.6 Å for C₆₀, based on the density of C₆₀.¹⁷ r^+ can be estimated using a similar approach, using a density of 1.5 g/cm³, the value for unsubstituted terthiophene.¹⁸ This calculation for the different oligomers yields the values given in table 5.2. On the basis of these data, we expect triplet absorptions in toluene, as observed (figure 5.3a), but photoinduced electron transfer in benzonitrile (figure 5.3b).

Table 5.2: Free energies for charge separation based on equation 5.2

n	E_{ox}^0 (ODCB) (V <i>vs.</i> Fc/Fc ⁺)	r^+ (Å)	ΔG_{CS} (eV)	
			toluene	benzonitrile
1	0	4.86	0.47	-0.59
2	-0.18	6.13	0.19	-0.75
3	-0.25	7.01	0.07	-0.81
4	-0.28	7.72	0.01	-0.83

The PIA spectra of (T-TP₂-T)_n-PCBM mixtures dissolved in benzonitrile (figure 5.3b) show two absorption peaks due the radical cation of the oligomer and a bleaching band at of the neutral compound at higher energy. In each of the spectra a weak band at 1.20 eV signifies the presence of the PCBM radical anion.¹³ The two absorption bands of the doublet-state radical cations correspond to dipole-allowed D₁ ← D₀ and D₂ ← D₀ transitions and result from electron excitations from HOMO → SOMO (singly occupied molecular orbital) and SOMO → LUMO. The transition energies of these bands (table 5.1, figure 5.2a) have been fitted to equation 5.1 to give $E_{\infty} = 0.82$ eV, $E_1 = 1.58$ eV, and $a = 1.97$ for the D₂ ← D₀ band and $E_{\infty} = 0.47$ eV, $E_1 = 0.96$ eV, and $a = 2.18$ for the D₁ ← D₀ band. The high values for a indicate a much faster saturation of the transition energies for the radical cation than for the absorption bands of the neutral molecule. Hence, the optical transitions are likely to be more localized in the radical cation than in the neutral molecule.

5.2.5 Chain length dependence in related systems

To obtain more insight into the effects that determine the band gap in thiophene-thieno[3,4-*b*]pyrazine-based donor-acceptor systems, the chain length dependence

of the maximum of absorption, E_{max} , and the redox potentials of the $(T-TP_2-T)_n$ series can be compared with data for related systems: T_n ,^{19,20} the $(T-TP-T)_n$ series (chapter 4), $T-TP_3-T$ (chapter 3), poly- T_n , and poly- TP_n .¹⁰ To be able to compare these different systems, we use the total number of rings N in the main chain as the common parameter. Figure 5.4 shows E_{max} , E_{ox} , and E_{red} versus $1/N$, as well as the calculated vertical transition energies E_{vert} and the calculated HOMO and LUMO levels for the different series (table 5.3).^{*} There is a fairly good agreement between the experimental E_{max} and calculated optical transitions E_{vert} , especially for the evolution with chain length N . Differences in the absolute positions might arise from the thermal population of torsion modes, which are neglected in the calculations,²¹ and from the neglect of solvent effects. The large HOMO–LUMO gaps provided by the INDO method are due to a conjunction between the inherent parametrization of ZINDO, the assumption of Koopmans’ theorem in the calculations, and the neglect of solvent effects. In any case, the evolution of the energies of the occupied or unoccupied levels among the different series is reliable with this theoretical approach.

Table 5.3: Calculated vertical transition energies (E_{vert}) and HOMO and LUMO energies *vs.* vacuum for T_n , $(T-TP-T)_n$, $(T-TP_2-T)_n$, and $(T-TP_3-T)_n$.

n	T_n			$(T-TP-T)_n$			$(T-TP_2-T)_n$			$(T-TP_3-T)_n$		
	E_{vert} (eV)	HOMO (eV)	LUMO (eV)	E_{vert} (eV)	HOMO (eV)	LUMO (eV)	E_{vert} (eV)	HOMO (eV)	LUMO (eV)	E_{vert} (eV)	HOMO (eV)	LUMO (eV)
1				2.67	-6.96	-0.57	2.17	-6.49	-0.94	1.84	-6.22	-1.12
2	3.94	-9.29	1.38	2.30	-6.66	-0.75	1.91	-6.30	-1.05	1.68	-6.09	-1.18
3	3.35	-8.19	0.33	2.11	-6.56	-0.82	1.82	-6.23	-1.09	1.61	-6.05	-1.20
4	3.04	-7.77	-0.09	2.04	-6.51	-0.85	1.76	-6.20	-1.10			
5	2.87	-7.56	-0.31	2.01	-6.49	-0.87						
6	2.75	-7.44	-0.44									
9	2.58	-7.37	-0.52									
12	2.51	-7.27	-0.64									
14	2.48	-7.22	-0.71									
23	2.43	-7.19	-0.74									

From figure 5.4 it is clear that the curvature of E_{max} (and its calculated equivalent E_{vert}) with $1/N$ is virtually identical for simple oligothiophenes (T_n) and for alternating $(T-TP-T)_n$ and $(T-TP_2-T)_n$ donor–acceptor systems. On the other hand, when comparing the $T-TP_n-T$ monomers ($n=0-3$) in the graphs (dashed line) it is evident that increasing the amount of thienopyrazine in the acceptor blocks causes a very strong reduction of E_{max} . The influence of adding one extra thienopyrazine unit to the repeat unit is almost as large as the total reduction in E_{max} upon going from one repeat unit to the polymer. This is further illustrated in figure 5.5, which shows E_{max} and E_g^{opt} for the polymers as a function of the fraction of TP units in the chain. The proportionality is much stronger than a simple linear relation such that already a fraction of $\sim 20\%$ thienopyrazine units is responsible for half the band gap reduction.

If the band gap reduction with increasing acceptor block size would be purely

^{*}The calculations were performed by L. Viani at the university of Mons–Hainaut.

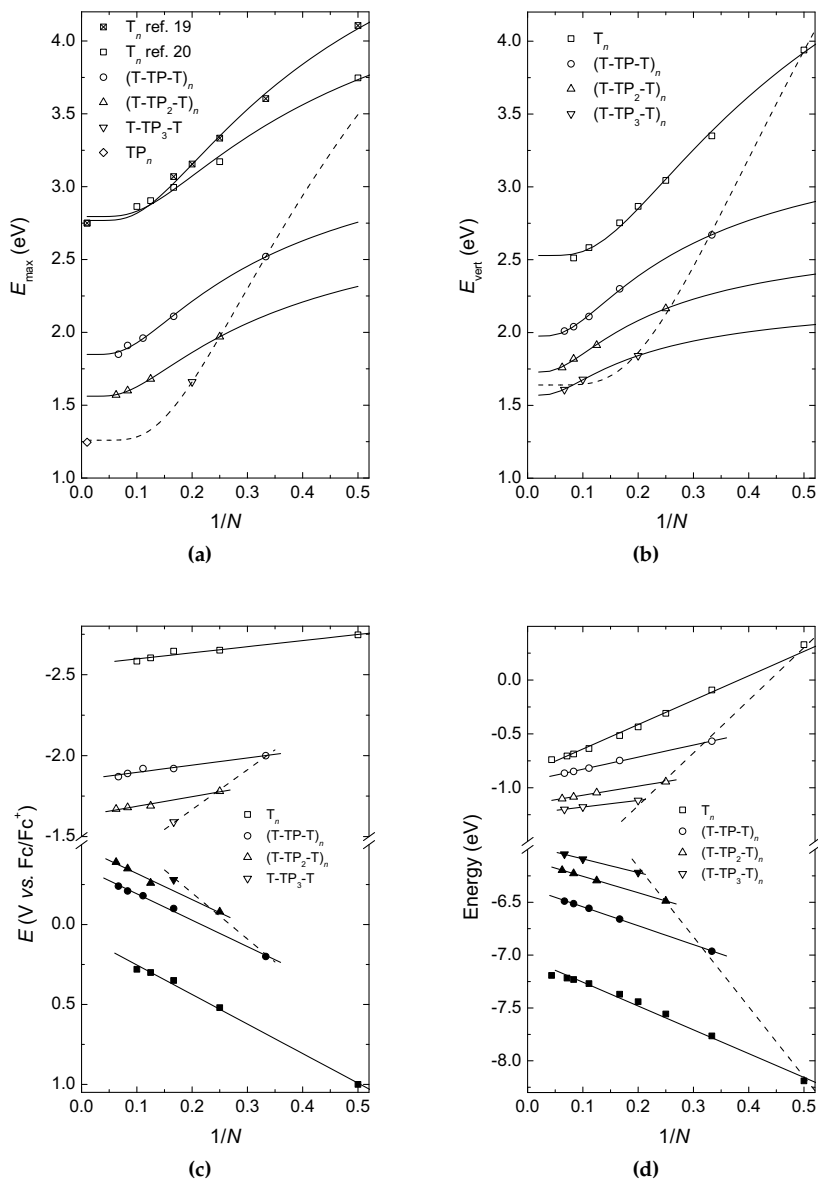


Figure 5.4: Experimental and calculated optical and electrochemical data for T_n , $(T-TP-T)_n$, $(T-TP_2-T)_n$, $(T-TP_3-T)_n$, and TP_n versus the inverse number of aromatic units. (a) Experimental E_{max} . (b) Calculated E_{vert} . (c) Experimental E_{ox} (solid markers) and E_{red} (open markers). (d) Calculated HOMO (solid markers) and LUMO (open markers) levels. Experimental data for T_n are from refs 19 and 20, for $(T-TP-T)_n$ from chapter 4, for $T-TP_3-T$ from chapter 3, and for TP_n from ref 10. Lines in graphs a and b are according to equation 5.1, and those in graphs c and d assume a linear relation. The redox potentials are given as the onset of oxidation or reduction, except for the T_n series, where E_0 was taken for the oxidation potential and the reduction potential was estimated by subtracting E_{max} from this value.

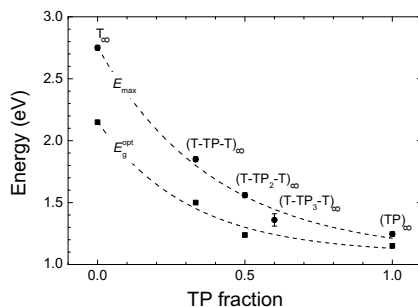


Figure 5.5: Experimental (T_n and TP_n) and extrapolated $(T-TP_x-T)_n$ values of E_{max} and E_g^{opt} for the polymers ($n = \infty$) versus the TP fraction in the chain. The value of $(T-TP_3-T)_\infty$ was estimated from the five-ring oligomer by extrapolating to $n = \infty$, using the chain length dependence found for $(T-TP_2-T)_n$ in figure 5.4a.

based on donor–acceptor effects, localization of both HOMO and LUMO on the respective donor and acceptor units will inevitably lead to smaller orbital coefficients on the atoms connecting the different units when the donor or acceptor blocks become larger. This effect would lead to a reduction of the chain length dependence and significantly reduce the slope of the curves of the HOMO–LUMO gap and E_{max} , when the thienopyrazine segment size increases. The absence of clear donor–acceptor character in these thienopyrazine oligomers originates from the fact that, according to the calculations, the thienopyrazine units are both a better electron acceptor *and* a better electron donor than thiophenes. This contrasts other more classical acceptor systems, like thiophene-*S,S*-dioxide, where mainly the LUMO levels are influenced by changing the acceptor content and donor character is absent.^{22,23} The donor character of thienopyrazine increases the delocalization of the HOMO and increases the chain length dependence of the band gap and E_{max} .² In fact, the delocalization of the HOMO level in T–TP systems is helpful because otherwise there would be, within a one-electron picture, no transition dipole moment between HOMO(D) and LUMO(A), and hence no significant absorption at low energy.

Figure 5.4c,d shows that for a fixed number of repeat units ($N = n + m$), the oxidation potential of a T_n-TP_m oligomer decreases when n decreases in favor of m . The lowering of the oxidation potential with increasing number of TP units implies that the T–TP systems are per se not “real” DA systems. For a DA system the HOMO of D should be well above that of A. We have calculated the frontier orbital levels of the T and TP monomers and of the T–T, T–TP, and TP–TP dimers (figure 5.6). It can be seen that while the concept works for the LUMO, it completely fails for the HOMO, due to the fact that the HOMO of T is lower than that of TP. Hence, T–TP has a lower HOMO than TP–TP and it is not a real DA pair. Hence, TP is a better donor and acceptor than T, and by admixing TP in the polymer, the lowest band gap is found for pure poly-TP and not for a mixed T_n-TP_m compound.

To explain the smaller band gap with increasing TP fraction, admixing of quinoid character into the ground state can be considered.³ By adding more thienopyrazine units, the quinoid character may increase and the band gap would decrease to ultimately reach the value for poly(thieno[3,4-*b*]pyrazine). We note that the band

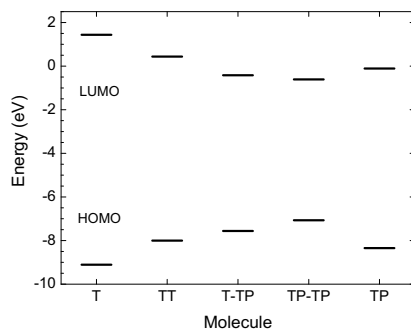


Figure 5.6: Calculated HOMO and LUMO levels of the monomers (T, TP) and dimers (T-T, T-TP, TP-TP).

gap for poly(thieno[3,4-*b*]pyrazine) is smaller than for any of the mixed thiophene–thienopyrazine systems and that poly(thieno[3,4-*b*]pyrazine) and related compounds like poly(isothianaphthene) are known to possess a quinoid ground state.^{24–27}

To investigate the possibility of quinoid character in the oligomers upon adding thienopyrazine units to the acceptor block, we compared the calculated bond length alternation (BLA) in T-TP₃-T with the BLA calculated for quinquethiophene (5T). The data are depicted in figure 5.7. From this graph, it can be seen that the bond length alternation inside the rings is around the value for 5T. The BLA in the connecting bonds in T-TP₃-T, however, is about half the value of 5T. If a quinoid resonance form would be the reason for the band gap reduction in these systems, both inter-ring bond length alternation and the alternation within the rings would be reduced, which is clearly not the case here. Hence, although the inter-ring bonds do indicate some admixing of quinoid character to T-TP₃-T, the bond length alternation is not necessarily quinoid. The strong reduction of the inter-ring bond lengths indicates a stronger interaction and bonding between the thienopyrazine moieties than between the thiophene rings. All together, the theoretical results demonstrate that the introduction of extra thienopyrazine rings does not induce significant geometric distortions, thus suggesting that the acceptor segments are too short to accommodate a fully developed quinoid structure. This is further supported by the fact that the lowest optical transition of a model oligothiophene segment, where the BLA pattern characteristic of the (T-TP₂-T)_{*n*} polymer was imposed, is only reduced by 0.06 eV compared to a regular oligothiophene.

The result that the interaction between neighboring thienopyrazine rings is more important than simple donor–acceptor effects is also supported by the electrochemistry data, depicted in figure 5.4c, and the calculated HOMO and LUMO levels for the different series, depicted in figure 5.4d. From these graphs it is clear that, for all series investigated (no, one, two, or three thienopyrazine units used as acceptor block), the chain length dependence is almost the same, the reduction of the band gap largely being caused by a rise of the HOMO level (reflected in a lowering of the oxidation potential) and to a lesser extent by a lowering of the LUMO level (lower reduction potential). The similar evolution and reduction of the oxidation potential

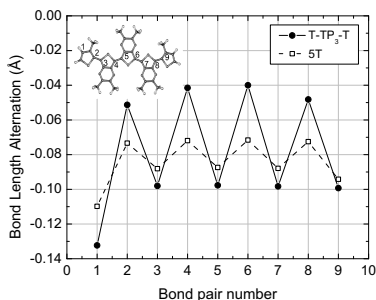


Figure 5.7: Calculated bond length alternation for T-TP₃-T and 5T. The even bond pair numbers describe the bond length difference between the single bond that connects two thiophene rings with a double bond. The odd bond pair numbers describe the bond length difference between a single and double bond in a ring.

in all series point to a delocalization of the HOMO over the entire molecule, also in the systems with high acceptor content, as supported by the theoretical calculations. This leads again to the conclusion that the donor character of the thienopyrazine moiety is important. At the same time, increasing the amount of thienopyrazine units in the repeating unit leads to an almost equal change in the oxidation and reduction potentials, meaning that the lowering of the LUMO level is accompanied by a concomitant rise of the HOMO level. This is contradictory to expectations based on a simple donor-acceptor approach, where the HOMO is located mainly on the donor part of the molecule and increasing the number of thienopyrazines would mainly affect the LUMO, leaving the HOMO unaltered.

5.3 Conclusions

A homologous series of well-defined, small band gap (T-TP₂-T)_n oligomers containing alternating blocks of two thiophene and two double thienopyrazine units has been prepared. The optical and electrochemical band gaps decrease with increasing chain length, leading to an extrapolated value of ~ 1.25 eV for the polymer. The absorption spectra of the triplet state and radical cations of these oligomers have been investigated by photoinduced absorption spectroscopy using triplet sensitization and electron transfer, employing excitation of a fullerene derivative (PCBM) in toluene and benzonitrile, respectively. The $T_n \leftarrow T_1$ absorptions shift to lower energy when going from dimer to tetramer, thereby showing the same trend as the $S_1 \leftarrow S_0$ absorption. In the more polar benzonitrile, electron transfer rather than energy transfer takes place, yielding the radical cation of the oligomers, as expected on the basis of calculations. Again, the optical transitions shift to lower energy as the oligomer length increases.

Comparison of the optical and electrochemical data with E_{max} and redox potentials of closely related T_n , (T-TP-T)_n, and T-TP₃-T, as well as the calculated E_{vert} and frontier orbital levels for the different series, leads to the conclusion that, in these thiophene-thienopyrazine systems, the reduction of the band gap cannot be

explained by simple donor–acceptor effects because the conjugation length dependence of E_{max} and the redox potentials for simple oligothiophenes and systems with one or two thienopyrazine units per repeating unit are all rather similar when plotted versus $1/N$. In these conjugated chains, the thienopyrazine unit is in fact rather electron-rich (poly-TP has a lower oxidation potential than poly-T) and has a tendency to provide the chain with a small quinoid-like character. The reduction of the band gap in polymers consisting of alternating thiophene and thienopyrazine blocks must therefore be attributed to the pronounced donor *and* acceptor character of thienopyrazine units and the strong interactions between neighboring thienopyrazine units, possibly with some admixing of quinoid character to the ground state.

5.4 Experimental

General methods NMR spectra were recorded in CDCl_3 on a 400 MHz NMR (Varian Mercury, 400 MHz for ^1H -NMR and 100 MHz for ^{13}C -NMR), chemical shifts are reported in ppm downfield from tetramethylsilane (TMS). IR spectra were recorded on a Perkin Elmer 1600 FT-IR. Matrix-assisted laser desorption ionization time-of-flight (MALDI-TOF) mass spectrometry was performed on a PerSeptive Biosystems Voyager–DE PRO spectrometer. UV/vis spectra were recorded on a Perkin Elmer Lambda 900 UV/vis/NIR spectrometer. Recycling GPC was performed on a LC system equipped with JAIGEL 2H and JAIGEL 2.5H columns and a UV-detector, using a preparative flow cell (path length 0.5 mm). The eluent was chloroform at 3.5 mL/min, the injection volume was 2 mL. Cyclic voltammograms were recorded in an inert atmosphere with 0.1 M tetrabutyl ammonium hexafluorophosphate (TBA-PF₆) in ODCB as supporting electrolyte. The working electrode was a platinum disc (0.2 cm²) and the counter electrode was a silver electrode. The samples were measured using an Ag/AgCl reference electrode with Fc/Fc⁺ as an internal standard using a μ Autolab II with a PGSTAT30 potentiostat at a scan speed of 200 mV/s. PIA spectra were recorded by exciting with a mechanically modulated cw Ar-ion laser ($\lambda = 351$ and 364 nm, 275 Hz) pump beam and monitoring the resulting change in transmission of a tungsten-halogen probe light through the sample (ΔT) with a phase-sensitive lock-in amplifier after dispersion by a grating monochromator and detection, using Si, InGaAs, and cooled InSb detectors. The pump power incident on the sample was typically 25 mW with a beam diameter of 2 mm. The PIA ($\Delta T/T$) was corrected for the photoluminescence, which was recorded in a separate experiment. Photoinduced absorption spectra and photoluminescence spectra were recorded with the pump beam in a direction almost parallel to the direction of the probe beam. The solutions were studied in a 1 mm near-IR grade quartz cell at room temperature.

Theoretical calculations Quantum-chemical calculations were performed to investigate the electronic and optical properties of the oligomers at a theoretical level. The quantum-chemical methods used in this work have been described and motivated in detail in chapter 4. Briefly it entails the following approach and approximations: (1) the conjugated backbone was imposed to be planar and the long alkyl side chains were replaced by methyl groups to minimize the computational efforts;

(2) the ground-state molecular geometries were optimized by the MNDO (Modified Neglect of Differential Overlap) method, as implemented in the AMPAC package;²⁸ (3) the electronic structure was calculated with the INDO (Intermediate Neglect of Differential Overlap) method, as parameterized by Zerner and co-workers, and using the Ohno-Klopman potential.²⁹ (4) the INDO results were coupled to a Single Configuration Interaction (SCI) scheme including all $\pi \rightarrow \pi^*$ transitions to calculate the vertical transition energy (E_{ver}^{cal}) between the ground and lowest excited states ($S_1 \leftarrow S_0$).

Materials Solvents were purchased from Biosolve and used without further purification, unless stated otherwise. THF was distilled over 4 Å molsieves before use. Chemicals were purchased from Acros or Aldrich and used without purification. PCBM was obtained from Solenne. The synthesis of 2,2',3,3'-tetrakis(2-ethylhexyl)-7,7'-bis(3-octylthiophen-2-yl)-5,5'-bithieno[3,4-*b*]pyrazine (**1**) was described in chapter 3. Oxygen and moisture-sensitive reactions were performed under an argon atmosphere.

Oligo(2,2',3,3'-tetrakis(2-ethylhexyl)-7,7'-bis(3-octylthiophen-2-yl)-5,5'-bithieno[3,4-*b*]pyrazine) (4**, *n* = 2, 3, 4)**

Monomer **1** (505 mg, 0.46 mmol) was dissolved in THF (20 mL). *N*-bromosuccinimide (89 mg, 0.50 mmol) was added at 0°C, in the absence of light. The mixture was stirred overnight, while warming to room temperature. Diethyl ether (100 mL) was added and the mixture was washed with water (3×50 mL) and saturated NaCl (2×50 mL). The organic phase was dried with MgSO₄ and the solvent was evaporated. The resulting monomer mixture (**2** + **3**) was brought under an argon atmosphere. Ni(COD)₂ (280 mg, 1.02 mmol) and 2,2'-bipyridyl (149 mg, 0.95 mmol) were dissolved in toluene (15 mL) and stirred for 0.5 h at 80°C. The Ni(COD)₂/bipyridyl mixture was added to the monomer mixture and stirred at 80°C for 21 h. A 1:1:1 methanol/acetone/0.1 M HCl mixture (200 mL) was added and the mixture was stirred for 1 h. The product was extracted with chloroform (2×100 mL), EDTA (disodium salt) (1.6 g) was added and the mixture was stirred for 3 h. The mixture was washed with water (3×200 mL), concentrated and precipitated in methanol (300 mL). The crude product mixture was filtered into a Soxhlet thimble and fractionated by Soxhlet extraction with methanol, hexane, and dichloromethane. The hexane and dichloromethane extracts were separated by recycling GPC, yielding pure oligomers. Yields: monomer: 10 mg, dimer: 80 mg, trimer: 68 mg, tetramer: 21 mg.

Dimer ¹H-NMR: δ 7.38 (s, 2H, Ar-*H*), 7.19 (s, 2H, Ar-*H*), 7.04 (s, 2H, Ar-*H*), 3.10 (m, 8H, -CH₂C₇H₁₅), 3.00–2.86 (m, 16H, -CH₂CH(C₄H₉)(C₂H₅)), 2.45–2.20 (m, 8H, -CH₂CH(C₄H₉)(C₂H₅)), 1.90–1.72 (m, 8H, -CH₂CH₂C₆H₁₃), 1.62–1.18 (m, 104H, -CH₂-), 1.07–0.81 (m, 60H, -CH₃). IR: $\tilde{\nu}_{max}$ (cm⁻¹) 2956, 2923, 2855, 1486, 1440, 1377, 1352, 1239, 1181, 1138, 1121, 826, 802, 725, 701. MALDI-TOF-MS: *m/z* 2211.11 (60%), 2212.10 (95), 2213.10 (100), 2214.09 (80), 2215.08 (50), 2216.08 (30), 2217.07 (15).

Trimer ¹H-NMR: δ 7.38 (d, *J* = 5.1 Hz, 2H, Ar-*H*), 7.19 (s, 4H, Ar-*H*), 7.04 (d, *J* = 5.2 Hz, 2H, Ar-*H*), 3.16–3.05 (m, 12H, -CH₂C₇H₁₅), 3.02–2.87 (m, 24H, -CH₂CH(C₄H₉)(C₂H₅)), 2.45–2.20 (m, 12H, -CH₂CH(C₄H₉)(C₂H₅)), 1.92–1.72 (m, 12H, -CH₂CH₂C₆H₁₃), 1.60–1.20 (m, 156H, -CH₂-), 1.07–0.80 (m, 90H, -CH₃). IR: $\tilde{\nu}_{max}$ (cm⁻¹) 2956, 2923, 2855, 1485, 1457, 1440, 1377, 1351, 1247, 1181, 1137, 1121,

825, 802, 724, 699. MALDI-TOF-MS: m/z 3315.56 (35%), 3316.55 (70), 3317.55 (95), 3318.55 (100), 3319.54 (85), 3320.55 (60), 3321.55 (45), 3322.57 (30).

Tetramer $^1\text{H-NMR}$: δ 7.38 (d, $J=5.0$ Hz, 2H, Ar-H), 7.19 (s, 6H, Ar-H), 7.04 (d, $J=4.9$ Hz, 2H, Ar-H), 3.17–3.06 (m, 16H, $-\text{CH}_2\text{C}_7\text{H}_{15}$), 3.02–2.86 (m, 32H, $-\text{CH}_2\text{CH}(\text{C}_4\text{H}_9)(\text{C}_2\text{H}_5)$), 2.46–2.20 (m, 16H, $-\text{CH}_2\text{CH}(\text{C}_4\text{H}_9)(\text{C}_2\text{H}_5)$), 1.92–1.73 (m, 16H, $-\text{CH}_2\text{CH}_2\text{C}_6\text{H}_{13}$), 1.64–1.20 (m, 208H, $-\text{CH}_2-$), 1.07–0.80 (m, 120H, $-\text{CH}_3$). IR: $\tilde{\nu}_{\text{max}}$ (cm^{-1}) 2956, 2923, 2854, 1485, 1457, 1440, 1377, 1350, 1250, 1181, 1137, 1121, 1097, 825, 802, 724. MALDI-TOF-MS: m/z 4425.43

References and notes

1. Roncali, J. *Chem. Rev.* **1997**, *97*, 173–205.
2. Van Mullekom, H. A. M.; Vekemans, J. A. J. M.; Havinga, E. E.; Meijer, E. W. *Mat. Sci. Eng. R.* **2001**, *32*, 1–40.
3. Kertesz, M.; Choi, C. H.; Yang, S. J. *Chem. Rev.* **2005**, *105*, 3448–3481.
4. Rasmussen, S. C.; Pomerantz, M. *Handbook of Conducting Polymers*, 3rd ed.; CRC Press: Boca Raton, FL, 2007.
5. Wudl, F.; Kobayashi, M.; Heeger, A. J. *J. Org. Chem.* **1984**, *49*, 3382–3384.
6. Kobayashi, M.; Colaneri, N.; Boysel, M.; Wudl, F.; Heeger, A. J. *J. Chem. Phys.* **1985**, *82*, 5717–5723.
7. Hoogmartens, I.; Adriaensens, P.; Vanderzande, D.; Gelan, J.; Quattrocchi, C.; Lazzaroni, R.; Brédas, J. L. *Macromolecules* **1992**, *25*, 7347–7356.
8. Pomerantz, M.; Chaloner-Gill, B.; Harding, L. O.; Tseng, J. J.; Pomerantz, W. J. *J. Chem. Soc. Chem. Commun.* **1992**, 1672–1673.
9. Nietfeld, J. P.; Heth, C. L.; Rasmussen, S. C. *Chem. Commun.* **2008**, 981–983.
10. Wen, L.; Duck, B. C.; Dastoor, P. C.; Rasmussen, S. C. *Macromolecules* **2008**, *41*, 4576–4578.
11. Yamamoto, T.; Morita, A.; Miyazaki, Y.; Maruyama, T.; Wakayama, H.; Zhou, Z.; Nakamura, Y.; Kanbara, T.; Sasaki, S.; Kubota, K. *Macromolecules* **1992**, *25*, 1214–1223.
12. Meier, H.; Stalmach, U.; Kolshorn, H. *Acta Polym.* **1997**, *48*, 379–384.
13. Van Hal, P. A.; Beckers, E. H. A.; Peeters, E.; Apperloo, J. J.; Janssen, R. A. J. *Chem. Phys. Lett.* **2000**, *328*, 403–408.
14. Janssen, R. A. J.; Hummelen, J. C.; Wudl, F. *J. Am. Chem. Soc.* **1995**, *117*, 544–545.
15. Weller, A. Z. *Phys. Chem. Neue Folge* **1982**, *133*, 93–98.
16. Kooistra, F. B.; Mihailetchi, V. D.; Popescu, L. M.; Kronholm, D.; Blom, P. W. M.; Hummelen, J. C. *Chem. Mater.* **2006**, *18*, 3068–3073.

17. Williams, R. M.; Zwier, J. M.; Verhoeven, J. W. *J. Am. Chem. Soc.* **1995**, *117*, 4093–4099.
18. Van Bolhuis, F.; Wynberg, H.; Havinga, E. E.; Meijer, E. W.; Staring, E. G. *J. Synth. Met.* **1989**, *30*, 381–389.
19. Bidan, G.; De Nicola, A.; Enee, V.; Guillerez, S. *Chem. Mater.* **1998**, *10*, 1052–1058.
20. Kirschbaum, T.; Azumi, R.; Mena-Osteritz, E.; Bäuerle, P. *New J. Chem.* **1999**, *23*, 241–250.
21. Gierschner, J.; Cornil, J.; Egelhaaf, H. *J. Adv. Mater.* **2007**, *19*, 173–191.
22. Barbarella, G.; Favaretto, L.; Sotgiu, G.; Zambianchi, M.; Antolini, L.; Pudova, O.; Bongini, A. *J. Org. Chem.* **1998**, *63*, 5497–5506.
23. Barbarella, G.; Favaretto, L.; Zambianchi, M.; Pudova, O.; Arbizzani, C.; Bongini, A.; Mastragostino, M. *Adv. Mater.* **1998**, *10*, 551–554.
24. Brédas, J. L.; Heeger, A. J.; Wudl, F. *J. Chem. Phys.* **1986**, *85*, 4673–4678.
25. Nayak, K.; Marynick, D. S. *Macromolecules* **1990**, *23*, 2237–2245.
26. Kastner, J.; Kuzmany, H.; Vegh, D.; Landl, M.; Cuff, L.; Kertesz, M. *Macromolecules* **1995**, *28*, 2922–2929.
27. Cuff, L.; Kertesz, M. *J. Chem. Phys.* **1997**, *106*, 5541–5553.
28. AMPAC 6.55, Semichem: Shawnee, KS, 1997.
29. Ridley, J.; Zerner, M. *Theor. Chim. Acta* **1973**, *32*, 111–134.

Chapter 6

Charge separation and recombination in small band gap oligomer – fullerene triads containing thieno[3,4-*b*]pyrazine units

Abstract In this chapter, synthesis and photophysics of a series of thiophene–thienopyrazine small band gap oligomers, end-capped at both ends with C₆₀, are presented. In these triads, a photoinduced electron transfer reaction occurs between the oligomer as a donor and the fullerene as an acceptor. Femtosecond photoinduced absorption has been used to determine the rates for charge separation and recombination. It was found that charge separation takes place within approximately 10 ps, and is situated close to the Marcus optimal region. Charge recombination is faster in *o*-dichlorobenzene (ODCB) (15–45 ps) than in toluene (90–730 ps), because in ODCB charge recombination takes place close to the optimal region. In toluene, the recombination is situated in the inverted region, with a much higher activation barrier. No signs of recombination into a triplet state were observed.

This work has been published: Karsten, B. P.; Bouwer, R. K. M.; Hummelen, J. C.; Williams, R. M.; Janssen, R. A. J. *J. Phys. Chem. B* **2010**, doi: 10.1021/jp906973d.

6.1 Introduction

Besides polymer properties like band gap and oxidation and reduction potentials, the kinetics of electron transfer from the polymer to an electron acceptor (most commonly a fullerene) are of crucial importance for polymer solar cells. Upon excitation of the polymer, fast charge separation is required after which the charges should be transported to the electrodes before recombination occurs. As triplet energy levels in small band gap polymers are generally low, even below the energy of the charge separated state, recombination to such a triplet state is likely to be a loss mechanism in solar cells based on these polymers.¹⁻³

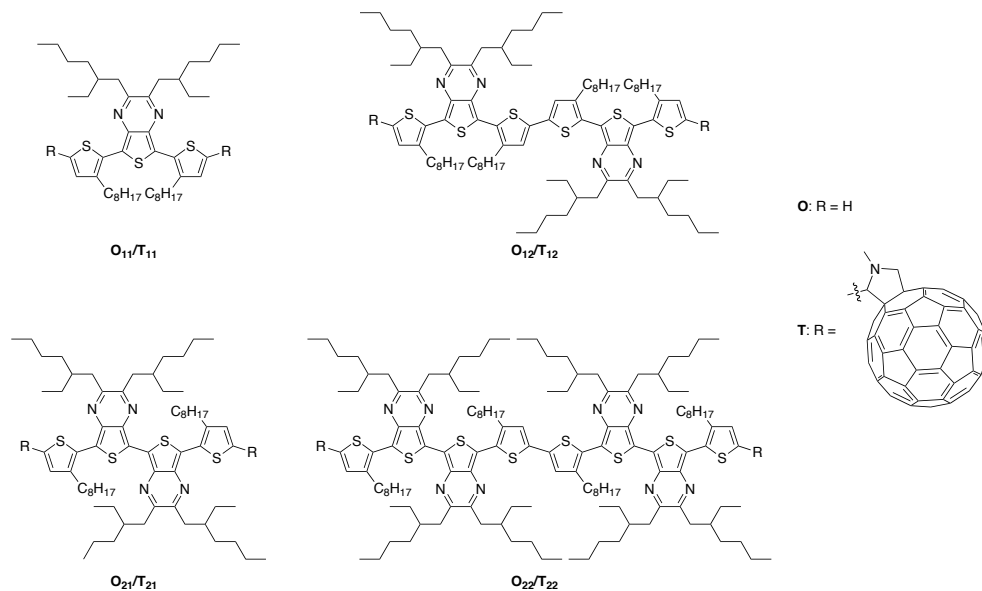
As the electron transfer is a key process in the operation of polymer solar cells, detailed knowledge about electron transfer processes might yield valuable information for the future design of new donor–acceptor combinations. Many detailed studies on electron transfer processes in linked donor–fullerene systems have emerged in the literature during the past decades.⁴⁻¹¹ Electron transfer in this type of donor–acceptor systems usually occurs rapidly, in the Marcus normal region. The electron transfer is followed by somewhat slower back-electron transfer to the ground state in the Marcus inverted region. Also, intersystem crossing in the charge separated state followed by charge recombination into a low-lying triplet state has been observed frequently.^{6,12-18}

In chapters 3, 4 and 5, studies on short thiophene–thienopyrazine oligomers and the factors that influence band gap and electrochemical properties in these systems, are presented. To investigate electron transfer and charge recombination in small band gap polymer–fullerene systems in more detail, we attached fullerene units to a number of these oligomers. The compounds studied are depicted in scheme 6.1. Fluorescence of the oligomers is quenched in the triads, indicating efficient charge separation. Photoinduced absorption measurements in the femtosecond to picosecond time range indicate very fast charge transfer on time scales < 10 ps. Charge recombination in the triads is also fast; recombination occurs within 15–50 ps in *o*-dichlorobenzene (ODCB) and within 90–730 ps in toluene. The results can be rationalized with Marcus–Jortner theory, indicating that charge separation occurs close to the optimal region, giving very low activation barriers for electron transfer. Charge recombination takes place close to the normal region in ODCB, and in the inverted region in toluene. No signs of charge recombination into a triplet state have been found.

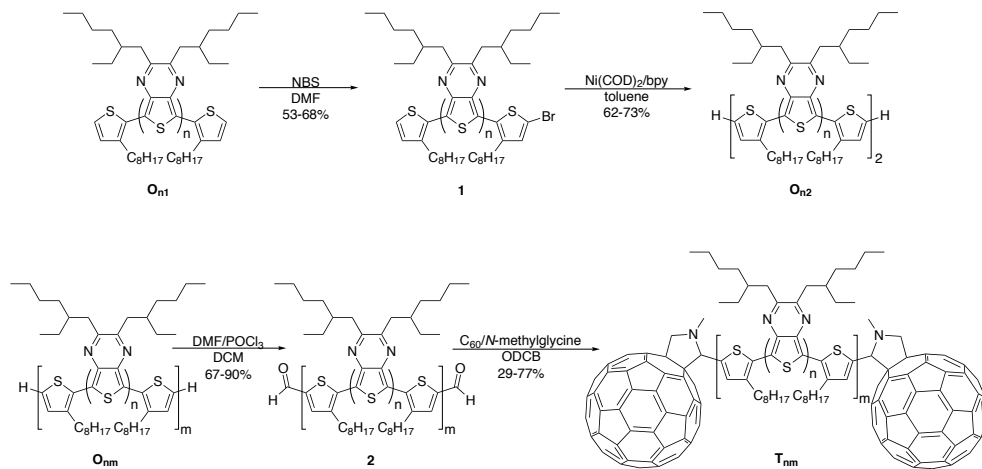
6.2 Results and discussion

6.2.1 Synthesis

Synthesis of the triads is outlined in scheme 6.2. The synthesis of monomers \mathbf{O}_{n1} has been described in previous chapters. The monomers were monobrominated with NBS and subsequently coupled *via* a nickel(0)-mediated Yamamoto coupling.¹⁹ The oligomers \mathbf{O}_{nm} were then formylated *via* Vilsmeier–Haack formylation,²⁰ and the C_{60} units were introduced in a Prato reaction.²¹ The triads \mathbf{T}_{nm} were further purified by preparative HPLC to yield the pure compounds. The triads were fully characterized by ¹H-NMR, ¹³C-NMR, FT-IR, MALDI-TOF-MS, and HPLC.



Scheme 6.1: Investigated oligomers and triads.


 Scheme 6.2: Synthesis of the oligomers O_{n2} and triads T_{nm} ($n = 1, 2$; $m = 1, 2$)

6.2.2 Optical properties

Optical absorptions of the oligomers \mathbf{O}_{nm} and the triads \mathbf{T}_{nm} are depicted in figure 6.1. It can be seen from this figure that the absorption of the triads is, in first approximation, close to an addition of the absorption spectra of the oligomers and *N*-methylfulleropyrrolidine (MP-C₆₀). Small differences in absorption coefficients and the small red shift upon addition of the C₆₀ units can be explained by the different end-groups attached to the oligomer (H in \mathbf{O}_{nm} and MP-C₆₀ in \mathbf{T}_{nm}). A summary of the optical data of the oligomers and the triads is given in table 6.1.

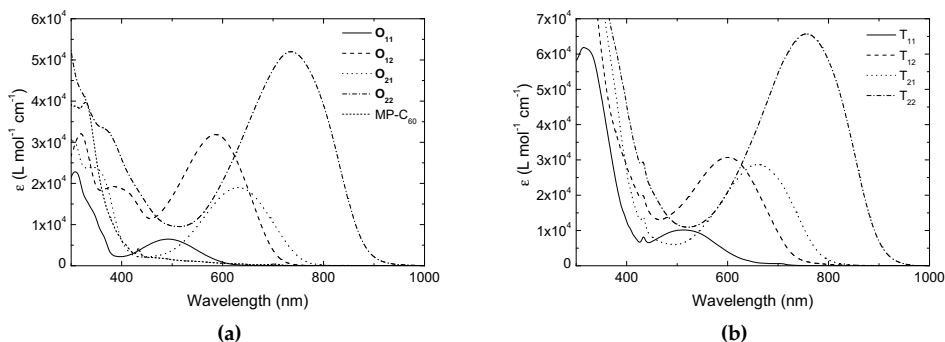


Figure 6.1: UV/vis/NIR absorption spectra of the unfunctionalized oligomers (a) and of the triads (b) recorded in toluene.

Table 6.1: Absorption and fluorescence data for the oligomers and triads in toluene.

	$\lambda_{max}(nm)$	E_{max} (eV)	λ_{onset} (nm)	E_{S1} (eV)	λ_{max}^{PL} (nm)
\mathbf{O}_{11}	493	2.52	605	2.05	659
\mathbf{T}_{11}	514	2.41	728	1.70	
\mathbf{O}_{12}	587	2.11	706	1.76	709
\mathbf{T}_{12}	601	2.06	732	1.69	
\mathbf{O}_{21}	629	1.97	756	1.64	772
\mathbf{T}_{21}	660	1.88	787	1.58	
\mathbf{O}_{22}	736	1.68	882	1.41	>850
\mathbf{T}_{22}	756	1.64	902	1.37	
MP-C ₆₀	328, 433	3.78, 2.86	725	1.71	713

MP-C₆₀ and the nonfunctionalized oligomers \mathbf{O}_{nm} are weakly fluorescent (fluorescence spectra are shown in figure 6.2). Fluorescence is absent for the \mathbf{T}_{nm} triads irrespective of exciting either the fullerene or the conjugated oligomer segment. Only for the shortest triad, \mathbf{T}_{11} , the quenching of the C₆₀ emission is not complete (70 % quenching in toluene and 90 % in ODCB). The strong quenching of both oligomer and C₆₀ emission in the triads indicates efficient electron transfer in these systems. In case of energy transfer instead of electron transfer, the fluorescence of only one of the units (oligomer or C₆₀) would have been quenched, leaving the fluorescence of the other unit unaffected.

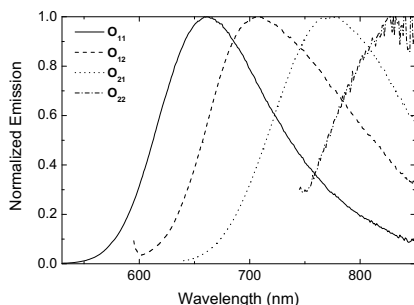


Figure 6.2: Photoluminescence spectra of the nonfunctionalized oligomers O_{nm} recorded in toluene.

6.2.3 Photoinduced absorption

In chapters 4 and 5, oligomers O_{nm} were studied by near steady-state photoinduced absorption (PIA). In these studies, PIA spectra of mixtures of O_{nm} and a fullerene (MP-C₆₀ or [6,6]-phenyl-C₆₁-butyric acid methyl ester, PCBM) were taken in both toluene and ODCB or benzonitrile. In toluene, the fullerene acts as a triplet sensitizer and triplet spectra of the oligomers O_{n2} were obtained. For oligomers O_{n1} only the (strongly quenched) signal of the fullerene triplet could be observed. The obtained triplet spectra are shown in figure 6.3. No PIA signal was obtained for the pure oligomers in either solvent.

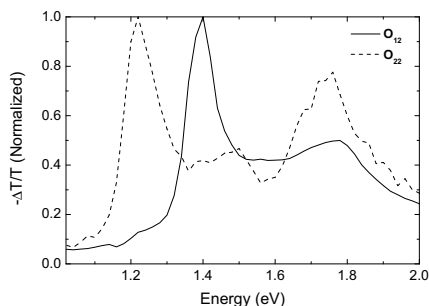


Figure 6.3: PIA spectra of mixtures of O_{12} with MP-C₆₀ and O_{22} with PCBM in toluene, showing the triplet absorption bands of the oligomers. The band around 1.8 eV is due to residual absorption of the fullerene triplet.

In ODCB and benzonitrile, more polar solvents than toluene, electron transfer from the oligomer to the fullerene takes place rather than triplet energy transfer. In this way, absorption spectra of the radical cations of the oligomers could be obtained, except for O_{11} where, again, only the fullerene triplet signal is observed. PIA spectra in ODCB and benzonitrile are depicted in figure 6.4.

In contrast to mixtures of oligomers O_{nm} with fullerenes, triads T_{nm} do not show any detectable signal in near steady-state PIA, probably because both charge separation and charge recombination in these systems take place on a much faster time scale than near steady-state PIA (in the millisecond to microsecond time range) can

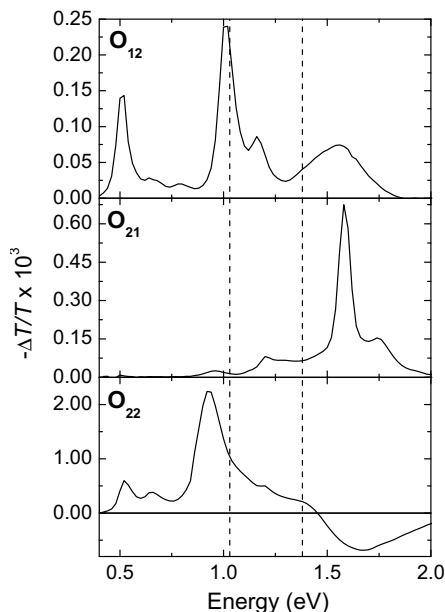


Figure 6.4: PIA spectra of mixtures of O_{12} with MP- C_{60} in ODCB and O_{22} with PCBM in benzonitrile, showing the absorption bands of the radical cation oligomers. The small band at 1.21 eV is due to the absorption of the fullerene anion.²² The dashed lines indicate the detection region in the fs-PIA experiments.

detect. To investigate the charge separation and charge recombination in the triads in detail, time resolved PIA experiments in the femtosecond to picosecond range were performed. In these experiments, the triad was excited by a 530 nm laser pulse of about 200 fs. Absorption spectra in the near infrared region were measured by a second pulse at short time intervals after excitation. The detection region of 900–1200 nm is indicated with dashed lines in figure 6.4. As an example, femtosecond-PIA (fs-PIA) results for O_{12} and T_{12} in toluene are depicted in figure 6.5. Data for the same compounds in ODCB are depicted in figure 6.6. For the other oligomers and triads, similar graphs were obtained.

As can be seen from these figures, the spectra of the bare oligomer show a broad absorption band in the near infrared. This band decays on a time scale of several hundred picoseconds and is attributed to the absorption of the singlet excited state ($S_n \leftarrow S_1$). The triad on the other hand shows a sharper absorption band that first increases in intensity and then decays. As can be seen from figure 6.4, this sharp band can be attributed to the absorption of the fullerene anion,²² and as a consequence, the intensity of this band is proportional to the amount of charge separated molecules present in solution. In both cases, no long-lived species are detected and no absorptions arise in the spectra that could be attributed to charge recombination into a triplet state.

Time constants for the decay of the singlet excited state of the oligomers (without C_{60}) could be fitted using a bi-exponential function, and the results are summarized

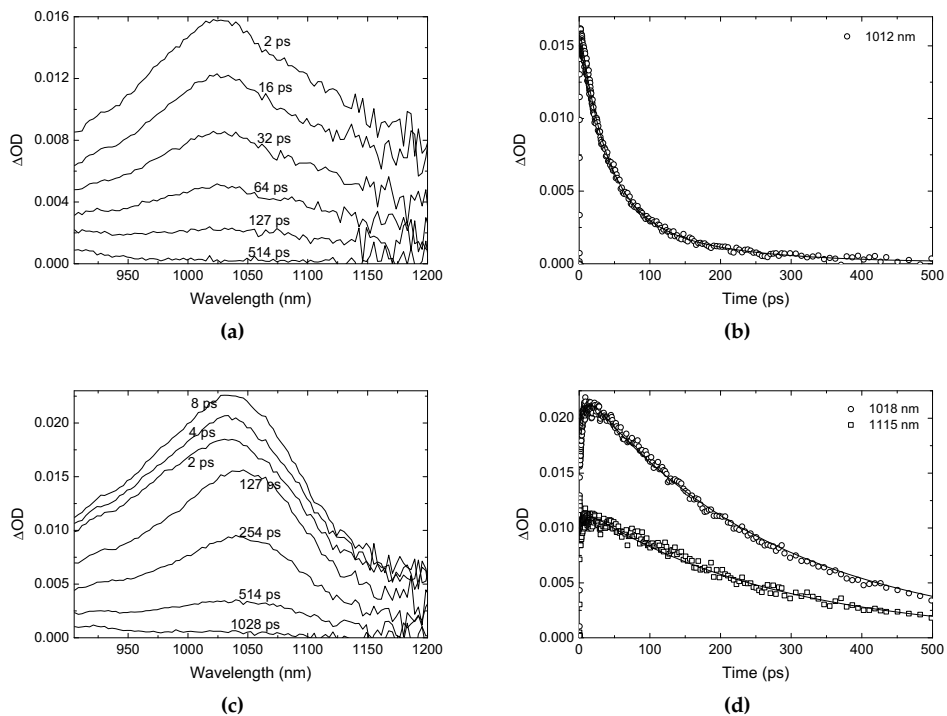


Figure 6.5: fs-PIA data for \mathbf{O}_{12} (a and b) and \mathbf{T}_{12} (c and d) in toluene. In graphs a and c, the evolution of the absorption spectra in time is visualized, and in graphs b and d, the PIA signal at selected wavelengths is displayed as a function of time. The solid lines in graphs b and d are bi-exponential fits of the data.

in table 6.2. For all oligomers \mathbf{O}_{nm} , fitting with mono-exponential decay did not give a very good fit, although lifetimes in the range of τ_1 are obtained. The exact cause for the second component in the fits is not known but might be related to, *e.g.*, solvation effects or structural rearrangements of the S_1 state.

For \mathbf{T}_{12} , the charge separated state absorbs more strongly than the singlet excited state. The signal shows a rise time of a few picoseconds, followed by a decay, as can be seen in figure 6.5d for toluene and in figure 6.6d for ODCB. The two traces in these figures, representing two different wavelengths, were fitted simultaneously, with bi-exponential functions, using one set of time constants, τ_{CS} and τ_{CR} , for charge separation and charge recombination, respectively, but different prefactors for the exponential functions at the two wavelengths. A summary of fitted time constants for the different triads is given in table 6.3.

As can be seen from table 6.3, charge separation in these triads is very fast, and generally occurs within 10 ps after excitation. Furthermore, the differences between the more polar solvent (ODCB) and the apolar solvent (toluene) are small. For charge recombination, however, large differences are found between the experiments in different solvents. In this case, the process in ODCB is much faster than that in toluene, although the charge separated state is thermodynamically more stable in a polar sol-

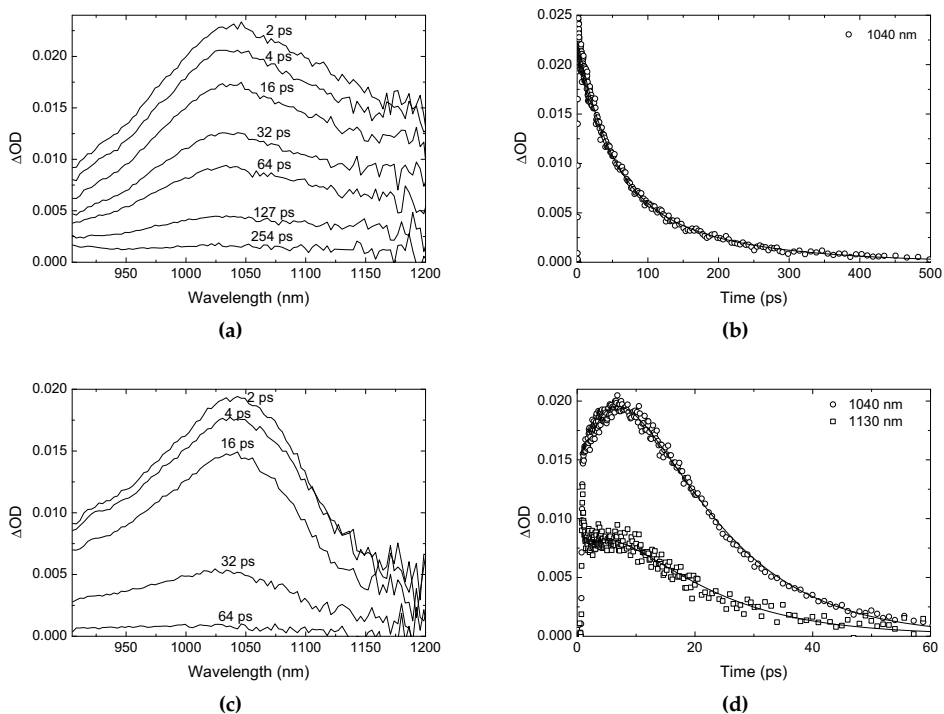


Figure 6.6: fs-PIA data for O_{12} (a and b) and T_{12} (c and d) in ODCB. In graphs a and c, the evolution of the absorption spectra in time is visualized, and in graphs b and d, the PIA signal at selected wavelengths is displayed as a function of time. The solid lines in graphs b and d are bi-exponential fits of the data.

Table 6.2: Fitted time constants for decay of the singlet excited state of the oligomers O_{nm} determined by femtosecond PIA.^a

	toluene		ODCB	
	τ_1 (ps)	τ_2 (ps)	τ_1 (ps)	τ_2 (ps)
O_{11}	7100 (1.7×10^{-3})	11 (3.9×10^{-4})	6700 (1.4×10^{-3})	21 (5.2×10^{-4})
O_{12}	36 (1.2×10^{-2})	133 (4.5×10^{-3})	45 (1.4×10^{-2})	154 (8.6×10^{-3})
O_{21}	435 (3.5×10^{-2})	2500 (2.4×10^{-3})	410 (3.1×10^{-2})	1000 ^b (4.2×10^{-3})
O_{22}	156 (4.6×10^{-3})	6.1 (7.1×10^{-3})	138 (5.2×10^{-3})	4.9 (6.4×10^{-3})

^a Prefactors of bi-exponential fits are given in parentheses.

^b Fixed during fitting.

Table 6.3: Time constants for charge separation (τ_{CS}) and charge recombination (τ_{CR}) obtained from a bi-exponential fit.

	τ_{CS} (ps)		τ_{CR} (ps)	
	toluene	ODCB	toluene	ODCB
T_{11}	21.5	10.1	727	44.9
T_{12}	6.3	7.1	275	13.5
T_{21}	4.3	6.2	201	15.8
T_{22}	2.7	7.2	91.4	15.1

vent.

The free energy for charge separation (ΔG_{CS}) in different solvents can be calculated with the following equation, based on a continuum model.²³

$$\Delta G_{CS} = e(E_{ox}(D) - E_{red}(A)) - E_{00} - \frac{e^2}{4\pi\epsilon_0\epsilon_s R_{cc}} - \frac{e^2}{8\pi\epsilon_0} \left(\frac{1}{r^+} + \frac{1}{r^-} \right) \left(\frac{1}{\epsilon_{ref}} - \frac{1}{\epsilon_s} \right) \quad (6.1)$$

In this equation, $E_{ox}(D)$ is the oxidation potential of the oligomer, $E_{red}(A)$ is the reduction potential of MP-C₆₀ (measured to be -1.2 V *vs.* Fc/Fc⁺ in ODCB), and E_{00} is the energy of the initial excited state (the energy of the singlet excited state of the oligomer). R_{cc} is the center-to-center distance of the positive and negative charges, which was determined for the triads using molecular modeling, assuming the positive charge to be located on the center of the oligomer and the negative charge at the center of the fullerene moiety. r^+ and r^- are the radii of the positive and negative ions formed. r^- is calculated in the literature to be 5.6 Å for C₆₀, based on the density of C₆₀.⁶ r^+ can be estimated using a similar approach, using a density of 1.5, the value for unsubstituted terthiophene.²⁴ ϵ_{ref} and ϵ_s are the permittivities of the reference solvent (used to measure oxidation and reduction potentials) and the solvent in which electron transfer is studied. It is well-known that solvents like toluene, with a low dipole moment and a high quadrupole moment, often show larger stabilization energies of charge separated states than predicted from their "bulk" relative permittivity. Because the relative permittivity does not describe the solvent-molecule interactions in these solvents well, an apparent permittivity can be used, such that the solvent behaves as a hypothetical solvent of polarity ϵ_{app} . For toluene, an apparent permittivity of 3.5 was used.^{25,26} The energy of the charge separated state (E_{CSS}) is then equal to the difference of E_{S_1} and ΔG_{CS} . Values calculated for r^+ , R_{cc} , E_{CSS} , and ΔG_{CS} are summarized in table 6.4.

Marcus theory estimates the activation barrier for photoinduced charge separation based on the free energy for charge separation, ΔG_{CS} , and the reorganization energy, λ , *i.e.* the energy needed to deform the excited donor-acceptor system to the geometry of the charge separated state. Assuming the same, parabolic energy curves for both the initial excited state and the charge separated state, this leads to:^{27,28}

$$\Delta G_{CS}^\ddagger = \frac{(\Delta G_{CS} + \lambda)^2}{4\lambda} \quad (6.2)$$

where λ is the sum of internal (λ_i) and solvent (λ_s) contributions. The internal re-

Table 6.4: Singlet energy level (E_{S_1}), half-wave oxidation potential (E_{ox} , vs. Fc/Fc⁺ in ODCB), and cation radius (r^+) of the oligomeric core of the triads, distance between positive and negative charges (R_{cc}) in the triads, energy of the charge separated state (E_{CSS}), reorganization energy (λ), free energy of charge separation (ΔG_{CS}), and activation energies for charge separation (ΔG_{CS}^\ddagger) and recombination (ΔG_{CR}^\ddagger) in toluene and ODCB.

	E_{S_1} (eV)	E_{ox} (V)	r^+ (Å)	R_{cc} (Å)	solvent	E_{CSS} (eV)	λ (eV)	ΔG_{CS} (eV)	ΔG_{CS}^\ddagger (eV)	ΔG_{CR}^\ddagger (eV)	k_{CS}/V^2 (s ⁻¹ eV ²)	k_{CR}/V^2 (s ⁻¹ eV ²)
T ₁₁	2.05	0.27	4.3	9.6	toluene	1.59	0.53	-0.46	0.003	0.52	1.4×10^{16}	5.2×10^{13}
					ODCB	1.32	0.76	-0.73	0.0004	0.10	1.3×10^{16}	2.0×10^{15}
T ₁₂	1.76	-0.01	5.4	15.4	toluene	1.41	0.57	-0.35	0.022	0.31	7.2×10^{15}	2.9×10^{14}
					ODCB	1.10	0.83	-0.66	0.0086	0.021	9.2×10^{15}	7.5×10^{15}
T ₂₁	1.64	-0.08	4.9	11.3	toluene	1.27	0.54	-0.37	0.014	0.25	1.0×10^{16}	6.0×10^{14}
					ODCB	0.99	0.77	-0.65	0.0052	0.016	1.1×10^{16}	8.6×10^{15}
T ₂₂	1.41	-0.26	6.1	18.3	toluene	1.17	0.57	-0.24	0.049	0.16	1.8×10^{15}	1.4×10^{15}
					ODCB	0.86	0.83	-0.55	0.024	0.0003	2.0×10^{15}	1.2×10^{16}
				11.3	toluene	1.04	0.49	-0.37	0.0069	0.15	1.4×10^{16}	1.9×10^{15}
					ODCB	0.81	0.68	-0.60	0.0023	0.072	1.3×10^{16}	1.1×10^{16}

organization energy is set to 0.3 eV in this case, based on the reported value for the C₆₀/diethylaniline couple.⁶ The solvent contribution can be calculated using the Born–Hush approach:²⁹

$$\lambda_s = \frac{e^2}{4\pi\epsilon_0} \left[\frac{1}{2} \left(\frac{1}{r^+} + \frac{1}{r^-} \right) - \frac{1}{R_{cc}} \right] \left(\frac{1}{n^2} - \frac{1}{\epsilon_s} \right) \quad (6.3)$$

In this formula, n is the refractive index of the solvent and the other parameters are the same as defined before. Reaction rates can be calculated using the nonadiabatic electron transfer theory by Jortner et al.:^{30,31}

$$k_0 = \sqrt{\frac{\pi}{\hbar^2 \lambda_s k_B T}} V^2 \sum_{n=0}^{\infty} e^{-S} \frac{S^n}{n!} \exp \left(-\frac{(\Delta G_0 + \lambda_s + n\hbar\omega)^2}{4\lambda_s k_B T} \right) \quad (6.4)$$

In this equation, V describes the electronic coupling between donor and acceptor and $S = \lambda_i/\hbar\omega$ the effective mode vibrational energy. $\hbar\omega$ was set to 0.186 eV (1500 cm⁻¹), a value characteristic for the carbon–carbon double bond stretching frequency. Reorganization energies, activation barriers, and calculated reaction rates are summarized in table 6.4. For charge recombination, $-E_{CSS}$ was used as the value for ΔG_{CR} . As V is not known, the rate constants in table 6.4 are given as k/V^2 .

From the values in table 6.4, a number of conclusions can be drawn. First, charge separation formally takes place in the Marcus normal region ($\lambda > -\Delta G_{CS}$). This would lead to faster charge separation in the more polar ODCB compared to toluene, due to stabilization of the charge separated state. The difference between λ and ΔG_{CS} however, is very small, indicating that charge separation takes place close to the Marcus optimal region, leading to very small activation barriers. These low activation barriers are also reflected in the high calculated rate constants and the small differences therein, which is consistent with experiment. In contrast to charge separation, charge recombination in toluene takes place in the Marcus inverted regime

($\lambda < E_{CSS}$), also explaining the slower charge recombination compared to charge separation. For the longer triads in ODCB, low activation barriers for recombination are calculated and very fast charge recombination in these systems has been observed. This leads to the conclusion that charge recombination in these triads, although possibly still in the Marcus inverted region, takes place close to the optimal region. This is due to the higher polarity of ODCB compared to toluene, leading to a smaller thermodynamic driving force for recombination. Measurements in more polar solvents, like benzonitrile, would be interesting here, but they were not performed due to solubility problems. The observed rates of recombination follow the trend expected based on the calculated rate constants, both in toluene and in ODCB. Dividing the experimentally determined $1/\tau$ by the calculated k/V^2 leads to values for V of 3.3 ± 1.5 meV for charge separation and 3.7 ± 1.4 meV for recombination for all triads, except for T_{22} , where $V = 14.4$ and 5.3 meV for charge separation in toluene and ODCB, respectively. Values for V of a few millielectronvolts are in the common range for donor–acceptor dyads and triads.^{7,26,32} Because thienopyrazine has a lower oxidation potential than thiophene, the positive charge in the radical cations of O_{22} and T_{22} might not localize in the center of the oligomer but rather asymmetrically on one of the two dithienopyrazine units. This will effectively reduce R_{cc} of T_{22} close to the value of T_{12} . Using $R_{cc} = 11.3$ Å, the electronic coupling V for charge separation is reduced to $V = 5.1$ meV (toluene) and 3.3 meV (OCDB), within the range of values observed for the other triads.

In previous chapters, we found that the pure oligomers have low-lying triplet levels (T_1). Triplet levels of O_{11} and O_{12} have been estimated to be ~ 1.14 eV and between 0.93 and 1.14 eV, respectively, by quenching experiments. Triplet energies of O_{21} and O_{22} have been estimated to be ≤ 0.93 eV. Because E_{CSS} is higher (except maybe for T_{2n} in ODCB), charge recombination into the low-lying triplet excited state might be a possible decay pathway for the charge separated state. Although for T_{21} and T_{22} the triplet absorptions are in the wavelength range studied in our experiments, no long-lived triplet absorptions are found for triads T_{nm} . The process of populating the T_1 state via an intermediate charge separated state has been extensively studied for donor–acceptor systems. In systems where the distance between the charges is large ($R_{cc} > 15$ Å), and hence the electronic coupling is weak, intersystem crossing (ISC) in the charge separated state is the commonly observed mechanism of triplet formation.^{12–15} In these systems, ISC occurs from the singlet charge separated state to the nearly degenerate triplet charge separated state, mainly *via* hyperfine interaction driven spin dephasing. At ambient temperatures, this process typically occurs on the order of 10 ns. For smaller systems, ISC via hyperfine interactions becomes less obvious, as the splitting energy between the singlet and triplet charge separated states becomes too large. Still, also for these systems, fast ISC via the charge separated state has been observed, with time scales on the order of 1 – 100 ns.^{16–18} As the reported time scales for ISC in the charge separated state are much longer than the lifetime of the charge separated state in T_{nm} ($\ll 1$ ns), ISC is not likely to occur. This rationalizes the fact that we do not see evidence for the formation of triplet excited states of the donor part in the triads.

6.3 Conclusions

Triads consisting of different short thiophene–thienopyrazine oligomers, with optical band gaps between 2.05 and 1.41 eV, and C₆₀ units have been prepared. It was found that the optical absorption of the triads was close to a superposition of the absorption spectra of the bare oligomers and MP-C₆₀. In these triads, fluorescence of both the oligomer and C₆₀ was quenched, indicating efficient electron transfer in these systems. To investigate in detail the charge separation and recombination in the small band gap oligomer–fullerene systems, femtosecond-PIA studies were performed. Charge separation in these systems takes place close to the Marcus optimal region, resulting in small activation barriers and very fast charge transfer, usually within 10 ps after excitation. Recombination of the charges occurs in the Marcus inverted region in toluene, and again close to the optimal region in ODCB. This leads to a much faster charge recombination in ODCB (15–45 ps) than in toluene (90–730 ps). No signs of recombination into a low-lying triplet state were observed, probably because the lifetime of the charge separated state is too short for intersystem crossing in the charge separated state.

6.4 Experimental

General methods ¹H-NMR and ¹³C-NMR spectra were recorded on a 400 MHz NMR (Varian Mercury or Varian 400-MR, 400 MHz for ¹H-NMR and 100 MHz for ¹³C-NMR) or on a 500 MHz NMR (Varian Unity Plus, 500 MHz for ¹H-NMR and 125 MHz for ¹³C-NMR). Spectra were recorded in CDCl₃, or in CS₂ using a D₂O insert for locking and shimming. Chemical shifts are reported in ppm downfield from tetramethylsilane (TMS). IR spectra were recorded on a Perkin Elmer 1600 FT-IR. Matrix-assisted laser desorption ionization time-of-flight (MALDI-TOF) mass spectrometry was performed on a PerSeptive Biosystems Voyager–DE PRO spectrometer. Recycling GPC was performed on a LC system equipped with JAIGEL 2H and JAIGEL 2.5H columns. The eluent was chloroform at 3.5 mL/min and the injection volume was 2 mL. Preparative HPLC was performed using a Cosmosil Buckyprep Waters packed column (10×250 mm), using toluene as the eluent at a flow rate of 10 mL/min. Analytical HPLC analysis was performed on a Hewlett Packard HP LC-Chemstation 3D (Agilent/HP1100 Series) using an analytical Cosmosil Buckyprep column (4.6×250 mm). UV/vis/NIR absorption spectra were recorded using a PerkinElmer Lambda 900 spectrophotometer. Fluorescence spectra were recorded on an Edinburgh Instruments FS920 double-monochromator spectrophotometer with a Peltier-cooled red-sensitive photomultiplier. The emission spectra were corrected for the wavelength dependence of the sensitivity of the detection system. Cyclic voltammograms were recorded in an inert atmosphere with 0.1 M tetrabutyl ammonium hexafluorophosphate (TBAPF₆) in ODCB as supporting electrolyte. The working electrode was a platinum disk (0.2 cm²), and the counter electrode was a silver electrode. The samples were measured using an Ag/AgCl reference electrode with Fc/Fc⁺ as an internal standard using a μ Autolab II with a PGSTAT30 potentiostat. Near steady-state PIA spectra were recorded by exciting with a mechanically modulated cw Ar-ion laser ($\lambda = 351$ and 364 nm, 275 Hz) pump beam and monitor-

ing the resulting change in transmission of a tungsten-halogen probe light through the sample (ΔT) with a phase-sensitive lock-in amplifier after dispersion by a grating monochromator and detection, using Si, InGaAs, and cooled InSb detectors. The pump power incident on the sample was typically 25 mW with a beam diameter of 2 mm. The PIA ($\Delta T/T$) was corrected for the photoluminescence, which was recorded in a separate experiment. Photoinduced absorption spectra and photoluminescence spectra were recorded with the pump beam in a direction almost parallel to the direction of the probe beam. The solutions were studied in a 1 mm near-IR grade quartz cell at room temperature. Femtosecond photoinduced absorption experiments were performed with a Spectra-Physics Hurricane titanium:sapphire regenerative amplifier system. The full spectrum setup was based on an optical parametric amplifier (Spectra-Physics OPA 800C) as the pump. The residual fundamental light, from the pump OPA, was used for white/probe light generation. The polarization of the pump light was controlled by a Berek Polarization Compensator (New Focus). The Berek polarizer was always included in the setup to provide the magic-angle conditions. The probe light was double-passed over a delay line (Physik Instrumente, M-531DD) that provides an experimental time window of 3.6 ns with a maximal resolution of 0.6 fs/step. The OPA was used to generate excitation pulses at 530 nm. The laser output was typically 3.5–5 μJ pulse⁻¹ (130 fs fwhm) with a repetition rate of 1 kHz. The samples were placed into cells of 2 mm path length (Hellma) and were stirred with a downward projected PTFE shaft, using a direct drive spectro-stir (SPECTROCELL). For femtosecond transient absorption in the NIR region, a Control Development NIR-256 L-1.7T1-USB, optical spectrometer system, InGaAs detector with 512 element arrays responding to wavelengths range from 900–1700 nm, was used. Detection light was generated with a sapphire plate. The exact optical layout has been described in literature.³³ All photophysical data reported here have a 5–10% error limit. All experiments were performed at room temperature. It has to be noted that T_{11} and T_{12} showed some signs of degradation in UV/vis absorption measurements conducted right before and after the time resolved PIA experiment. In the case of T_{11} , about 20% degradation was observed in toluene and about 8% in ODCB, as inferred from the decrease of the $\pi \rightarrow \pi^*$ absorption band. T_{12} showed about 14% degradation in toluene and was stable in ODCB. As the time resolved PIA measurement consisted of four sweeps that were averaged afterward, the degradation during one sweep is limited to only a few percent; furthermore, comparing the individual sweeps did not show marked changes. Therefore, we think that effects of degradation on the fitted parameters are very limited and do not affect the general trends.

Materials Solvents were purchased from Biosolve and used without further purification. THF was distilled over 4Å molsieves before use. Dichloromethane was distilled over P₂O₅ before use. C₆₀, MP-C₆₀ and PCBM were obtained from Solenne, other chemicals were purchased from Acros or Aldrich and used without purification. *N*-bromosuccinimide (NBS) was recrystallized from water. Synthesis of 2,3-Bis(2'-ethylhexyl)-5,7-bis(3-octylthiophen-2-yl)thieno[3,4-*b*]pyrazine (**O**₁₁) and 2,2',3,3'-tetrakis(2-ethylhexyl)-7,7'-bis(3-octylthiophen-2-yl)-5,5'-bithieno[3,4-*b*]pyrazine (**O**₂₁) was described in chapter 3. Oxygen and moisture-sensitive reactions were performed under an argon atmosphere.

5-(5-Bromo-3-octyl-2-thienyl)-2,3-bis(2-ethylhexyl)-7-(3-octyl-2-thienyl)-thieno[3,4-*b*]pyrazine (1, *n* = 1) Compound **O**₁₁ (1.0 g, 1.35 mmol) was dissolved in THF (50 mL). NBS (0.22 g, 1.24 mmol) was added in small portions at 0°C and the mixture was stirred overnight, while warming to room temperature. Diethyl ether (150 mL) was added and the mixture was washed with water (3×50 mL) and saturated NaCl (2×50 mL). The organic phase was dried with MgSO₄ and the solvent was evaporated. The compound was purified by flash chromatography on silica, using dichloromethane/heptane as the eluent. Yield: 0.69 g (68 %). ¹H-NMR (400 MHz, CDCl₃): δ 7.36 (d, *J* = 5.0 Hz, 1H, Ar-*H*), 7.00 (d, *J* = 5.0 Hz, 1H, Ar-*H*), 6.94 (s, 1H, ArBr-*H*), 2.97–2.87 (m, 4H, Ar-CH₂-), 2.87–2.82 (m, 4H, Ar-CH₂-), 2.26–2.16 (m, 2H, -CH₂CH(C₄H₉)(C₂H₅)), 1.77–1.66 (m, 4H, -CH₂CH₂C₆H₁₃), 1.55–1.20 (m, 36H, -CH₂-), 0.99–0.83 (m, 18H, -CH₃). ¹³C-NMR (100 MHz, CDCl₃): δ 155.81, 155.65, 140.27, 139.79, 137.66, 137.47, 131.62, 130.26, 129.24, 128.15, 126.36, 123.87, 122.61, 113.53, 39.42, 39.37, 37.58, 37.43, 32.82, 32.73, 31.89, 30.58, 30.40, 30.34, 29.99, 29.79, 29.73, 29.55, 29.52, 29.33, 29.29, 28.91, 28.89, 25.91, 23.13, 22.66, 14.20, 14.14, 14.08, 10.91, 10.87. IR: $\tilde{\nu}_{max}$ (cm⁻¹) 2956, 2923, 2854, 1523, 1494, 1459, 1427, 1378, 1354, 1271, 1250, 1184, 1136, 1122, 817, 724, 696, 660. MALDI-TOF-MS: *m/z* 826.25 (80 %), 827.25 (45), 828.25 (100), 829.25 (50), 830.26 (25), 831.27 (10).

7-(5-Bromo-3-octyl-2-thienyl)-2,2',3,3'-tetrakis(2-ethylhexyl)-7'-(3-octyl-2-thienyl)-5,5'-bithieno[3,4-*b*]pyrazine (1, *n* = 2) Compound **O**₂₁ (1.0 g, 0.91 mmol) was dissolved in THF (30 mL). NBS (0.15 g, 0.82 mmol) was added in small portions at 0°C and the mixture was stirred overnight, while warming to room temperature. Diethyl ether (100 mL) was added and the mixture was washed with water (3×30 mL) and saturated NaCl (2×30 mL). The organic phase was dried with MgSO₄ and the solvent was evaporated. The compound was purified by flash chromatography on silica, using dichloromethane/heptane as the eluent. Yield: 0.52 g (53 %). ¹H-NMR (400 MHz, CDCl₃): δ 7.37 (d, *J* = 5.2 Hz, 1H, Ar-*H*), 7.03 (d, *J* = 5.2 Hz, 1H, Ar-*H*), 6.97 (s, 1H, ArBr-*H*), 3.10–3.01 (m, 4H, Ar-CH₂-), 2.93 (d, *J* = 6.9 Hz, 4H, -CH₂CH(C₄H₉)(C₂H₅)), 2.88 (d, *J* = 6.7 Hz, 4H, -CH₂CH(C₄H₉)(C₂H₅)), 2.33–2.19 (m, 4H, -CH₂CH(C₄H₉)(C₂H₅)), 1.80–1.71 (m, 4H, -CH₂CH₂C₆H₁₃), 1.56–1.18 (m, 52H, -CH₂-), 1.00–0.80 (m, 30H, -CH₃). ¹³C-NMR (100 MHz, CDCl₃): δ 155.95, 155.87, 155.36, 155.22, 140.33, 139.92, 138.11, 137.91, 137.76, 131.74, 131.13, 129.34, 129.12, 126.46, 126.30, 124.74, 123.31, 122.84, 133.49, 39.59, 39.52, 37.99, 37.89, 37.81, 37.62, 33.03, 32.87, 32.83, 32.78, 32.74, 31.89, 30.58, 30.40, 30.27, 30.01, 29.72, 29.65, 29.32, 29.29, 28.97, 28.93, 25.96, 25.90, 23.19, 23.15, 22.65, 14.21, 14.17, 14.11, 14.06, 10.93, 10.87. IR: $\tilde{\nu}_{max}$ (cm⁻¹) 2957, 2924, 2856, 1490, 1458, 1378, 1354, 1182, 1137, 828, 802, 725, 697. MALDI-TOF-MS: *m/z* 1184.6 (70 %), 1185.64(55), 1186.63 (100), 1187.63 (70), 1188.63 (40), 1189.63 (20), 1190.63 (5).

5,5'-(4,4'-Dioctyl[2,2'-bithiophene]-5,5'-diyl)bis[2,3-bis(2-ethylhexyl)-7-(3-octyl-2-thienyl)-thieno[3,4-*b*]pyrazine] (O**₁₂)** A solution of Ni(COD)₂ (0.45 g, 1.64 mmol) and 2,2'-bipyridyl (0.26 g, 1.64 mmol) in toluene (15 mL) was stirred for 30 min, while heating to 80°C. This solution was added to compound **1** (*n* = 1) (0.68 g, 0.82 mmol) and the mixture was stirred at 80°C overnight. The mixture was precipitated in methanol (150 mL), the suspension was filtered over celite and the solids were washed with methanol. The product was recovered from the celite

by redissolution in dichloromethane. The solvent was evaporated and the product was purified by flash chromatography on silica, using dichloromethane/heptane as the eluent. Yield: 0.38 g (62 %). $^1\text{H-NMR}$ (400 MHz, CDCl_3): δ 7.36 (d, $J=4.6$ Hz, 2H, Ar- H), 7.14 (s, 2H, Ar- H), 7.01 (d, $J=4.8$ Hz, 2H, Ar- H), 2.97 (t, $J=7.5$ Hz, 8H, Ar- CH_2-), 2.89 (d, $J=7.7$ Hz, 4H, $-\text{CH}_2\text{CH}(\text{C}_4\text{H}_9)(\text{C}_2\text{H}_5)$), 2.86 (d, $J=7.1$ Hz, 4H, $-\text{CH}_2\text{CH}(\text{C}_4\text{H}_9)(\text{C}_2\text{H}_5)$), 2.34 (m, 2H, $-\text{CH}_2\text{CH}(\text{C}_4\text{H}_9)(\text{C}_2\text{H}_5)$), 2.21 (m, 2H, $-\text{CH}_2\text{CH}(\text{C}_4\text{H}_9)(\text{C}_2\text{H}_5)$), 1.85–1.69 (m, 8H, $-\text{CH}_2\text{CH}_2\text{C}_6\text{H}_{13}$), 1.55–1.20 (m, 72H, $-\text{CH}_2-$), 1.04–0.84 (m, 36H, $-\text{CH}_3$). $^{13}\text{C-NMR}$ (100 MHz, CDCl_3): δ 155.81, 155.31, 140.88, 140.24, 137.76, 137.69, 129.33, 128.37, 127.79, 126.26, 125.79, 123.80, 123.49, 39.49, 39.36, 37.70, 37.52, 32.83, 31.93, 31.92, 30.84, 30.41, 30.02, 29.87, 29.82, 29.60, 29.57, 29.34, 29.00, 28.94, 25.93, 25.87, 23.16, 22.68, 14.17, 14.10, 10.93, 10.90. IR: $\tilde{\nu}_{\text{max}}$ (cm^{-1}) 2956, 2922, 2853, 1517, 1487, 1457, 1428, 1377, 1350, 1239, 1182, 1122, 929, 824, 814, 724, 696. MALDI-TOF-MS: m/z 1494.97 (90 %), 1495.97 (100), 1496.97 (80), 1497.97 (50), 1498.97 (25), 1499.97 (10).

7,7''-(4,4'-Dioctyl[2,2'-bithiophene]-5,5'-diyl)bis[2,2',3,3'-tetrakis(2-ethylhexyl)-7'-(3-octyl-2-thienyl)-5,5'-bithieno[3,4-*b*]pyrazine] (O₂₂) A solution of Ni(COD)₂ (0.24 g, 0.87 mmol) and 2,2'-bipyridyl (0.14 g, 0.87 mmol) in toluene (7.5 mL) was stirred for 30 min, while heating to 80°C. This solution was added to compound **1** ($n = 2$) (0.52 g, 0.43 mmol) and the mixture was stirred at 80°C overnight. The mixture was precipitated in methanol (75 mL), the suspension was filtered over celite and the solids were washed with methanol. The product was recovered from the celite by redissolution in dichloromethane. The solvent was evaporated and the product was purified by flash chromatography on silica, using dichloromethane/heptane as the eluent. Yield: 0.35 g (73 %). $^1\text{H-NMR}$ (400 MHz, CDCl_3): δ 7.37 (d, $J=5.2$ Hz, 2H, Ar- H), 7.19 (s, 2H, Ar- H), 7.04 (d, $J=5.2$ Hz, 2H, Ar- H), 3.15–3.05 (m, 8H, Ar- CH_2-), 2.99–2.86 (m, 16H, $-\text{CH}_2\text{CH}(\text{C}_4\text{H}_9)(\text{C}_2\text{H}_5)$), 2.44–2.20 (m, 8H, $-\text{CH}_2\text{CH}(\text{C}_4\text{H}_9)(\text{C}_2\text{H}_5)$), 1.90–1.72 (m, 8H, $-\text{CH}_2\text{CH}_2\text{C}_6\text{H}_{13}$), 1.80–1.20 (m, 104H, $-\text{CH}_2-$), 1.06–0.81 (m, 60H, $-\text{CH}_3$). $^{13}\text{C-NMR}$ (100 MHz, CDCl_3): δ 155.87, 155.45, 155.33, 155.06, 141.02, 140.24, 138.10, 137.96, 137.82, 129.36, 129.21, 128.82, 126.19, 125.98, 125.92, 123.18, 122.84, 39.62, 39.54, 39.37, 38.04, 37.95, 37.84, 37.61, 33.06, 32.88, 31.95, 31.90, 30.95, 30.42, 30.30, 29.97, 29.84, 29.78, 29.73, 29.66, 29.36, 29.34, 28.99, 26.01, 25.96, 25.90, 25.85, 25.80, 23.19, 23.16, 22.66, 14.18, 14.13, 14.06, 10.90. IR: $\tilde{\nu}_{\text{max}}$ (cm^{-1}) 2956, 2923, 2855, 1513, 1485, 1457, 1440, 1378, 1351, 1239, 1180, 1138, 1121, 824, 804, 724, 708. MALDI-TOF-MS: m/z 2211.45 (60 %), 2212.45 (100), 2213.45 (100), 2214.44 (75), 2215.44 (50), 2216.43 (25), 2217.42 (15).

5,5'-[2,3-Bis(2-ethylhexyl)thieno[3,4-*b*]pyrazine-5,7-diyl]bis[4-octyl-2-thiophenecarboxaldehyde] (2, $n = 1$, $m = 1$) O₁₁ (315 mg, 0.42 mmol), DMF (130 μL , 1.7 mmol) and POCl₃ (160 μL , 1.7 mmol) were dissolved in dry dichloromethane (2 mL). The mixture was stirred at 40°C for 48 h. 1 M NaOH (5 mL) was added, the mixture was stirred vigorously and the phases were separated. The aqueous phase was extracted with dichloromethane. The combined organic phases were dried with MgSO₄ and the solvent was evaporated. The crude product was purified by flash chromatography on silica, using dichloromethane/heptane as the eluent. Yield: 227 mg (67 %). $^1\text{H-NMR}$ (400 MHz, CDCl_3): δ 9.92 (s, 2H, $-\text{COH}$), 7.66 (s, 2H, Ar- H), 3.02 (t, $J=7.9$ Hz, 4H, Ar- CH_2-), 2.92 (d, $J=6.8$ Hz, 4H, $-\text{CH}_2\text{CH}(\text{C}_4\text{H}_9)(\text{C}_2\text{H}_5)$), 2.24

(m, 2H, $-\text{CH}_2\text{CH}(\text{C}_4\text{H}_9)(\text{C}_2\text{H}_5)$), 1.80 (m, 4H, $-\text{CH}_2\text{CH}_2\text{C}_6\text{H}_{13}$), 1.53–1.24 (m, 36H, $-\text{CH}_2-$), 0.96 (t, $J = 7.4$ Hz, 6H, $-\text{CH}_3$), 0.91–0.85 (m, 12H, $-\text{CH}_3$). ^{13}C -NMR (100 MHz, CDCl_3): δ 182.75, 157.32, 142.58, 141.12, 139.06, 138.08, 137.76, 124.76, 39.56, 37.61, 32.79, 31.85, 30.86, 29.77, 29.74, 29.49, 29.26, 28.84, 25.90, 23.09, 22.63, 14.08, 14.05, 10.87. IR: $\tilde{\nu}_{\text{max}}$ (cm^{-1}) 2958, 2924, 2854, 1652, 1528, 1463, 1417, 1243, 1155, 744, 669. MALDI-TOF-MS: m/z 804.34 (100%), 805.34 (60), 806.34 (30), 807.35 (10).

5,5'-[(4,4'-Dioctyl[2,2'-bithiophene]-5,5'-diyl)bis[2,3-bis(2-ethylhexyl)thieno[3,4-*b*]pyrazine-7,5-diyl]bis[4-octyl-2-thiophenecarboxaldehyde] (2, $n = 1$, $m = 2$) O_{12} (300 mg, 0.20 mmol), DMF (70 μL , 0.9 mmol) and POCl_3 (80 μL , 0.9 mmol) were dissolved in dry dichloromethane (1.5 mL). The mixture was stirred at 40°C for 48 h. 1 M NaOH (5 mL) was added, the mixture was stirred vigorously and the phases were separated. The organic phase was dried with MgSO_4 and the solvent was evaporated. The crude product was purified by flash chromatography on silica, using dichloromethane/heptane as the eluent. Yield: 280 mg (90%). ^1H -NMR (400 MHz, CDCl_3): δ 9.90 (s, 2H, $-\text{COH}$), 7.65 (s, 2H, Ar-*H*), 7.18 (s, 2H, Ar-*H*), 3.07–2.96 (m, 8H, Ar- CH_2-), 2.95–2.89 (m, 8H, $-\text{CH}_2\text{CH}(\text{C}_4\text{H}_9)(\text{C}_2\text{H}_5)$), 2.40–2.32 (m, 2H, $-\text{CH}_2\text{CH}(\text{C}_4\text{H}_9)(\text{C}_2\text{H}_5)$), 2.29–2.21 (m, 2H, $-\text{CH}_2\text{CH}(\text{C}_4\text{H}_9)(\text{C}_2\text{H}_5)$), 1.86–1.76 (m, 8H, $-\text{CH}_2\text{CH}_2\text{C}_6\text{H}_{13}$), 1.55–1.23 (m, 72H, $-\text{CH}_2-$), 1.04–0.80 (m, 36H, $-\text{CH}_3$). ^{13}C -NMR (100 MHz, CDCl_3): δ 182.69, 156.97, 155.79, 141.98, 141.62, 141.09, 139.18, 139.07, 138.60, 138.05, 137.75, 127.77, 127.04, 126.11, 121.47, 39.63, 39.27, 37.67, 37.50, 32.80, 31.93, 31.89, 31.11, 30.85, 29.91, 29.85, 29.80, 29.61, 29.55, 29.34, 29.32, 28.98, 28.88, 25.90, 25.80, 23.14, 22.67, 14.15, 14.13, 14.08, 10.93. IR: $\tilde{\nu}_{\text{max}}$ (cm^{-1}) 2957, 2923, 2854, 1655, 1528, 1440, 1421, 1391, 1337, 1243, 1157, 862, 825, 743, 723, 670. MALDI-TOF-MS: m/z 1550.97 (85%), 1551.97 (100), 1552.97 (80), 1553.97 (45), 1554.96 (25), 1555.96 (10).

5,5'-[2,2',3,3'-Tetrakis(2-ethylhexyl)[5,5'-bithieno[3,4-*b*]pyrazine]-7,7'-diyl]bis[4-octyl-2-thiophenecarboxaldehyde] (2, $n = 2$, $m = 1$) O_{21} (280 mg, 0.25 mmol), DMF (80 μL , 1.0 mmol) and POCl_3 (100 μL , 1.1 mmol) were dissolved in dry dichloromethane (2 mL). The mixture was stirred at 40°C for 48 h. 1 M NaOH (5 mL) was added, the mixture was stirred vigorously and the phases were separated. The aqueous phase was extracted with dichloromethane. The combined organic phases were dried with MgSO_4 and the solvent was evaporated. The crude product was purified by flash chromatography on silica, using dichloromethane/heptane as the eluent. The product was further purified by recycling GPC. Yield: 202 mg (68%). ^1H -NMR (400 MHz, CDCl_3): δ 9.92 (s, 2H, $-\text{COH}$), 7.68 (s, 2H, Ar-*H*), 3.14 (t, $J = 7.1$ Hz, 4H, Ar- CH_2-), 2.99 (d, $J = 6.5$ Hz, 4H, $-\text{CH}_2\text{CH}(\text{C}_4\text{H}_9)(\text{C}_2\text{H}_5)$), 2.95 (d, $J = 6.3$ Hz, 4H, $-\text{CH}_2\text{CH}(\text{C}_4\text{H}_9)(\text{C}_2\text{H}_5)$), 2.28 (m, 4H, $-\text{CH}_2\text{CH}(\text{C}_4\text{H}_9)(\text{C}_2\text{H}_5)$), 1.84 (qu, $J = 7.2$ Hz, 4H, $-\text{CH}_2\text{CH}_2\text{C}_6\text{H}_{13}$), 1.58–1.20 (m, 52H, $-\text{CH}_2-$), 1.02–0.93 (m, 12H, $-\text{CH}_3$), 0.92–0.82 (m, 18H, $-\text{CH}_3$). ^{13}C -NMR (100 MHz, CDCl_3): δ 182.67, 157.15, 156.16, 141.93, 140.63, 139.52, 139.38, 138.64, 137.88, 125.56, 125.32, 39.65, 38.11, 37.76, 33.02, 32.82, 32.78, 31.85, 30.81, 29.73, 29.68, 29.64, 29.27, 28.95, 28.88, 28.86, 25.98, 25.91, 25.87, 23.16, 23.12, 22.63, 14.12, 14.09, 14.04, 10.90, 10.88. IR: $\tilde{\nu}_{\text{max}}$ (cm^{-1}) 2957, 2921, 2854, 1651, 1525, 1458, 1439, 1427, 1402, 1387, 1352, 1336, 1246, 1162, 887, 747, 726, 677, 662. MALDI-TOF-MS: m/z 1162.71 (100%), 1163.71 (80), 1164.71 (50), 1165.71 (25), 1166.72 (10).

5,5'-[(4,4'-Dioctyl[2,2'-bithiophene]-5,5'-diyl)bis[2,2',3,3'-tetrakis(2-ethylhexyl)[5,5'-bithieno[3,4-*b*]pyrazine]-7',7'-diyl]]bis[4-octyl-2-thiophenecarboxaldehyde] (2, *n* = 2, *m* = 2) O₂₂ (304 mg, 0.14 mmol), DMF (50 μL, 0.6 mmol) and POCl₃ (60 μL, 0.7 mmol) were dissolved in dry dichloromethane (1 mL). The mixture was stirred at 40°C for 48 h. 1 M NaOH (3 mL) was added, the mixture was stirred vigorously and the phases were separated. The organic phase was dried with MgSO₄ and the solvent was evaporated. The crude product was purified by flash chromatography on silica, using dichloromethane/heptane as the eluent. Yield: 257 mg (82%). ¹H-NMR (400 MHz, CDCl₃): δ 9.91 (s, 2H, -COH), 7.68 (s, 2H, Ar-*H*), 7.21 (s, 2H, Ar-*H*), 3.18–3.10 (m, 8H, Ar-CH₂-), 3.02–2.92 (m, 16H, -CH₂CH(C₄H₉)(C₂H₅)), 2.45–2.37 (m, 2H, -CH₂CH(C₄H₉)(C₂H₅)), 2.33–2.24 (m, 6H, -CH₂CH(C₄H₉)(C₂H₅)), 1.91–1.80 (m, 8H, -CH₂CH₂C₆H₁₃), 1.60–1.20 (m, 104H, -CH₂-), 1.07–0.82 (m, 60H, -CH₃). ¹³C-NMR (100 MHz, CDCl₃): δ 182.61, 157.00, 155.95, 155.60, 155.47, 141.70, 141.35, 140.10, 140.05, 139.48, 138.84, 138.34, 138.13, 138.03, 128.89, 128.25, 126.39, 126.09, 123.59, 121.99, 39.68, 39.60, 39.35, 38.13, 37.80, 37.61, 33.06, 32.85, 31.94, 31.87, 31.09, 30.80, 29.87, 29.78, 29.71, 29.67, 29.35, 29.30, 28.98, 28.88, 26.01, 25.93, 25.88, 25.83, 25.77, 23.19, 23.14, 22.66, 14.17, 14.14, 14.11, 14.06, 10.96, 10.89. IR: $\tilde{\nu}_{max}$ (cm⁻¹) 2956, 2923, 2855, 1655, 1527, 1457, 1414, 1391, 1378, 1332, 1244, 1154, 825, 803, 745, 725, 672. MALDI-TOF-MS: *m/z* 2267.47 (60%), 2268.47 (95), 2269.46 (100), 2270.45 (75), 2271.44 (50), 2272.44 (25), 2273.44 (15).

2',2''-[[2,3-Bis(2-ethylhexyl)thieno[3,4-*b*]pyrazine-5,7-diyl]bis(4-octyl-5,2-thiophenediyl)]bis[1',5'-dihydro-1'-methyl-2'-H-[5,6]fullereno-C₆₀-I_h-[1,9-*c*]pyrrole] (T₁₁) Compound 2 (*n* = 1, *m* = 1) (226 mg, 0.28 mmol), C₆₀ (2.0 g, 2.8 mmol), and *N*-methylglycine (0.26 g, 3.0 mmol) were dissolved in ODCB (250 mL) and stirred at 120°C for 5 h. The solvent was evaporated. The excess of C₆₀ was removed by column chromatography on silica, using CS₂ as the eluent. The product was subsequently eluted with toluene and the solvent was evaporated. The product was redissolved in ODCB, precipitated in methanol and dried in a vacuum oven. Yield: 453 mg (67%). About 7 mg of the product was further purified by preparative HPLC. ¹H-NMR (500 MHz, CS₂): δ 7.19 (s, 2H, Ar-*H*), 5.16 (s, 2H, MP-*H*), 4.93 (d, *J* = 9.4 Hz, 2H, MP-*H*), 4.23 (d, *J* = 9.4 Hz, 2H, MP-*H*), 2.93 (s, 6H, N-CH₃), 2.89 (t, *J* = 7.2 Hz, 4H, Ar-CH₂-), 2.77 (d, *J* = 6.8 Hz, 4H, -CH₂CH(C₄H₉)(C₂H₅)), 2.30–2.19 (m, 2H, -CH₂CH(C₄H₉)(C₂H₅)), 1.65 (m, 4H, -CH₂CH₂C₆H₁₃), 1.50–1.14 (m, 36H, -CH₂-), 0.97–0.80 (m, 18H, -CH₃). ¹³C-NMR (125 MHz, CS₂): δ 155.71, 155.67, 154.90, 153.55, 153.07, 152.98, 147.06, 147.04, 146.73, 146.72, 146.16, 146.11, 146.02, 146.00, 145.95, 145.89, 145.84, 145.71, 145.51, 145.42, 145.25, 145.20, 145.12, 145.10, 145.02, 145.00, 144.92, 144.48, 144.45, 144.14, 142.93, 142.90, 142.80, 142.49, 142.40, 142.01, 141.95, 141.89, 141.84, 141.78, 141.71, 141.68, 141.66, 141.45, 141.39, 140.54, 140.03, 139.95, 139.72, 139.54, 138.75, 137.37, 136.77, 136.69, 136.60, 136.54, 135.62, 135.47, 130.35, 129.82, 129.79, 127.37, 123.75, 79.23, 79.15, 77.04, 77.02, 69.91, 69.89, 68.46, 40.24, 40.22, 39.34, 39.21, 37.19, 36.91, 33.31, 33.29, 33.25, 33.23, 32.24, 30.83, 30.81, 30.21, 30.19, 29.95, 29.85, 29.70, 29.37, 29.27, 26.46, 26.42, 26.30, 26.27, 23.77, 23.74, 23.24, 14.74, 14.57, 11.37, 11.36, 11.23, 11.21. IR: $\tilde{\nu}_{max}$ (cm⁻¹) 2953, 2920, 2850, 2777, 1461, 1260, 1088, 1016, 796, 768. MALDI-TOF-MS: *m/z* 2298.30 (50%), 2299.30 (100), 2300.30 (95), 2301.31 (70), 2302.28 (50). HPLC: 1 peak at 5.3 min.

2',2'''-[(4,4'-Diocetyl[2,2'-bithiophene]-5,5'-diyl)bis[2,3-bis(2-ethylhexyl)thieno[3,4-*b*]pyrazine-7,5-diyl](4-octyl-5,2-thiophenediyl)]bis[1',5'-dihydro-1'-methyl-2'H-[5,6]fullereno-C₆₀-I_h-[1,9-*c*]pyrrole] (**T₁₂**) Compound **2** ($n=1$, $m=2$) (281 mg, 0.18 mmol), C₆₀ (1.3 g, 1.8 mmol), and *N*-methylglycine (0.18 g, 2.0 mmol) were dissolved in ODCB (225 mL) and stirred at 120°C for 5 h. The solvent was evaporated. The excess of C₆₀ was removed by column chromatography on silica, using CS₂ as the eluent. The product was subsequently eluted with toluene and the solvent was evaporated. The product was redissolved in ODCB, precipitated in methanol and dried in a vacuum oven. Yield: 161 mg (29%). About 15 mg of the product was further purified by preparative HPLC. ¹H-NMR (400 MHz, CS₂): δ 7.19 (s, 2H, Ar-*H*), 6.92 (s, 2H, Ar-*H*), 5.15 (s, 2H, MP-*H*), 4.91 (d, *J* = 9.4 Hz, 2H, MP-*H*), 4.22 (d, *J* = 9.4 Hz, 2H, MP-*H*), 2.92 (s, 6H, N-CH₃), 2.92–2.70 (m, 16H, Ar-CH₂-), 2.31–2.20 (m, 4H, -CH₂CH(C₄H₉)(C₂H₅)), 1.76–1.61 (m, 8H, -CH₂CH₂C₆H₁₃), 1.52–1.10 (m, 72H, -CH₂-), 0.99–0.77 (m, 36H, -CH₃). ¹³C-NMR (100 MHz, CS₂): δ 155.74, 155.69, 154.90, 154.57, 153.58, 153.11, 153.02, 147.07, 147.05, 146.76, 146.75, 146.19, 146.13, 146.03, 146.01, 145.96, 145.91, 145.85, 145.72, 145.52, 145.43, 145.42, 145.26, 145.21, 145.13, 145.04, 145.01, 144.93, 144.49, 144.47, 144.16, 142.94, 142.91, 142.81, 142.50, 142.41, 142.03, 142.01, 141.96, 141.91, 141.85, 141.79, 141.73, 141.70, 141.68, 141.46, 141.41, 140.44, 140.04, 139.96, 139.73, 139.56, 138.62, 137.83, 137.50, 137.37, 136.78, 136.70, 136.62, 136.56, 135.62, 135.48, 129.97, 129.85, 129.83, 128.00, 125.59, 124.00, 123.36, 79.25, 79.19, 77.07, 69.92, 68.48, 40.25, 40.23, 39.36, 39.24, 39.14, 37.26, 37.21, 36.98, 36.93, 33.31, 33.26, 33.06, 33.03, 32.26, 31.03, 30.86, 30.21, 30.16, 30.10, 29.97, 29.86, 29.72, 29.39, 29.29, 29.20, 26.46, 26.44, 26.29, 26.25, 23.79, 23.76, 23.62, 23.25, 23.23, 14.73, 14.56, 11.38, 11.30, 11.28, 11.24. IR: $\tilde{\nu}_{max}$ (cm⁻¹) 2952, 2960, 2851, 2780, 1494, 1462, 1376, 1332, 1241, 1216, 1179, 1121, 1107, 1030, 825, 768, 725. MALDI-TOF-MS: *m/z* 3045.55 (30%), 3046.53 (75), 3047.53 (100), 3048.53 (100), 3049.53 (80), 3050.53 (55), 3051.52 (30), 3052.55 (15). HPLC: 1 peak at 4.6 min.

2',2'''-[[2,2',3,3'-Tetrakis(2-ethylhexyl)[5,5'-bithieno[3,4-*b*]pyrazine]-7,7'-diyl]bis(4-octyl-5,2-thiophenediyl)]bis[1',5'-dihydro-1'-methyl-2'H-[5,6]fullereno-C₆₀-I_h-[1,9-*c*]pyrrole] (**T₂₁**) Compound **2** ($n=2$, $m=1$) (135 mg, 0.12 mmol), C₆₀ (0.86 g, 1.2 mmol), and *N*-methylglycine (0.12 g, 1.4 mmol) were dissolved in ODCB (150 mL) and stirred at 120°C for 5 h. The solvent was evaporated. The excess of C₆₀ was removed by column chromatography on silica, using CS₂ as the eluent. The product was subsequently eluted with toluene and the solvent was evaporated. The product was redissolved in ODCB, precipitated in methanol and dried in a vacuum oven. Yield: 238 mg (77%). About 50 mg of the product was further purified by preparative HPLC. ¹H-NMR (400 MHz, CS₂): δ 7.19 (s, 2H, Ar-*H*), 5.15 (s, 2H, MP-*H*), 4.91 (d, *J* = 9.4 Hz, 2H, MP-*H*), 4.22 (d, *J* = 9.4 Hz, 2H, MP-*H*), 2.98 (t, *J* = 7.0 Hz, 4H, Ar-CH₂-), 2.92 (s, 6H, N-CH₃), 2.84 (d, *J* = 6.8 Hz, 4H, -CH₂CH(C₄H₉)(C₂H₅)), 2.79 (d, *J* = 6.6 Hz, 4H, -CH₂CH(C₄H₉)(C₂H₅)), 2.31–2.18 (m, 4H, -CH₂CH(C₄H₉)(C₂H₅)), 1.67 (qu, *J* = 7.0 Hz, 4H, -CH₂CH₂C₆H₁₃), 1.50–1.10 (m, 52H, -CH₂-), 0.97–0.75 (m, 30H, -CH₃). ¹³C-NMR (100 MHz, CS₂): δ 155.75, 155.71, 154.95, 154.43, 153.57, 153.59, 153.15, 153.05, 147.06, 147.03, 146.79, 146.22, 146.11, 146.00, 145.95, 145.90, 145.84, 145.71, 145.51, 145.42, 145.40, 145.26, 145.18, 145.13, 145.11, 145.13, 145.02, 144.99, 144.92, 144.46, 144.14, 142.92, 142.89, 142.80, 142.48, 142.39, 142.02, 142.01, 141.95, 141.89, 141.83, 141.79, 141.73, 141.69, 141.67,

141.45, 141.39, 140.45, 140.03, 139.94, 139.71, 139.57, 138.72, 137.73, 137.69, 136.74, 136.67, 136.63, 136.57, 135.60, 135.49, 130.69, 129.88, 126.13, 123.14, 79.18, 77.46, 77.07, 69.90, 68.47, 40.21, 40.18, 39.36, 39.25, 37.70, 37.34, 37.09, 33.24, 33.20, 32.21, 30.74, 30.07, 30.02, 29.64, 29.61, 29.36, 29.28, 29.14, 26.35, 26.31, 23.75, 23.71, 23.68, 23.19, 14.68, 14.53, 14.50, 11.33, 11.22, 11.19, 11.17, 11.14. IR: $\tilde{\nu}_{max}$ (cm⁻¹) 2952, 2921, 2852, 2779, 1541, 1495, 1462, 1429, 1376, 1331, 1242, 1179, 1122, 1030, 900, 768, 726. MALDI-TOF-MS: m/z 2656.52 (40%), 2657.51 (85), 2658.51 (100), 2659.51 (85), 2660.50 (60), 2661.51 (40), 2662.46 (20). HPLC: 1 peak at 4.7 min.

2',2'''-[(4,4'-Dioctyl[2,2'-bithiophene]-5,5'-diyl)bis[[2,2',3,3'-tetrakis(2-ethylhexyl)[5,5'-bithieno[3,4-*b*]pyrazine]-7,7'-diyl](3-octyl-5,2-thiophenediyl)]]bis[1',5'-dihydro-1'-methyl-2'-H-[5,6]fullereno-C₆₀-I_h-[1,9-*c*]pyrrole] (T₂₂) Compound 2 ($n=2$, $m=2$) (243 mg, 0.11 mmol), C₆₀ (0.98 g, 1.4 mmol), and *N*-methylglycine (0.12 g, 1.4 mmol) were dissolved in ODCB (225 mL) and stirred at 120°C for 5 h. The solvent was evaporated. The excess of C₆₀ was removed by column chromatography on silica, using CS₂ as the eluent. The product was subsequently eluted with toluene and the solvent was evaporated. The product was redissolved in ODCB, precipitated in methanol and dried in a vacuum oven. Yield: 260 mg (64%). About 50 mg of the product was further purified by preparative HPLC. ¹H-NMR (400 MHz, CS₂): δ 7.21 (s, 2H, Ar-*H*), 6.97 (s, 2H, Ar-*H*), 5.16 (s, 2H, MP-*H*), 4.92 (d, $J=9.5$ Hz, 2H, MP-*H*), 4.22 (d, $J=9.4$ Hz, 2H, MP-*H*), 3.04–2.95 (m, 8H, Ar-CH₂-), 2.93 (s, 6H, N-CH₃), 2.90–2.79 (m, 16H, -CH₂CH(C₄H₉)(C₂H₅)), 2.35–2.18 (m, 8H, -CH₂CH(C₄H₉)(C₂H₅)), 1.81–1.65 (m, 8H, -CH₂CH₂C₆H₁₃), 1.56–1.10 (m, 104H, -CH₂-), 1.02–0.75 (m, 60H, -CH₃). ¹³C-NMR (100 MHz, CS₂): δ 155.77, 155.73, 154.95, 154.56, 154.48, 154.35, 153.60, 153.18, 153.08, 147.08, 147.05, 146.82, 146.80, 146.24, 146.13, 146.03, 146.01, 145.97, 145.91, 145.85, 145.72, 145.54, 145.44, 145.42, 145.27, 145.21, 145.15, 145.05, 145.02, 145.01, 144.93, 144.49, 144.17, 144.15, 142.93, 142.91, 142.81, 142.50, 142.40, 142.04, 142.02, 141.96, 141.91, 141.85, 141.80, 141.74, 141.71, 141.46, 141.41, 140.59, 140.38, 140.35, 140.04, 139.95, 139.73, 139.60, 138.64, 137.98, 137.81, 137.77, 136.77, 136.69, 136.65, 136.60, 135.61, 135.50, 130.77, 129.89, 129.03, 126.61, 125.86, 125.70, 123.34, 122.73, 79.26, 77.12, 77.10, 69.93, 68.50, 40.25, 40.22, 39.48, 39.40, 39.28, 37.87, 37.75, 37.40, 37.12, 33.32, 33.27, 33.24, 33.20, 33.10, 33.07, 32.26, 31.05, 30.80, 30.11, 30.08, 29.70, 29.66, 29.41, 29.32, 29.25, 29.23, 29.19, 26.36, 26.32, 26.28, 26.23, 23.80, 23.77, 23.74, 23.72, 23.64, 23.24, 23.21, 14.74, 14.58, 14.55, 14.52, 11.38, 11.31, 11.28, 11.26, 11.21, 11.19, 11.18, 11.15. IR: $\tilde{\nu}_{max}$ (cm⁻¹) 2953, 2921, 2852, 2780, 1541, 1490, 1456, 1376, 1332, 1242, 1179, 1121, 1030, 900, 829, 769, 726. MALDI-TOF-MS: m/z 3762.9 (50%), 3063.9 (70), 3764.9 (90), 3765.87 (100), 3766.90 (70), 3767.82 (50). HPLC: 1 peak at 4.3 min.

References and notes

1. Ford, T. A.; Avilov, I.; Beljonne, D.; Greenham, N. C. *Phys. Rev. B* **2005**, *71*, 125212.
2. Offermans, T.; Van Hal, P. A.; Meskers, S. C. J.; Koetse, M. M.; Janssen, R. A. J. *Phys. Rev. B* **2005**, *72*, 045213.

3. Ford, T. A.; Ohkita, H.; Cook, S.; Durrant, J. R.; Greenham, N. C. *Chem. Phys. Lett.* **2008**, *454*, 237–241.
4. Imahori, H. *Bull. Chem. Soc. Jpn.* **2007**, *80*, 621–636.
5. Guldi, D. M.; Illescas, B. M.; Atienza, C. M.; Wielopolskia, M.; Martin, N. *Chem. Soc. Rev.* **2009**, *38*, 1587–1597.
6. Williams, R. M.; Zwier, J. M.; Verhoeven, J. W. *J. Am. Chem. Soc.* **1995**, *117*, 4093–4099.
7. Williams, R. M.; Koeberg, M.; Lawson, J. M.; An, Y. Z.; Rubin, Y.; PaddonRow, M. N.; Verhoeven, J. W. *J. Org. Chem.* **1996**, *61*, 5055–5062.
8. Schuster, D. I.; Cheng, P.; Wilson, S. R.; Prokhorenko, V.; Katterle, M.; Holzwarth, A. R.; Braslavsky, S. E.; Klihm, G.; Williams, R. M.; Luo, C. P. *J. Am. Chem. Soc.* **1999**, *121*, 11599–11600.
9. Schuster, D. I.; Cheng, P.; Jarowski, P. D.; Guldi, D. M.; Luo, C. P.; Echegoyen, L.; Pyo, S.; Holzwarth, A. R.; Braslavsky, S. E.; Williams, R. M.; Klihm, G. *J. Am. Chem. Soc.* **2004**, *126*, 7257–7270.
10. McClenaghan, N. D.; Grote, Z.; Darriet, K.; Zimine, M.; Williams, R. M.; De Cola, L.; Bassani, D. M. *Org. Lett.* **2005**, *7*, 807–810.
11. Galloni, P.; Floris, B.; De Cola, L.; Cecehetto, E.; Williams, R. M. *J. Phys. Chem. C* **2007**, *111*, 1517–1523.
12. Verhoeven, J. W. *J. Photochem. Photobiol. C. Photochem. Rev.* **2006**, *7*, 40–60.
13. Dance, Z. E. X.; Mi, Q.; McCamant, D. W.; Ahrens, M. J.; Ratner, M. A.; Wasielewski, M. R. *J. Phys. Chem. B* **2006**, *110*, 25163–25173.
14. Wasielewski, M. R.; Johnson, D. G.; Svec, W. A.; Kersey, K. M.; Minsek, D. W. *J. Am. Chem. Soc.* **1988**, *110*, 7219–7221.
15. Wiederrecht, G. P.; Svec, W. A.; Wasielewski, M. R.; Galili, T.; Levanon, H. *J. Am. Chem. Soc.* **2000**, *122*, 9715–9722.
16. Okada, T.; Karaki, I.; Matsuzawa, E.; Mataga, N.; Sakata, Y.; Misumi, S. *J. Phys. Chem.* **1981**, *85*, 3957–3960.
17. Benniston, A. C.; Harriman, A.; Li, P.; Rostron, J. P.; Van Ramesdonk, H. J.; Groeneveld, M. M.; Zhang, H.; Verhoeven, J. W. *J. Am. Chem. Soc.* **2005**, *127*, 16054–16064.
18. Harriman, A.; Mallon, L. J.; Ulrich, G.; Ziessel, R. *Chemphyschem* **2007**, *8*, 1207–1214.
19. Yamamoto, T.; Morita, A.; Miyazaki, Y.; Maruyama, T.; Wakayama, H.; Zhou, Z.; Nakamura, Y.; Kanbara, T.; Sasaki, S.; Kubota, K. *Macromolecules* **1992**, *25*, 1214–1223.

20. Vilsmeier, A.; Haack, A. *Ber. Dtsch. Chem. Ges.* **1927**, *60B*, 119–122.
21. Maggini, M.; Scorrano, G.; Prato, M. *J. Am. Chem. Soc.* **1993**, *115*, 9798–9799.
22. Van Hal, P. A.; Beckers, E. H. A.; Peeters, E.; Apperloo, J. J.; Janssen, R. A. J. *Chem. Phys. Lett.* **2000**, *328*, 403–408.
23. Weller, A. Z. *Phys. Chem. Neue Folge* **1982**, *133*, 93–98.
24. Van Bolhuis, F.; Wynberg, H.; Havinga, E. E.; Meijer, E. W.; Staring, E. G. J. *Synth. Met.* **1989**, *30*, 381–389.
25. Reynolds, L.; Gardecki, J. A.; Frankland, S. J. V.; Horng, M. L.; Maroncelli, M. J. *Phys. Chem.* **1996**, *100*, 10337–10354.
26. Veldman, D.; Chopin, S. M. A.; Meskers, S. C. J.; Janssen, R. A. J. *J. Phys. Chem. A* **2008**, *112*, 8617–8632.
27. Marcus, R. A. *J. Chem. Phys.* **1965**, *43*, 679–701.
28. Marcus, R. A. *Angew. Chem. Int. Ed.* **1993**, *32*, 1111–1121.
29. Oevering, H.; Paddon-Row, M. N.; Heppener, M.; Oliver, A. M.; Cotsaris, E.; Verhoeven, J. W.; Hush, N. S. *J. Am. Chem. Soc.* **1987**, *109*, 3258–3269.
30. Kestner, N. R.; Logan, J.; Jortner, J. *J. Phys. Chem.* **1974**, *78*, 2148–2166.
31. Ulstrup, J.; Jortner, J. *J. Chem. Phys.* **1975**, *63*, 4358–4368.
32. Beckers, E. H. A.; Meskers, S. C. J.; Schenning, A. P. H. J.; Chen, Z. J.; Würthner, F.; Janssen, R. A. J. *J. Phys. Chem. A* **2004**, *108*, 6933–6937.
33. Baffreau, J.; Leroy-Lhez, S.; Vân Anh, N.; Williams, R. M.; Hudhomme, P. *Chem. Eur. J.* **2008**, *14*, 4974–4992.

Chapter 7

Charge separation and (triplet) recombination in diketopyrrolopyrrole – fullerene triads

Abstract Synthesis and photophysics of two diketopyrrolopyrrole-based small band gap oligomers, end-capped at both ends with C₆₀ are presented. Upon photoexcitation of the oligomer, ultrafast energy transfer to the fullerene occurs (~0.5 ps), followed by an electron transfer reaction. Femtosecond photoinduced absorption has been used to determine the rates for charge separation and recombination. Charge separation occurs in the Marcus normal region with a time constant of 18–47 ps and recombination occurs in the inverted regime, with a time constant of 37 ps to 1.5 ns. Both processes are faster in *o*-dichlorobenzene (ODCB) than in toluene. Analysis of the charge transfer rates by Marcus–Jortner theory leads to the view that the positive charge must be located on the thiophene/bithiophene unit closest to the fullerene. Approximately 14% of the charge transfer state was found to recombine into the low-lying triplet state of the oligomer for the smaller system in ODCB.

This work has been published: Karsten, B. P.; Bouwer, R. K. M.; Hummel, J. C.; Williams, R. M.; Janssen, R. A. J. *Photochem. Photobiol. Sci.* **2010**, doi: 10.1039/c0pp00098a.

7.1 Introduction

One class of compounds that has attracted much interest recently for use as donor materials in organic photovoltaics, is based on alternating electron-rich thiophene units and electron-poor diketopyrrolopyrrole (DPP) units. Using polymers¹⁻⁴ and short oligomers⁵⁻⁷ containing the DPP unit, device efficiencies approaching 5 % have been reported. A common feature of these DPP-based materials is their relatively high oxidation potential, leading to high-energy charge separated states when combined with fullerenes, and to correspondingly high voltages when used in solar cells.

Despite the advantage of having light absorption extending into the near-IR region of the spectrum, one of the drawbacks of small-band gap systems like the DPP-based polymers is their generally low triplet energy. If the triplet energy is lower than the energy of the charge separated state, this leads to the possibility of charge recombination into the triplet state. This triplet recombination is therefore likely to be a loss mechanism in solar cells based on small band gap polymers and oligomers.⁸⁻¹⁰

As electron transfer reactions are key steps in the charge separation and recombination processes, detailed knowledge about these reactions could be of great help in designing new donor-acceptor combinations. Many studies of electron transfer processes in linked donor–fullerene systems have been performed in the past decades.¹¹⁻¹⁸ In general, charge separation occurs rapidly, in the Marcus normal regime, followed by charge recombination in the Marcus inverted regime. Also charge recombination into a triplet state has been observed frequently.^{13,19-22}

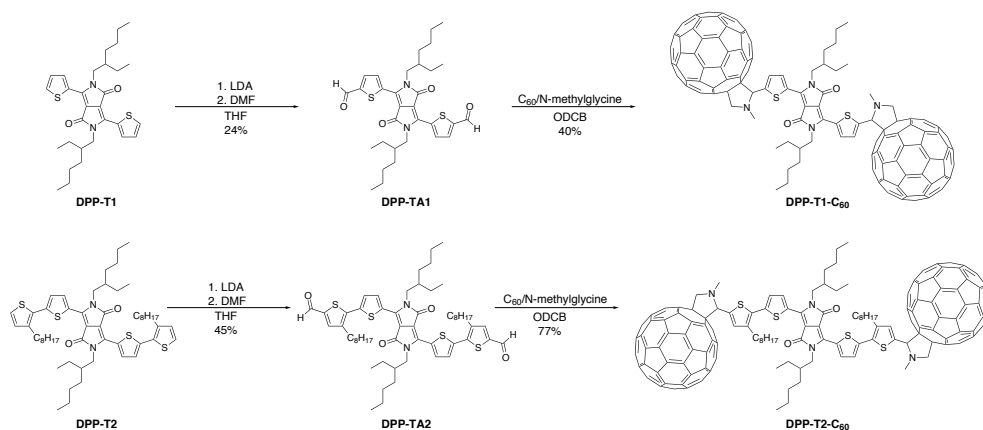
In chapter 6 studies on several small band gap oligomer – fullerene triads are described, using thienopyrazines (TPs) as the electron-deficient unit in the oligomer. We found, that in these systems very fast charge separation took place close to the Marcus optimal region. Charge recombination occurred in the Marcus inverted region. In these systems no recombination into the low-lying triplet state could be observed, most probably due to the short lifetime of the charge separated state, preventing intersystem crossing in that state. Here, we present a similar series of oligomer – fullerene triads, based on the DPP-core as the electron-deficient unit in the oligomers. In these systems, charge transfer takes place in a two-step fashion, upon photoexcitation of the oligomer. In the first step, energy transfer to the C₆₀ moiety takes place, followed by electron transfer in the Marcus normal region. As the energy of the charge separated state in the DPP-systems is higher than in the TP-systems, and charge recombination takes place in the Marcus inverted regime, the lifetime of the charge separated state is long enough to allow relatively slow intersystem crossing followed by much faster charge recombination into the triplet excited state of the oligomer.

7.2 Results and discussion

7.2.1 Synthesis

Synthesis of the compounds is depicted in scheme 7.1. Oligomers **DPP-T1** and **DPP-T2** were synthesized according to (modified) literature procedures.^{3,23} Lithiation

with lithium diisopropylamide (LDA), followed by quenching of the anion by *N,N*-dimethylformamide (DMF) gave the corresponding aldehydes. These were reacted with C_{60} and *N*-methylglycine in a Prato reaction,²⁴ yielding triads **DPP-T1-C₆₀** and **DPP-T2-C₆₀**. Small amounts of the crude triads were purified by preparative HPLC for the analysis described in this chapter. The compounds were characterized by ¹H-NMR, ¹³C-NMR, FT-IR and MALDI-TOF-MS.



Scheme 7.1: Synthesis of the compounds under study

7.2.2 Optical and electrochemical properties

UV/vis absorption spectra of the oligomers and triads are given in figure 7.1a. It can be seen, that the absorption of the triads resembles a superposition of the spectra of the separate oligomer and *N*-methylfulleropyrrolidine (MP- C_{60}) units, although a distinct red-shift in the absorption is observed. The most likely cause for this red-shift is the fact that the end-groups connected to the oligomer (H in the bare oligomer and MP- C_{60} in the triads) differ, thereby slightly influencing the electronic energy levels of the polymer. No other electronic interactions (*e.g.* charge-transfer absorptions) can be observed in the absorption spectrum of **DPP-T2-C₆₀**. Due to the low solubility of **DPP-T1-C₆₀**, some scattering occurred in the UV-experiment, reflected in the low-energy tail of the spectrum. Therefore, no definite conclusions about other electronic interactions can be drawn from these spectra, although there are no clear indications for their existence. From the onsets of absorption, the optical band gaps of the oligomers can be calculated as 2.15 eV for **DPP-T1** and 1.88 eV for **DPP-T2**. The UV/vis absorption data of the oligomers are summarized in table 7.1.

Cyclic voltammograms of the separate oligomers and MP- C_{60} are depicted in figure 7.1b. In both oligomers, one or two reversible oxidations and one reversible reduction were observed. From the onsets of oxidation and reduction, the electrochemical band gaps of the oligomers can be calculated as 2.09 eV for **DPP-T1**, and 1.81 eV for **DPP-T2**. These values are in good agreement with the optical band gaps. The electrochemical data for the oligomers are summarized in table 7.1.

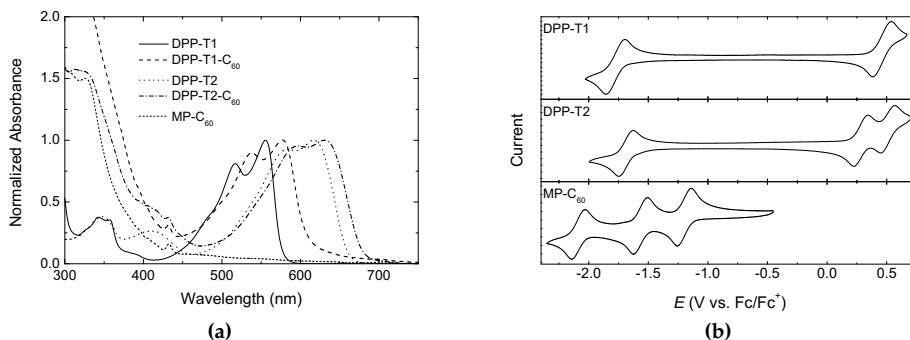


Figure 7.1: Normalized UV/vis absorption spectra of the oligomers, triads and MP-C₆₀ recorded in ODCB (a) and cyclic voltammograms of the oligomers and MP-C₆₀ recorded in ODCB (b).

Table 7.1: UV/vis absorption and fluorescence and electrochemical data in ODCB for the oligomers and MP-C₆₀. Oxidation and reduction potentials are relative to ferrocene.

	λ_{onset} (nm)	E_{S1} (eV)	λ_{max} (nm)	λ_{max}^{PL} (nm)	Φ_F	τ_F (ns)	E_{ox}^{onset} (V)	E_{ox}^0 (V)	E_{red}^{onset} (V)	E_{red}^0 (V)	E_g^{CV} (eV)
DPP-T1	576	2.15	555	569	0.62	5.9	0.38	0.46	-1.71	-1.78	2.09
DPP-T2	660	1.88	617	653	> 0.23 ^a	2.5	0.21	0.29	-1.60	-1.69	1.81
MP-C₆₀	726	1.71	433	717		1.3			-1.13	-1.20	

^a Not the full fluorescence band could be detected. Therefore, a lower limit for the fluorescence quantum yield is given.

7.2.3 Triplet excited states and cations of the oligomers

The absorptions of the triplet excited states of **DPP-T1** and **DPP-T2** were investigated by near steady-state photoinduced absorption (PIA) spectroscopy. As direct excitation of the oligomers did not result in a detectable signal, due to the low quantum yield for intersystem crossing to the triplet state, triplet sensitization with MP-C₆₀ in toluene solution was employed.²⁵ In these experiments MP-C₆₀ is excited, leading to the triplet excited state of MP-C₆₀ with a quantum yield of near unity. The energy of this triplet state can then be transferred from MP-C₆₀ to the oligomer, provided that the latter triplet state has a lower energy than the triplet of MP-C₆₀. The obtained spectra are shown in figure 7.2. Both spectra show a bleaching band at the absorption wavelength of the oligomer, and a strong absorption at lower energy. The triplet spectrum of **DDP-T1** shows a $T_n \leftarrow T_1$ absorption at 1.44 eV with two vibronic progressions to higher energies with spacings of 0.16 (strong) and 0.08 eV (weak). In **DPP-T2** the lowest energy $T_n \leftarrow T_1$ absorption has red shifted to 1.08 eV, again with a vibronic peak shifted by 0.16 eV, but the spectrum is dominated by an absorption at 1.88 eV.

The energies of the triplet states can be estimated by adding quenchers with a known triplet energy to the oligomer/MP-C₆₀ mixture. If the triplet energy of the oligomer is lower than the triplet energy of the quencher, the spectrum is not af-

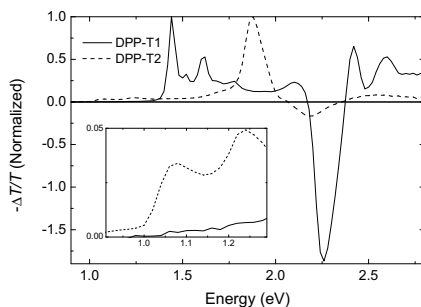


Figure 7.2: Near steady-state PIA spectra of mixtures of **DPP-T1** or **DPP-T2** (0.1 mM) and **MP-C₆₀** (0.4 mM) recorded in toluene, at an excitation wavelength of 351/364 nm. The inset shows an enlargement of the low-energy part of the spectra.

ected and the triplet state of the oligomer is still visible. If however, the triplet energy of the quencher is lower than that of the oligomer, the triplet of the oligomer is quenched, and the triplet absorption of the quencher is observed. In case both absorptions are visible, both triplets have about the same energy. In this way, the energies of the triplet states of the oligomers can be estimated as being around 1.1 eV for **DPP-T1** (partial quenching of the rubrene triplet, at 1.14 eV,²⁶ and visibility of both **DPP-T1** and rubrene triplet signals in the spectrum) and around 0.9 eV for **DPP-T2** (partial quenching of the bis(trihexylsiloxy)silicon-2,3-naphthalocyanine triplet, at 0.93 eV).²⁷ The triplet energy of **MP-C₆₀** is known to be 1.50 eV.¹³ Triplet energies and absorption maxima are summarized in table 7.2.

Table 7.2: Triplet $T_n \leftarrow T_1$ absorption maxima and triplet energies (E_T) of the oligomers and absorption maxima ($D_1 \leftarrow D_0$ and $D_2 \leftarrow D_0$) of the radical cations (RC) of the oligomers.

	$T_n \leftarrow T_1$ (eV)	E_T (eV)	RC $D_1 \leftarrow D_0$ (eV)	RC $D_2 \leftarrow D_0$ (eV)
DPP-T1	1.44	1.1	1.45	2.03
DPP-T2	1.08	1.88	1.21	1.45

The absorption spectra of the radical cations, formed upon oxidation of **DPP-T1** and **DPP-T2** can be investigated by chemical oxidation with thianthrenium hexafluorophosphate.²⁸ In these experiments the oxidant is added to a solution of the oligomer in small aliquots, and the UV/vis spectra are recorded. Spectra obtained in this way are shown in figure 7.3. In both cases, the original $\pi \rightarrow \pi^*$ absorption band of the neutral oligomer disappears and two bands appear at lower energy. These bands can be attributed to the HOMO \rightarrow SOMO (Singly Occupied Molecular Orbital) and SOMO \rightarrow LUMO transitions of the newly formed doublet-state radical. The absorption maxima of the radical cations are summarized in table 7.2.

7.2.4 Photoluminescence of oligomers and triads

Photoluminescence spectra of oligomers **DPP-T1** and **DPP-T2** dissolved in toluene are depicted in figure 7.4a. Fluorescence maxima, quantum yields and lifetimes are

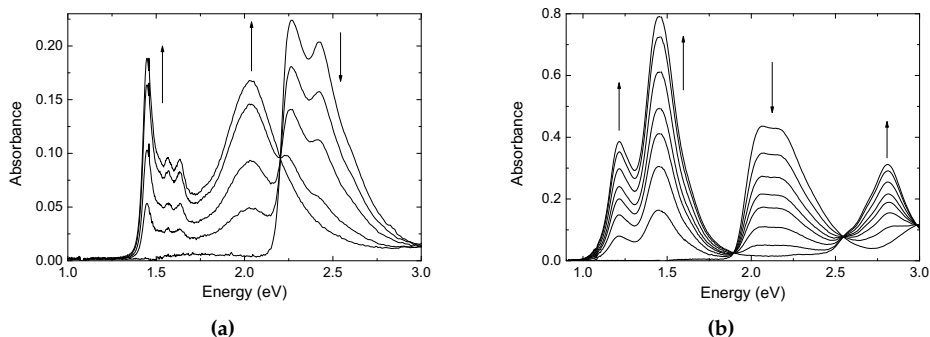


Figure 7.3: Chemical oxidation of oligomers **DPP-T1** (a) and **DPP-T2** (b) by adding a solution of thianthrenium hexafluorophosphate. The appearance and disappearance of bands is indicated with arrows.

summarized in table 7.1. Whereas the bare oligomers are strongly fluorescent, the fluorescence of the DPP oligomer in the triads is fully quenched due to the very fast decay of the S1 state of the DPP moiety, either by energy transfer to the C₆₀ units or by electron transfer from the C₆₀ to the DPP oligomer.

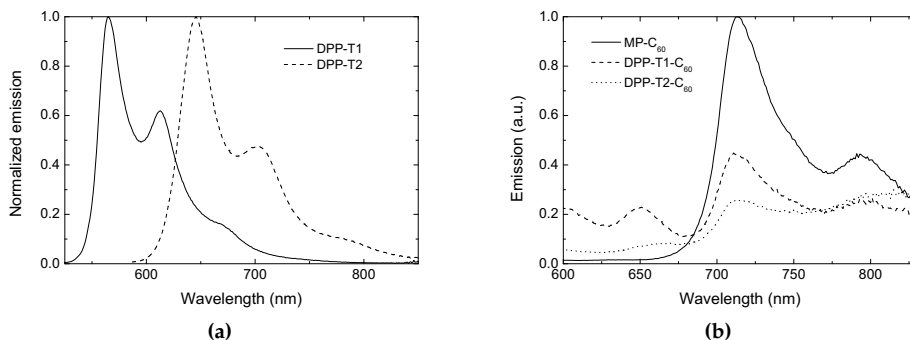


Figure 7.4: Normalized photoluminescence spectra of the oligomers (a) and quenching of the fullerene fluorescence in the triads in toluene, recorded with excitation at 433 nm (b).

Some insight into the processes occurring after excitation can be obtained, when the fluorescence of the C₆₀ units is examined. Quenching of the fluorescence of MP-C₆₀ in the triads is shown in figure 7.4b. For this graph, MP-C₆₀ and the oligomers were excited at 433 nm, corresponding to the small absorption maximum in the fullerene spectrum, and the emission spectra of all compounds were recorded without changing the settings of the spectrometer. The spectra were corrected for the optical density at the excitation wavelength, and hence the height of the fluorescent peaks is proportional to the relative quantum yields for fluorescence of the different compounds. It is clear from figure 7.4b that in toluene, the fluorescence of the C₆₀-units is partially quenched ($\sim 55\%$ for **DPP-T1-C₆₀** and $\sim 75\%$ for **DPP-T2-C₆₀**), indicating some, but incomplete charge transfer in these systems. In ODCB complete quenching of the C₆₀ fluorescence is observed for **DPP-T1-C₆₀** and **DPP-T2-C₆₀**, in-

dicating complete charge separation as a result of the higher solvent polarity that stabilizes the charge separated state.

7.2.5 Charge separation and recombination processes

Near steady-state PIA spectra of the triads **DPP-T1-C₆₀** and **DPP-T2-C₆₀** are shown in figure 7.5. For both oligomers, clear signals are observed in both toluene and ODCB, that can be attributed to the absorption of the triplet excited state of the DPP-oligomers. As the bare oligomers do not show any detectable amount of triplet absorptions, the observed triplet states must be formed *via* another process than direct intersystem crossing from the singlet excited state of the DPP-oligomer. This process can either be triplet sensitization by the MP-C₆₀ part of the molecules, as shown previously for mixtures of the oligomers and MP-C₆₀, or recombination of the charge separated state into the triplet state of the oligomer. The latter is possible *via* intersystem crossing (ISC) in the charge separated state, provided that the lifetime of this state is long enough. The fact that triplet excited oligomers are still observed in ODCB, with full quenching of the MP-C₆₀ fluorescence, is in correspondence with the latter explanation. The smaller amount of observed triplets, reflected in the weaker signal, could be explained by the shorter lifetime of the charge separated state that is expected in ODCB, compared to toluene. This is due to the observation in chapter 6, that charge recombination in this kind of systems takes place in the Marcus inverted regime, leading to a shorter lifetime for the thermodynamically more stable charge separated state in ODCB.

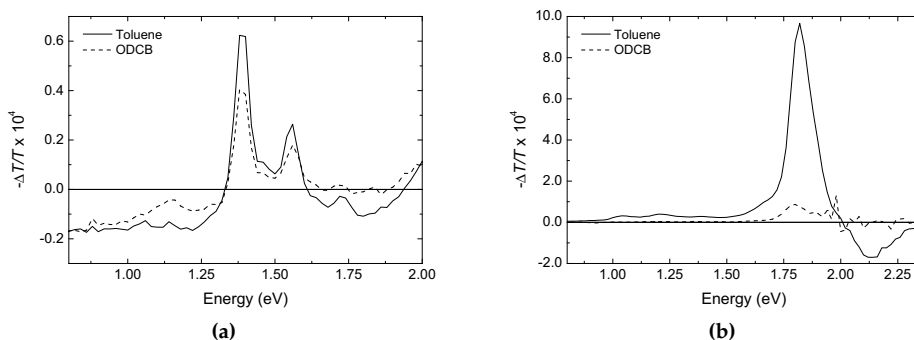


Figure 7.5: Near steady-state PIA spectra of **DPP-T1-C₆₀** (a) and **DPP-T2-C₆₀** (b) recorded in toluene and ODCB, at an excitation wavelength of 514 nm.

To obtain more insight into the processes occurring after excitation of the triads, the compounds were investigated by femtosecond photoinduced absorption spectroscopy (fs-PIA). fs-PIA spectra of the oligomers in ODCB are shown in figure 7.6. For both compounds, a negative band consisting of the ground state bleaching and stimulated emission (SE) peaks (visible as the low-energy shoulder), and positive bands at lower and higher energy were observed. The latter bands can be attributed to the $S_n \leftarrow S_1$ absorptions of the oligomers. In both cases, the bands show a mono-exponential decay, with a time constant of 3–4 ns, close to the fluorescence lifetimes of the oligomers determined by time-correlated single photon counting (table 7.1).

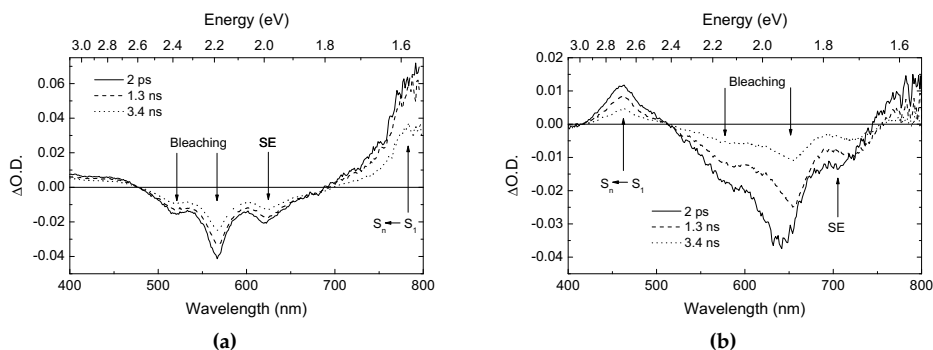


Figure 7.6: fs-PIA spectra of the oligomers **DPP-T1** (a) and **DPP-T2** (b) in ODCB.

fs-PIA data for the triads in toluene and ODCB are shown in figure 7.7. fs-PIA spectra of **DPP-T1-C₆₀** in toluene could not be recorded, due to the very low solubility of the triad in that solvent. In all spectra shown in figure 7.7, the initially formed singlet excited state of the DPP-oligomer has decayed within 2 ps after excitation, as evidenced from the absence of the stimulated emission feature in the negative band. Therefore, the observed bleaching band is associated with the formation of the charge separated state (CSS), in which an electron has been transferred from the oligomer to the MP-C₆₀ unit. In the next 20–140 ps, an increase of the bleaching band is observed, combined with a concomitant rise of absorptions in the regions where the cations of the oligomers absorb. This is due to charge separation from the singlet excited state of the MP-C₆₀ unit, which has formed within the first ~0.5 picoseconds. The formed charged separated state then recombines partially to the ground state, and partially to the triplet excited state of the DPP oligomer. This is evidenced by the clear signal observed after a few ns at 690 nm (1.8 eV) for **DPP-T2-C₆₀** (most clearly visible in toluene), which is at the same position as the triplet absorption of the bare oligomer. For **DPP-T1-C₆₀**, the triplet absorption itself is not observed, as it is probably too weak, but the bleaching band of the oligomer does not completely vanish, indicating the presence of a long-lived excited state.

A schematic depiction of the charge separation and recombination process, following from the discussion above, is depicted in figure 7.8. In summary, excitation of the DPP-oligomer leads to partial charge transfer and partial energy transfer to the fullerene. The excited C₆₀ moiety then leads to electron transfer from the DPP-oligomer to the fullerene, yielding the (singlet) charge separated state (¹CSS). This charge separated state then recombines to the ground state, or intersystem crossing to the triplet charge separated state (³CSS) occurs, which recombines into the triplet excited state of the DPP oligomer. It has to be noted that the ³CSS is not detected as a separate species because its formation (from ¹CSS) is much slower than its decay (to the triplet state localized on the DPP oligomer). Its intermediacy is assumed.

To access the rates for the different charge separation and recombination processes, global analysis of the data using the Glotaran²⁹ software has been performed. In this procedure, the time traces at all wavelengths are simultaneously fitted to a tri-exponential model. In case of **DPP-T2-C₆₀** in ODCB, only 3 time traces (shown in figure 7.7f), characteristic for the different excited states, were fitted, because the global

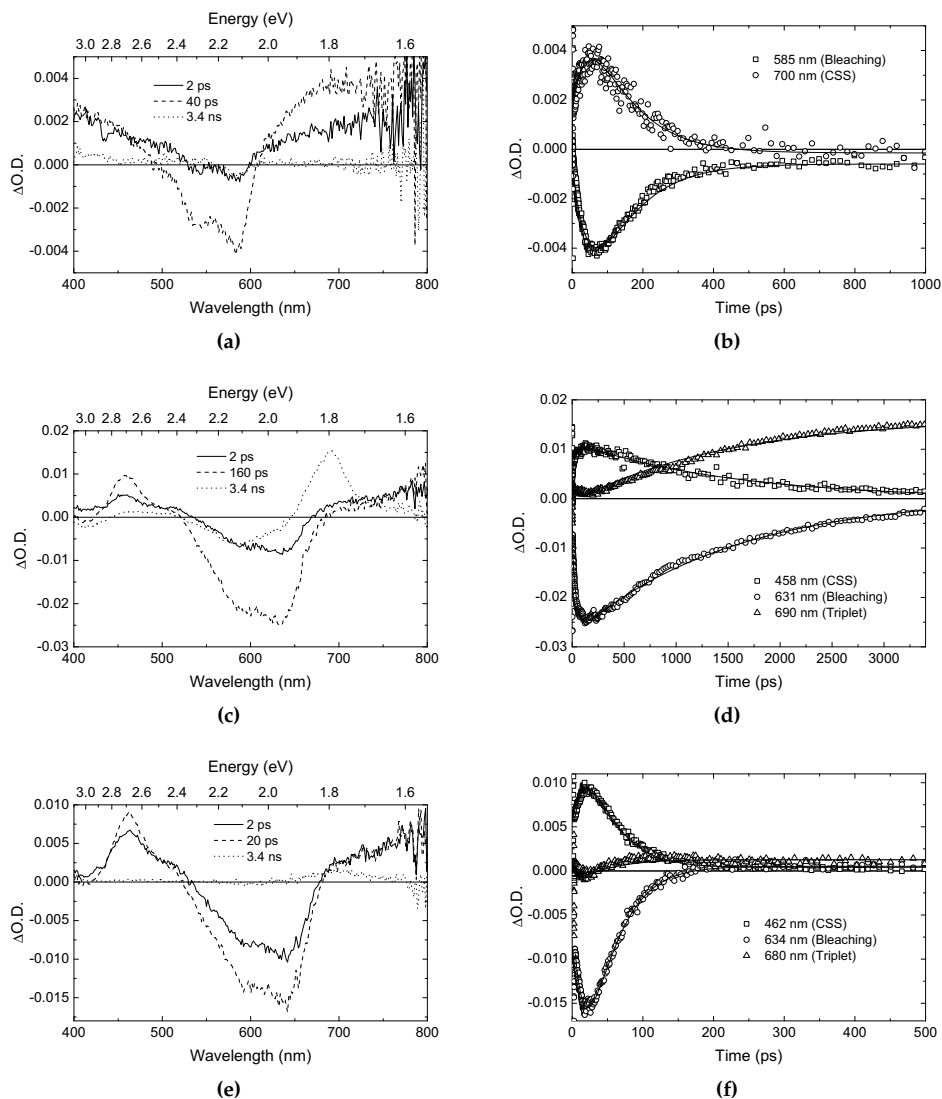


Figure 7.7: fs-PIA data for DPP-T1-C₆₀ in ODCB (a, b) and DPP-T2-C₆₀ in toluene (c, d) and ODCB (e, f). Graphs a, c, e show the evolution of the spectra with time, graphs b, d, f show time traces at selected wavelengths. The solid lines in the latter graphs are triexponential fits of the data, obtained by a global analysis procedure.

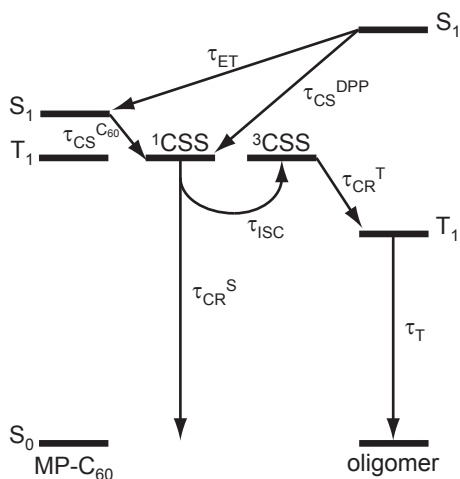


Figure 7.8: Schematic depiction of the charge separation and recombination processes occurring after excitation of the triads.

analysis did not converge. This procedure yielded time constants for charge separation ($\tau_{CS}^{C_{60}}$), charge recombination (τ_{CR}) and a very long component for the decay of the long-living triplet state of the oligomer. The time constants for charge separation and recombination are summarized in table 7.3. Time constants for charge separation and recombination are summarized in table 7.3. Time constants for energy transfer from the initially formed singlet excited DPP unit to C₆₀ (τ_{ET}) and for charge transfer from the same state (τ_{CS}^{DPP}) fall within the time resolution of the fs-PIA setup (0.2 ps), but their spectral characteristics were obscured by the coherent artifact (pulse related phenomena).

Table 7.3: Time constants for charge separation in the triad from the excited C₆₀ unit ($\tau_{CS}^{C_{60}}$), and recombination of the charges to either the ground state or the triplet excited state (τ_{CR}).

	$\tau_{CS}^{C_{60}}$ (ps)		τ_{CR} (ps)	
	toluene	ODCB	toluene	ODCB
DPP-T1-C ₆₀		47		110
DPP-T2-C ₆₀	41	18	1500	37

Fitting the time traces results in only one, overall time constant (τ_{CR}) for charge recombination. From the scheme in figure 7.8 however, it is clear that this time constant is composed of the time constants for two different processes: recombination into the ground state (with τ_{CR}^S) and recombination into a triplet state (with τ_{ISC} , provided that ISC is the rate limiting step for charge recombination into the triplet). A rough estimate of the quantum yield for charge recombination into the triplet state from the charge separated state can be made, by looking at the residual bleaching of the oligomer at long times. This bleaching, divided by the maximum bleaching obtained, is approximately equal to the fraction of the charge separated molecules that recombines into the triplet state. For DPP-T1-C₆₀ in ODCB, approximately 14 % of

the formed charge separated states recombines into the triplet, meaning that τ_{CR}^S is about 6 times smaller than τ_{ISC} (*i.e.* recombination into the ground state is 6 times faster than ISC), resulting in τ_{ISC} of about 0.8 ns, using the relation:

$$\frac{1}{\tau_{CR}} = \frac{1}{\tau_{CR}^S} + \frac{1}{\tau_{ISC}} \quad (7.1)$$

For **DPP-T2-C₆₀** in toluene, the fraction of charge separated molecules that recombine into the triplet state is about 10%, meaning that τ_{CR}^S is about 9 times smaller than τ_{ISC} , resulting in τ_{ISC} of about 15 ns. For **DPP-T2-C₆₀** in ODCB, this analysis could not be performed, as the fraction recombination into triplet states is too small, due to the short lifetime of the charge separated state.

The energy of the charge separated state (E_{CSS}) in different solvents can be calculated with the following equation, based on a continuum model:³⁰

$$E_{CSS} = e(E_{ox}(D) - E_{red}(A)) - \frac{e^2}{4\pi\epsilon_0\epsilon_s R_{cc}} - \frac{e^2}{8\pi\epsilon_0} \left(\frac{1}{r^+} + \frac{1}{r^-} \right) \left(\frac{1}{\epsilon_{ref}} - \frac{1}{\epsilon_s} \right) \quad (7.2)$$

In this equation, $E_{ox}(D)$ is the oxidation potential of the oligomer and $E_{red}(A)$ is the reduction potential of MP-C₆₀ (-1.2 V *vs.* Fc/Fc⁺ in ODCB). R_{cc} is the center-to-center distance of the positive and negative charges, which was determined for the triads using molecular modeling, assuming the positive charge to be located either on the center of the oligomer (the DPP-unit) or asymmetrically on the center of the thiophene/bithiophene unit next to the fullerene, and the negative charge at the center of the fullerene moiety. r^+ and r^- are the radii of the positive and negative ions formed. r^- is calculated in literature to be 5.6 Å for C₆₀, based on the density of C₆₀.¹³ r^+ can be estimated using a similar approach, using a density of 1.5, the value for unsubstituted terthiophene.³¹ ϵ_{ref} and ϵ_s are the permittivities of the reference solvent (used to measure oxidation and reduction potentials) and the solvent in which electron transfer is studied. It is well known that solvents like toluene, with a low dipole moment and a high quadrupole moment, often show larger stabilization energies of charge separated states than predicted from their "bulk" relative permittivity. Because the relative permittivity does not describe the solvent-molecule interactions in these solvents well, an apparent permittivity can be used, such that the solvent behaves as a hypothetical solvent of polarity ϵ_{app} . For toluene, an apparent permittivity of 3.5 was used.^{32,33} Values calculated for r^+ , R_{cc} , E_{CSS} , and ΔG for the different charge transfer processes are summarized in table 7.4.

Marcus theory estimates the activation barrier for photoinduced charge separation based on the free energy for charge separation, ΔG_{CS} , and the reorganization energy, *i.e.* the energy needed to deform the excited donor-acceptor system to the geometry of the charge separated state. Assuming the same parabolic energy curves for both the initial excited state and the charge separated state, this leads to:^{34,35}

$$\Delta G_{CS}^\ddagger = \frac{(\Delta G_{CS} + \lambda)^2}{4\lambda} \quad (7.3)$$

Where λ is the sum of internal (λ_i) and solvent (λ_s) contributions. The internal reorganization energy is set to 0.3 eV in this case, based on the reported value for the

Table 7.4: Singlet (E_{S1}) and triplet (E_{T1}) energy levels, half-wave oxidation potentials (E_{ox} , vs. Fc/Fc⁺ in ODCB), cation radius (r^+), distance between positive and negative charges (R_{cc}), energy of the charge separated state (E_{CSS}) and free energies (ΔG) for the different charge separation and recombination processes (using the same sub- and superscripts as in figure 7.8). Energies are calculated for toluene and ODCB when the center of the positive charge is located on the center of the oligomer ("DPP") or on the thiophene/bithiophene unit next to the fullerene ("T").

	E_{S1} (eV)	E_{T1} (eV)	E_{ox} (V)	r^+ (Å)	Location charge	R_{cc} (Å)	Solvent	E_{CSS} (eV)	ΔG_{CS}^{DPP} (eV)	ΔG_{CS}^{C60} (eV)	ΔG_{CR}^S (eV)	ΔG_{CR}^T (eV)
DPP- T1-C₆₀	2.15	1.1	0.46	4.3	DPP	9.7	toluene	1.79	-0.36	0.09	-1.79	-0.69
							ODCB	1.51	-0.64	-0.19	-1.51	-0.41
					T	6.9	toluene	1.62	-0.53	-0.08	-1.62	-0.52
							ODCB	1.45	-0.70	-0.25	-1.45	-0.35
DPP- T2-C₆₀	1.88	0.9	0.29	5.0	DPP	13.1	toluene	1.69	-0.19	-0.01	-1.69	-0.79
							ODCB	1.38	-0.50	-0.32	-1.38	-0.48
					T	8.5	toluene	1.52	-0.36	-0.18	-1.52	-0.62
							ODCB	1.32	-0.56	-0.38	-1.32	-0.72

C₆₀/diethylaniline couple.¹³ The solvent contribution can be calculated using the Born-Hush approach:³⁶

$$\lambda_s = \frac{e^2}{4\pi\epsilon_0} \left[\frac{1}{2} \left(\frac{1}{r^+} + \frac{1}{r^-} \right) - \frac{1}{R_{cc}} \right] \left(\frac{1}{n^2} - \frac{1}{\epsilon_s} \right) \quad (7.4)$$

In this formula, n is the refractive index of the solvent, and the other parameters are the same as defined before. Reaction rates can be calculated using the non-adiabatic electron transfer theory by Jortner *et al.*:^{37,38}

$$k_0 = \sqrt{\frac{\pi}{\hbar^2 \lambda_s k_B T}} V^2 \sum_{n=0}^{\infty} e^{-S} \frac{S^n}{n!} \exp \left(-\frac{(\Delta G_0 + \lambda_s + n\hbar\omega)^2}{4\lambda_s k_B T} \right) \quad (7.5)$$

In this equation, V describes the electronic coupling between donor and acceptor and $S = \lambda_i/\hbar\omega$, the effective mode vibrational energy. $\hbar\omega$ was set to 0.186 eV (1500 cm⁻¹), a value characteristic for the carbon-carbon double bond stretching frequency. Because the value of V is not known in our case, rates are calculated as k/V^2 . Values calculated for λ , ΔG^\ddagger , and k/V^2 for the different charge transfer processes are summarized in table 7.5.

From the values in tables 7.4 and 7.5, it is clear that for charge separation from the initial excited state on the oligomer, λ is close to ΔG_{CS}^{DPP} . This means that this charge separation takes place close to the Marcus optimal region, leading to low activation barriers and very fast charge separation, in line with experimental observations. Charge separation when the excited state is located on the fullerene unit is clearly located in the Marcus normal region ($-\Delta G_{CS}^{DPP} < \lambda$), reflected in higher activation barriers and lower charge transfer rates. The fact that this charge separation process takes place in the Marcus normal region also explains the experimental observation that this process is faster in ODCB (where the charge separated state is

Table 7.5: Reorganization energy (λ), activation barriers (ΔG^\ddagger) and calculated rate constants (k/V^2) for the different charge transfer processes (using the same sub- and superscripts as in figure 7.8), in toluene and ODCB when the center of the positive charge is located on the center of the oligomer ("DPP") or on the thiophene/bithiophene unit next to the fullerene ("T").

	Location charge	Solvent	λ (eV)	$\Delta G_{CS}^{\ddagger DPP}$ (eV)	$\Delta G_{CS}^{\ddagger C60}$ (eV)	$\Delta G_{CR}^{\ddagger S}$ (eV)	$\Delta G_{CR}^{\ddagger T}$ (eV)	k_{CS}^{DPP}/V^2 ($s^{-1} eV^2$)	k_{CS}^{C60}/V^2 ($s^{-1} eV^2$)	k_{CR}^S/V^2 ($s^{-1} eV^2$)	k_{CR}^T/V^2 ($s^{-1} eV^2$)
DPP-T1-C₆₀	DPP	toluene	0.54	0.015	0.18	0.73	0.011	1.0×10^{16}	2.0×10^{11}	1.0×10^{13}	1.1×10^{16}
		ODCB	0.77	0.006	0.11	0.18	0.041	1.1×10^{16}	8.0×10^{13}	6.8×10^{14}	2.5×10^{15}
	T	toluene	0.44	0.005	0.073	0.79	0.003	1.3×10^{16}	2.3×10^{14}	1.6×10^{13}	1.3×10^{16}
		ODCB	0.58	0.006	0.047	0.33	0.021	1.2×10^{16}	2.0×10^{15}	2.3×10^{14}	7.2×10^{15}
DPP-T2-C₆₀	DPP	toluene	0.56	0.060	0.13	0.56	0.022	9.5×10^{14}	8.9×10^{12}	3.2×10^{13}	8.5×10^{15}
		ODCB	0.81	0.031	0.076	0.099	0.034	3.8×10^{15}	4.7×10^{14}	2.0×10^{15}	3.3×10^{15}
	T	toluene	0.47	0.006	0.043	0.59	0.012	1.5×10^{16}	2.5×10^{15}	5.2×10^{13}	1.1×10^{16}
		ODCB	0.63	0.002	0.025	0.19	0.017	1.3×10^{16}	5.8×10^{15}	8.2×10^{14}	8.3×10^{15}

stabilized) than in toluene. Charge recombination to the ground state clearly takes place in the Marcus inverted region ($-\Delta G_{CR}^S > \lambda$), which is in agreement with the results described in chapter 6. Because this charge recombination is located in the inverted region, charge recombination is faster in ODCB than in toluene. In all cases the calculated $\Delta G_{CR}^{\ddagger S}$ is larger than $\Delta G_{CS}^{\ddagger C60}$, in line with experimental observations. Energetically, charge recombination to the triplet state again takes place close to the Marcus normal region, which would lead to very high reaction rates. The experimental observation of slow triplet recombination can however be explained by a rate-limiting ISC process, instead of a rate-limiting charge transfer process.

For the general trends discussed above, the location of the positive charge is not of great importance. When calculating rate constants however, using equation 7.5, it does matter if the charge is located on the center of the DPP-oligomer, or more asymmetrically, on the center of the thiophene/bithiophene unit next to the fullerene. If rate constants are estimated using the value of R_{cc} calculated for the positive charge being located on the oligomer center, the general trends are not reproduced. Here, the calculated values for k_{CR}^S/V^2 are larger than k_{CS}^{C60}/V^2 , in contrast to the experimental observation that charge recombination is slower than charge separation. Furthermore, when calculating V , by comparing the observed $1/\tau_{CS}^{C60}$ and the calculated k_{CS}^{C60}/V^2 , values for V of 11 to 52 meV are obtained. These are unrealistically large, as values of a few meV are generally obtained for donor-acceptor dyads and triads.^{14,33,39} Recalculating the values with a smaller R_{cc} , obtained by placing the positive charge on the center of the thiophene/bithiophene unit next to the fullerene, accurately reproduces the experimental trends. The calculation results in very fast initial charge separation from the excited oligomer, somewhat slower recombination from the excited fullerene, and even slower charge recombination to the ground state. Moreover, the obtained value for V is 3.2 ± 0.1 meV, which is completely in line with commonly observed values. Therefore, we can conclude that the positive charge is most probably located on the thiophene/bithiophene unit next to the fullerene. This conclusion is consistent with the idea that the DPP units are electron deficient compared to the electron rich thiophene/bithiophenes and that radi-

cal cations are preferentially formed on the latter units. Furthermore, similar cationic charge localization on an oligomeric unit (influencing the center-to-center distance) has been suggested before to occur in perylenemonoimide/oligothiophene donor-acceptor systems.⁴⁰

7.3 Conclusions

Triads consisting of DPP-containing oligomers, end capped with fullerenes were prepared and photoinduced energy and electron transfer reactions were investigated by photoluminescence, near steady-state PIA and fs-PIA techniques. After excitation of the DPP oligomer, charge transfer takes place *via* two simultaneously occurring routes. The first route is direct electron transfer, in the Marcus optimal regime, from the excited DPP oligomer to the fullerene. The second route is a two-step process consisting of ultrafast energy transfer from the DPP-oligomer to the fullerene, followed by charge separation from the formed excited state. In the latter case, the charge transfer process occurs in the Marcus normal regime, with time constants in the range of 18–47 ps. The formed charge separated state subsequently recombines *via* two distinct pathways. The first pathway is direct recombination to the ground state, which occurs in the Marcus inverted region, with time constants in the range of 37 ps to 1.5 ns. Because the charge separated state has a lower energy in the more polar ODCB, this process is much faster in ODCB than in toluene. The other pathway consists of intersystem crossing in the charge separated state, with time constants of 0.8 to 15 ns, and subsequent recombination into the triplet excited state of the DPP oligomer. ISC in the charge separated state is the rate-limiting step in this process. Clear signals for the triplet absorption of the oligomer could be observed by near steady-state PIA and fs-PIA. As the ISC process is slow compared to direct recombination to the ground state, triplet recombination was found to be of more importance in toluene than in ODCB, because of the slower direct recombination process in toluene. Analysis of the observed rates by Marcus–Jortner theory leads to the conclusion that the positive charge in the charge separated state is most likely not located on the center of the DPP oligomer, but rather asymmetrically on the thiophene/bithiophene unit next to the fullerene.

7.4 Experimental

General methods ¹H-NMR and ¹³C-NMR spectra were recorded on a 400 MHz NMR (Varian Mercury or Varian 400-MR, 400 MHz for ¹H-NMR and 100 MHz for ¹³C-NMR) or on a 500 MHz NMR (Varian Unity Plus, 500 MHz for ¹H-NMR and 125 MHz for ¹³C-NMR). Spectra were recorded in CDCl₃, or in CS₂, using a D₂O insert for locking and shimming. Chemical shifts are reported in ppm downfield from tetramethylsilane (TMS). IR spectra were recorded on a Perkin Elmer 1600 FT-IR. Matrix-assisted laser desorption ionization time-of-flight (MALDI-TOF) mass spectrometry was performed on a PerSeptive Biosystems Voyager–DE PRO spectrometer. Preparative HPLC was performed using a Cosmosil Buckyprep Waters packed column (10×250 mm), using toluene as the eluent at a flow rate of 5 mL/min. Analytical

HPLC analysis was performed on a Hewlett Packard HP LC-Chemstation 3D (Agilent/HP1100 Series) using an analytical Cosmosil Buckyprep column (4.6 × 250 mm). Cyclic voltammograms were recorded in an inert atmosphere with 0.1 M tetrabutyl ammonium hexafluorophosphate (TBAPF₆) in ODCB as supporting electrolyte. The working electrode was a platinum disc (0.2 cm²) and the counter electrode was a silver electrode. The samples were measured using an Ag/AgCl reference electrode with Fc/Fc⁺ as an internal standard using a μ Autolab II with a PGSTAT30 potentiostat. UV/vis/nearIR absorption spectra were recorded using a PerkinElmer Lambda 900 spectrophotometer. Fluorescence spectra were recorded on an Edinburgh Instruments FS920 double-monochromator spectrophotometer with a Peltier-cooled red-sensitive photomultiplier. The emission spectra were corrected for the wavelength dependence of the sensitivity of the detection system. Time-correlated single photon counting fluorescence studies were performed on an Edinburgh Instruments LifeSpec-PS spectrometer by photoexcitation with a 400 nm picosecond laser (PicoQuant PDL 800B) operated at 2.5 MHz and by detection with a Peltier-cooled Hamamatsu microchannel plate photomultiplier (R3809U-50). The data were deconvoluted with the instrument response function of the instrument, recorded using dispersed light, and fitted to a monoexponential function using the Fluofit package (PicoQuant, Berlin). Near steady-state PIA spectra were recorded by exciting with a mechanically modulated cw Ar-ion laser ($\lambda = 351$ and 364 nm or 514 nm, 275 Hz) pump beam and monitoring the resulting change in transmission of a tungsten-halogen probe light through the sample (ΔT) with a phase-sensitive lock-in amplifier after dispersion by a grating monochromator and detection, using Si, InGaAs, and cooled InSb detectors. The pump power incident on the sample was typically 25 mW with a beam diameter of 2 mm. The PIA ($\Delta T/T$) was corrected for the photoluminescence, which was recorded in a separate experiment. Photoinduced absorption spectra and photoluminescence spectra were recorded with the pump beam in a direction almost parallel to the direction of the probe beam. The solutions were studied in a 1 mm near-IR grade quartz cell at room temperature. Femtosecond photoinduced absorption experiments were performed with a Spectra-Physics Hurricane Titanium:Sapphire regenerative amplifier system. The full spectrum setup was based on an optical parametric amplifier (Spectra-Physics OPA 800C) as the pump. The residual fundamental light, from the pump OPA, was used for white/probe light generation, which was detected with a CCD spectrograph (Ocean Optics) for Vis detection. The polarization of the pump light was controlled by a Berek Polarization Compensator (New Focus). The Berek-Polarizer was always included in the setup to provide the Magic-Angle conditions. The probe light was double-passed over a delay line (Physik Instrumente, M-531DD) that provides an experimental time window of 3.6 ns with a maximal resolution of 0.6 fs/step. The OPA was used to generate excitation pulses at 530 nm. The laser output was typically 3.5-5 μ J pulse⁻¹ (130 fs FWHM) with a repetition rate of 1 kHz. The samples were placed into cells of 2 mm path length (Hellma) and were stirred with a downward projected PTFE shaft, using a direct drive spectro-stir (SPECTROCELL). This stir system was also used for the white light generation in a 2 mm water cell. The exact optical layout has been described in literature.⁴¹ All photophysical data reported here have a 5 to 10 % error limit. All experiments were performed at room temperature.

Materials Solvents were purchased from Biosolve and used without further purification. THF was purified using a solvent purification system before use. C₆₀ and MP-C₆₀ were obtained from Solenne, other chemicals were purchased from Acros or Aldrich and used without purification. *N*-bromosuccinimide (NBS) was recrystallized from water. Oxygen and moisture-sensitive reactions were performed under an argon atmosphere. 3,6-Bis(thiophen-2-yl)-2,5-bis(2-ethylhexyl)pyrrolo[3,4-*c*]pyrrole-1,4-dione (**DPP-T1**),²³ 3,6-bis(5-bromothiophen-2-yl)-2,5-bis(2-ethylhexyl)pyrrolo[3,4-*c*]pyrrole-1,4-dione,⁴² and tributyl(3-octyl-thiophen-2-yl)stannane⁴³ were synthesized following literature procedures.

3,6-di([2,2'-bithiophen]-5-yl)-2,5-bis(2-ethylhexyl)pyrrolo[3,4-*c*]pyrrole-1,4-(2H,5H)-dione (DPP-T2) 3,6-bis(5-bromothiophen-2-yl)-2,5-bis(2-ethylhexyl)pyrrolo[3,4-*c*]pyrrole-1,4-dione (1.50 g, 2.2 mmol) and tributyl(3-octyl-thiophen-2-yl)stannane (2.37 g, 4.8 mmol) were dissolved in THF (50 mL). Pd(PPh₃)₂Cl₂ (77 mg) was added and the mixture was stirred for 22 h at 70°C. The solvent was evaporated and the crude product was purified by flash chromatography on silica, using dichloromethane/heptane as the eluent. The product was subsequently recrystallized from ethanol and hexane. Yield: 0.38 g (19%). ¹H-NMR (400 MHz, CDCl₃): δ 9.02 (d, J = 4.1 Hz, 2H, Ar-*H*), 7.28 (d, J = 4.2 Hz, 2H, Ar-*H*), 7.26 (d, J = 5.0 Hz, 2H, Ar-*H*), 6.98 (d, J = 5.2 Hz, 2H, Ar-*H*), 4.06 (m, 4H, -CH₂CH(C₄H₉)(C₂H₅)), 2.83 (t, J = 7.8 Hz, 4H, -CH₂C₇H₁₅), 1.95 (m, 2H, -CH₂CH(C₄H₉)(C₂H₅)), 1.67 (qu, J = 7.6 Hz, 4H, -CH₂CH₂C₆H₁₃), 1.45–1.20 (m, 36H, -CH₂-), 0.94–0.83 (m, 18H, -CH₃). ¹³C-NMR (100 MHz, CDCl₃): δ 161.70, 142.09, 141.20, 139.70, 136.42, 130.55, 129.73, 128.86, 126.70, 125.21, 108.13, 46.05, 39.28, 31.86, 30.57, 30.25, 29.63, 29.48, 29.27, 28.41, 23.57, 23.13, 22.65, 14.08, 14.05, 10.52. IR: $\tilde{\nu}_{max}$ (cm⁻¹) 2956, 2923, 2855, 1641, 1548, 1527, 1450, 1432, 1227, 1080, 1023, 836, 802, 718. MALDI-TOF-MS: m/z 912.58 (100%), 913.58 (75), 914.58 (45), 915.58 (20), 916.58 (5). Melting point: 135°C.

5,5'-(2,5-bis(2-ethylhexyl)-3,6-dioxo-2,3,5,6-tetrahydropyrrolo[3,4-*c*]pyrrole-1,4-diyl)bis(thiophene-2-carbaldehyde) (DPP-TA1) Compound DPP-T1 (1.0 g, 1.91 mmol) was dissolved in THF (20 mL). At -78°C, LDA (1 M, 7.6 mL) was added dropwise. The mixture was stirred at -78°C for 2 h and DMF (0.75 mL, 10 mmol) was added dropwise at that temperature. The mixture was then stirred at room temperature for 1 h. Dichloromethane (100 mL) was added and the organic phase was washed with saturated NaCl (3×50 mL), dried over MgSO₄ and the solvent was evaporated. The crude product was purified by flash chromatography on silica, using dichloromethane/heptane as the eluent. Yield: 0.26 g (24%). ¹H-NMR (400 MHz, CDCl₃): δ 10.03 (s, 2H, -COH), 9.04 (d, J = 4.3 Hz, 2H, Ar-*H*), 7.88 (d, J = 4.1 Hz, 2H, Ar-*H*), 4.05 (m, 4H, -CH₂CH(C₄H₉)(C₂H₅)), 1.84 (m, 2H, -CH₂CH(C₄H₉)(C₂H₅)), 1.43–1.18 (m, 16H, -CH₂-), 0.94–0.81 (m, 12H, -CH₃). ¹³C-NMR (100 MHz, CDCl₃): δ 182.75, 161.34, 146.51, 140.54, 136.70, 136.10, 135.96, 110.82, 46.13, 39.24, 30.07, 28.23, 23.47, 22.98, 13.96, 10.38. IR: $\tilde{\nu}_{max}$ (cm⁻¹) 2962, 2929, 2858, 1672, 1647, 1553, 1541, 1451, 1436, 1405, 1379, 1354, 1209, 1095, 835, 734, 713. MALDI-TOF-MS: m/z 580.18 (100%), 581.18 (60), 582.18 (25), 583.19 (5). Melting point: 192°C.

5',5'''-(2,5-bis(2-ethylhexyl)-3,6-dioxo-2,3,5,6-tetrahydropyrrolo[3,4-c]pyrrole-1,4-diy)bis([2,2'-bithiophene]-5-carbaldehyde) (DPP-TA2) Compound DPP-T2 (250 mg, 0.27 mmol) was dissolved in THF (5 mL). At -78°C , LDA (1 M, 1.1 mL) was added dropwise. The mixture was stirred at -78°C for 2 h and DMF (0.1 mL, 1.4 mmol) was added dropwise at that temperature. The mixture was stirred overnight, while warming to room temperature. Dichloromethane (5 mL) was added and the organic phase was washed with saturated NaCl ($3\times 5\text{ mL}$), dried over MgSO_4 and the solvent was evaporated. The crude product was purified by flash chromatography on silica, using dichloromethane/heptane as the eluent. Yield: 120 mg (45 %). $^1\text{H-NMR}$ (400 MHz, CDCl_3): δ 9.87 (s, 2H, $-\text{COH}$), 9.03 (d, $J=4.2\text{ Hz}$, 2H, Ar- H), 7.64 (s, 2H, Ar- H), 7.44 (d, $J=4.2\text{ Hz}$, 2H, Ar- H), 4.06 (m, 4H, $-\text{CH}_2\text{CH}(\text{C}_4\text{H}_9)(\text{C}_2\text{H}_5)$), 2.86 (t, $J=7.8\text{ Hz}$, 4H, $-\text{CH}_2\text{C}_7\text{H}_{15}$), 1.92 (m, 2H, $-\text{CH}_2\text{CH}(\text{C}_4\text{H}_9)(\text{C}_2\text{H}_5)$), 1.72 (qu, $J=7.7\text{ Hz}$, 4H, $-\text{CH}_2\text{CH}_2\text{C}_6\text{H}_{13}$), 1.45–1.23 (m, 36H, $-\text{CH}_2-$), 0.95–0.84 (m, 18H, $-\text{CH}_3$). $^{13}\text{C-NMR}$ (100 MHz, CDCl_3): δ 182.46, 161.50, 141.81, 141.42, 140.22, 139.57, 139.43, 138.78, 136.42, 130.73, 128.38, 108.93, 46.12, 39.33, 31.81, 30.21, 29.73, 29.52, 29.41, 29.22, 28.36, 23.56, 23.09, 22.63, 14.06, 14.02, 10.49. IR: $\tilde{\nu}_{\text{max}}$ (cm^{-1}) 2955, 2925, 2853, 1655, 1548, 1528, 1419, 1393, 1242, 1152, 1117, 1084, 1024, 807, 731, 711, 671. MALDI-TOF-MS: m/z 968.50 (100 %), 969.50 (85), 970.49 (60), 971.49 (25), 972.49 (10). Melting point: 174°C .

2',2'''-[[2,5-bis(2-ethylhexyl)pyrrolo[3,4-c]pyrrole-1,4(2H,5H)-dione-3,6-diy]-bis(4-octyl-5,2-thiophenediy)]bis[1',5'-dihydro-1'-methyl-2'H-[5,6]fullereno- C_{60} - I_h -[1,9-c]pyrrole] (DPP-T1- C_{60}) Compound DPP-TA1 (50 mg, 0.086 mmol), C_{60} (0.63 g, 0.87 mmol) and *N*-methylglycine (77 mg, 0.87 mmol) were dissolved in ODCB (125 mL). The mixture was stirred at 120°C for 5 h. The reaction mixture was concentrated *in vacuo* and purified by column chromatography on silica, using CS_2 as the eluent to remove unreacted C_{60} , the product was subsequently eluted with toluene. Yield: 42 mg (40 %). 14 mg of the product was further purified by preparative HPLC. $^1\text{H-NMR}$ (500 MHz, CS_2): δ 8.92 (s, 2H, Ar- H), 5.32 (s, 2H, MP- H), 4.97 (d, $J=9.0\text{ Hz}$, 2H, MP- H), 4.28 (d, $J=10.0\text{ Hz}$, 2H, MP- H), 3.92 (m, 4H, $-\text{CH}_2\text{CH}(\text{C}_4\text{H}_9)(\text{C}_2\text{H}_5)$), 2.95 (s, 6H, N- CH_3). IR: $\tilde{\nu}_{\text{max}}$ (cm^{-1}) 2948, 2923, 2856, 2782, 1668, 1574, 1456, 1091, 746, 736, 706. MALDI-TOF-MS: m/z 2074.39 (50 %), 2075.36 (100), 2076.40 (90), 2077.37 (70), 2078.4 (40), 2079.38 (25). HPLC: 1 peak at 13.7 min.

2',2'''-[[2,5-bis(2-ethylhexyl)pyrrolo[3,4-c]pyrrole-1,4(2H,5H)-dione-3,6-diy]bis(3'-octyl-5,5'-[2,2'-bithiophene]diy)]bis[1',5'-dihydro-1'-methyl-2'H-[5,6]fullereno- C_{60} - I_h -[1,9-c]pyrrole] (DPP-T2- C_{60}) Compound DPP-TA2 (59 mg, 0.05 mmol), C_{60} (0.45 g, 0.62 mmol) and *N*-methylglycine (58 mg, 0.65 mmol) were dissolved in ODCB (125 mL). The mixture was stirred at 120°C for 5 h. The reaction mixture was concentrated *in vacuo* and purified by column chromatography on silica, using CS_2 as the eluent to remove unreacted C_{60} , the product was subsequently eluted with toluene/ethyl acetate. Yield: 95 mg (77 %). 20 mg of the product was further purified by preparative HPLC. $^1\text{H-NMR}$ (500 MHz, CS_2): δ 8.98 (d, $J=4.1\text{ Hz}$, 2H, Ar- H), 7.20 (s, 2H, Ar- H), 7.18 (d, $J=4.1\text{ Hz}$, 2H, Ar- H), 5.14 (s, 2H, MP- H), 4.93 (d, $J=9.5\text{ Hz}$, 2H, MP- H), 4.23 (d, $J=9.5\text{ Hz}$, 2H, MP- H), 3.92 (d, $J=7.5\text{ Hz}$, 4H, $-\text{CH}_2\text{CH}(\text{C}_4\text{H}_9)(\text{C}_2\text{H}_5)$), 2.93 (s, 6H, N- CH_3), 2.80 (t, $J=7.3\text{ Hz}$, 4H, $-\text{CH}_2\text{C}_7\text{H}_{15}$), 1.84 (m, 2H, $-\text{CH}_2\text{CH}(\text{C}_4\text{H}_9)(\text{C}_2\text{H}_5)$), 1.63 (m, 4H, $-\text{CH}_2\text{CH}_2\text{C}_6\text{H}_{13}$), 1.40–1.16 (m,

36H, $-CH_2-$), 0.92–0.82 (m, 18H, $-CH_3$). ^{13}C -NMR (125 MHz, CS_2): δ 160.61, 155.82, 153.76, 153.01, 152.83, 147.49, 146.85, 146.55, 146.51, 146.41, 146.39, 146.34, 146.29, 146.15, 145.92, 145.88, 145.83, 145.62, 145.57, 145.47, 145.44, 145.38, 144.92, 144.85, 144.57, 144.54, 143.38, 143.24, 142.94, 142.84, 142.47, 142.38, 142.30, 142.28, 142.24, 142.16, 142.14, 142.07, 141.88, 141.82, 141.45, 141.44, 140.47, 140.45, 140.22, 140.20, 139.96, 138.87, 137.31, 136.88, 136.86, 136.11, 135.78, 131.45, 130.74, 129.55, 129.54, 127.76, 126.87, 126.85, 108.73, 104.99, 79.30, 77.17, 70.27, 68.80, 45.83, 40.69, 39.76, 32.62, 30.85, 30.63, 30.38, 30.29, 30.25, 30.07, 28.96, 24.14, 24.11, 23.65, 14.96, 11.10. IR: $\tilde{\nu}_{max}$ (cm^{-1}) 2951, 2922, 2851, 2781, 1663, 1543, 1456, 1429, 733. MALDI-TOF-MS: m/z 2462.50 (40%), 2463.50 (80), 2464.49 (100), 2465.47 (80), 2466.46 (55), 2467.44 (30), 2468.43 (10). HPLC: 1 peak at 9.0 min.

References and notes

1. Wienk, M. M.; Turbiez, M.; Gilot, J.; Janssen, R. A. J. *Adv. Mater.* **2008**, *20*, 2556–2560.
2. Bijleveld, J. C.; Zoombelt, A. P.; Mathijssen, S. G. J.; Wienk, M. M.; Turbiez, M.; De Leeuw, D. M.; Janssen, R. A. J. *J. Am. Chem. Soc.* **2009**, *131*, 16616–16617.
3. Zou, Y.; Gendron, D.; Neagu-Plesu, R.; Leclerc, M. *Macromolecules* **2009**, *42*, 6361–6365.
4. Zhou, E.; Wei, Q.; Yamakawa, S.; Zhang, Y.; Tajima, K.; Yang, C.; Hashimoto, K. *Macromolecules* **2010**, *43*, 821–826.
5. Tamayo, A. B.; Walker, B.; Nguyen, T. Q. *J. Phys. Chem. C* **2008**, *112*, 11545–11551.
6. Tamayo, A. B.; Dang, X. D.; Walker, B.; Seo, J.; Kent, T.; Nguyen, T. Q. *Appl. Phys. Lett.* **2009**, *94*, 103301.
7. Walker, B.; Tamayo, A. B.; Dang, X. D.; Zalar, P.; Seo, J. H.; Garcia, A.; Tantiwivat, M.; Nguyen, T. Q. *Adv. Funct. Mater.* **2009**, *19*, 3063–3069.
8. Ford, T. A.; Avilov, I.; Beljonne, D.; Greenham, N. C. *Phys. Rev. B* **2005**, *71*, 125212.
9. Offermans, T.; Van Hal, P. A.; Meskers, S. C. J.; Koetse, M. M.; Janssen, R. A. J. *Phys. Rev. B* **2005**, *72*, 045213.
10. Ford, T. A.; Ohkita, H.; Cook, S.; Durrant, J. R.; Greenham, N. C. *Chem. Phys. Lett.* **2008**, *454*, 237–241.
11. Imahori, H. *Bull. Chem. Soc. Jpn.* **2007**, *80*, 621–636.
12. Guldi, D. M.; Illescas, B. M.; Atienza, C. M.; Wielopolskia, M.; Martin, N. *Chem. Soc. Rev.* **2009**, *38*, 1587–1597.
13. Williams, R. M.; Zwier, J. M.; Verhoeven, J. W. J. *J. Am. Chem. Soc.* **1995**, *117*, 4093–4099.
14. Williams, R. M.; Koeberg, M.; Lawson, J. M.; An, Y. Z.; Rubin, Y.; PaddonRow, M. N.; Verhoeven, J. W. J. *Org. Chem.* **1996**, *61*, 5055–5062.

15. Schuster, D. I.; Cheng, P.; Wilson, S. R.; Prokhorenko, V.; Katterle, M.; Holzwarth, A. R.; Braslavsky, S. E.; Klihm, G.; Williams, R. M.; Luo, C. P. *J. Am. Chem. Soc.* **1999**, *121*, 11599–11600.
16. Schuster, D. I.; Cheng, P.; Jarowski, P. D.; Guldi, D. M.; Luo, C. P.; Echegoyen, L.; Pyo, S.; Holzwarth, A. R.; Braslavsky, S. E.; Williams, R. M.; Klihm, G. *J. Am. Chem. Soc.* **2004**, *126*, 7257–7270.
17. McClenaghan, N. D.; Grote, Z.; Darriet, K.; Zimine, M.; Williams, R. M.; De Cola, L.; Bassani, D. M. *Org. Lett.* **2005**, *7*, 807–810.
18. Galloni, P.; Floris, B.; De Cola, L.; Cecehetto, E.; Williams, R. M. *J. Phys. Chem. C* **2007**, *111*, 1517–1523.
19. Verhoeven, J. W. *J. Photochem. Photobiol. C. Photochem. Rev.* **2006**, *7*, 40–60.
20. Dance, Z. E. X.; Mi, Q.; McCamant, D. W.; Ahrens, M. J.; Ratner, M. A.; Wasielewski, M. R. *J. Phys. Chem. B* **2006**, *110*, 25163–25173.
21. Wasielewski, M. R.; Johnson, D. G.; Svec, W. A.; Kersey, K. M.; Minsek, D. W. *J. Am. Chem. Soc.* **1988**, *110*, 7219–7221.
22. Wiederrecht, G. P.; Svec, W. A.; Wasielewski, M. R.; Galili, T.; Levanon, H. *J. Am. Chem. Soc.* **2000**, *122*, 9715–9722.
23. Tamayo, A. B.; Tantiwivat, M.; Walker, B.; Nguyen, T. Q. *J. Phys. Chem. C* **2008**, *112*, 15543–15552.
24. Maggini, M.; Scorrano, G.; Prato, M. *J. Am. Chem. Soc.* **1993**, *115*, 9798–9799.
25. Van Hal, P. A.; Beckers, E. H. A.; Peeters, E.; Apperloo, J. J.; Janssen, R. A. *J. Chem. Phys. Lett.* **2000**, *328*, 403–408.
26. Herkstroeter, W. G.; Merkel, P. B. *J. Photochem.* **1981**, *16*, 331–341.
27. Firey, P. A.; Ford, W. E.; Sounik, J. R.; Kenney, M. E.; Rodgers, M. A. *J. Am. Chem. Soc.* **1988**, *110*, 7626–7630.
28. Shine, H. J.; Zhao, B. J.; Marx, J. N.; Ould-Ely, T.; Whitmire, K. H. *J. Org. Chem.* **2004**, *69*, 9255–9261.
29. Glotaran 0.2.1, <http://timpgui.org>.
30. Weller, A. *Z. Phys. Chem. Neue Folge* **1982**, *133*, 93–98.
31. Van Bolhuis, F.; Wynberg, H.; Havinga, E. E.; Meijer, E. W.; Staring, E. G. *J. Synth. Met.* **1989**, *30*, 381–389.
32. Reynolds, L.; Gardecki, J. A.; Frankland, S. J. V.; Horng, M. L.; Maroncelli, M. *J. Phys. Chem.* **1996**, *100*, 10337–10354.
33. Veldman, D.; Chopin, S. M. A.; Meskers, S. C. J.; Janssen, R. A. *J. Phys. Chem. A* **2008**, *112*, 8617–8632.

34. Marcus, R. A. *J. Chem. Phys.* **1965**, *43*, 679–701.
35. Marcus, R. A. *Angew. Chem. Int. Ed.* **1993**, *32*, 1111–1121.
36. Oevering, H.; Paddon-Row, M. N.; Heppener, M.; Oliver, A. M.; Cotsaris, E.; Verhoeven, J. W.; Hush, N. S. *J. Am. Chem. Soc.* **1987**, *109*, 3258–3269.
37. Kestner, N. R.; Logan, J.; Jortner, J. *J. Phys. Chem.* **1974**, *78*, 2148–2166.
38. Ulstrup, J.; Jortner, J. *J. Chem. Phys.* **1975**, *63*, 4358–4368.
39. Beckers, E. H. A.; Meskers, S. C. J.; Schenning, A. P. H. J.; Chen, Z. J.; Würthner, F.; Janssen, R. A. J. *J. Phys. Chem. A* **2004**, *108*, 6933–6937.
40. Petrella, A.; Cremer, J.; De Cola, L.; Bäuerle, P.; Williams, R. M. *J. Phys. Chem. A* **2005**, *109*, 11687–11695.
41. Baffreau, J.; Leroy-Lhez, S.; Vân Anh, N.; Williams, R. M.; Hudhomme, P. *Chem. Eur. J.* **2008**, *14*, 4974–4992.
42. Zhou, E.; Yamakawa, S.; Tajima, K.; Yang, C.; Hashimoto, K. *Chem. Mater.* **2009**, *21*, 4055–4061.
43. Campos, L. M.; Tontcheva, A.; Gunes, S.; Sonmez, G.; Neugebauer, H.; Sariciftci, N. S.; Wudl, F. *Chem. Mater.* **2005**, *17*, 4031–4033.

Chapter 8

Diketopyrrolopyrroles as acceptor materials in organic photovoltaics

Abstract In the search for new electron acceptor, *n*-type materials for organic solar cells that combine a strong absorption over a broad range with good electrical characteristics we explore the use of diketopyrrolopyrrole (DPP) derivatives with low reduction potentials. A series of small molecule DPP-derivatives is presented and the compounds are tested as electron acceptors, in combination with poly(3-hexylthiophene) (P3HT) as donor material. Working photovoltaic devices are obtained that show a photoresponse in the wavelength region where the DPP molecules absorb. The best device shows a power conversion efficiency of 0.31 % in simulated solar light, with a photon to electron conversion efficiency of $\sim 10\%$ up to 700 nm. The efficiency seems to be limited by the coarse morphology of the blend.

This work has been published: Karsten, B. P.; Bijleveld, J. C.; Janssen, R. A. J. *Macromol. Rapid Commun.* **2010**, doi: 10.1002/marc.201000133.

8.1 Introduction

Most polymer solar cells consist of a conjugated polymer that acts under illumination as an electron donor towards an electron accepting material. After photoexcitation of the polymer, the formed exciton migrates to the donor–acceptor interface where it dissociates, generating free charges. Virtually all high-efficiency polymer solar cells use fullerenes, in particular [6,6]-phenyl-C₆₁-butyric acid methyl ester (PC₆₁BM), as electron accepting material, mainly because of its favorable high electron mobility. One drawback of fullerenes is their relatively low light absorption in the visible region of the spectrum. Although higher fullerenes like PC₇₁BM¹ partially solve this problem, there is use for *n*-type materials that can contribute to light absorption in the visible and near-IR region of the solar spectrum.

Very recently, solar cells based on polymers^{1–4} and oligomers,^{5–7} containing the diketopyrrolopyrrole (DPP) core have attracted attention. When used as an electron donor, *p*-type, material in combination with fullerenes, device efficiencies close to 5% have been reported in simulated solar light.² A common feature of these DPP-based materials is their low-lying HOMO, leading to relatively high open-circuit voltages, even for small band gap organic solar cells. Having a small band gap and a low lying HOMO, however implies that also the LUMO level of the oligomers and polymers is low. Hence these materials might be suitable as acceptor towards polymers with higher lying energy levels in organic solar cells. Moreover, DPP-based polymers possess a relatively high electron mobility in FET devices.^{2,8} In this chapter, we present a series of small DPP-core oligomers (figure 8.1) with different reduction potentials. When applied in bulk heterojunction solar cells, using poly(3-hexylthiophene) (P3HT) as the donor material, power conversion efficiencies up to 0.31% are obtained.

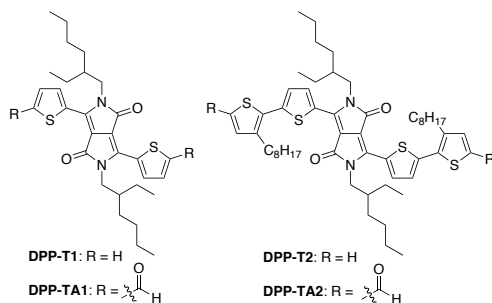


Figure 8.1: Structure of DPP acceptor materials.

8.2 Results and discussion

8.2.1 Optical and electrochemical properties

The UV/vis/near-IR absorption and steady-state photoluminescence spectra in toluene and of thin films of the acceptor materials are depicted in figure 8.2. A summary of the absorption and fluorescence data is given in table 8.1. Compared to the

spectra recorded in toluene solution, the thin films show a marked red-shift in both absorption and fluorescence, indicative of strong aggregation behavior of the pure materials.

Table 8.1: UV/vis absorption onsets (λ_{ons}), maxima (λ_{max}) and optical band gaps (E_g), and fluorescence maxima (λ_{max}^{PL}) in toluene solution and in thin films. Field-effect electron mobilities (μ_e) in thin films. Oxidation (E_{ox}) and reduction (E_{red}) onsets and electrochemical band gaps (E_{CV}^{sol}) measured in ODCB solution. Potentials are relative to ferrocene.

	Solution							Thin film				
	λ_{ons} (nm)	E_g^{sol} (eV)	λ_{max} (nm)	λ_{max}^{PL} (nm)	E_{ox} (V)	E_{red} (V)	E_{CV}^{sol} (eV)	λ_{ons} (nm)	E_g^{film} (eV)	λ_{max} (nm)	λ_{max}^{PL} (nm)	μ_e^a (cm ² /Vs)
DPP-T1	572	2.17	553	565	0.38	-1.71	2.09	612	2.03	510	691	
DPP-TA1	643	1.93	612	636	0.67	-1.15	1.82	686	1.81	580	745	3×10^{-3}
DPP-T2	651	1.90	609	646	0.21	-1.60	1.81	726	1.71	615	724	
DPP-TA2	684	1.81	601	677	0.39	-1.38	1.77	776	1.60	636	> 850	2×10^{-3}
P3HT					0.06	-2.34	2.4	650	1.91			

^a For **DPP-T1** and **DPP-T2** electron mobilities could not be obtained, due to the high LUMO level of the compounds.

Cyclic voltammograms of the materials recorded in *o*-dichlorobenzene (ODCB) solution are depicted in figure 8.3. All compounds show one or more reversible oxidation and reduction waves. As can be seen, the aldehydes (**DDP-TAn**) have a much lower reduction potential than their parent compounds (**DPP-Tn**) and at the same time the oxidation potential is increased. The result is a net lowering of the electrochemical band gap. Oxidation and reduction onsets are summarized in table 8.1. As can be seen from this table, the electrochemical band gap calculated from the oxidation and reduction potential onsets ($E_{CV}^{sol} = E_{ox} - E_{red}$) is slightly higher than the optical band gaps (E_g^{film}) calculated from the onset of the optical absorption in thin films. Explanations for this can (amongst others) be found in the fact that the electrochemical experiment takes place in solution, where stacking of the molecules is absent, resulting in a higher band gap.

8.2.2 Acceptor behavior of the compounds

To verify whether these DPP materials can fulfill the requirements to act as an acceptor for P3HT as donor we determined the "effective" optical HOMO (E_{HOMO}^{OPT}) and LUMO (E_{LUMO}^{OPT}) energies of the separate materials in thin solid films from E_{ox} and E_{red} and correcting for the experimental difference between E_{CV}^{sol} and E_g^{film} , following a method described recently:⁹

$$E_{HOMO}^{OPT} = -5.23 \text{ eV} - eE_{ox} + \frac{1}{2} \left(E_{CV}^{sol} - E_g^{film} \right) \quad (8.1)$$

$$E_{LUMO}^{OPT} = -5.23 \text{ eV} - eE_{red} - \frac{1}{2} \left(E_{CV}^{sol} - E_g^{film} \right) \quad (8.2)$$

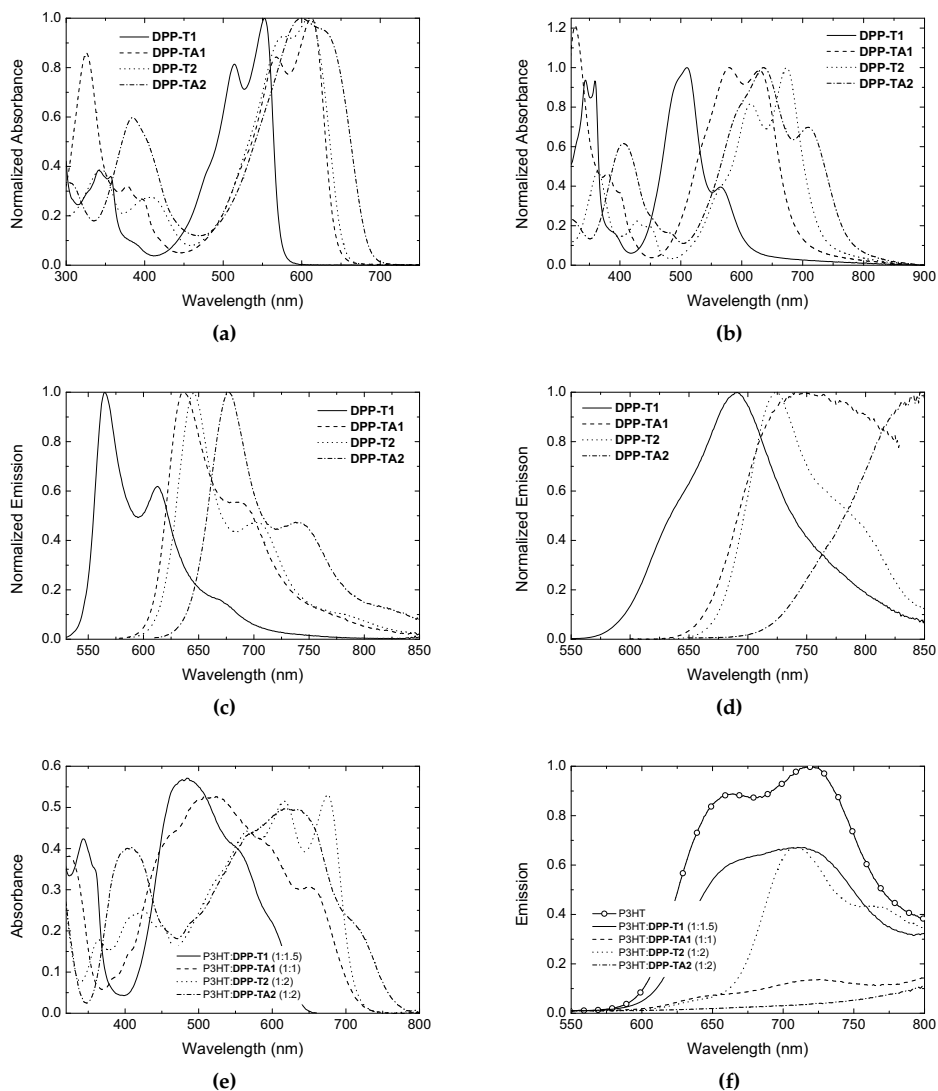


Figure 8.2: UV/vis/near-IR absorption spectra steady-state photoluminescence spectra in toluene (a and c) and of thin films (b and d) of the acceptor materials, spin cast from chloroform solution. (e) UV/vis/near-IR absorption spectra of the prepared solar cell devices, measured in reflection. (f) Photoluminescence spectra of the devices, the PL spectrum of a pure P3HT film is plotted as a reference.

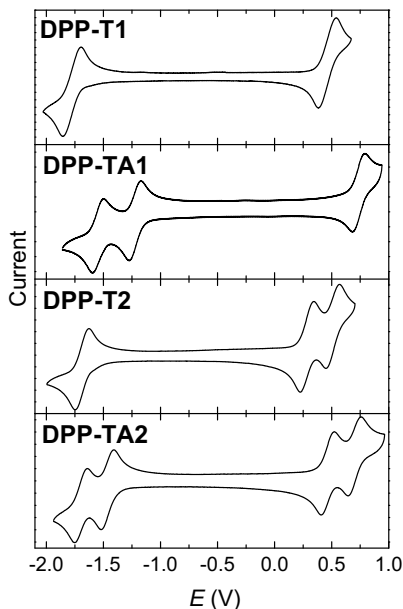


Figure 8.3: Cyclic voltammograms of the acceptor materials, recorded in ODCB solution, containing 0.1 M TBAPF₆ as the supporting electrolyte. Potentials are relative to ferrocene.

By this definition the $|E_{HOMO}^{OPT} - E_{LUMO}^{OPT}|$ value of a single material is equal to its optical gap E_g^{film} in the film, and hence one could argue that the effective HOMO and LUMO levels incorporate the intramolecular exciton binding energy in the solid state. The resulting values are collected in table 8.2. In a next step the energy of the donor-acceptor charge transfer (CT) state can be estimated from E_{HOMO}^{OPT} and E_{LUMO}^{OPT} energies via the empirical relation:⁹

$$E_{CT} = |E_{HOMO}^{OPT}(D) - E_{LUMO}^{OPT}(A)| + 0.29 \text{ eV} \quad (8.3)$$

where E_{HOMO}^{OPT} is the value of P3HT and E_{LUMO}^{OPT} of the acceptor. This gives values ranging from 1.25–1.75 eV. As was previously shown,⁹ the criterion for photoinduced electron transfer from the locally excited state with energy E_g to the CT state is:

$$\Delta = E_g - E_{CT} > 0.08 (\pm 0.02) \text{ eV} \quad (8.4)$$

where E_g corresponds to the lowest optical gap in the donor:acceptor blend. The values for $E_g - E_{CT}$ are collected in table 8.2 and reveal that photoinduced electron transfer from P3HT to **DPP-T2** is unlikely ($\Delta = 0.06$ eV); that transfer to **DPP-T1** and **DPP-TA2** just fulfills the criterion ($\Delta = 0.16$ – 0.20 eV); and transfer from P3HT to **DPP-TA1** is really favorable ($\Delta = 0.56$ eV).

These predictions correlate rather well with the observed quenching (or absence thereof) of the photoluminescence as shown in figure 8.2f in the blends. For P3HT:**DPP-T1** and P3HT:**DPP-T2**, with the lowest Δ values, photoinduced electron transfer appears not very efficient because either the P3HT luminescence is hardly quen-

Table 8.2: Effective optical HOMO (E_{HOMO}^{OPT}) and LUMO (E_{LUMO}^{OPT}) levels, estimated energy of the donor-acceptor charge transfer state (E_{CT}), and $E_g - E_{CT}$. P3HT is used as the donor material.

	E_{HOMO}^{OPT} (eV)	E_{LUMO}^{OPT} (eV)	E_{CT} (eV)	$E_g - E_{CT}$ (eV)
DPP-T1	-5.55	-3.59	1.75	0.16
DPP-TA1	-5.90	-4.09	1.25	0.56
DPP-T2	-5.39	-3.68	1.66	0.06
DPP-TA2	-5.54	-3.94	1.40	0.20
P3HT	-5.05	-3.14		

ched (in P3HT:DPP-T1) or energy transfer occurs leading to predominant DPP-T2 emission (in P3HT:DPP-T2). Only for P3HT:DPP-TA1 and P3HT:DPP-TA2, the P3HT photoluminescence is significantly quenched, without generating significant DPP-TA n emission. For these blends electron transfer seems more likely.

8.2.3 Photovoltaic devices

Solar cells were prepared by spin casting a blend of P3HT and the acceptor molecule from chloroform (P3HT:DPP-T1 and P3HT:DPP-TA1) or chlorobenzene (CB, for P3HT:DPP-T2 and P3HT:DPP-TA2) solution. All devices were annealed, as this increased solar cell performance by a factor of about 2 (for P3HT:DPP-T1) to 250 (for P3HT:DPP-TA2). As the morphology of the layers is rather coarse, morphology improvements by annealing cannot be the reason for these large improvements in performance. A possible explanation for the positive effect of annealing might an improvement in the crystallinity of both P3HT and acceptor phases, improving the transport properties of the layer. J - V characteristics and external quantum efficiency (EQE) spectra are depicted in figure 8.4. Device parameters of the best cells are summarized in table 8.3. Devices show efficiencies of 0.15–0.31 %, the main limiting parameters in these cells are the low fill factor and short-circuit current. The open-circuit voltages of the cells follow the trend with the E_{CT} , but their values are less than could have been expected.⁹

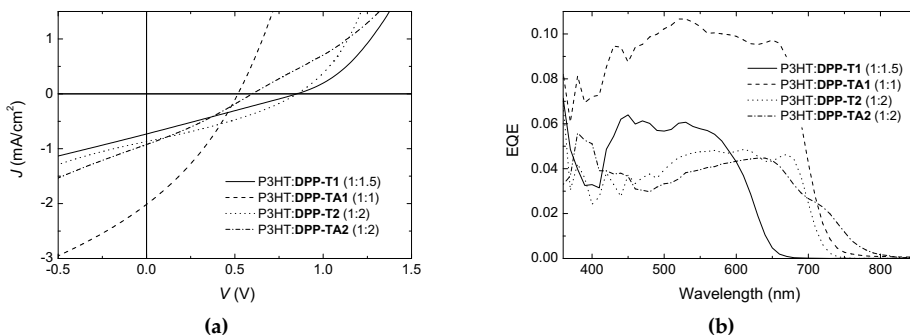


Figure 8.4: J - V characteristics under 100 mW/cm² illumination (a) and EQE spectra (b) of the devices.

Table 8.3: Device parameters of solar cells consisting of P3HT and the acceptor materials.

Acceptor	P3HT: acceptor ratio	Solvent	Layer thickness (nm)	Annealing (°C, min)	Device area (cm ²)	V_{oc} (V)	J_{sc} (mA/cm ²)	FF	η (%)
DPP-T1	1:1.5	CHCl ₃	134	80, 5	0.091	0.85	0.79	0.25	0.17
DPP-TA1	1:1	CHCl ₃	111	80, 5	0.091	0.52	1.93	0.31	0.31
DPP-T2	1:2	CB	66	100, 5	0.091	0.85	0.87	0.32	0.24
DPP-TA2	1:2	CB	67	100, 10	0.162	0.60	0.86	0.29	0.15

In agreement with the above analysis of $E_g - E_{CT}$, the highest photocurrent is observed for P3HT:DPP-TA1. Figure 8.4b reveals that the contribution of the strongly absorbing DPP-based acceptor materials (figure 8.2e) to the photocurrent is significant. As a result of this strong absorption in the acceptor material, the spectral response of the solar cells is approximately constant over all wavelengths below the band gaps of the absorbing materials. Low fill factors (i.e. < 0.45) are commonly observed for solar cells incorporating n -type polymers, even for the most efficient materials,^{10–12} and often associated with imbalanced charge transport because the occurrence of space-charge limited photocurrents is known to reduce the fill factor to about 42%.¹³ This is supported by the obtained electron mobilities (table 8.1) of 10^{-3} cm²/Vs, which are 1–2 orders of magnitude lower than values reported for P3HT.^{14,15} When the fill factor is lower than 42%, as observed here, a poor dissociation efficiency of the initially created electron-hole pairs or poor morphology may explain the strongly field-dependent photogeneration efficiency and the low fill factor.¹⁶ AFM images of the active layers (figure 8.5) reveal rather smooth films (± 10 nm height differences on a $5 \mu\text{m} \times 5 \mu\text{m}$ area) but do show relatively coarse domains, with sizes of several hundred nanometers or more. This indicates that further optimization of DPP type acceptor materials should primarily focus on improving the morphology when blended with P3HT, optimizing the degree and characteristic size of the phase separation. Suitable strategies for this goal may be found in varying the number, length, branching, or nature of the solubilizing side chains in combination with exploring a broader range of deposition methods, *e.g.* by using solvent mixtures or processing agents, to create optimized morphologies.

8.3 Conclusions

We prepared four DPP-based small molecules and tested these as acceptor materials in bulk-heterojunction solar cells with P3HT as a donor. Working solar cells based on n -type DPP materials were obtained and show a clear contribution of the DPP molecules to the photocurrent. Device efficiencies are in the range of 0.15–0.31% and are presently limited by a low fill factor and low photocurrent. The results show, that DPP based compounds are possibly suitable as acceptor material in future polymer solar cells but that their performance has to be improved considerably. This may be expected by designing new molecules or developing deposition procedures that lead to improved morphologies in the blends.

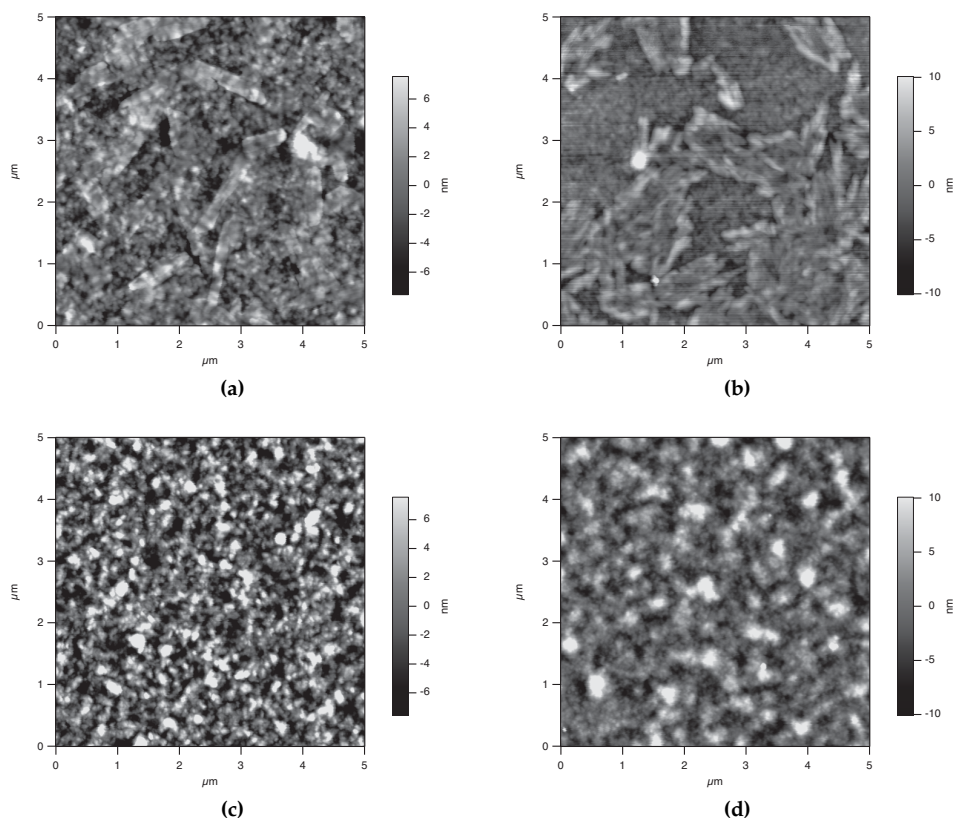


Figure 8.5: AFM height images of the active layers of the prepared P3HT:acceptor devices. (a) P3HT:DPP-T1. (b) P3HT:DPP-TA1. (c) P3HT:DPP-T2. (d) P3HT:DPP-TA2.

8.4 Experimental

General Methods Synthesis of all compounds is described in chapter 7. Cyclic voltammograms were recorded in an inert atmosphere with 0.1 M tetrabutyl ammonium hexafluorophosphate (TBAPF₆) in ODCB as supporting electrolyte. The working electrode was a platinum disc (0.2 cm²) and the counter electrode was a silver electrode. The samples were measured using an Ag/AgCl reference electrode with Fc/Fc⁺ as an internal standard using a μ Autolab II with a PGSTAT30 potentiostat at a scan speed of 200 mV/s. UV/vis/near-IR absorption spectra were recorded using a PerkinElmer Lambda 900 spectrophotometer. Fluorescence spectra were recorded on an Edinburgh Instruments FS920 double-monochromator spectrophotometer with a Peltier-cooled red-sensitive photomultiplier. The emission spectra were corrected for the wavelength dependence of the sensitivity of the detection system. Tapping mode AFM was performed on a MFP-3D atomic force microscope (Asylum research) using PPP-NCHR probes (Nanosensors).

Photovoltaic devices Photovoltaic devices were made by spin coating poly(ethylenedioxythiophene):poly(styrene sulfonate) (PEDOT:PSS) (Clevios P, VP A14083) onto pre-cleaned, patterned indium tin oxide (ITO) substrates (14Ω per square) (Naranjo Substrates). The photoactive layer was deposited by spin coating at 3000 rpm from a solution of acceptor and 10 mg/ml P3HT in chloroform (for P3HT:DPP-T1 and P3HT:DPP-TA1) or chlorobenzene (for P3HT:DPP-T2 and P3HT:DPP-TA2). The counter electrode, consisting of LiF (1 nm) and Al (100 nm), was deposited by vacuum evaporation at 3×10^{-7} mbar. The active area of the cells was 0.091 cm^2 or 0.16 cm^2 . J - V characteristics were measured under $\sim 100 \text{ mW/cm}^2$ white light from a tungsten halogen lamp filtered by a Schott GG385 UV filter and a Hoya LB120 daylight filter, using a Keithley 2400 source meter. Short-circuit currents under AM1.5G conditions were estimated from the spectral response and convolution with the AM1.5G solar spectrum. The spectral response was measured under simulated 1 sun light intensity operation conditions using bias light from a 532 nm solid state laser (Edmund Optics). Monochromatic light from a 50 W tungsten halogen lamp (Philips focusline) in combination with monochromator (Oriel, Cornerstone 130) was modulated with a mechanical chopper. The response was recorded as the voltage over a 50Ω resistance, using a lock-in amplifier (Stanford research Systems SR830). A calibrated Si cell was used as reference. The device was kept behind a quartz window in a nitrogen filled container. The thickness of the active layers in the photovoltaic devices was measured on a Veeco Dektak150 profilometer.

Field-effect transistors Field-effect transistors were fabricated using heavily doped silicon wafers as the common gate electrode with a 200 nm thermally oxidized SiO_2 layer as the gate dielectric. Using conventional photolithography, gold source and drain electrodes were defined in a bottom contact device configuration with channel width and length of $2500 \mu\text{m}$ and $10 \mu\text{m}$, respectively. A 10 nm layer of titanium was used acting as an adhesion layer for the gold on SiO_2 . The SiO_2 layer was exposed to the vapor of the primer hexamethyldisilazane for 60 min prior to semiconductor deposition in order to passivate the surface of the dielectric. Semiconductor films were deposited by drop casting. Freshly prepared devices were annealed in a dynamic vacuum of 10^{-5} mbar at 80°C for 72 h to remove traces of solvent. All electrical measurements were performed in vacuum using an HP 4155C semiconductor parameter analyzer.

References and notes

1. Wienk, M. M.; Kroon, J. M.; Verhees, W. J. H.; Knol, J.; Hummelen, J. C.; Van Hal, P. A.; Janssen, R. A. J. *Angew. Chem. Int. Ed.* **2003**, *42*, 3371–3375.
2. Bijleveld, J. C.; Zoombelt, A. P.; Mathijssen, S. G. J.; Wienk, M. M.; Turbiez, M.; De Leeuw, D. M.; Janssen, R. A. J. *J. Am. Chem. Soc.* **2009**, *131*, 16616–16617.
3. Zou, Y.; Gendron, D.; Neagu-Plesu, R.; Leclerc, M. *Macromolecules* **2009**, *42*, 6361–6365.
4. Zhou, E.; Wei, Q.; Yamakawa, S.; Zhang, Y.; Tajima, K.; Yang, C.; Hashimoto, K. *Macromolecules* **2010**, *43*, 821–826.

5. Tamayo, A. B.; Walker, B.; Nguyen, T. Q. *J. Phys. Chem. C* **2008**, *112*, 11545–11551.
6. Tamayo, A. B.; Dang, X. D.; Walker, B.; Seo, J.; Kent, T.; Nguyen, T. Q. *Appl. Phys. Lett.* **2009**, *94*, 103301.
7. Walker, B.; Tamayo, A. B.; Dang, X. D.; Zalar, P.; Seo, J. H.; Garcia, A.; Tantiwiwat, M.; Nguyen, T. Q. *Adv. Funct. Mater.* **2009**, *19*, 3063–3069.
8. Bürgi, L.; Turbiez, M.; Pfeiffer, R.; Bienewald, F.; Kirner, H. J.; Winnewisser, C. *Adv. Mater.* **2008**, *20*, 2217–2224.
9. Veldman, D.; Meskers, S. C. J.; Janssen, R. A. J. *Adv. Funct. Mater.* **2009**, *19*, 1939–1948.
10. McNeill, C. R.; Abrusci, A.; Zaumseil, J.; Wilson, R.; McKiernan, M. J.; Burroughes, J. H.; Halls, J. J. M.; Greenham, N. C.; Friend, R. H. *Appl. Phys. Lett.* **2007**, *90*, 193506.
11. Koetse, M. M.; Sweelssen, J.; Hoekerd, K. T.; Schoo, H. F. M.; Veenstra, S. C.; Kroon, J. M.; Yang, X. N.; Loos, J. *Appl. Phys. Lett.* **2006**, *88*, 083504.
12. Zhan, X. W.; Tan, Z. A.; Domercq, B.; An, Z. S.; Zhang, X.; Barlow, S.; Li, Y. F.; Zhu, D. B.; Kippelen, B.; Marder, S. R. *J. Am. Chem. Soc.* **2007**, *129*, 7246–7247.
13. Mihailetchi, V. D.; Wildeman, J.; Blom, P. W. M. *Phys. Rev. Lett.* **2005**, *94*, 126602.
14. Bao, Z.; Dodabalapur, A.; Lovinger, A. J. *Appl. Phys. Lett.* **1996**, *69*, 4108–4110.
15. Sirringhaus, H.; Tessler, N.; Friend, R. H. *Science* **1998**, *280*, 1741–1744.
16. Mandoc, M. M.; Veurman, W.; Koster, L. J. A.; De Boer, B.; Blom, P. W. M. *Adv. Funct. Mater.* **2007**, *17*, 2167–2173.

Epilogue

The aim of this thesis was to obtain more insight into the properties of small band gap materials and the processes involved in charge separation and recombination in solar cells utilizing these materials. This was achieved by detailed studies on oligomeric model compounds. Although much work has already been done in the past on extended oligothiophenes, such studies had not yet been performed on small band gap compounds relevant for the next generation organic photovoltaics. The thesis focusses on the optical and electrochemical properties of small band gap materials and the actual charge separation process in combination with fullerenes. Some of the prepared oligomers are applied as acceptor materials in actual solar cells.

First, the influence of the type of acceptor in small band gap materials based on the donor–acceptor concept has been studied. Many different acceptor systems have successfully been used for decreasing the band gap of π -conjugated polymers, but the reasons for this band gap reduction were not always fully understood. The acceptors under study fall in two different groups: benzene-based and thiophene-based, the latter are usually more effective in reducing the band gap. Although the thiophene-based acceptors are effective, the oxidation potentials are generally low, and the HOMO does not seem to be localized on the “donor” unit, but is delocalized over the entire molecule. This is not consistent with the generally accepted donor–acceptor view, where the HOMO would be localized on the donor units, and the LUMO would be localized on the acceptor. Systems with benzene-based acceptors are more consistent with the donor–acceptor idea, with some more localization of the HOMO, leading to higher oxidation potentials (lower HOMO levels), which would be beneficial for the voltage, when applied in solar cells. This difference between the two groups of acceptors might explain why 2,1,3-benzothiadiazole is often present in the more successful small band gap polymers, whereas acceptors like thienopyrazine and thienothiadiazole have only been used with limited success. As triplet recombination might be an important loss mechanism in polymer solar cells, it would be useful if we were able to predict the triplet energies, or the singlet–triplet splitting energies, of small band gap materials. Unfortunately, no clear correlation between the acceptor type and these properties could be observed.

One specific acceptor, thieno[3,4-*b*]pyrazine, has been studied in great detail. A number of different mixed oligothiophenes, with varying amounts of thienopyrazine in the acceptor blocks have been prepared, and their properties were investigated, both experimentally and theoretically. It was found that for all series the chain length dependence of the properties is identical to simple oligothiophenes, contrary to the common donor–acceptor view. The band gap reduction upon chain elongation was found to be mainly determined by a rise of the HOMO level. Overall, adding thienopyrazine units to the acceptor block led to a much stronger band gap reduction than simple chain elongation. The commonly accepted explanation for the small band gaps in polymers like poly(isothianaphthene) or poly(thienopyrazine) is their quinoid ground state. Here, it was found by theoretical calculations that for oligomers with thiophene, no quinoid ground state is obtained and therefore, this effect cannot explain the band gap reduction in thiophene–thienopyrazine systems. Calculating the frontier orbital levels for different dimers of thiophene and thienopyrazine leads to the conclusion that thienopyrazine is not only a good acceptor but

also a better donor than thiophene. This explains the strong delocalization of the HOMO and the low oxidation potentials found for the oligomers with thiophene-based acceptors.

The second main topic of this thesis is the charge separation and recombination in small band gap oligomer – fullerene triads. These compounds serve as model systems for the donor–acceptor interface in polymer solar cells. Two different series of triads have been prepared: systems with an oligomer part based on the previously described thieno[3,4-*b*]pyrazine and systems based on the diketopyrrolopyrrole (DPP) unit. The main difference between the two series is the energy of the charge separated state in the triads. Due to the higher oxidation potential (lower HOMO) of the DPP-based compounds the energy of the charge separated state is higher than in the thienopyrazine-based systems. Charge separation is very fast (<50 ps) in both systems and takes place in the Marcus normal regime. Charge recombination takes place in the Marcus inverted regime and, consequently the lifetime of the charge separated system is much higher in the DPP-based triads than in the thienopyrazine systems. The very efficient charge recombination in the thienopyrazine-based systems might be one of the reasons for the low photocurrents observed in thienopyrazine-based solar cells. In the DPP-based systems, the lifetime of the charge separated state is long enough to allow for intersystem crossing to the triplet charge separated state, which is then followed by charge recombination into the triplet state of the oligomer. This observation leads to the conclusion that triplet recombination might indeed be an important recombination pathway for high voltage, small band gap polymer solar cells.

Due to the limited light absorption by fullerenes, there would be use for alternative *n*-type materials for solar cells. So far however, other materials than fullerenes, either polymers or small molecules, have only been applied with limited success. As DPP-based materials do possess some *n*-type characteristics, they were used in solar cells, combined with polythiophene as the donor material. Although the efficiencies of the obtained devices were low, and mainly limited by morphology issues, the results do show that DPP-based materials can act as acceptors and might form a suitable alternative to the omnipresent fullerenes, provided that morphology and mobility issues can be solved.

Overall, the results described in this thesis shed more light on the effects causing the small band gaps in donor–acceptor systems based on thiophene and a variety of acceptors. Moreover, more insight into the processes relevant for charge separation has been obtained. The results described here, might therefore help in the design of new materials for more efficient polymer photovoltaics.

Oligomer studies on polymer photovoltaics

Summary

Solar cells based on polymers are an attractive alternative to silicon-based photovoltaics, because of their low cost and processing advantages. To increase the efficiency of polymer solar cells, however polymers are required that absorb light also in the near infrared part of the solar cells. The research described in this thesis aims to address some fundamental questions related to these so-called small band gap polymers. The method followed consists of the synthesis of small molecular model systems and detailed investigation of their properties by a variety of spectroscopic and electrochemical methods.

In chapter 2, oligomers consisting of two cyclopentadithiophenes and different acceptor units are described. These oligomers were synthesized to investigate the influence of the type of acceptor unit on the band gaps and energy levels of small band gap polymers. It was found that oligomers having thiophene-based acceptors generally have lower HOMO and LUMO levels than oligomers having benzene-based acceptors. This will ultimately lead to lower voltages when these acceptor systems are applied in solar cells. No clear correlation was found between the acceptor strength and the singlet-triplet splitting energy.

Chapters 3 to 5 deal with several series of donor-acceptor oligomers consisting of thiophene and thieno[3,4-*b*]pyrazine moieties. The series described in chapter 3 consists of oligomers formed by one, two or three thienopyrazines end capped with thiophene units. The effect of increasing the chain length of the systems with one or two thienopyrazines in the acceptor block is described in chapters 4 and 5. The optical and electrochemical properties of the series are evaluated both experimentally and theoretically. It is found that the dependence of these properties on the chain length is identical in all series.

In literature, a number of possible causes for the small band gaps in this kind of systems are given, *e.g.* donor-acceptor effects and induction of a quinoid structure in the polymer chain. In the work described in this thesis, it is concluded that the main cause for the small band gaps in these systems is none of the previously mentioned possibilities. Rather, the strong acceptor *and* donor character of thienopyrazine (usually only regarded as a strong acceptor), combined with strong interactions between the neighboring thienopyrazine units, explains the observed small band gaps.

Besides light absorption, charge separation and recombination processes are of crucial importance to photovoltaic cells. A detailed study of these processes in small band gap oligomer – fullerene triads is described in chapters 6 and 7. Triads containing oligomers using the thienopyrazine unit, described in previous chapters, are presented in chapter 6. In these systems very fast charge separation takes place close to the Marcus optimal region, followed by fast recombination in the inverted regime. Because of the short lifetime of the charge separated state, no recombination into triplet states could be observed.

Systems using the diketopyrrolopyrrole unit in the oligomer part of the triads are described in chapter 7. Charge separation in these systems takes place in the Marcus normal regime, followed by recombination in the inverted regime. As the energy of the charge separated state is higher in these systems than in systems using

the thienopyrazine unit, the lifetime of this state is long enough to allow intersystem crossing to the triplet state. Clear evidence for triplet recombination was observed in these systems.

In the last chapter, the use of diketopyrrolopyrrole containing oligomers as acceptor materials in solar cells is explored. Although diketopyrrolopyrrole-containing polymers are normally used as donor materials, acceptor behavior was also present and solar cells were prepared consisting of polythiophene as the donor material and the oligomers as acceptor materials. The best device shows a power conversion efficiency of 0.31% in simulated solar light, with a photon to electron conversion efficiency of $\sim 10\%$ up to 700 nm. The efficiency seems to be limited by the coarse morphology of the blend.

Oligomerenstudies aan polymere zonnecellen

Samenvatting

Zonnecellen gebaseerd op polymeren vormen, vanwege de geringe kosten en voordelen bij het verwerken, een aantrekkelijk alternatief voor de huidige siliciumgebaseerde zonnecellen. Om het rendement van deze cellen te verhogen zijn er echter wel materialen nodig die beter gebruik maken van het beschikbare zonlicht en ook licht in het nabij-infrarode deel van het zonlicht spectrum gebruiken. Het onderzoek dat beschreven is in dit proefschrift tracht een aantal fundamentele vragen te beantwoorden die verbonden zijn aan deze zogenaamde kleinebandafstandpolymeren. De gevolgde methode bestaat uit de synthese van modelsystemen bestaande uit kleine moleculen en een gedetailleerde studie van hun eigenschappen met behulp van een aantal spectroscopische en elektrochemische technieken.

In hoofdstuk 2 worden oligomeren beschreven bestaande uit twee cyclopentadithiofenen en een aantal verschillende acceptorgroepen. Deze oligomeren zijn gesynthetiseerd om de invloed van het type acceptor te onderzoeken op de bandafstand en de energieniveaus in kleinebandafstandpolymeren. Uit de resultaten in dit hoofdstuk blijkt, dat oligomeren met een thiofeengebaseerde acceptor in het algemeen lagere HOMO- en LUMO-niveaus hebben dan oligomeren met een benzeengebaseerde acceptor. Als dit soort acceptorsystemen wordt toegepast in zonnecellen zal dit uiteindelijk leiden tot een lagere spanning. Er kon geen duidelijk verband worden gevonden tussen de sterkte van de acceptor en afstand tussen de singlet- en tripletenergieniveaus.

Hoofdstukken 3 tot en met 5 beschrijven verschillende series donor-acceptoroligomeren bestaande uit thiofeen- en thieno[3,4-*b*]pyrazine-eenheden. In hoofdstuk 3 wordt een serie oligomeren beschreven bestaande één, twee of drie thienopyrazine-eenheden die aan het uiteinde worden afgeschermd door thiofenen. Het effect van toename van de ketenlengte in de systemen met één of twee thienopyrazines in het acceptorblok wordt beschreven in hoofdstukken 4 en 5. De optische en elektrochemische eigenschappen van de verschillende series zijn onderzocht met zowel experimentele als theoretische technieken. Het verband tussen ketenlengte en eigenschappen van de systemen blijkt bij alle onderzochte series identiek te zijn.

In de literatuur wordt een aantal mogelijke oorzaken genoemd voor de kleine bandafstanden in dit type systemen, bijvoorbeeld donor-acceptoreffecten en een deels quinoïde structuur in de polymeerketen. Uit de resultaten in dit proefschrift kunnen we echter concluderen dat geen van deze mogelijkheden de kleine bandafstanden in deze systemen verklaart. In deze systemen blijken de kleine bandafstanden verklaard te kunnen worden uit het sterke acceptor- *en* donorgedrag van thienopyrazine (normaal gesproken wordt thienopyrazine uitsluitend gezien als een sterke acceptor), gecombineerd met sterke interacties tussen naburige thienopyrazine-eenheden.

Behalve lichtabsorptie zijn ook ladingsscheidings- en ladingsrecombinatieprocessen van cruciaal belang voor het functioneren van zonnecellen. Een gedetailleerde studie van deze processen in triaden bestaande uit kleinebandafstandoligomeren en fullerenen wordt beschreven in hoofdstukken 6 en 7. Triaden op basis van oligomeren met de thienopyrazine-eenheid, zoals beschreven in voorgaande hoofd-

stukken, worden beschreven in hoofdstuk 6. In deze systemen treedt zeer snelle ladingsscheiding op nabij het Marcus-optimale gebied, dit wordt gevolgd door snelle recombinatie in het Marcus-omgekeerde gebied. Vanwege de korte levensduur van de ladingsgescheiden toestand kon geen recombinatie naar een triplettoestand worden waargenomen.

Systemen met een diketopyrrolopyrroleenheid in het oligomeergedeelte van de triaden worden beschreven in hoofdstuk 7. In deze systemen vindt de ladingsscheiding plaats in het Marcus-normale gebied, gevolgd door recombinatie in het omgekeerde gebied. Omdat de energie van de ladingsgescheiden toestand in deze systemen hoger ligt dan bij thienopyrazinegebaseerde systemen is de levensduur van deze toestand lang genoeg voor de vorming van een triplettoestand. Recombinatie naar een triplettoestand kon in deze systemen duidelijk worden waargenomen.

In het laatste hoofdstuk wordt het gebruik van oligomeren met een diketopyrrolopyrroleenheid onderzocht als acceptormateriaal in zonnecellen. Hoewel polymeren gebaseerd op diketopyrrolopyrrolen normaal gesproken worden gebruikt als donormaterialen, kan er ook acceptorgedrag worden waargenomen in deze materialen en er zijn zonnecellen gemaakt bestaande uit polythiofeen als donormateriaal en diketopyrrolopyrrololigomeren als acceptormaterialen. De beste cel heeft een rendement van 0.31 % in gesimuleerd zonlicht, met een foton-naar-elektron omzettingsrendement van $\sim 10\%$ tot een golflengte van 700 nm. Het rendement lijkt met name beperkt te worden door de grove morfologie van de actieve laag.

Curriculum vitae



Bram Karsten is geboren op 23 mei 1983 te Rotterdam. Na het behalen van zijn VWO-diploma aan het Christelijk Lyceum Veenendaal begon hij in 2001 met zijn studie Scheikundige Technologie aan de Technische Universiteit Eindhoven. Zijn afstudeeropdracht in de homogene katalyse heeft hij gedaan in de vakgroep "Anorganische Chemie en Katalyse" onder leiding van prof. D. Vogt. Na het afronden van zijn studie in 2006 is hij begonnen met zijn promotieonderzoek in de groep "Molecular Materials and Nanosystems" onder leiding van prof. R.A.J. Janssen. De belangrijkste resultaten van dit onderzoek zijn beschreven in dit proefschrift.

Bram Karsten was born on May 23rd, 1983 in Rotterdam, The Netherlands. After finishing his secondary education at the Christelijk Lyceum Veenendaal in Veenendaal, he studied Chemical Engineering and Chemistry at Eindhoven University of Technology. His graduation project in homogeneous catalysis was conducted in the "Inorganic Chemistry and Catalysis" group under supervision of prof. D. Vogt. After completion of this study, he started his doctoral research in the "Molecular Materials and Nanosystems" group under supervision of prof. R.A.J. Janssen. The most important results of this research are described in this thesis.

List of publications

Small band gap oligothieno[3,4-b]pyrazines

Karsten, B. P.; Janssen, R. A. J. *Org. Lett.* **2008**, *10*, 3513–3516.

An oligomer study on small band gap polymers

Karsten, B. P.; Viani, L.; Gierschner, J.; Cornil, J.; Janssen, R. A. J. *J. Phys. Chem. A* **2008**, *112*, 10764–10773.

Electronic structure of small band gap oligomers based on cyclopentadithiophenes and acceptor units

Karsten, B. P.; Bijleveld, J. C.; Viani, L.; Cornil, J.; Gierschner, J.; Janssen, R. A. J. *J. Mater. Chem.* **2009**, *19*, 5343–5350.

On the origin of small band gaps in alternating thiophene – thienopyrazine oligomers

Karsten, B. P.; Viani, L.; Gierschner, J.; Cornil, J.; Janssen, R. A. J. *J. Phys. Chem. A* **2009**, *113*, 10343–10350.

Charge separation and recombination in small band gap oligomer – fullerene triads

Karsten, B. P.; Bouwer, R. K. M.; Hummelen, J. C.; Williams, R. M.; Janssen, R. A. J. *J. Phys. Chem. B* **2010**, doi: 10.1021/jp906973d.

Diketopyrrolopyrroles as acceptor materials in organic photovoltaics

Karsten, B. P.; Bijleveld, J. C.; Janssen, R. A. J. *Macromol. Rapid Commun.* **2010**, doi: 10.1002/marc.201000133.

Charge separation and (triplet) recombination in diketopyrrolopyrrole – fullerene triads

Karsten, B. P.; Bouwer, R. K. M.; Hummelen, J. C.; Williams, R. M.; Janssen, R. A. J. *Photochem. Photobiol. Sci.* **2010**, doi: 10.1039/c0pp00098a.

Dankwoord

Na vier jaar SMO/M2N/MST ben ik nu toch echt toe aan het laatste en waarschijnlijk meest gelezen deel van mijn proefschrift. Hoewel er maar één naam op de kaft vermeld staat, was dit boekje niet tot stand gekomen zonder de hulp van een groot aantal mensen, die ik hier zoveel mogelijk zal proberen te benoemen, wetende dat ik waarschijnlijk heel veel mensen zal vergeten.

De eerste die veel dank verdient is natuurlijk mijn promotor. René, ik weet nog goed dat ik jou een e-mail stuurde met de vraag of ik eventueel in jou groep zou mogen promoveren. Ik geloof dat ik al binnen een kwartier antwoord van je had en we waren er snel uit dat ik in september 2006 zou beginnen. Ik heb er geen moment spijt van gehad, ik geloof niet dat je als promovendus een betere begeleider zou kunnen treffen. Ik heb in de afgelopen jaren keer op keer kunnen profiteren van de grote breedheid van je kennis en je wetenschappelijke inzichten. Ik ben ervan overtuigd dat de discussies met jou mij tot een beter en zeker ook kritischer onderzoeker hebben gemaakt dan zonder jou mogelijk was geweest. Naast je wetenschappelijke kant heb ik ook altijd bewondering gehad voor de altijd plezierige manier waarop je met mensen om kunt gaan. Ook als het wetenschappelijk even tegen zat wist jij altijd de moed er weer in te krijgen. René, hartelijk bedankt voor alle vertrouwen en begeleiding de afgelopen jaren!

Vijf van de zeven inhoudelijke hoofdstukken van dit proefschrift zijn tot stand gekomen in samenwerking met groepen van andere universiteiten. Here, I would like to thank our friends from Mons: Lucas, Johannes and Jérôme. Lucas, it has been a pleasure for me to work with you, and without all your calculations three of the chapters in this thesis would have been much less interesting. Moreover, our collaboration has led to three nice publications. Jérôme, the same holds for you, and I am very pleased that you were willing to take part in my reading committee. De twee hoofdstukken over fullereenderivaten zijn tot stand gekomen met hulp van mensen uit Groningen en Amsterdam. Ricardo Bouwer verdient hier veel dank voor al zijn hulp met de synthese en vooral zuivering van de verbindingen. Ricardo, ik heb onze samenwerking altijd zeer plezierig gevonden en ik ben blij dat al het werk tot twee mooie papers heeft geleid. Kees Hummelen en René Williams verdienen uiteraard ook veel dank voor hun bijdrage en ik ben zeer verheugd dat zij plaats wilden nemen in mijn lees- c.q. promotiecommissie.

Naast mensen van buiten de universiteit ben ik natuurlijk ook veel collega's uit Eindhoven dank verschuldigd. Ten eerste Johan Bijleveld. Johan, onze samenwerking is altijd zeer plezierig geweest en ik heb onze discussies en gezamenlijke syntheseroutes altijd zeer op prijs gesteld. Ik ben blij dat jij één van mijn paranimfen wilde worden. Ook ben ik veel dank verschuldigd aan Dirk Veldman. In de eerste paar jaar van mijn promotie heb ik hem altijd kunnen benaderen met alle mogelijke problemen op het gebied van optische spectroscopie. Dirk, zonder jou als kantoorgenoot was het een stuk lastiger geweest om me al die technieken eigen te maken. Martijn Wienk wil ik graag bedanken voor al zijn hulp bij het draaiende houden van de gloveboxen en dergelijke. Simon Mathijssen wordt vriendelijk bedankt voor zijn hulp met het dropcasten, afpompen en op START duwen (kortom: het meten van mobiliteiten aan een aantal van mijn verbindingen, beschreven in het laatste hoofdstuk).

Ook de hulp van alle ondersteunende mensen is van grote waarde geweest voor mijn tijd in de groep. Ralf, Lou en Joost verdienen dank voor hun hulp bij alles wat met analyse te maken had. Hans verdient grote dank voor al zijn hulp bij het bestellen van chemicaliën en het draaiende houden van alle apparatuur op het lab. De dames van het secretariaat verdienen veel lof voor de uitstekende manier waarop zij de groep al die tijd hebben ondersteund. Verder is een proefschrift natuurlijk niet af als Henk niet bedankt wordt voor de koffie... Henk, de koffie was prima!

Als je op een groot kantoor zit zijn er natuurlijk ook een hoop kantoorgenoten om te bedanken voor de goede sfeer. Hier komen ze: Dirk, Robert, De Herrik, Rafael, Christophe, Girish, Wolfie, Stefan, Marie-France, Arantxa, Di Nuzzo, Jan Anton en Irén. Verder verdienen natuurlijk nog alle mensen van Lab 1 een bedankje. Ik zal ze niet verder specificeren, behalve dan dat ik even wil zeggen dat met name de contacten met Mindaugas en de Appel altijd zeer goed waren. De rest van de vakgroep zal ik niet met naam en toenaam vermelden, dan vergeet ik alleen maar heel veel mensen die in belangrijke mate hebben bijgedragen aan de goede sfeer.

Wat betreft de allerlaatste fase van mijn promotietijd moet ik ook nog de mensen bedanken die zitting hebben willen nemen in de lees- en promotiecommissie (voor zover ze nog niet genoemd zijn): Bert Meijer, Stefan Meskers en Han Zuilhof.

De laatste alinea is uiteraard bestemd voor bijzondere personen. Mark, ik wil je graag bedanken voor de goede vriendschap in de afgelopen >20 jaar en ik stel het dan ook zeer op prijs dat je als paranimf wilt optreden. Veel succes met je eigen promotie! Tot slot verdient mijn familie natuurlijk de grootst mogelijke dank voor alle steun in de vele jaren voorafgaande aan mijn promotie. Zonder jullie was dit allemaal niet mogelijk geweest!

Bram